USAAMRDL-TR- 75-39A

DESIGN CRITERIA FOR ELASTOMERIC BEARINGS

Volume I - Final Report

Thiokol/Wasatch Division
A Division of Thiokol Corporation
Brigham City, Utah 84302

March 1976

Final Report

Prepared for

EUSTIS DIRECTORATE
U. S. ARMY AIR MOBILITY RESEARCH AND DEVELOPMENT LABORATORY
Fort Eustis, Va. 23604

EUSTIS DIRECTORATE POSITION STATEMENT

The data contained in this report are the results of an effort designed to improve the state of the art of elastomeric bearing design for helicopter rotor head applications. The products of this effort are a design manual and a computer program based on finite-element techniques. The results of this program are contained in the following four volumes:

Volume I - Final Report
Volume II - Design Manual
Volume III - Program User's Manual
Volume IV - Programmer's Manual

Volume I contains the development and background information used in producing the design manual.

Volume II presents design considerations and procedures, bearing applications, methods of analysis, and techniques for predicting bearing performance.

Volumes III and IV contain the computer code and examples of problems showing sample inputs and outputs.

The products of this effort provide a good foundation for building a comprehensive manual and computer code for the design and analysis of elastomeric bearings for helicopter rotor head applications. It was recognized at the onset of this program that both the manual and the code would be first editions. The results of this effort were expected to define areas requiring further development. Further investigations coupled with feedback from users and/or evaluators are expected to provide material for upgrading the content and format of the manual and codes.

Mr. John Sobczak of the Military Operations Technology Division served as project engineer for this effort.

UNCLASSIFIED

SECURITY CLASSIFICATION OF THIS PAGE (When Data Entered)

REPORT DOCUMENTATION PAGE	READ INSTRUCTIONS BEFORE COMPLETING FORM
1. REPORT NUMBER: USAAMRDL-TR-75-39A	2. GOVT ACCESSION NO. / 3. RECIPIENT'S CATALOG NUMBER
4. TITLE (and Subtitle): DESIGN CRITERIA FOR ELASTOMERIC BEARINGS, Volume I - Final Report	5. TYPE OF REPORT & PERIOD COVERED: Final Report
	6. PERFORMING ORG. REPORT NUMBER
7. AUTHOR(s): Arnold R. Thompson	8. CONTRACT OR GRANT NUMBER(s): DAAJ02-73-C-0091
9. PERFORMING ORGANIZATION NAME AND ADDRESS: Thiokol/Wasatch Division, A Division of Thiokol Corporation, Brigham City, Utah 84302	10. PROGRAM ELEMENT, PROJECT, TASK AREA & WORK UNIT NUMBERS: 62205A 1F162205A119 01 013 EK
11. CONTROLLING OFFICE NAME AND ADDRESS: Eustis Directorate, U. S. Army Air Mobility Research and Development Laboratory, Fort Eustis, Va. 23604	12. REPORT DATE: March 1976 / 13. NUMBER OF PAGES: 266
14. MONITORING AGENCY NAME & ADDRESS(if different from Controlling Office): 267 p.	15. SECURITY CLASS. (of this report): Unclassified / 15a. DECLASSIFICATION/DOWNGRADING SCHEDULE

16. DISTRIBUTION STATEMENT (of this Report)

Approved for public release; distribution unlimited.

DA-1-F-162205-A-119

17. DISTRIBUTION STATEMENT (of the abstract entered in Block 20, if different from Report)

18. SUPPLEMENTARY NOTES

None

19. KEY WORDS (Continue on reverse side if necessary and identify by block number)

Elastomeric Bearings
Helicopter Rotor
Natural Rubber
Finite Element Analysis
Stability
Service Life

20. ABSTRACT (Continue on reverse side if necessary and identify by block number)

The contract with the Eustis Directorate included the evaluation, development, and selection of analytic and experimental techniques required for the design and/or evaluation of elastomeric bearings for rotor head applications. Axially laminated cylindrical (Type I), radially laminated cylindrical (Type II), and spherical laminated (Type III) bearings were considered.

This report reviews three major areas of development: (1) the development and selection of experimental procedures for the determination of required design and

NEXT Page

DD FORM 1 JAN 73 1473 EDITION OF 1 NOV 65 IS OBSOLETE

UNCLASSIFIED

SECURITY CLASSIFICATION OF THIS PAGE (When Data Entered)

20.
analysis parameters, (2) the evaluation and definition of predictive techniques for stability of buckling of laminated bearings, and (3) the development of procedures for predicting the service life of bearings.

The products of this effort are a finite-element computer code and a first edition of a design manual.

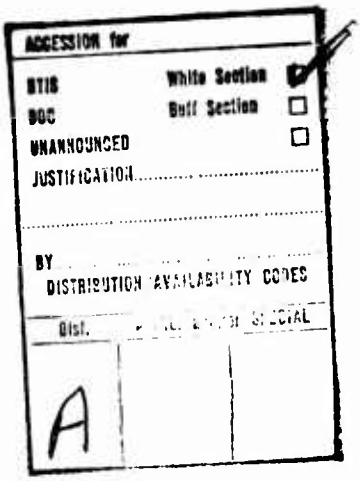

SUMMARY

The application of elastomeric bearings in helicopter systems is of current interest. This report presents the results of the contract on Design Criteria for Elastomeric Bearings conducted for the Eustis Directorate, U.S. Army Air Mobility Research and Development Laboratory, Fort Eustis, Virginia. The products of this effort are a design manual and a computer program based on finite-element techniques. These developments are an extension of prior solid rocket motor thrust vector control elastomeric bearing and elastomer mechanics technology.

The program scope includes bearing configurations with potential application in rotor heads. Type I (flat laminate) bearings react the main thrust or CF loads and provide for lateral and torsional motion. Type II (radial or cylindrically laminated) bearings react radial loads and provide for torsional motion with some axial motion in the case of cylindrical shims and out-of-plane rotation in the case of spherical shims. Type III (spherically laminated) bearings react axial or CF loads while providing for three degrees of rotational motion.

Several levels of design analysis are presented: closed-form equations, computer developed design curves, and finite-element computer analyses. The material properties to make these calculations are determined for a selected representative elastomer. Test specimens and methods are included in this discussion.

Design procedures are verified to show the accuracy of these results. The limits or regions of applicability are pointed out.

The design restraints determined by stability and service life are also developed.

The results of this contract on Design Criteria for Elastomeric Bearings are presented in four volumes:

Volume I	Final Report
Volume II	Design Manual
Volume III	Program User's Manual
Volume IV	Programmer's Manual

PREFACE

This report contains the results of testing and analysis performed by Thiokol/Wasatch Division under Eustis Directorate, U.S. Army Air Mobility Research and Development Laboratory (USAAMRDL) Contract DAAJ02-73-C-0091.

The contracted work was conducted under the technical cognizance of Mr. John Sobczak of the Eustis Directorate.

The work was performed under the direction of Principal Investigators C. W. Vogt and A. R. Thompson with the support of B. W. Law of the Program Management Directorate.

The principal contributors were:

Dr. G. Anderson -- Material Properties and Service Life

Dr. S. Kulkarni -- Analysis and Stability

W. E. Berndt -- Type I Bearing Verification

L. E. Jensen -- Type II Bearing Verification

G. J. Bakken -- Type III Bearing Verification

D. R. Trauntvein -- Fabrication

D. H. Lee - Programming

TABLE OF CONTENTS

TABLE OF CONTENTS (Cont)

LIST OF ILLUSTRATIONS

LIST OF ILLUSTRATIONS (Cont)

LIST OF ILLUSTRATIONS (Cont)

LIST OF ILLUSTRATIONS (Cont)

LIST OF TABLES

1.0 INTRODUCTION

The primary objectives of this contract were to develop a design manual and a computer code for the design and analysis of elastomeric bearings for helicopter rotor head application.

The program approach was to use the analytic, experimental, design, and process expertise developed for the design of solid rocket motor propellant grains and thrust vector control (TVC) systems. Solid propellant is a nonlinear, viscoelastic material with physical property and response characteristics of an elastomer. Elastomeric bearings for TVC are spherical (Type III) with core (elastomeric pad and reinforcing shim composite) geometries proportional to that required for rotor head application.

This final report (Volume I) contains the development and background information necessary to produce the design manual (Volume II). Such background information includes: (1) selection of an elastomeric material representative of currently used elastomers, (2) development of test methods and specimens for physical properties, (3) development of service life data, (4) determination of stability parameters, and (5) verification of design and analytical techniques.

For this report elastomeric bearings in rotor head applications are classified into four types. The Type I axial bearing (Figure 1-1) is constructed by laminating flat annulars of elastomeric pads and reinforcing shims between end rings. The primary loads and motions for this type bearing are the reaction of axial loads, F_z, and torsional displacement, θ_z. The bearing will allow some compliance to the asymmetric motions and loads in the x-y plane or about the x and y axes; however, these asymmetric loads and motions will severely compromise the service life and stability of the design. The Type II radial bearing (Figure 1-2) is constructed of cylindrical laminates of elastomer and reinforcement. This bearing is difficult to fabricate when residual cure and thermal induced tensile stresses

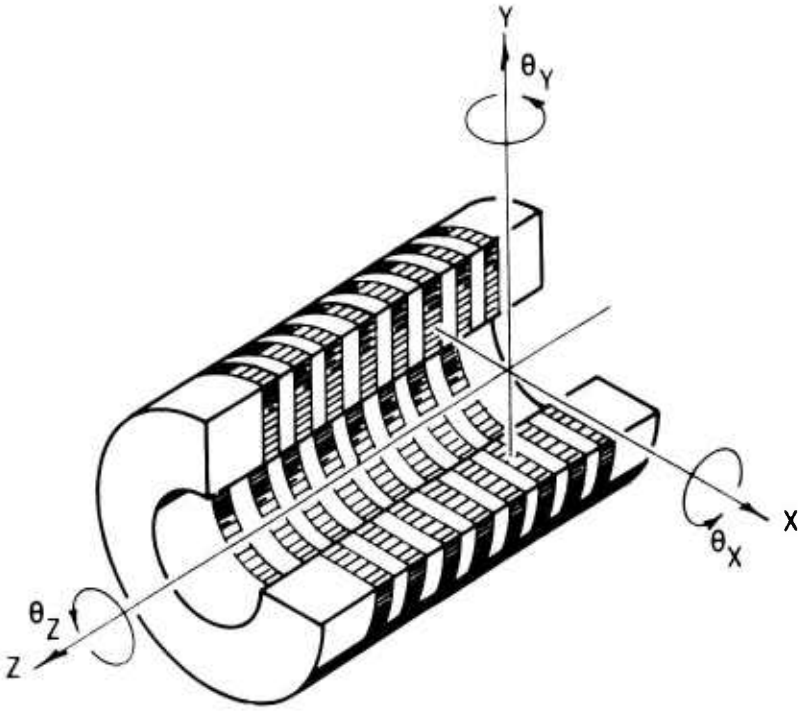

Figure 1-1. Type I Axial Bearing

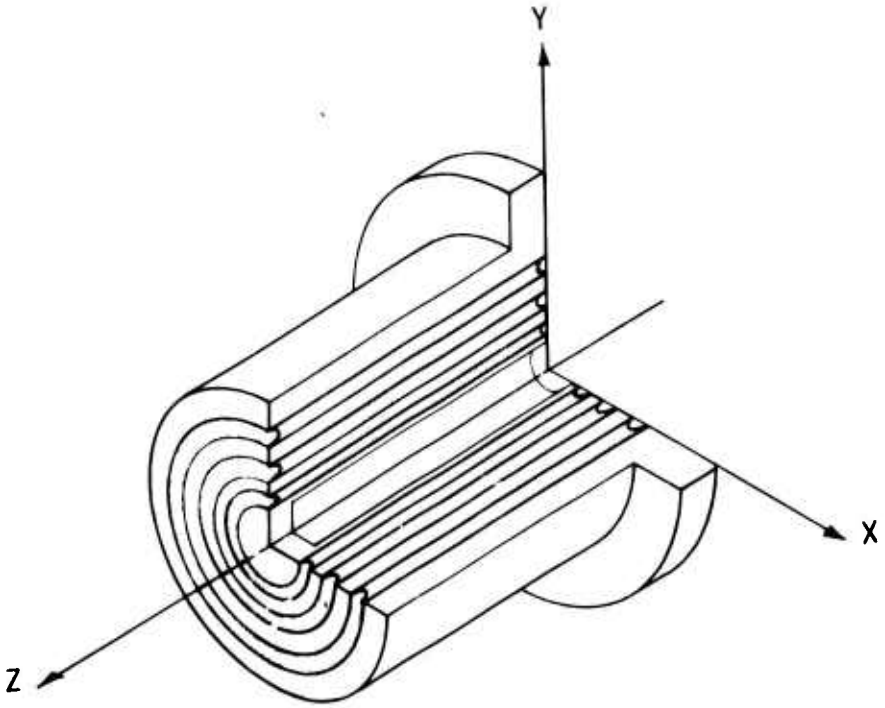

Figure 1-2. Type II Radial Bearing

must be minimized. The primary loads and motions are the reaction of the radial forces, F_r, in the x-y plane and torsional displacement, θ_z, about the z axis. The bearing will also react moments about the x and y axes and will provide minimal compliance in the axial or z direction. The Type III spherical bearing (Figure 1-3) is constructed of spherical segment of elastomer and reinforcement between end rings. Compression, transfer, and injection molding techniques are applicable. This bearing provides for rotational motion about all axes while reacting axial and lateral loads. The Type IV conical bearing (Figure 1-4) is constructed by laminating conical segments of elastomer and reinforcement between end rings. This bearing primarily provides for torsional displacement about the z axis, while reacting axial and lateral loads. Some compliance to rotation and moments about the x and y axes is provided.

The design of Type I, II and III bearings is presented in this manual. The computer code presented in Volumes III and IV can be used to design the Type IV bearings, and the basic design procedures can be extended to this bearing. It was recognized that the manual and code will be first editions. That is, the results of the analytic and experimental phases would provide definition of technology requiring further development. Also, the feedback from users and evaluators would further define requirements for highly applicable and user-oriented design tools.

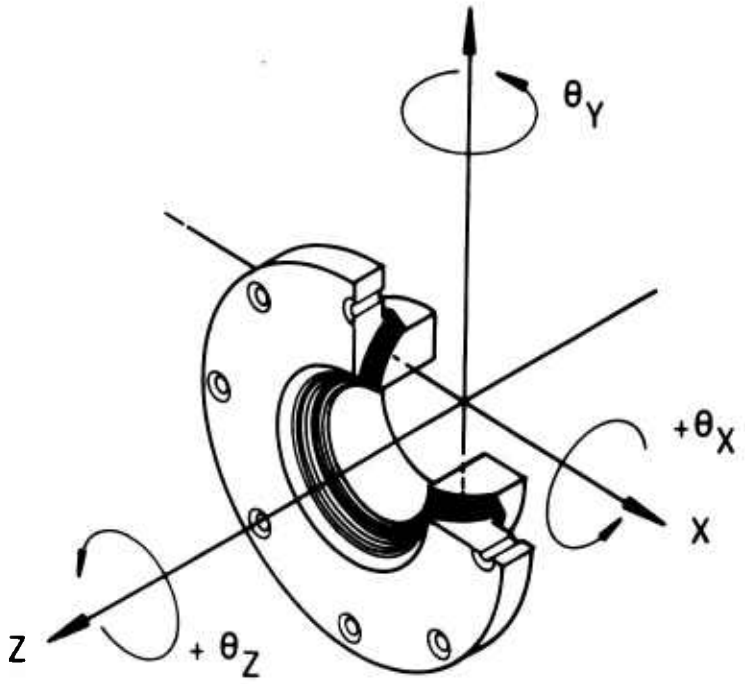

Figure 1-3. Type III Spherical Bearing

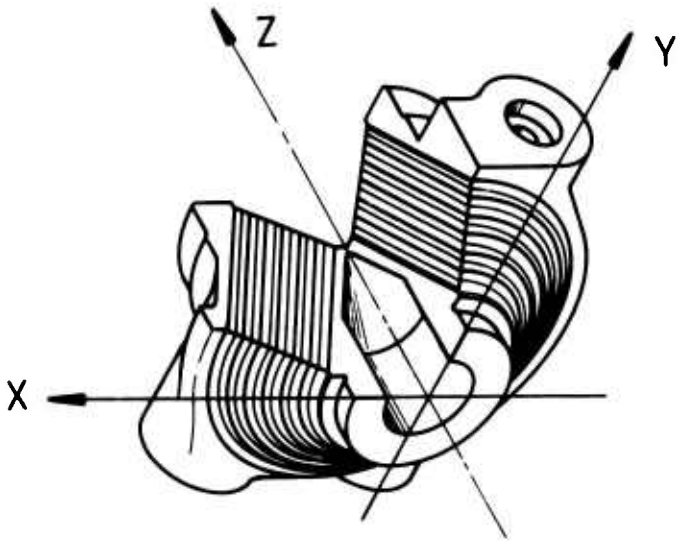

Figure 1-4. Type IV Conical Bearing

2.0 MATERIAL SELECTION

2.1 MATERIAL SELECTION FOR ELASTOMERIC BEARINGS

Recent work in industry on elastomeric bearings for helicopter and rocket motor nozzles, respectively, has identified natural rubber (NR) as probably the best "all around" material for mechanical application. Some NR characteristics make it advantageous for use in mechanical system subjected to a fatigue-type environment:

1. Strain induced crystallization tends to resist crack tip propagation.
2. Low stress/strain hysteresis keeps internal heat buildup to a minimum.
3. NR is readily bondable to metals.
4. Inherent low temperature crystallization (-25°C) and a high post-vulcanization temperature (+140°C) make it compatible with a wide temperature service application.

NR stock was therefore naturally specified (contract requirements) for use on this program, and only the task of selecting a representative formulation or recipe that would be applicable to a helicopter bearing was at hand.

2.1.1 NR Formulation Constituents

The criteria for compounding the NR formulation were based on meeting the following requirements:

1. Good elasticity combined with high strength.
2. Long fatigue life.
3. High resistance for age degradation.

4. Low creep or stress relaxation.
5. Minimum internal heat generation.
6. Resistance to tear and abrasion.

These requirements may be met and even optimized by a proper combination of the basic categories of ingredients:

1. Raw latex--technically referred to as "cis-polyisoprene" and obtained from the "hevea brasilienis" tree.
2. Vulcanization agents--notably sulfur, and usually supplemented by stearic acid, zinc oxide and cure accelerators.
3. Fillers--"reinforcing" and "nonreinforcing" carbon black.
4. Plasticizers--paraffinic or naphthenic oil.
5. Protective agents--antioxidants and antiozonants.

All categories are influential on the mechanical, bondability, and aging properties of the material.

2.1.2 Latex

Natural rubber stock extracted from the sap of the rubber tree in the form of latex is processed into a smoked sheet and crepe for subsequent mixing and processing. This initial processing establishes the grades of NR as a function of cleanliness and uniformity of viscosity. The grades commonly employed for quality mechanical systems are: RSS1, SMR5, SMR5L, and SMR5CV, where:

RSS = Ribbed smoked sheet

SMR = Standard Malaysian rubber

1, 5 = Grades 1 and 5, which are "best quality" for their respective type (RSS, SMR)

L = Low viscosity

CV = Constant viscosity

RSS1 and SMR5CV are the two types most commonly available, where the latter is considered the highest quality (free from foreign material) and proven most reproducible from lot to lot. SMR5CV was selected based on these considerations.

2.1.3 Vulcanization Agents

The Natural Rubber Producers Research Association (NRPRA) has recently summarized (ref 2-1 and 2-2) the results of compounding research performed for the development of NR formulations that exhibit improved dynamic/fatigue properties.

This work has been centered on the reduction of sulfur within the compound to enhance its thermal stability and reduce its susceptibility to age degradation. Apparently sulfur in excess of one part per hundred of rubber (phr), as is the case of "conventional" formulations, results in predominant polysulfide crosslinking which is known to be unstable to heat and thus prone to "reversion" or a postheating deterioration. A similar degradation in physical properties will also follow accordingly at a rate dependent on the working temperatures.

The two aforementioned references classify NR compounds as a function of sulfur and accelerator content:

Type	Sulfur (phr)	Accelerator (phr)
Conventional	2.0-3.0	0.5-1.0
Semiefficient vulcanizing	1.0-1.8	1.0-2.5
Efficient vulcanizing (EV)	0.3-1.0	2.0-5.0

Fatigue data (ref 2-2) as obtained from an NRPRA ring fatigue test for both unaged and aged (7 days at 100° C in air) conditions (Figure 2-1) depicts the EV system as having the best "aged" fatigue characteristics.

Anticipating that heat buildup and thermal aging will be inherent in a bearing and will affect the fatigue life of the elastomeric, the EV system was selected for use in this program. The remaining task was to establish the filler or reinforcement content that would yield optimum fatigue strength.

2.1.4 Filler

NR compounds employed for engineering applications are normally filled with a "reinforcing" type carbon black to improve strength and increase modulus (Figure 2-2).

Chrysler Corporation performed an optimization study (ref 2-3) to determine the best type and optimum quantity of carbon black that would give the best fatigue strength. The types of carbon black considered were:

FEF = Fast extrusion furnace
MT = Medium thermal
MPC = Medium process channel
SRF = Semireinforcing furnace
HAF = High abrasion furnace

Of these five candidates, the HAF and SRF yielded the best and equivalent fatigue strength characteristics, both at a content of around 30 phr.

The results from this Chrysler study fall in line with the work of NRPRA, which recommends (ref 2-4) an EV formulation containing SRF for specific use in mechanical components (i.e., springs, couplings, mountings, bearings, etc).

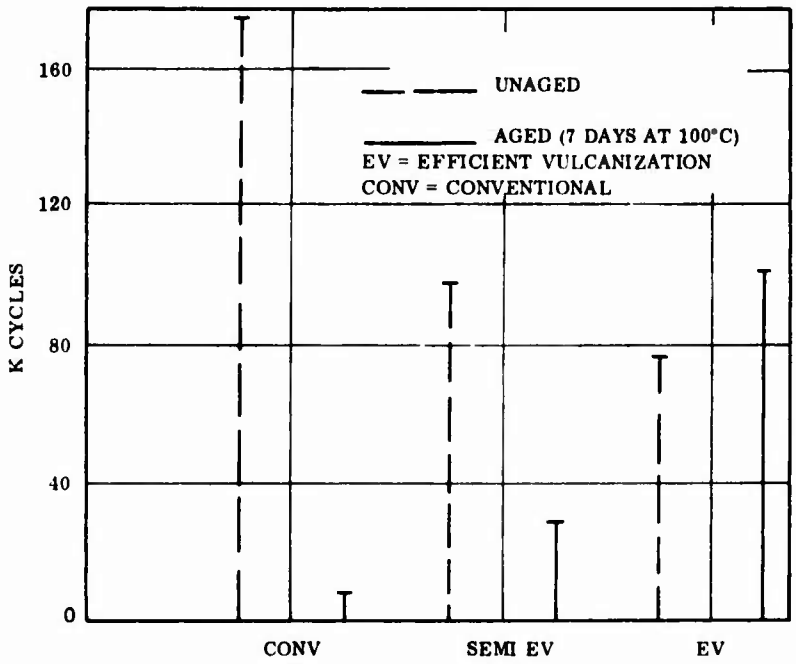

Figure 2-1. Fatigue Characteristics of Three Types of NR Compounds

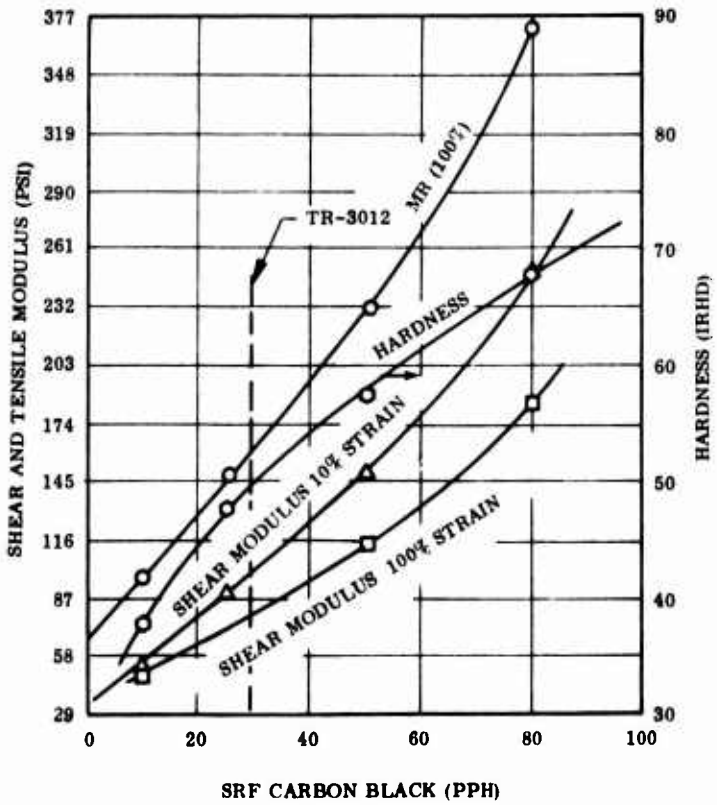

Figure 2-2. Physical Properties Comparison of TR-3012 Elastomer vs Carbon Black

2.1.5 Plasticizer

A plasticizer is commonly employed to facilitate processing by improving the flow and extrusion characteristics for injection molding or to reduce the stiffness (modulus) of a cured rubber system. Our requirements did not warrant the use of this additive.

2.1.6 Protective Agents

Oxygen and ozone readily degrade NR if protection is not given. Commercially available antioxidants are universally used to prevent oxidation and are extremely effective with NR in preventing the long-term creep and stress relaxation inherent to this form of deterioration. Ozone attack, which appears on the surface of the rubber in the form of cracks or craze marks, occurs when the rubber is in a stressed condition and can be arrested by the addition of antiozonant ingredients. However, because of the migratory nature of such ingredients, bonding problems have been identified with the use of this material as it readily permeates and coats the surface of the rubber crepe.

The formulation recommended by ref 2-4 includes an antioxidant but not an antiozonant because of (1) the relative low outdoor ozone concentration, (2) the low amount of exposed surface area of a pad, and (3) the criticality of the bond to the steel shims associated with a helicopter bearing.

2.1.7 NR Formulation

The formulation as selected from ref 2-4 is summarized as follows:

Constituent	Category	Quantity (parts)
Natural rubber (SMR5CV)	Latex	100.00
Carbon black (SRF, ASTM Type N770)	Filler	30.00
Sulfur	Curative	0.60

Constituent	Category	Quantity (parts)
Zinc oxide	Curative	5.00
Zinc 2-ethyl hexanoate	Curative	2.00
2-morpholinothis - benzothiazote	Cure accelerator	1.44
Tetrabutylthiuran - disulfide	Cure accelerator	0.60
Poly-2,2,4-trimethyl - 1,2-dihydroquinoline	Antioxidant	2.00

This formulation was unchanged during the course of the program. The task at hand was to develop a representative, workable formulation and to evaluate the influence and sensitivities of mechanical parameters related to the design of an elastomeric helicopter bearing. Compound optimization was outside the program scope.

2.1.8 Formulation Designation

ASTM D2000 depicts a method of classification for rubber compounds based on their physical properties as measured by standard ASTM/SAE test methods.

The ASTM/SAE designation for the material employed for this program is:

4AA530A13B13C20F17K11L14P20

where

4 = Grade number

A = Type (150° F test temperature)

A = Class (no maximum swell requirement)

5 = Durometer hardness

30 = 3,000 psi minimum tensile strength

A13 = Heat resistance (ASTM D573)

B13 = Compression set (ASTM D395, Method B)

C20 = Outdoor aging (ASTM D1171)

F17 = Low-temperature brittleness (ASTM D746, Process B)

K11 = Adhesion (ASTM D429, Method A)

L14 = Water resistance (ASTM D471)

P20 = Straining resistance (ASTM D925, Method B)

These tests were not performed by Thiokol but were by NRPRA (ref 2-1) in support of characterizing the EV type of compound. This formulation will be identified by Thiokol's designation TR-3012 for the purpose of this contract.

2.2 OXIDATION AND OZONE PROTECTION

Natural rubber is subject to oxidation by air and ozone, as is all unsaturated (not all carbon atoms are bonded but some are left free) rubbers. However, natural rubber can be protected by additives which provide several years of protection under normal atmospheric conditions. Ozone protection also improves resistance to flex cracking, which can be significant under some dynamic conditions.

The initial low sulfur rubber compound, designated TR-3012, contained an antioxidant (Flectol H, polymerized 2, 2, 4 trimethyl hydroquinoline) but no antiozonant. As a result of a consultation with Dr. Gent (as reported in Appendix B), two formulations were compounded using Santoflex 17. Santoflex 17 chemically is N, N' bis (1-ethyl-3 methyl pentyl) p-phenylene diamine and is a dark red-brown mobile liquid. This mobility is a disadvantage as far as bondability is concerned because of its tendency to migrate to the bond zone.

A study was initiated to determine the adhesive effect of antiozonant additives. Three formulations were prepared as shown in Table 2-1. The first column represents contact rubber TR-3012; the second and third have one part and two

TABLE 2-1

EFFECT OF ANTIOZONANT ON OZONE AGING OF ELASTOMERIC BEARINGS

Formulation (pph)	TR-3012			347A			347B		
SMR-CV (SL)	100			100			100		
Zinc Oxide	5			5			5		
Zinc-2-Ethexoate	2			2			2		
Flectol H	2			1			1		
Santoflex 17	--			1			2		
Sulfur	0.6			0.6			0.6		
Santocure MOR	1.44			1.44			1.44		
Butyl Tuads	0.6			0.6			0.6		
SRF Black	30			30			30		
QLS Determined Shear Properties	- 0 -	4 wk	12 wk	- 0 -	4 wk	12 wk	- 0 -	4 wk	12 wk
Strain at 10%*									
S_B (psi)	1,284	2,104	1,800	1,705	1,264	1,099	1,542	1,102	1,174
ϵ_B (%)	520	598	600	611	583	582	610	563	576
G50 (psi)	--	58.5	39.5	27.1	29.5	32.3	29.5	28.9	33.7
G100 (psi)	80.6	91.0	70.8	58.8	54.3	57.9	60.2	51.2	60
G300 (psi)	350	369	284	250	200	188	256	194	217.5
Failure (% COA)	100	100	100	100	40	70	100	20	65
Strain at 25%*									
S_B (psi)		2,119	2,232		1,222			1,208	1,050
ϵ_B (%)		612	600		571			559	508
G50 (psi)		43	43.5		27.8			34.3	30.2
G100 (psi)		77	78.5		52.2			56.3	52.9
G300 (psi)		335	360		193			203	184
Failure (% COA)		100	100		45			20	65
Strain at 50%*									
S_B (psi)		1,986	1,895		922			1,152	1,095
ϵ_B (%)		589	603		552			627	577
G50 (psi)		42	38.5		27.6			28.4	29.0
G100 (psi)		75	73.3		50.3			51.0	50.3
G300 (psi)		329	260		183			181	183
Failure (% COA)		100	100		25			10	50

*Storage Strain Level: S_B = shear stress at breaking
ϵ_B = shear stress at breaking
G50 = secant modulus at 50% shear strain
COA = percent cohesive failure

parts of antiozonant additives, respectively. Quadruple lap shear specimens (Figure 2-3) were fabricated using the three formulas.

The specimens were then subjected to shear strains of 10, 25, and 50% in an atmosphere of 50 ppm ozone and aged for 4 and 12 weeks at room temperatures.

The formulation containing only the antioxidant (TR-3012) showed good retention of properties through the 12-week aging program with some increase in shear strength but with essentially no change in elongation. The moduli values had only slight variations.

The compositions containing the Santoflex antiozonant (347A and 347B) showed a slight decrease in shear strength, shear modulus, and elongation with age. The changes appeared to be nearly the same for each imposed strain level. Of prime concern is the change in failure mode from 100% cohesive failure to partly adhesive failure.

Based upon these results, it was concluded that the formulation (TR-3012) without added antiozonant should be carried forth and no further work done with the antiozonant containing materials. A communication with Dr. P. B. Lindley (ref 2-5) indicates how to avoid this bond degradation. He makes the following comments: "The antiozonant has an opportunity to migrate to the surface before vulcanization. With compounds containing this class of chemical antiozonants it is advisable to remill immediately before moulding, or to use an indirect (e.g., transfer moulding) process."

Waxes are recommended for ozone protection under static conditions, but the amount needed may lead to undesirable blooms and also may interfere with, bonding. However, wax/chemical antiozonant combinations can be effective at

fairly low concentrations and we would therefore suggest trying the following blend of a wax and a slightly less mobile antiozonant than Santoflex 17.

Microcrystalline wax (e.g., Sunolite 240)	1.5 phr
Santoflex 13	2.0 phr

The bonding integrity was determined to be more important than ozone protection of small exposed surface area; therefore, the Santoflex 17 additive was dropped from the recipe.

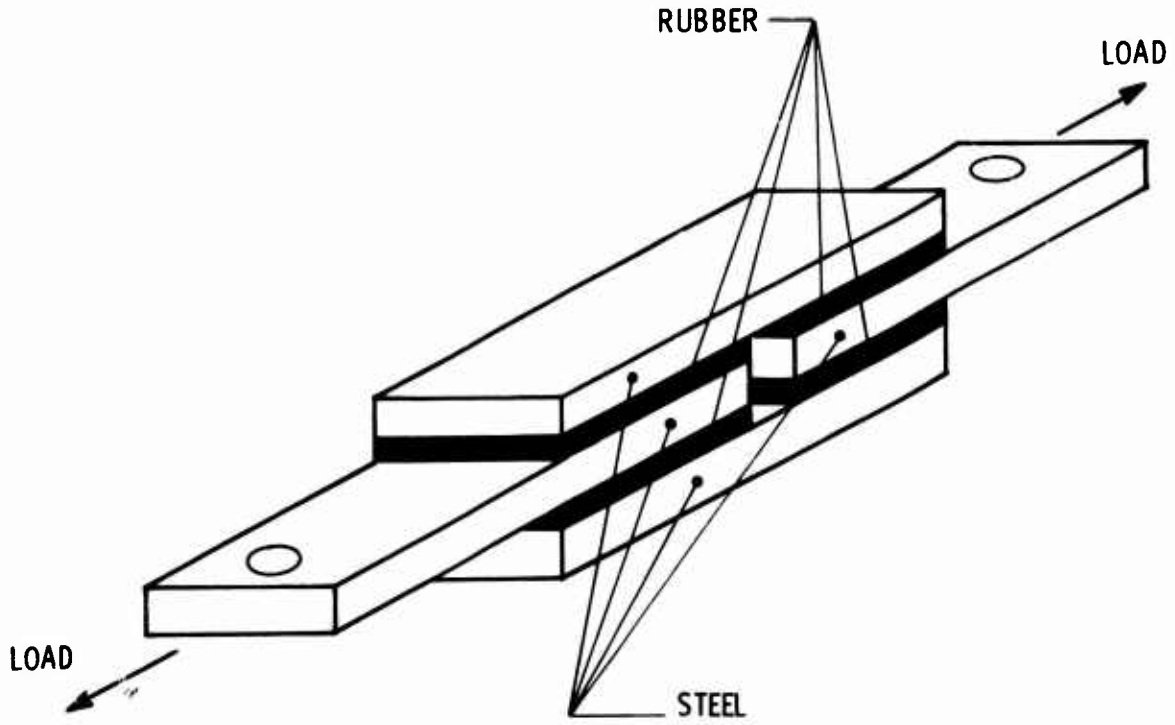

Figure 2-3. Quadruple Lap Shear (QLS) Test Specimen

2.3 CHARACTERIZATION

2.3.1 Uniaxial Tensile Data

Most helicopter elastomeric bearing designs use the elastomer in compression; however, the limited tensile data obtained reveals some interesting phenomena. Elastomers at standard temperatures for military and/or commercial use in the range of -65° to +140° F show properties that are both temperature and load rate dependent. Testing to determine the materials' response to both variations can be performed in a number of different ways: (1) relaxation testing, (2) dynamic testing, and (3) broad spectrum testing. The latter refers to a test matrix of various combinations of temperatures and rates of loading of a tensile specimen (Figure 2-4 shows the tensile specimen used). Data (Table 2-2) from typical tensile tests are shown in Figures 2-5 through 2-7. The uniaxial stress versus strain is noted for various testing temperatures (-20°, +75°, and +140°F) for different crosshead rates. The data are plotted as temperature corrected stress,

$$\sigma_c = \sigma \frac{T_s}{T}$$

where T_s = reference temperature = 77° + 460° F

to yield absolute units. Figure 2-5 shows the effect of crosshead speed at -20° F. At these rates and temperature, the material is in the transition range (between glassy and equilibrium) which shows a sizable response to load rate. At room temperature (Figure 2-6), the material is less responsive to rate, and at +140° F it should be even less sensitive to rate because of its nearness to equilibrium.

Gage marks must be used to obtain accurate data, particularly at the high temperatures (140° F). The material flows out of the jaws and makes the data somewhat inaccurate. It is recommended that the material be scragged or stress-softened 4 to 5 cycles before measurements are taken.

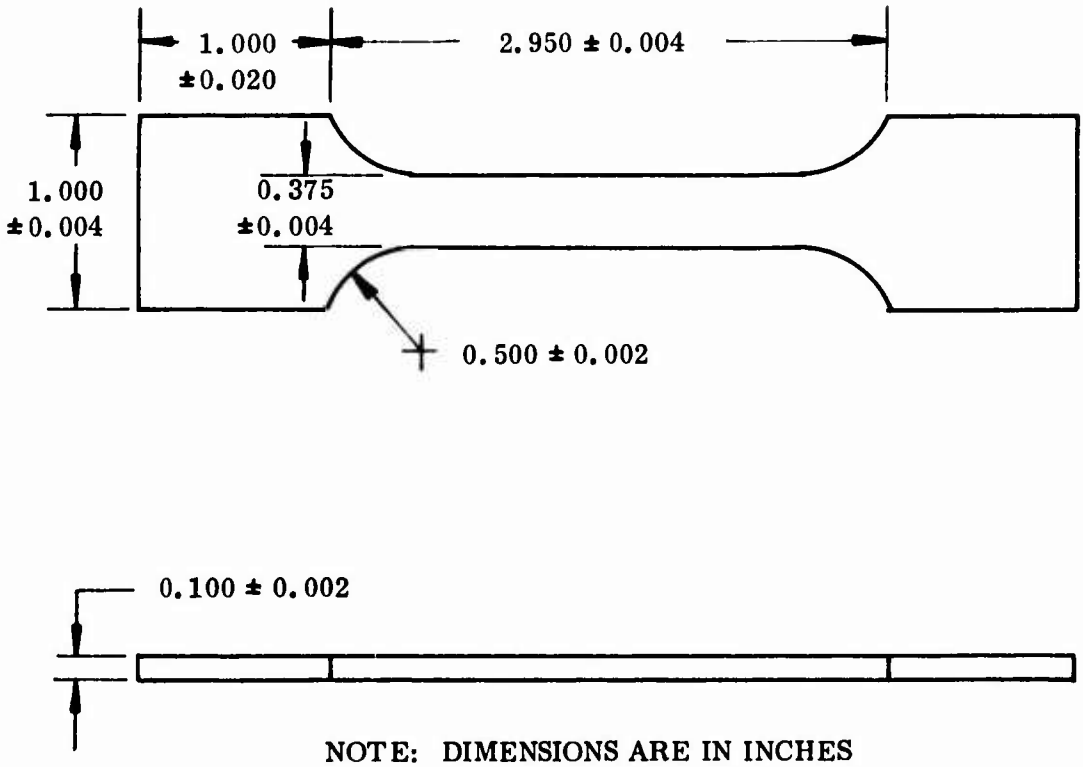

Figure 2-4. Uniaxial Tensile Test Specimen

TABLE 2-2

FLEXIBLE BEARING MATERIALS UNIAXIAL TENSILE DATA

Sample Number	Test Temp (°F)	Crosshead Rate (in/min)	Sample Cross Section (in^2)	Force at Strain Levels (lb)						Stress at Strain Levels (psi)						Modulus at Strain Levels (psi)					
				2.5%	5%	10%	15%	20%	30%	2.5%	5%	10%	15%	20%	30%	2.5%	5%	10%	15%	20%	30%
1-1	-20	0.05	0.022	0.10	0.37	0.57	0.77	0.93	1.25												
2-1	-20	0.05	0.022	0.07	0.28	0.48	0.65	0.79	1.10												
	Avg		0.022	0.09	0.33	0.53	0.71	0.86	1.18	3.5	13.2	21.3	28.8	34.8	47.6	195	377	320	302	286	282
3-1	-20	0.10	0.021	0.14	0.23	0.38	0.55	0.70	0.97												
4-1	-20	0.10	0.020	0.12	0.28	0.47	0.58	0.75	1.00												
4-2	-20	0.10	0.020	0.07	0.30	0.53	0.73	0.86	1.09												
	Avg		0.020	0.11	0.27	0.46	0.62	0.77	1.02	6.6	16.2	27.6	37.1	46.0	61.0	271	340	304	286	277	265
5-1	-20	20	0.016	0.22	0.31	0.61	0.94	1.20	1.58												
5-2	-20	20	0.016	0.21	0.32	0.61	1.00	1.28	1.60												
6-1	-20	20	0.022	0.28	0.35	0.65	0.88	1.10	1.31												
6-2	-20	20	0.022	0.27	0.34	0.64	0.84	0.98	1.24												
	Avg		0.019	0.25	0.33	0.63	0.92	1.14	1.43	15.8	21.4	41.1	60.8	75.9	95.7	647	450	452	466	456	413
7-1	75	0.1	0.019	0.14	0.20	0.48	0.72	0.84	1.16												
8-1	75	0.1	0.023	0.14	0.23	0.60	0.80	1.04	1.38												
9-1	75	0.1	0.026	0.07	0.37	0.67	0.98	1.22	1.63												
10-1	75	0.1	0.017	0.05	0.23	0.44	0.63	0.80	1.08												
	Avg		0.021	0.09	0.26	0.53	0.75	0.95	1.28	4.3	12.4	25.5	35.9	45.6	61.8	178	260	281	276	274	268
12-1	75	20	0.020	0.23	0.32	0.48	0.76	1.02	1.28												
13-1	75	20	0.020	0.28	0.34	0.52	0.78	1.04	1.34												
	Avg		0.020	0.26	0.33	0.50	0.77	1.03	1.32	12.8	16.5	25.0	38.5	51.5	65.5	524	346	275	295	309	284
14-1	140	0.1	0.022	0.14	0.22	0.50	0.66	0.88	1.20												
15-1	140	0.1	0.021	0.14	0.26	0.46	0.66	0.86	1.10												
	Avg		0.021	0.14	0.24	0.48	0.66	0.87	1.15	6.0	10.2	20.4	28.1	37.0	48.9	146	216	224	216	222	211
16-1	140	20	0.023	0.26	0.38	0.58	0.74	0.86	1.18												
17-1	140	20	0.016	0.14	0.20	0.34	0.46	0.56	0.74												
	Avg		0.020	0.20	0.29	0.46	0.60	0.71	0.93	9.0	12.9	20.7	27.2	32.3	41.2	371	271	227	208	193	178

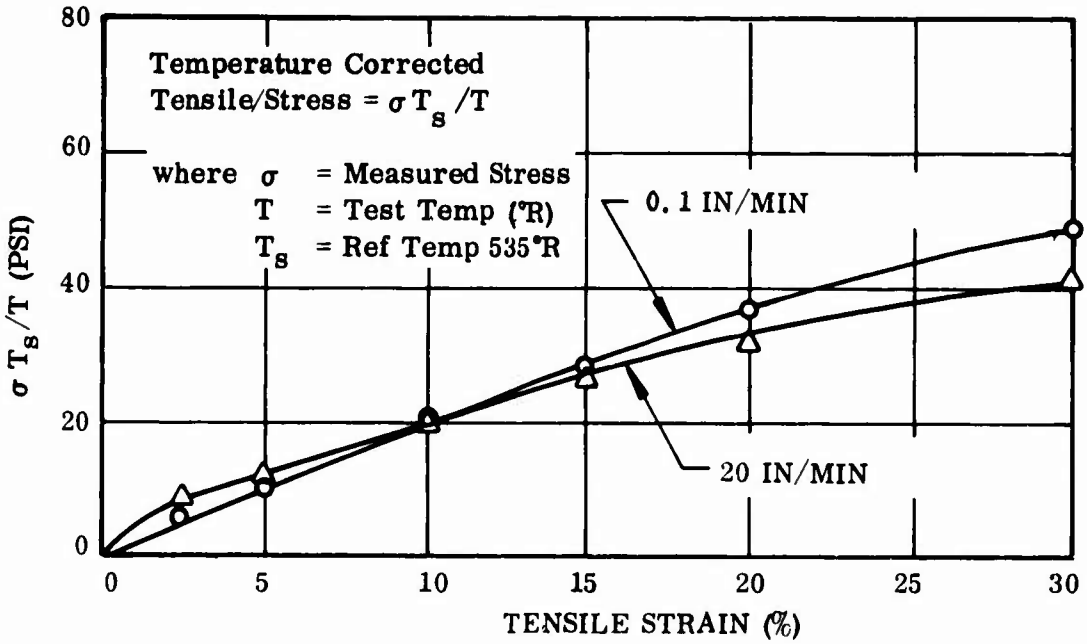

Figure 2-5. Tensile Data, 140°F

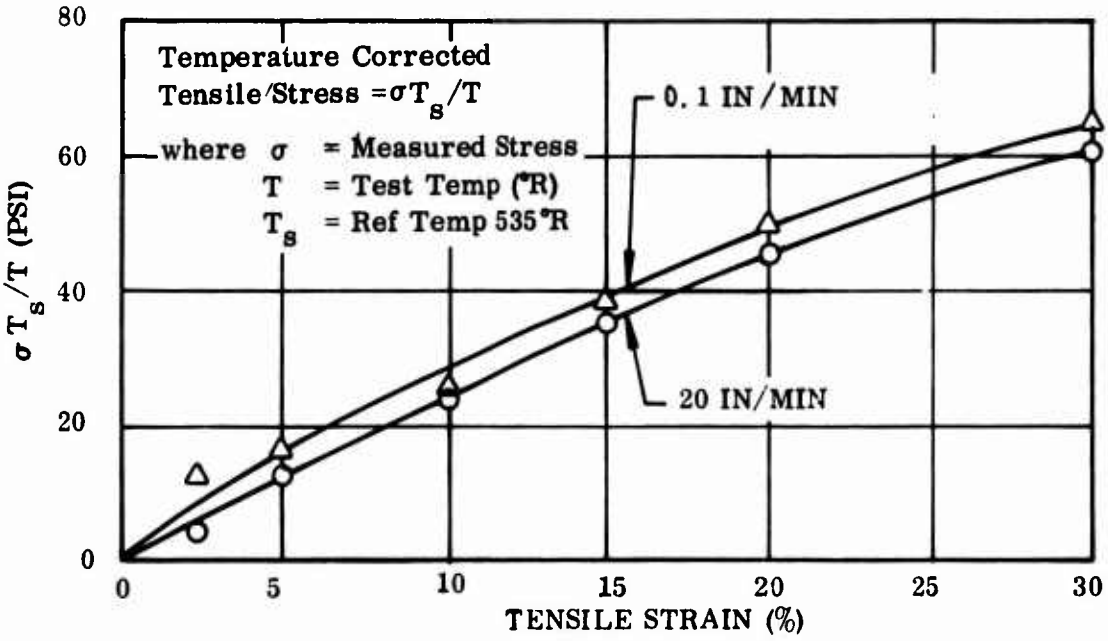

Figure 2-6. Tensile Data, 75°F

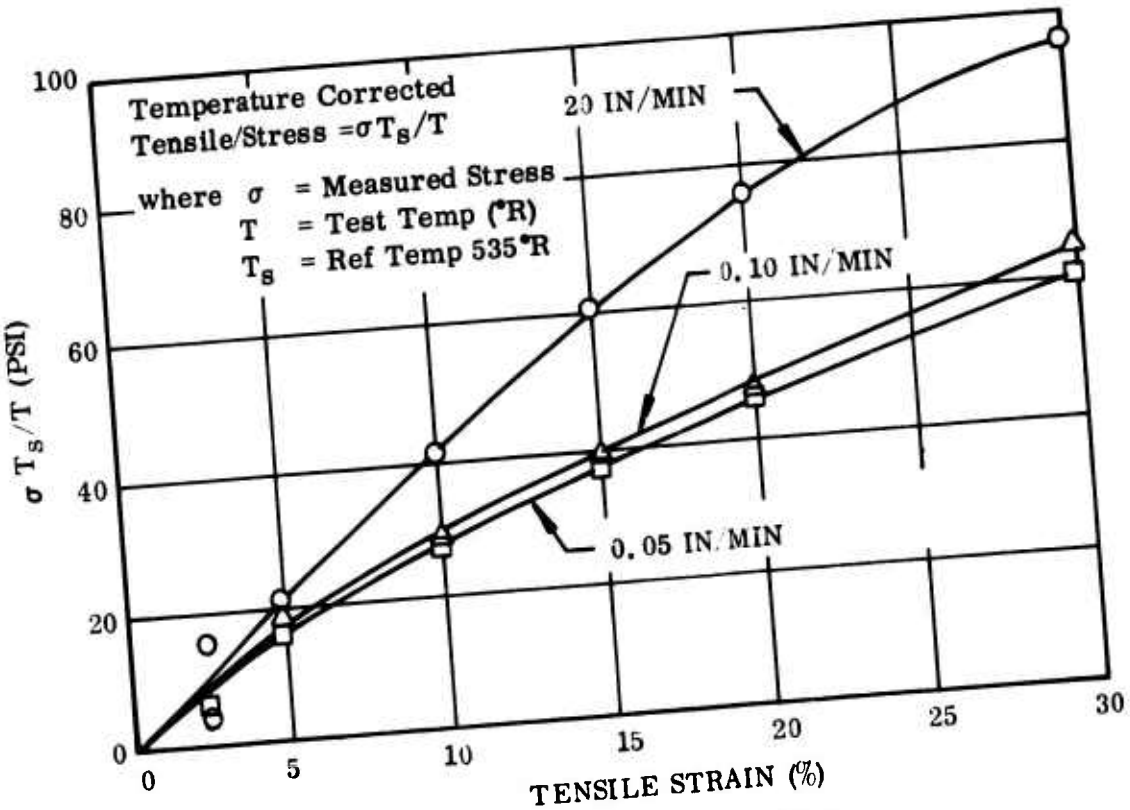

Figure 2-7. Tensile Data, -20°F

2.3.2 Shear Modulus

The response of an elastomeric material in shear has a marked effect on the elastomeric bearing. Shear data are much more difficult to obtain than tensile data because of the geometrical sensitivity. Over the years, a specimen has been developed that yields relatively good engineering data. The specimen is also used for Quality Control. Figure 2-8 shows the geometry of the specimen.

Per TWR-7405, quadruple lap shear specimens were fabricated and tested per the test plan. The processing steps are outlined below.

1. Use two 1 in. x 3 in. steel plates with drilled holes and two steel plates without holes.
2. Solvent clean all surfaces of all four plates.
3. Grit blast, with silica sand, bonding surfaces of each of the four plates.
4. Solvent clean all surfaces of metal plates.
5. Use Chemlok 205; stir thoroughly, and brush a coat on the bonding surfaces of each of the four steel plates. Air dry 15 minutes.
6. Obtain Chemlok 220; stir thoroughly, and brush a coat on the 205 painted surfaces. Air dry for 30 minutes.
7. Obtain elastomer, and cut four pads 1 in. by 1 in. square.
8. Solvent wipe mold and spacers. Allow to dry.
9. Place one steel plate, without hole, in bottom of mold with Chemlok surface UP; insert a spacer, noted on Figure 2-9 as (B), on each side of plate. Place a 1 in. by 1 in. elastomer pad on each end of the exposed Chemlok area. Insert the two steel plates, with holes, into the spacer, identified as (A) on the

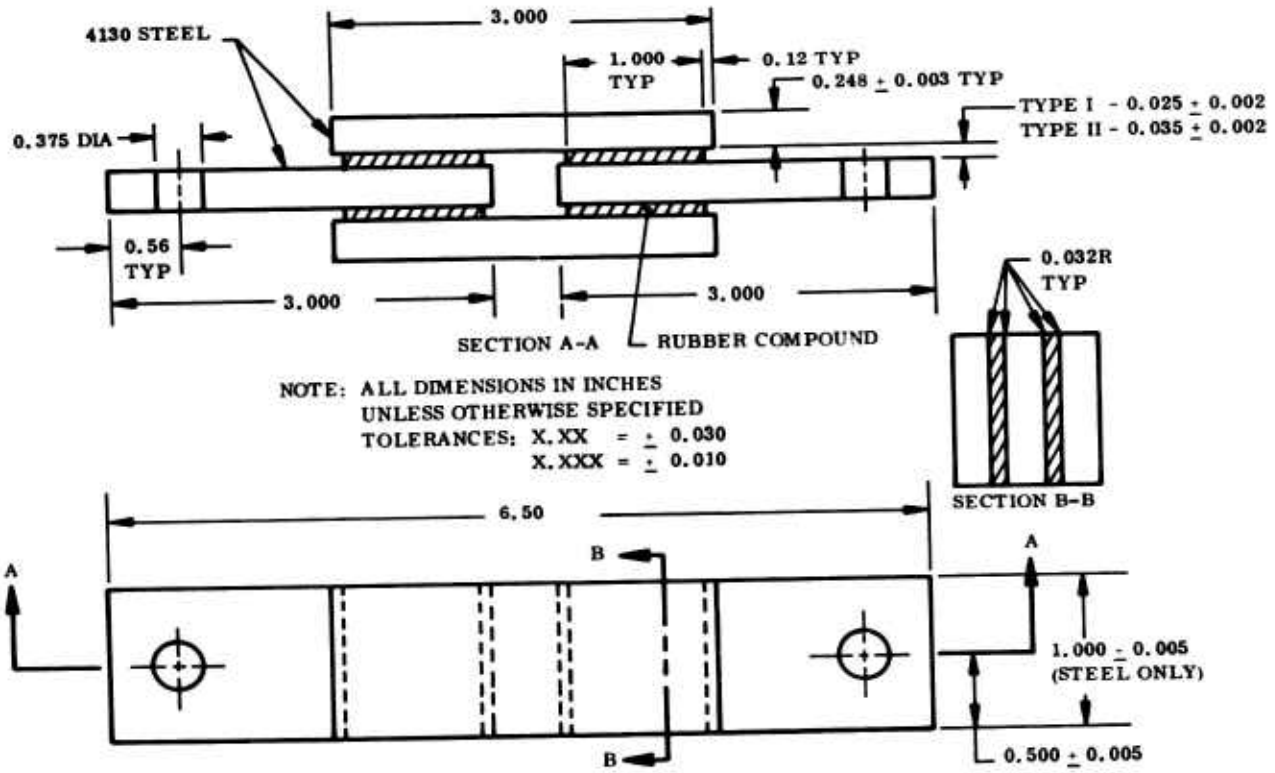

Figure 2-8. Configuration of QLS Specimen

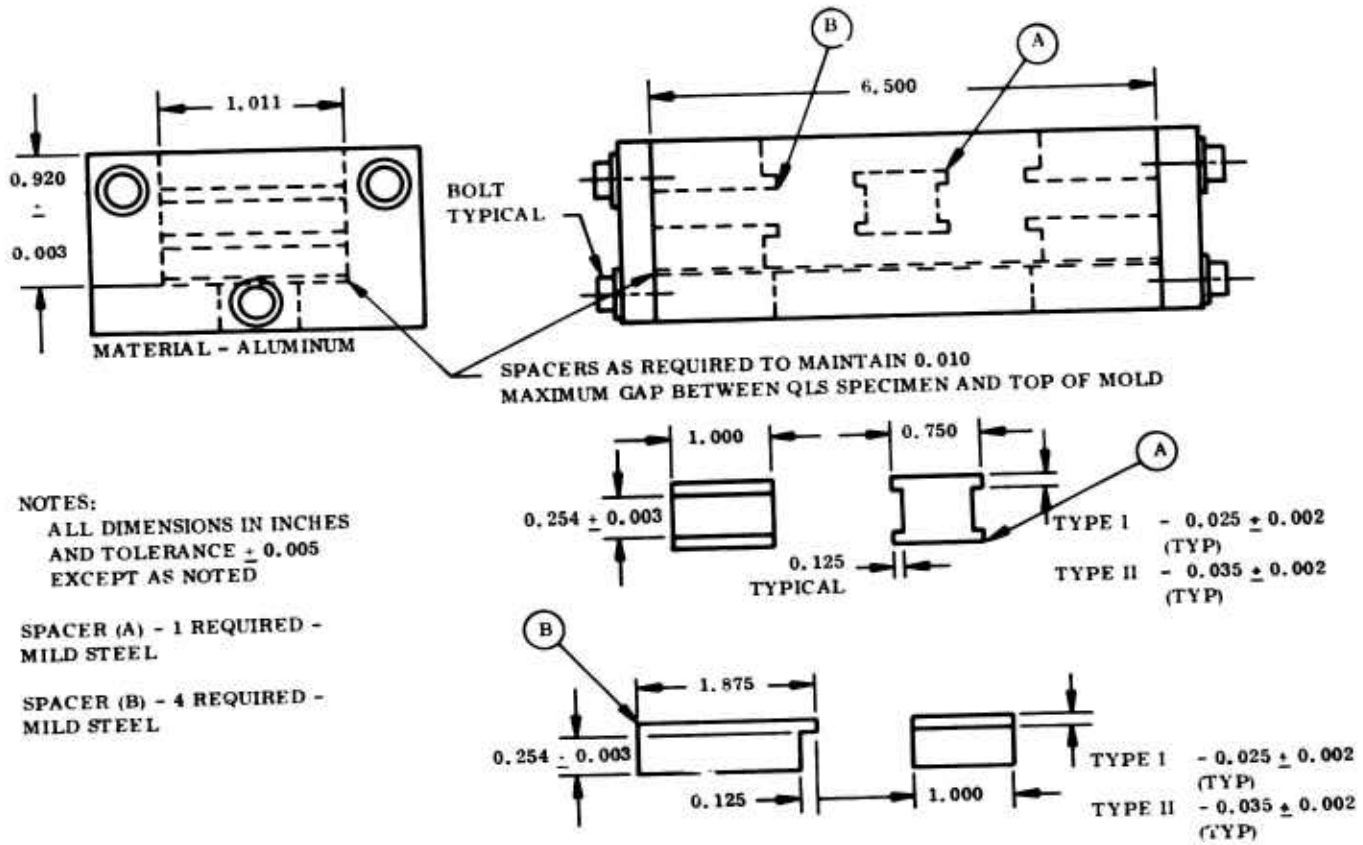

Figure 2-9. Specimen Mold

sketch, with the hole side to the outside. Place this assembly in the mold. Place two spacers, identified as (B), in the mold on outside ends; place a 1 in. by 1 in. elastometer pad on each side of the spacer (B). Place the steel plate, without holes, in the mold between the spacers, with the Chemlok side down.

10. Put mold assembly in preheated press (300°F) and cure for 1 hr.
11. Disassemble by removing specimen from the mold; using a plastic hammer, tap off spacers (B) and push spacer (A) out with an arbor press. Mark specimen with applicable identification.

The quadruple lap shear (QLS) specimen allows the two outside plates to adjust in thickness due to shear loading.

2.3.2.1 Applicable Documents

The following specifications, standards, and other documents apply.

Specifications:

Federal

TT-M-261	Methyl ethyl ketone (for use in organic coatings)

Military

MIL-T-81533	Trichloroethane 1,1,1 (methylchloroform) Inhibited, vapor degreasing

Department of the Navy
Strategic Systems Project Office

XWS 15274 (ref)	Cement, natural rubber base
XWS 15585 (ref)	Primer, adhesive, rubber-to-glass cloth
XWS 15586 (ref)	Adhesive, rubber-to-glass cloth

Standards:

Federal

FED-STD-102	Preservation, packaging, and packing levels
FED-STD-601	Rubber, sampling and testing

Military

MIL-STD-129	Marking for shipment and storage

Other Publications:

ASTM D 2240-68	Indentation hardness of rubber and plastics by means of a durometer

2.3.2.2 Preparation of Specimens

A minimum of eight quadruple lap shear (QLS) specimens were prepared for determination of shear strength and modulus. The specimens were fabricated from 4130 steel heat treated to 180,000 psi minimum tensile strength. The specimens were prepared in accordance with Figures 2-8 and 2-9 and the following process steps.

1. Degrease the steel plates in vapor conforming to MIL-T-81533 for a minimum of 10 minutes and allow them to dry for a minimum of 10 minutes.
2. Grit-blast the steel plates with 100 to 200 mesh zirconium silicate to remove any remaining visible contamination from the mating surfaces.
3. Wipe the steel plates with methyl ethyl ketone (MEK) conforming to TT-M-261 to remove any remaining grit, and allow to dry for a minimum of 15 minutes at 80° $\pm$ 20°F.
4. Arrange the steel plates in groups of four for each specimen, and record the thickness of each set to the nearest 0.001 in. (Figure 2-8).

NOTE: Do not touch the mating surface with fingers. Thoroughly stir the primer and adhesive before using.

5. Using a clean brush, apply a uniform coat of primer conforming to XLS 15585 to the mating surfaces of the steel plates, and allow to dry for a minimum of 15 minutes at 80° ± 20°F.

6. Using a clean brush, apply a uniform coat of adhesive conforming to XWS 15585 to the primed surfaces, and allow to dry for a minimum of 30 minutes at 80° ± 20°F.

7. Using a clean brush, apply a uniform coat of cement conforming to XWS 15274 to the primed and adhesive-coated surfaces, and allow to dry for a minimum of 60 minutes at 80° ± 20°F.

   NOTE: Clean, lint-free cotton gloves shall be worn while completing the remaining operations of specimen preparation.

8. From the uncured rubber sample, cut the required size and number of pieces to fabricate the QLS specimens. The specimens shall be made normally using only one layer of rubber from the uncured rubber roll per pad.

9. Fabricate each specimen in a clean mold in accordance with Figure 2-9; place each mold and test specimen under a press heated to 300° ± 5°F.

10. Exert 25,000 ± 5,000 lb force to seat the specimen in the mold, and maintain this condition for 55 ± 5 minutes. This includes 10 minutes necessary to bring the test specimen to the cure temperature (300°F).

11. Repeat the test specimen preparation to fabricate a minimum of eight QLS specimens.
12. Remove the test specimens from the molds and allow to postcondition cure at 75° ± 5°F and 50 ± 20% relative humidity for a minimum of 16 hr.
13. Measure the thickness of each QLS test specimen through the steel plates and rubber pads, subtract the thickness of the steel plates, and record the difference as the thickness of the rubber pads.

2.3.2.3 Test Procedure

The shear strength and shear modulus tests were performed at 75° ± 5°F, using a tensile testing machine and the following process steps.

1. Install the specimen in the grips of the machine and test at a crosshead speed of 0.5 in. per minute (indicated) and with the automatic chart recorder speed at 5 in. per minute (indicated).
2. Calculate shear strength and shear modulus values using the following formulas:

$$\text{Shear modulus at 50 psi} = \frac{A\ 50}{C_s}$$

where A = thickness of the two rubber pads, inch

C_s = distance crosshead separated at 100 pounds load, inch

50 = shear stress, psi

$$\text{Shear strength, psi} = \frac{L_f}{2(\text{in}^2)}$$

where L_f = chart load at failure, lb

in^2 = total surface area of the pads

3. Report the following valid test results for the samples as follows:

   a. Average shear modulus to the nearest 0.1 psi.

   b. Minimum shear strength to the nearest 0.0 psi.

2.3.2.4 Data

Some typical data using this specimen are shown in Figure 2-10. Notice that the shear properties are very linear up to 100-150%; then the apparent stiffness begins to increase with strain amplitude. Shear strains of about 500% are typical for this formulation. Shear stresses of about 2,000 psi are also noted.

The QLS is particularly useful for helicopter bearings because a second transverse loading can be applied to simulate a compressive stress field simultaneously with the shear loading.

2.3.3 Compression Modulus Testing

Compression modulus tests were conducted with specimens prepared from TR-3012 rubber formulation.

The compression testing was conducted using "sandwich" specimens comprising two metal plates with a rubber sample bonded between. Both metal plates (top and bottom) and intermediate rubber layer were prepared in round disc configuration. All metal plates measured a nominal 0.25 in. thickness by 3.0 in. diameter, and rubber sample thickness was 0.10 or 0.38 in. Figure 2-11 shows the configurations.

Compression testing was accomplished using a floor model Instron tester equipped with a model CF 10,000-lb-capacity compression load cell. Axial compressive loading was applied normal to the surface of the metal plates at a rate of 0.1 in. per minute. The load was applied at this rate with intermittent stops made at designated strain (deflection) levels for photographs and measurements of compressed rubber sample diameter.

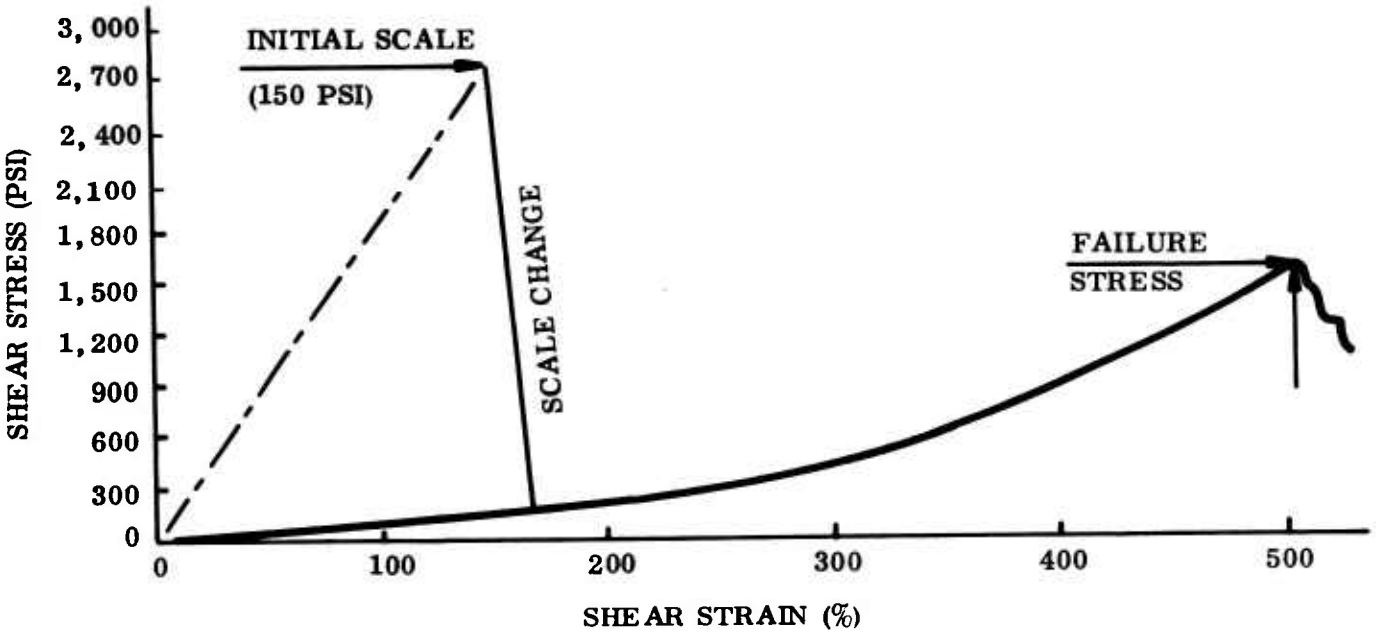

Figure 2-10. Typical QLS Data
(TR-3012 Elastomer, Room Temp, 0.5 in/min)

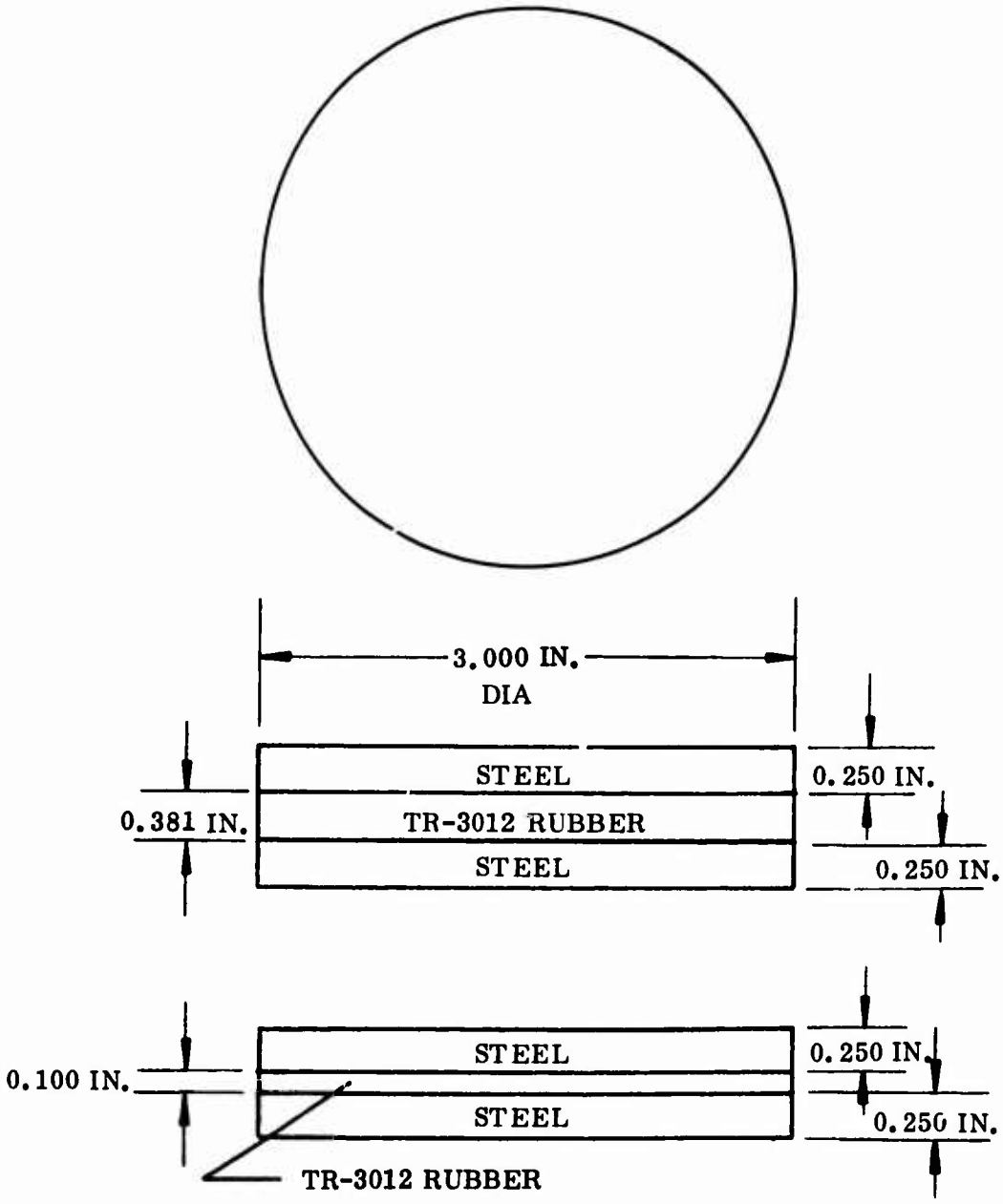

Figure 2-11. Compressive Specimens

Photographs were taken at various deflection levels using a Beattie-Coleman sequence camera at an F-32 shutter stop setting. Diameter measurements were made with a Brown and Sharpe precision vernier caliper, and samples tested at other than ambient temperature were conditioned in either (1) a Precision Scientific forced air recirculating oven (160°F) or (2) a Missimers environmental conditioning chamber (-40°F).

Compression test load limitations were encountered due to load cell capacity. Maximum available capacity of 10,000 lb did not allow compression deflection levels greater than 52.5% on the thicker (0.38 in.) samples, and these tests were terminated upon achieving the 10,000-lb load limit. Deflection was measured at this point, and these measurements were used to compile the load-deflection values for this maximum compression level.

Compression load levels represented by 10, 15, 30, 40 and maximum (44-52.5) percentage of deflections, accompanied by photographs and rubber diameter measurements, are reported for specimens tested at ambient conditions (75°F). Samples tested at temperatures other than ambient required thermal conditioning plates whose position disallowed measurements of the deflected rubber layer diameter, and the need to maintain constant specimen temperature further necessitated a rapid and nearly continuous load application with no intermittent stops for diameter measurements. Tables 2-3 and 2-4 display these data.

Some typical photographs at 160°F are shown for 0, 10, 15, 30 and 48.6% strains in Figures 2-12 through 2-16.

Figure 2-17 shows the load deflection patterns for 0.100-in.-thick specimens at 75°F. Figure 2-18 shows the effective modulus for the same 0.100-in.-thick specimens at 75°F. Figure 2-19 shows some typical measured radial displacements. The load deflection curves for the 0.381-in.-thick specimens at -40°, 75°, and 160°F are shown in Figure 2-20. The effective modulus data for these same specimens are shown in Figure 2-21 using the same temperatures.

TABLE 2-3

COMPRESSION SPECIMEN TEST DATA
(Tested at 75° F, 160° F and -40° F and 0.1 In/Min Loading Rate)

Sample Number	Sample Thickness (in.)	Sample Deflection (in.)	Load at 10% Def (lb)	Def (in.)	Load at 15% Def (lb)	Def (in.)	Load at 30% Def (lb)	Def (in.)	Load at 50% Def (lb)	Max Def (in.)	Max Def (%)	Max Load (lb)	Test Temp (°F)	Load Rate (in/min)
1-1	0.100	0.01	575	0.015	1,760	0.03	4,670	0.05	9,150				75	0.1
1-2	0.100	0.01	1,020	0.015	1,900	0.03	5,140	0.05	9,700				75	0.1
Orig Diam	3.000		3,006		3,014		3,026		3,057					
2-1	0.100	0.01	775	0.015	1,540	0.03	4,320	0.05	8,980				75	0.1
2-2	0.100	0.01	740	0.015	1,580	0.03	4,550	0.05	9,000				75	0.1
Orig Diam	3.000		3,007		3,015		3,031		3,059					
3-1	0.100	0.01	1,070	0.015	2,040	0.03	5,470	0.05	9,800				75	0.1
3-2	0.100	0.01	1,175	0.015	2,200	0.03	5,330	0.05	9,900				75	0.1
Orig Diam	3.000		3,008		3,018		3,027		3,054					
									Load at 40% Def (lb)					
4-1	0.381	0.038	1,285	0.057	2,170	0.114	5,550	0.152	8,760	0.165	43	10,000	75	0.1
4-2	0.381	0.038	1,170	0.057	1,970	0.114	4,820	0.152	8,170	0.168	44	10,000	75	0.1
Orig Diam	2.990		3,112		3,192		3,377		3,462					
5-1	0.381	0.038	1,370	0.057	2,150	0.114	5,370	0.152	8,810	0.166	44	10,000	75	0.1
5-2			1,300		2,200		5,020		8,850	0.168	44	10,000	75	0.1
Orig Diam	2.987		3,134		3,209		3,353		3,475			3,504		
6-1	0.381	0.038	1,290	0.057	1,910	0.114	5,320	0.152	8,880	0.164	43	10,000	75	0.1
6-2			1,200		2,010		4,960		8,150	0.169	44	10,000	75	0.1
Orig Diam	2.987		3,108		3,185		3,351		3,466			3,488		
7-1	0.381	0.038	1,280	0.057	2,100	0.114	5,240	0.152	8,790	0.164	43	10,000	75	0.1
7-2			1,220		2,010		4,970		8,360	0.168	44	10,000	75	0.1
Orig Diam	2.990		3,130		3,200		3,351		3,530			--		
8-1	0.381	0.038	1,275	0.057	2,090	0.114	5,100	0.152	8,510	0.166	44	10,000	75	0.1
8-2			1,270		2,000		4,820		8,070	0.169	44	10,000	75	0.1
Orig Diam	2.987		3,120		3,213		3,370		3,480			3,510		
9-1	0.381	0.038	1,340	0.057	2,160	0.114	5,410	0.152	8,800	0.164	43	10,000	75	0.1
9-2			1,300		2,020		5,030		8,400	0.167	44	10,000	75	0.1
Orig Diam	2.987		3,135		3,211		3,392		3,475			3,497		
10-1	0.381	0.038	1,120	0.057	1,892	0.114	4,600	0.152	7,300	1.85	48.6	10,000	160	0.1
11-1	0.381	0.038	1,250	0.057	1,150	0.114	4,840	0.152	7,900	1.80	47.2	10,000	150	0.1
12-1	0.381	0.038	1,200	0.057	1,900	0.114	4,600	0.152	7,450	1.84	48.3	10,000	160	0.1
13-1	0.381	0.038	700	0.057	1,100	0.114	3,400	0.152	6,000	1.92	50.4	10,000	-40	0.1
14-1	0.381	0.038	550	0.057	987	0.114	3,100	0.152	5,635	2.00	52.5	10,000	-40	0.1
14-2	0.381	0.038	750	0.057	1,140	0.114	3,300	0.152	5,900	1.93	50.7	10,000	-40	0.1

*Increased specimen thickness results in greater load/deflection values and necessitates use of 40% deflection/maximum load measurement level.

TABLE 2-4

COMPRESSION MODULUS TEST DATA

Sample Number (Average)	Thick. (in.)	Diam (in.)	Temp (°F)	Crosshead (in/min)	10% Deflection				15% Deflection				30% Deflection			
					Load (lb)	σ (psi)	E_c (psi)	Diam (in.)	Load (lb)	σ (psi)	E_c (psi)	Diam (in.)	Load (lb)	σ (psi)	E_c (psi)	Diam (in.)
1	0.100	3.000	75	0.1	800	85	850	3.006	1,830	194	1,290	3.014	4,910	521	1,740	3.026
2	0.100	3.000	75	0.1	760	81	810	3.007	1,560	166	1,110	3.015	4,440	471	1,570	3.031
3	0.100	3.000	75	0.1	1,120	119	1,190	3.008	2,120	225	1,500	3.018	5,400	573	1,910	3.027
4	0.381	2.990	75	0.1	1,230	131	1,310	3.112	2,070	220	1,470	3.192	5,190	551	1,840	3.377
5	0.381	2.987	75	0.1	1,340	142	1,420	3.134	2,180	231	1,540	3.209	5,200	552	1,840	3.353
6	0.381	2.987	75	0.1	1,250	133	1,330	3.108	1,960	208	1,390	3.185	5,140	545	1,820	3.351
7	0.381	2.990	75	0.1	1,250	133	1,330	3.130	2,060	219	1,460	3.200	5,110	542	1,810	3.351
8	0.381	2.987	75	0.1	1,270	135	1,350	3.120	2,050	218	1,450	3.213	4,960	526	1,750	3.370
9	0.381	2.987	75	0.1	1,370	145	1,450	3.135	2,090	222	1,480	3.211	5,220	554	1,850	3.392
10	0.381		160	0.1	1,120	119	1,190		1,892	201	1,340		4,600	488	1,630	
11	0.381		160	0.1	1,250	133	1,330		2,150	228	1,520		4,840	514	1,710	
12	0.381		160	0.1	1,200	127	1,270		1,900	202	1,350		4,600	488	1,630	
13	0.381		-40	0.1	700	74	740		1,100	117	780		3,400	361	1,200	
14-1	0.381		-40	0.1	550	58	580		990	105	700		3,100	330	1,100	
14-2	0.381		-40	0.1	750	80	800		1,140	121	810		3,300	350	1,170	

$E_c = \frac{\sigma}{\epsilon}$ (Deflection) = Compression Modulus

TABLE 2-4 (Cont)

COMPRESSION MODULUS TEST DATA

Sample Number (Average)	40% Deflection				50% Deflection				Maximum Deflection				
	Load (lb)	σ (psi)	E_c (psi)	Diam (in.)	Load (lb)	σ (psi)	E_c (psi)	Diam (in.)	Def (%)	Load (lb)	σ (psi)	E_c (psi)	Diam (in.)
1					9,450	1,003	2,010	3.057					
2					8,990	954	1,910	3.059					
3					9,850	1,045	2,090	3.054					
4	8,470	899	2,250	3.462					44	10 K	1,060	2,410	--
5	8,830	937	2,340	3.475					44	10 K	1,060	2,410	3.504
6	8,520	904	2,260	3.466					44	10 K	1,060	2,410	3.488
7	8,580	910	2,280	3.530					44	10 K	1,060	2,410	--
8	8,290	880	2,200	3.480					44	10 K	1,060	2,410	3.510
9	8,600	912	2,280	3.475					44	10 K	1,060	2,410	3.497
10	7,300	775	1,940						48.6	10 K	1,060	2,180	
11	7,900	838	2,100						47.2	10 K	1,060	2,250	
12	7,450	790	1,980						48.3	10 K	1,060	2,190	
13	6,000	637	1,590						50.4	10 K	1,060	2,100	
14-1	5,640	598	1,500						52.5	10 K	1,060	2,020	
14-2	5,900	626	1,570						50.7	10 K	1,060	2,090	

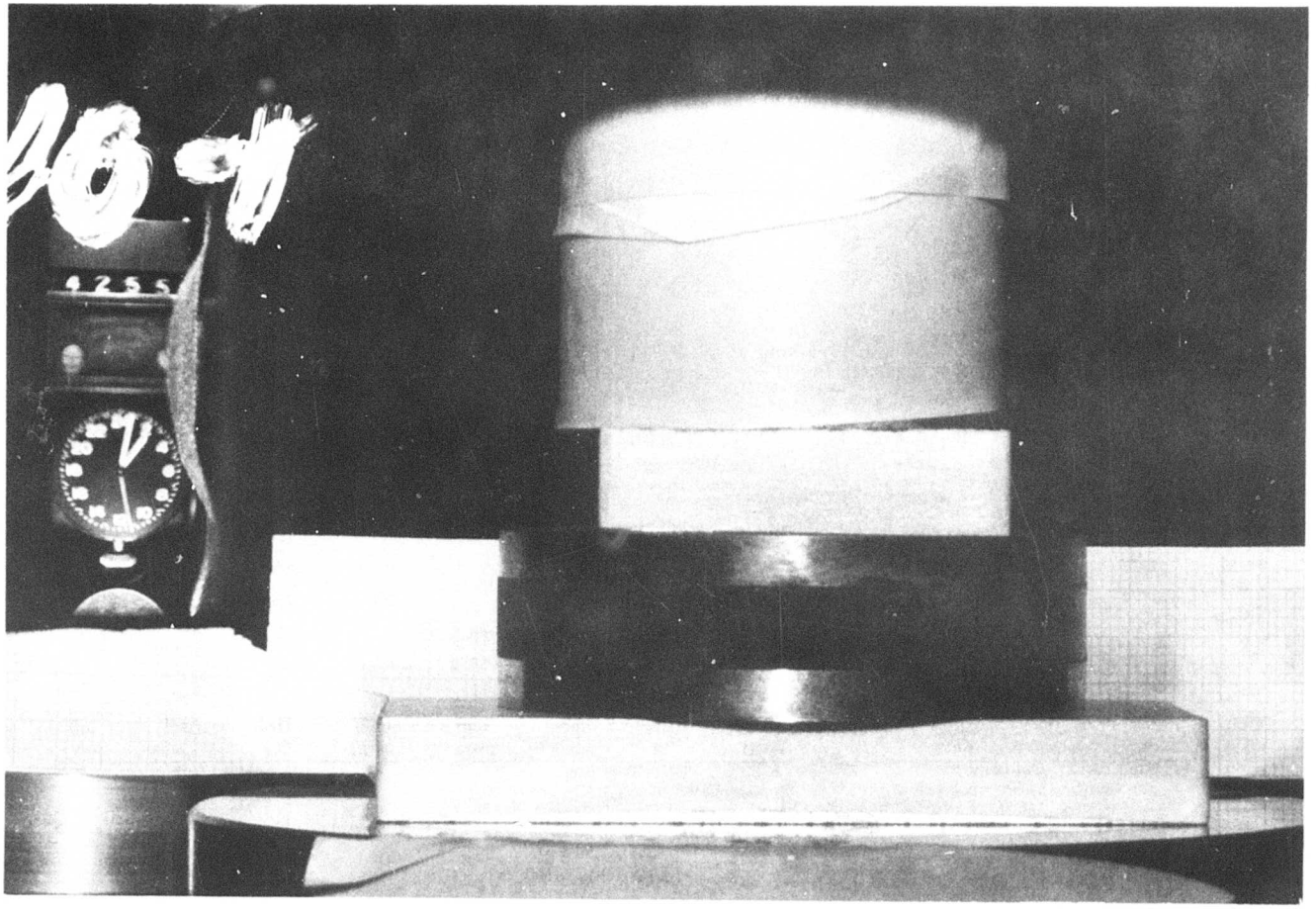

Figure 2-12. Typical Compressive Testing at 160°F, Specimen 10-1, 0% Deflection

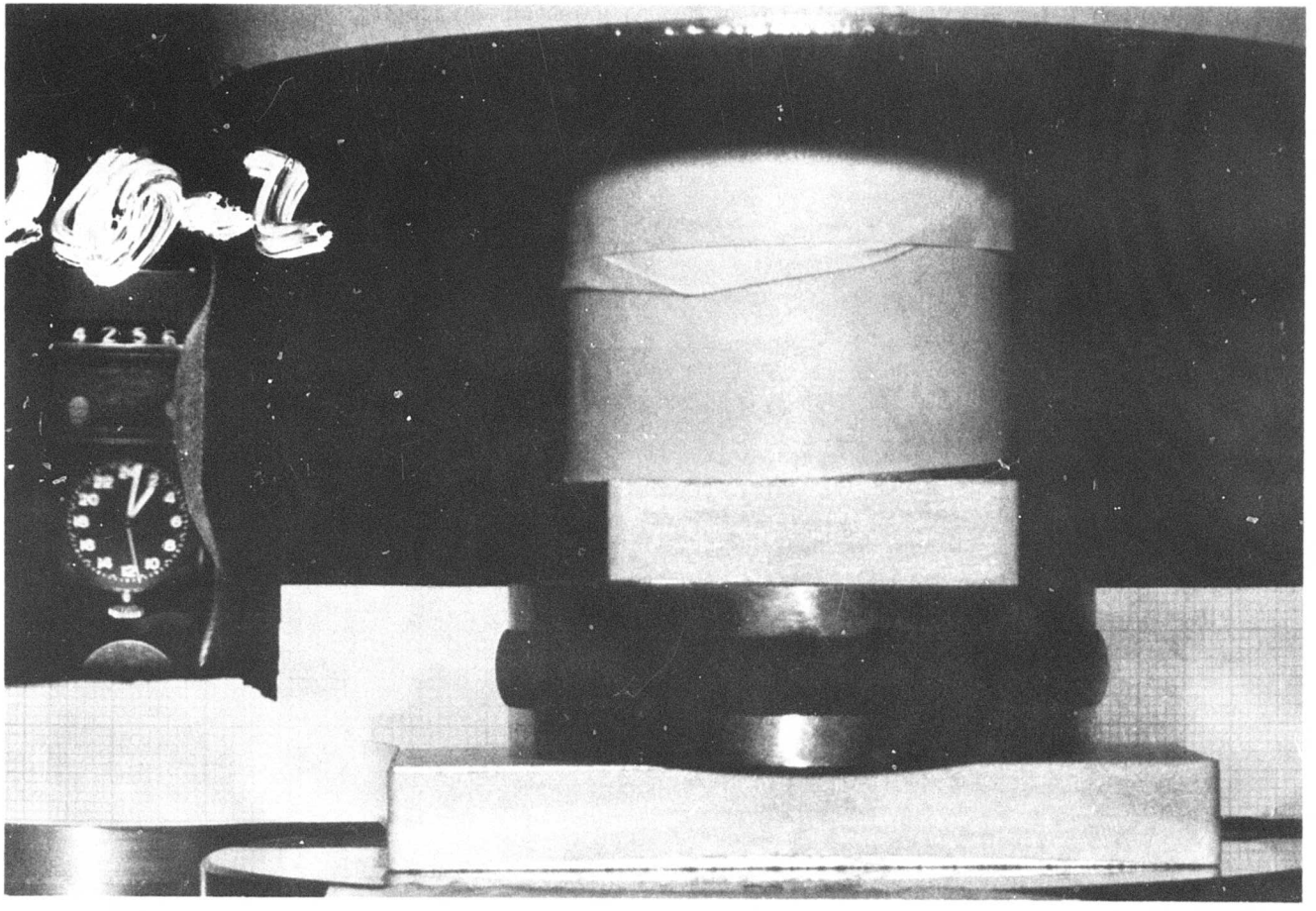

Figure 2-13. Typical Compressive Testing at 160°F, Specimen 10-1, 10% Deflection

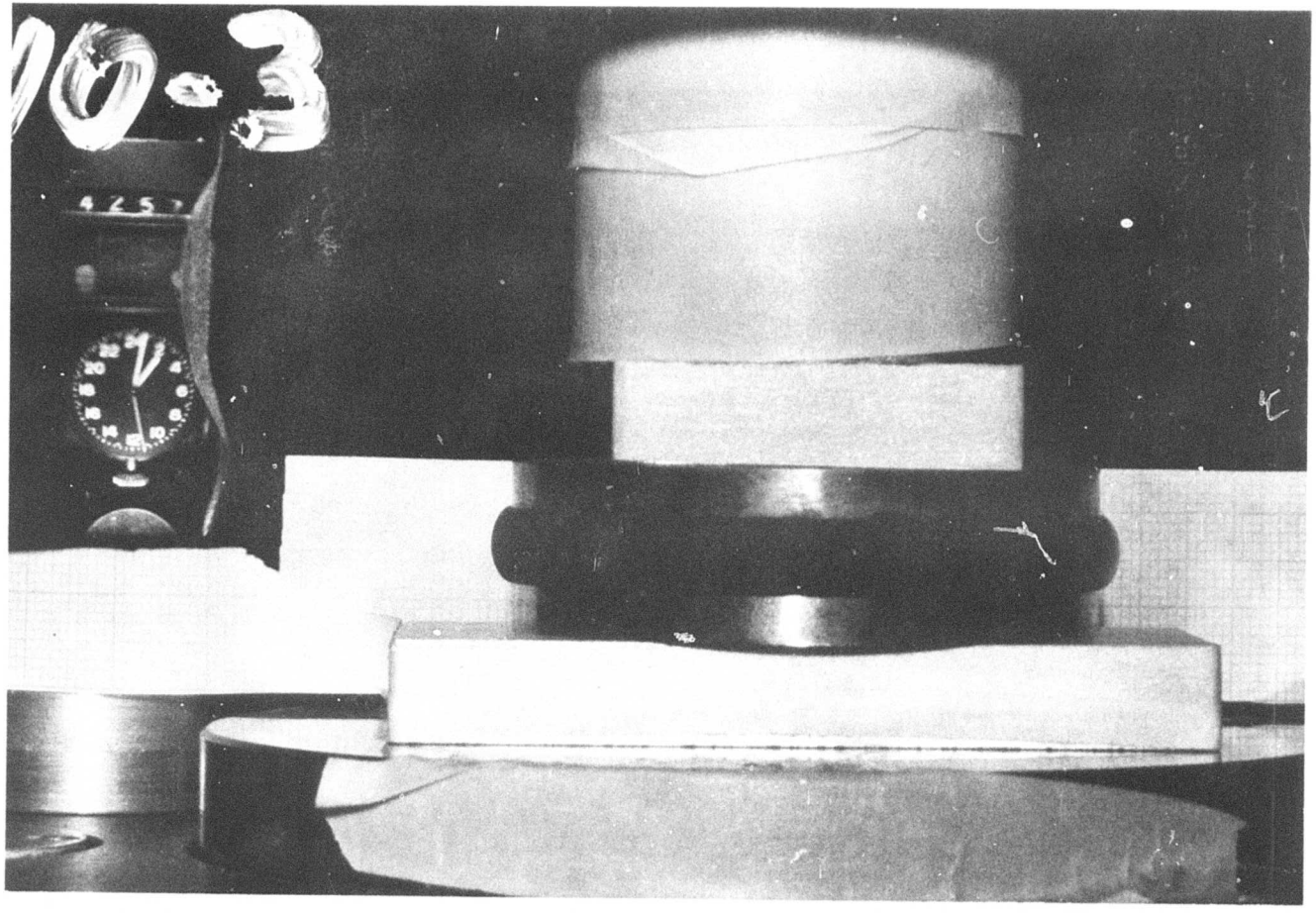

Figure 2-14. Typical Compressive Testing at 160°F, Specimen 10-1, 15% Deflection

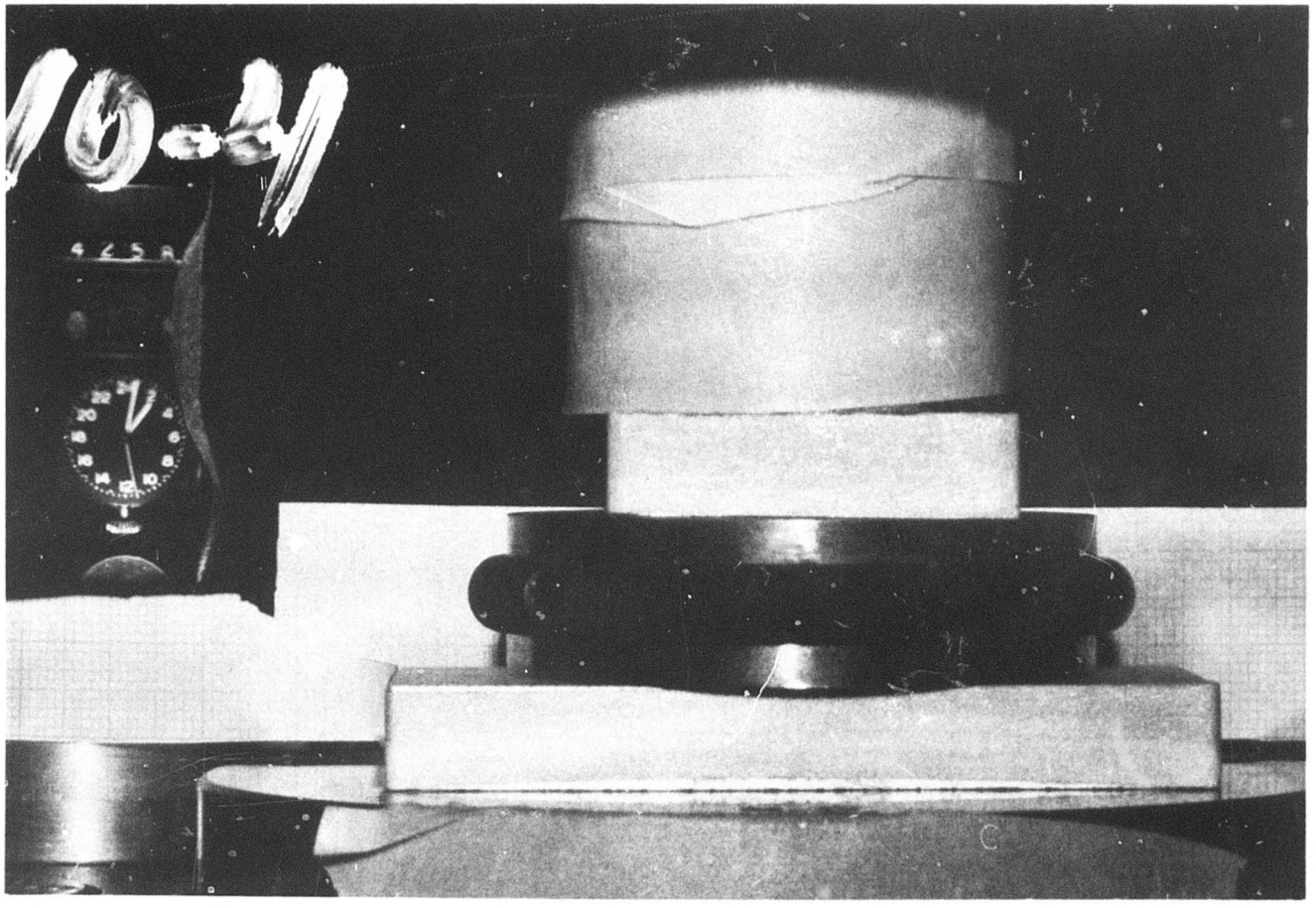

Figure 2-15. Typical Compressive Testing at 160°F, Specimen 10-1, 30% Deflection

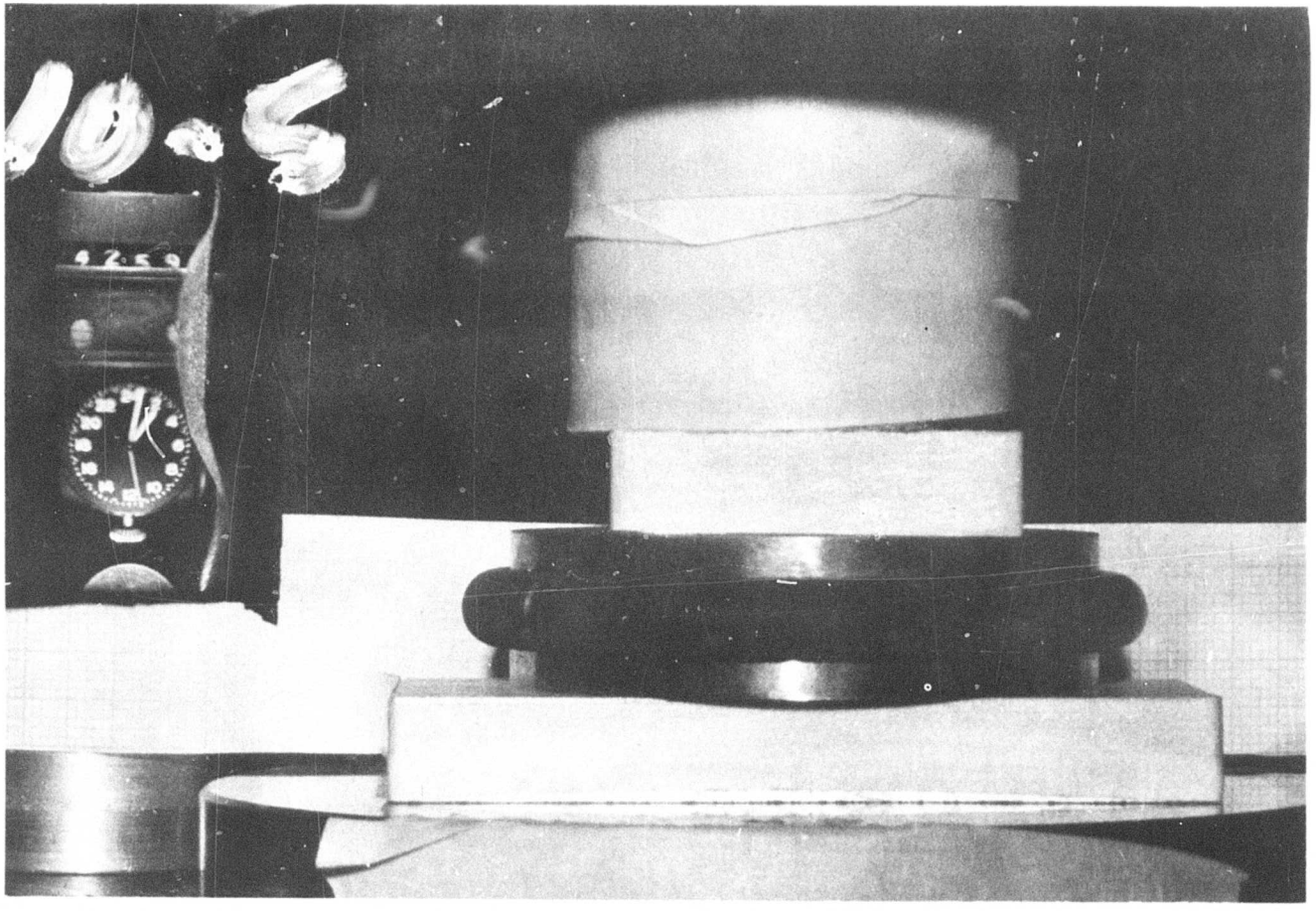

Figure 2-16. Typical Compressive Testing at 160°F, Specimen 10-1, 48.6% Deflection

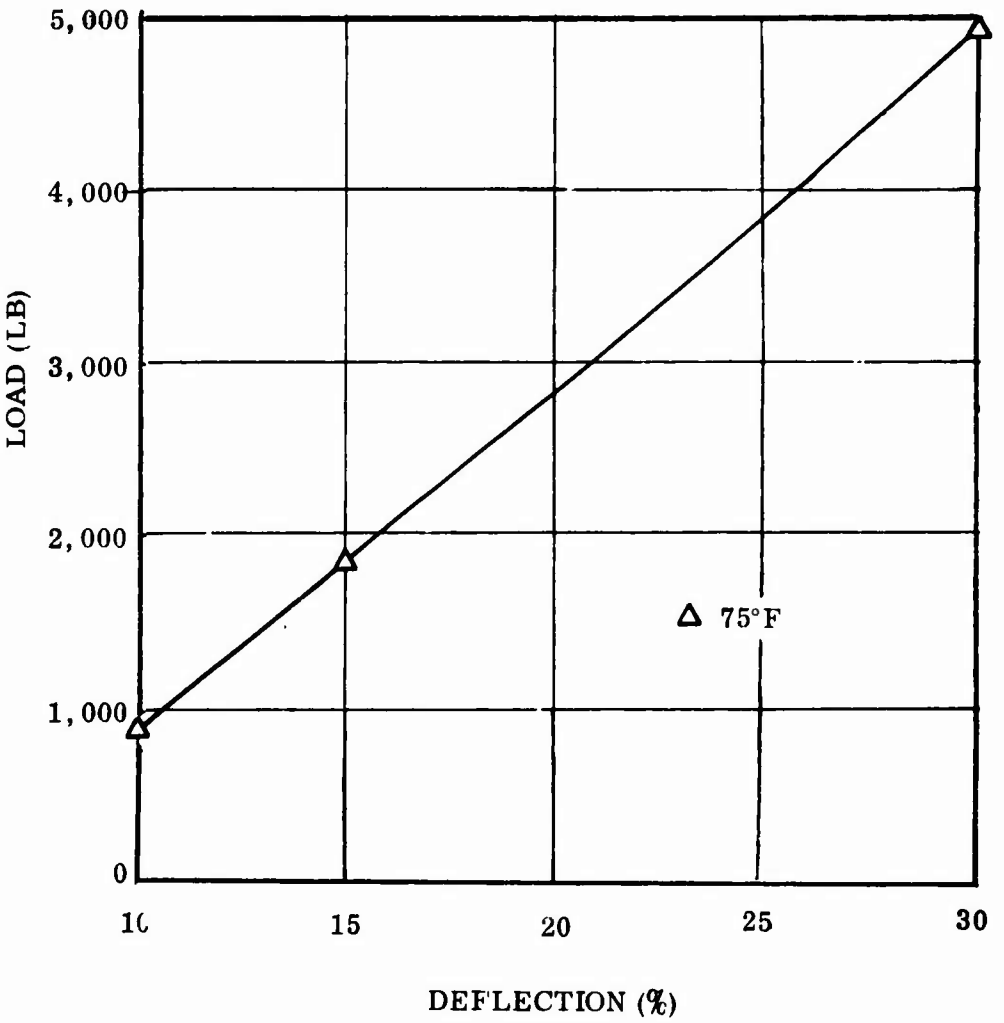

Figure 2-17. Typical Compressive Load vs Percentage of Strain (0.0100 In. Specimen)

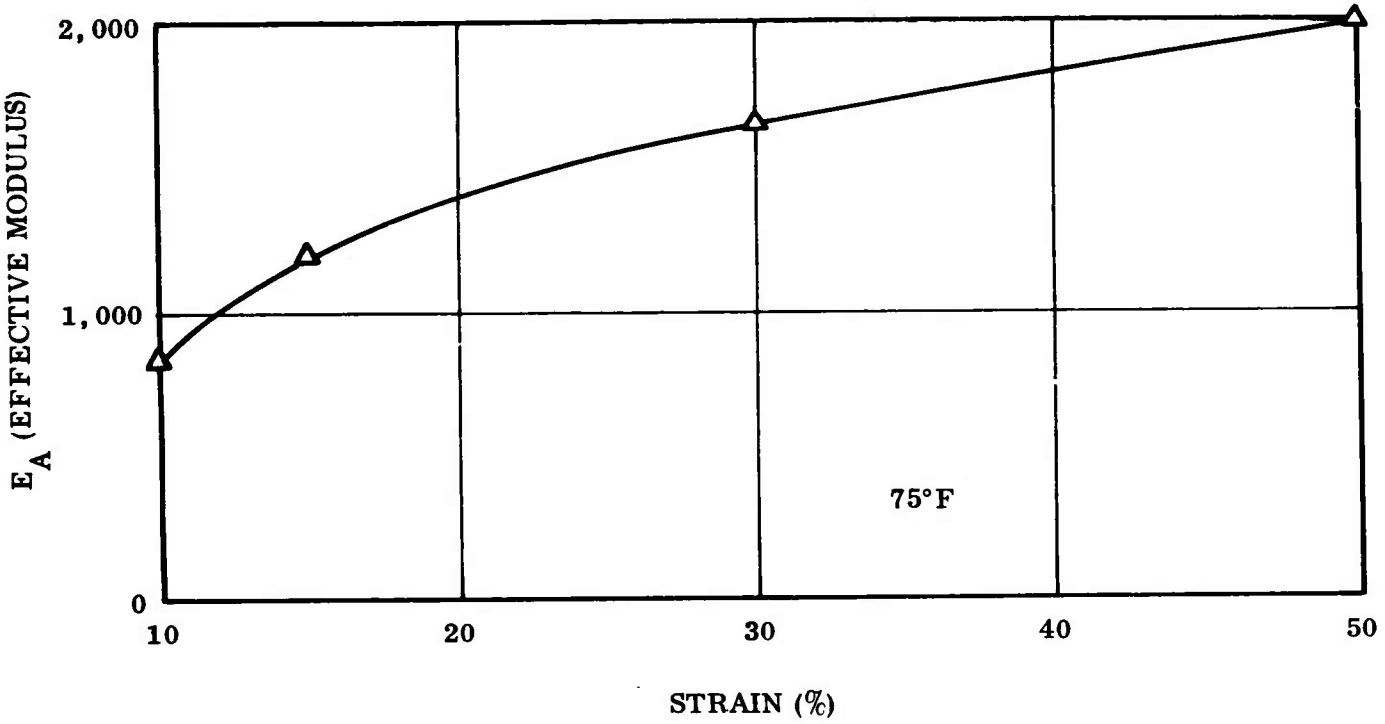

Figure 2-18. Typical Effective Modulus vs Percentage of Strain (0.0100 In. Specimen)

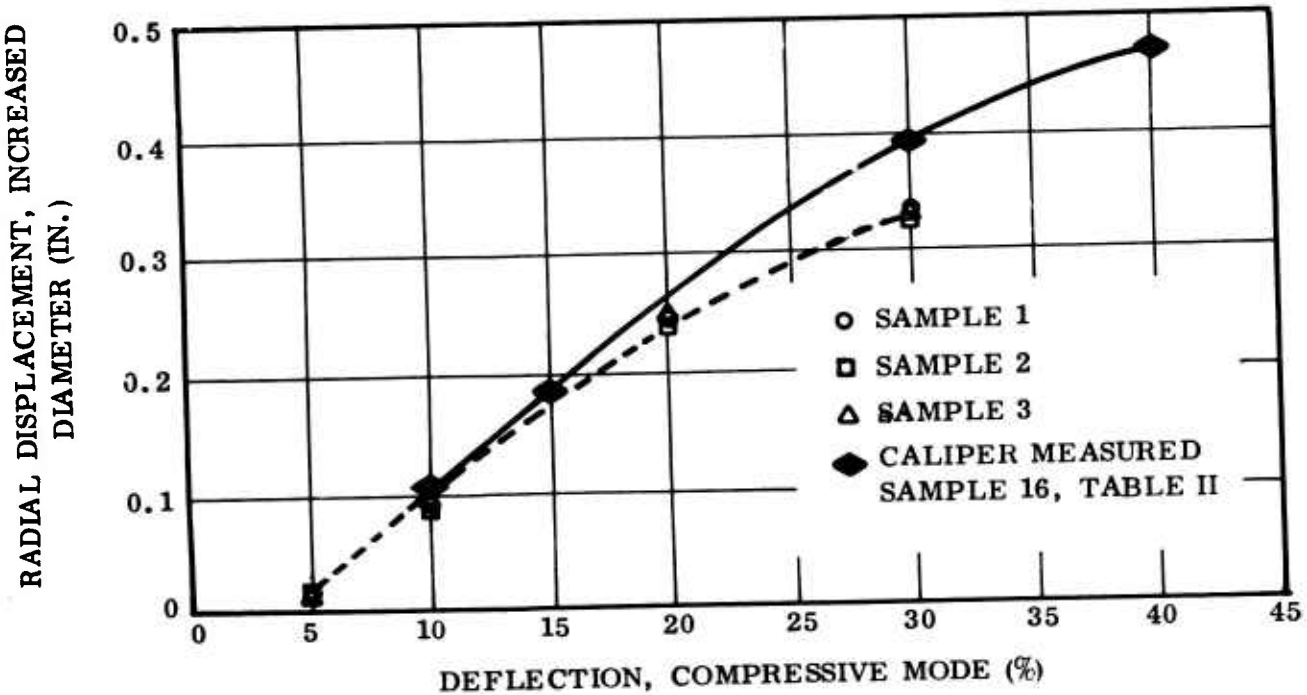

Figure 2-19. Typical Radial Displacements

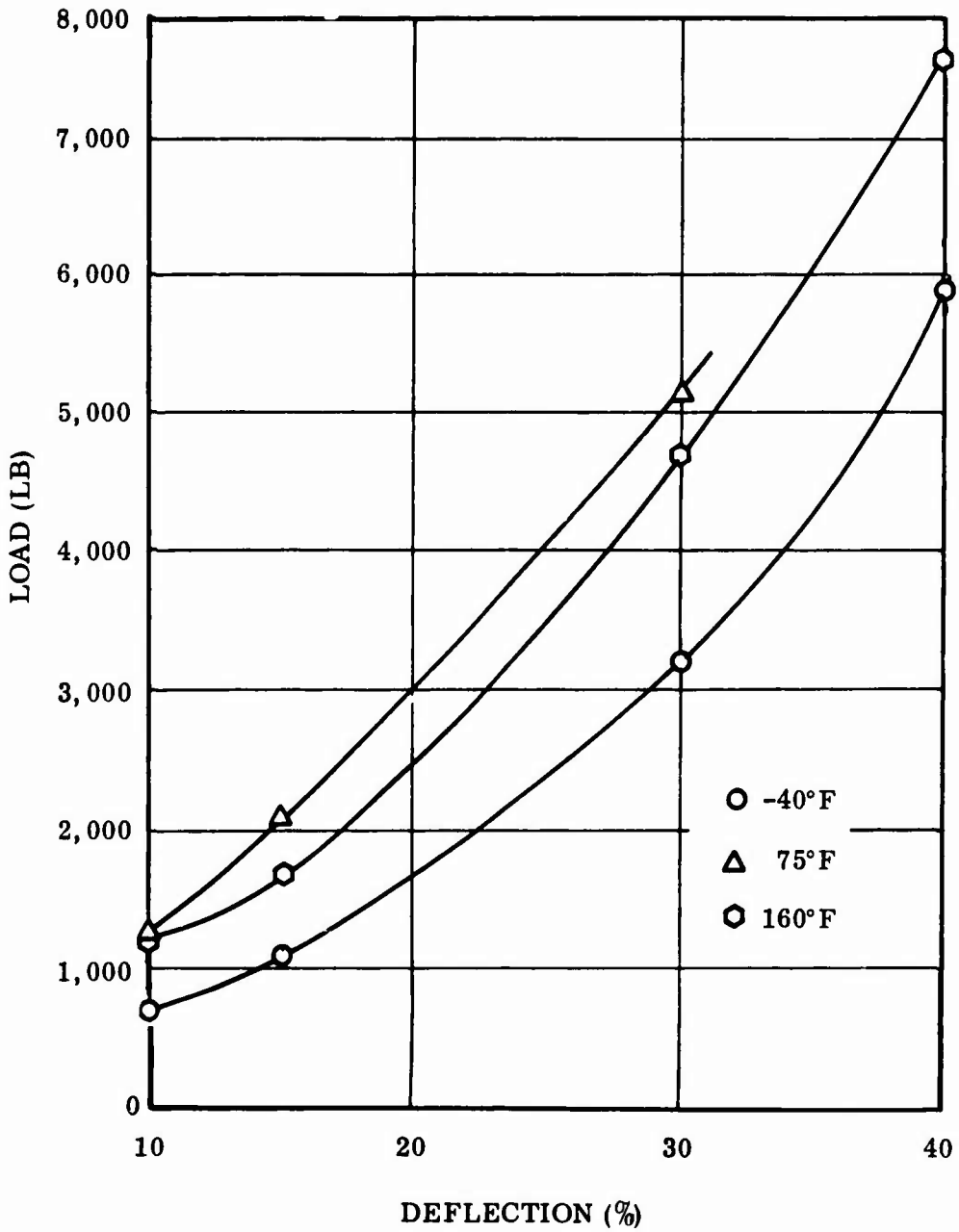

Figure 2-20. Typical Compressive Load vs Percentage of Strain (0.381 In. Specimen)

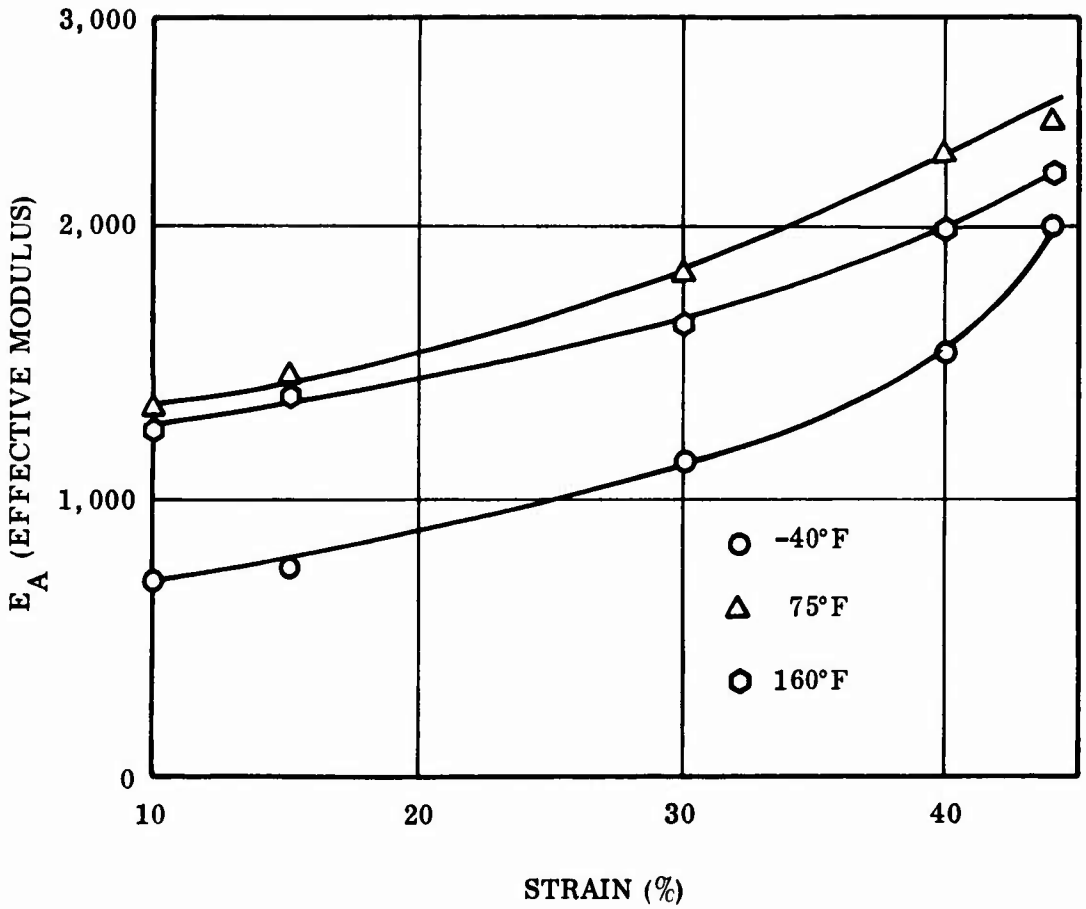

Figure 2-21. Typical Effective Modulus vs Percentage of Strain (0.381 In. Specimen)

3.0 PHYSICAL PROPERTY DEVELOPMENT

3.1 RELAXATION MODULUS AND DYNAMIC MODULUS

Relaxation modulus data were obtained at -20°, 77° and 120° F for applied strains of 5, 10, and 30% with the TR-3012 rubber formulation. The use of relaxation modulus data in bearing stress analysis is discussed in Volume II.

We have suggested the use of a Williams, Landel, Ferry (WLF) equation for time-temperature superposition, and a temperature shift factor of T_s/T. In the process of evaluating mechanical properties of natural rubber for bearing pads, several characteristics were noted which affect testing techniques and the use of the rubber. These characteristics are: (1) a stress softening as repeated loads are applied (Mullins' effect) and (2) an increase in relaxation modulus when rubber is maintained at a relatively low temperature for an extended period of time.

At all strain levels (even as low as 1% prior to exhibiting measurable dilatation), most filled rubber vulcanites exhibit a stress softening and hysteresis phenomenon. This phenomenon is normally associated with microstructural failure prior to the formulation of vacuoles and is termed the Mullins' effect. Approximately five cycles are required before a constant stress-strain behavior is noted. This number would be smaller if the specimens were strained to a higher level on the first cycle. Figure 3-1 shows this scragging phenomenon.

Prestrains on test specimens should, therefore, be carefully avoided if material properties are desired for first cycle loads (such as thermally induced loads applied after rubber cure). On the other hand, test specimens should be preloaded (scragged) to a level greater than the test level for a number of cycles before testing for mechanical properties used in predicting stresses due to cyclic loads.

When maintained at low temperatures, many rubber formulations crystallize. The rate of crystallization is greatest in the -15° to -40°F range and may take from 24 hr to several weeks to reach the 50% crystallized level. This crystallization can

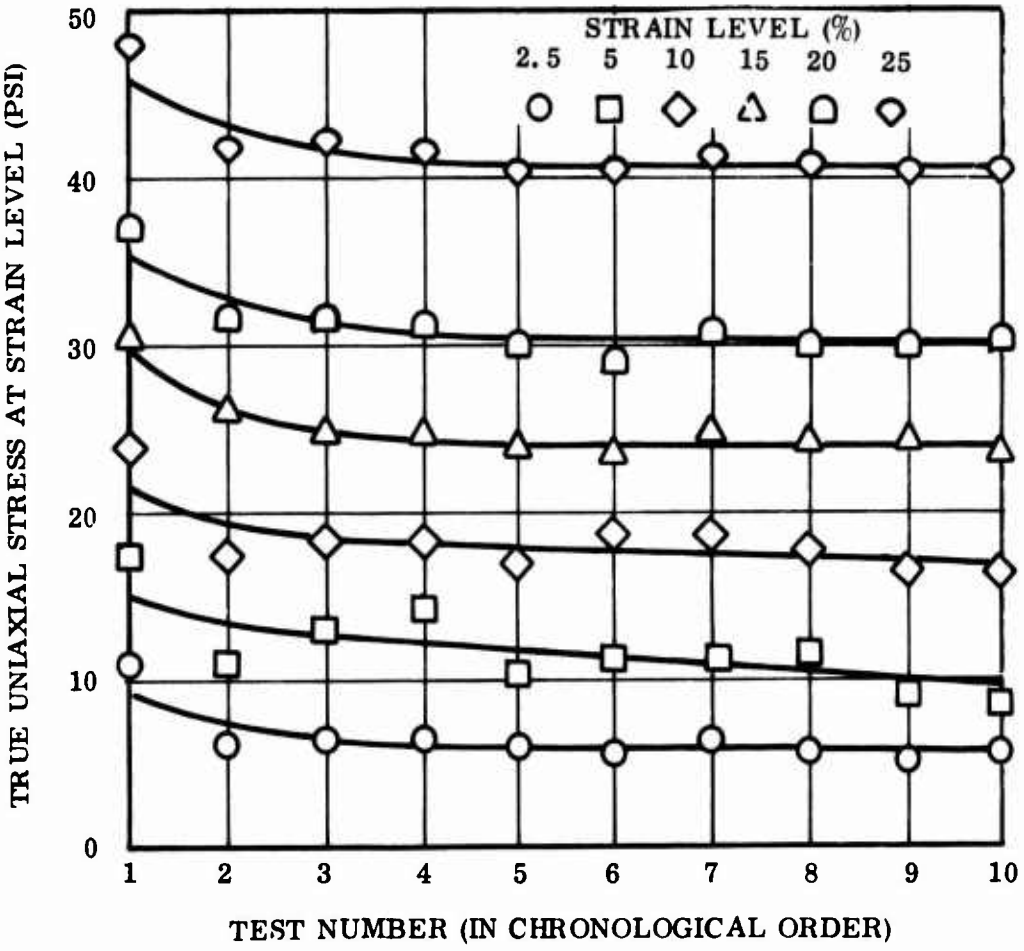

Figure 3-1. Flexible Bearing Uniaxial Tensile Tests

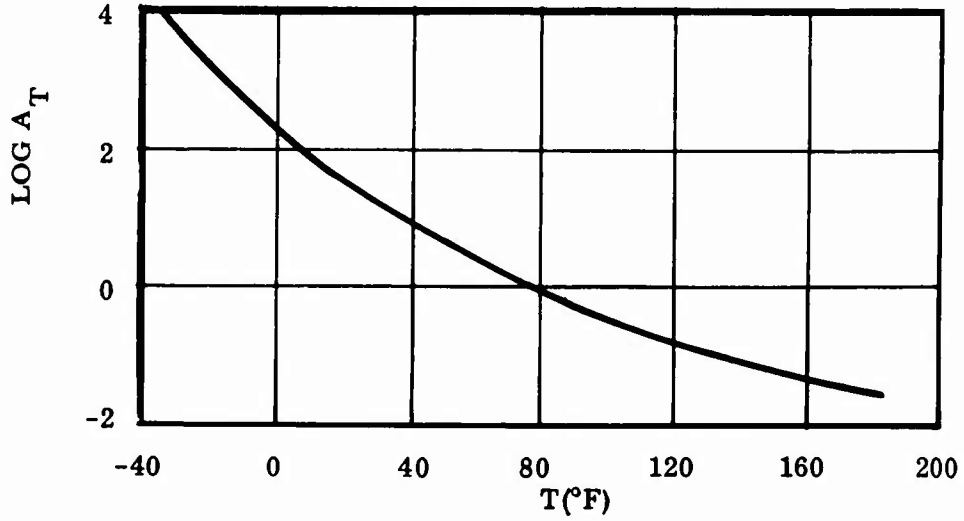

Figure 3-2. WLF Shift Factor

occur at higher or lower temperature levels but at a reduced rate. Crystallization disappears rapidly as the temperature is increased. After crystallization, the modulus may be orders of magnitude greater than in the noncrystallized state.

The WLF shift equation normally provides a smooth master relaxation curve. However, as noted above, crystallization occurs at temperatures below 0°F, which changes the rubber modulus. For temperatures below 0° F, the WLF equation cannot always be applied. A best curve fit using rubber exposed to environmental temperature-time combinations of interest is suggested. The shifted curves are termed master curves.

A curve of the WLF shift factor is given in Figure 3-2. It is noted that the WLF shift factor is normally given in °C; however, conversion to ° F is given by

$$\log A_T = \frac{797.4 - 8.86\,(T - Tg)}{93.24 + T - Tg}$$

where Tg is the glass transition temperature in ° F.

The temperature correction factor T_s/T is essentially a vertical shift of the data and is introduced to compensate for the equilibrium (long time) modulus' being directly proportional to absolute temperature. This factor was first introduced from theoretical studies by Treloar and is now widely used. As shown in Volume II, this factor is essential in rubber characterization. The cross-sectional area change is

$$E_R^c = \frac{\sigma_{true}}{\epsilon_o} = \frac{P(1 + \epsilon_o)}{A_o \epsilon_o}$$

where P = applied load

A_o = initial cross-sectional area

By this correction we have attempted to correct the relaxation modulus for large deformations. However, when analyses using small deformation theory are being conducted on bearings, the correction should be dropped.

In solid propellants, the relaxation modulus obtained from uniaxial tensile tests normally increases (up to 100%) with applied hydrostatic pressure. This has

been attributed to the prevention of void formation. Relaxation modulus tests of TR-3012 rubber were therefore conducted at ambient and 1,000 psi superimposed pressures (see Figure 3-3 and Table 3-1). A decrease of approximately 9% is noted. We feel that this drop is not physically realistic and attribute the error to data scatter possibly caused by inconsistent scragging procedures. We, therefore, feel that hydrostatic stresses up to 1,000 psi will have negligible effect on rubber relaxation modulus.

All of the relaxation modulus testing completed during this program used uniaxial tensile samples. It has been shown that rubber behavior in uniaxial tension is nonlinear and of the form

$$\sigma = G(\lambda - \lambda^{-2}) = E(\epsilon - \epsilon^2 + \frac{4}{3}\epsilon^3 + \ldots)$$

where $\lambda = 1 + \epsilon$ is the extension ratio. Therefore, in a linear characterization the modulus must change with strain, i.e.,

$$\frac{\sigma}{\epsilon} = E(\epsilon)$$

To examine this dependence, relaxation modulus values were tested at strains of 5, 10, and 30% as shown in Figure 3-4 and Tables 3-1 through 3-3. When low-temperature crystallization problems are neglected, a consistent trend of decreasing modulus with strain is noted.

To avoid this problem in the future, we suggest the use of a quadruple lap shear specimen (QLS), Figure 3-5, for relaxation modulus testing. The QLS specimen is loaded in a state of pure shear, in which case the shear stress is directly proportional to the shear strain. Thus, the relaxation modulus would be independent of strain. The shear modulus G_R values could then be converted to tensile values as required by our finite-element computer program by multiplying by a factor of 3 ($E_R = 3\,G_R$).

During the period covered by this program, we performed three sets of relaxation modulus tests as experience was gained in test procedures (scragging, time-temperature shifting, etc.).

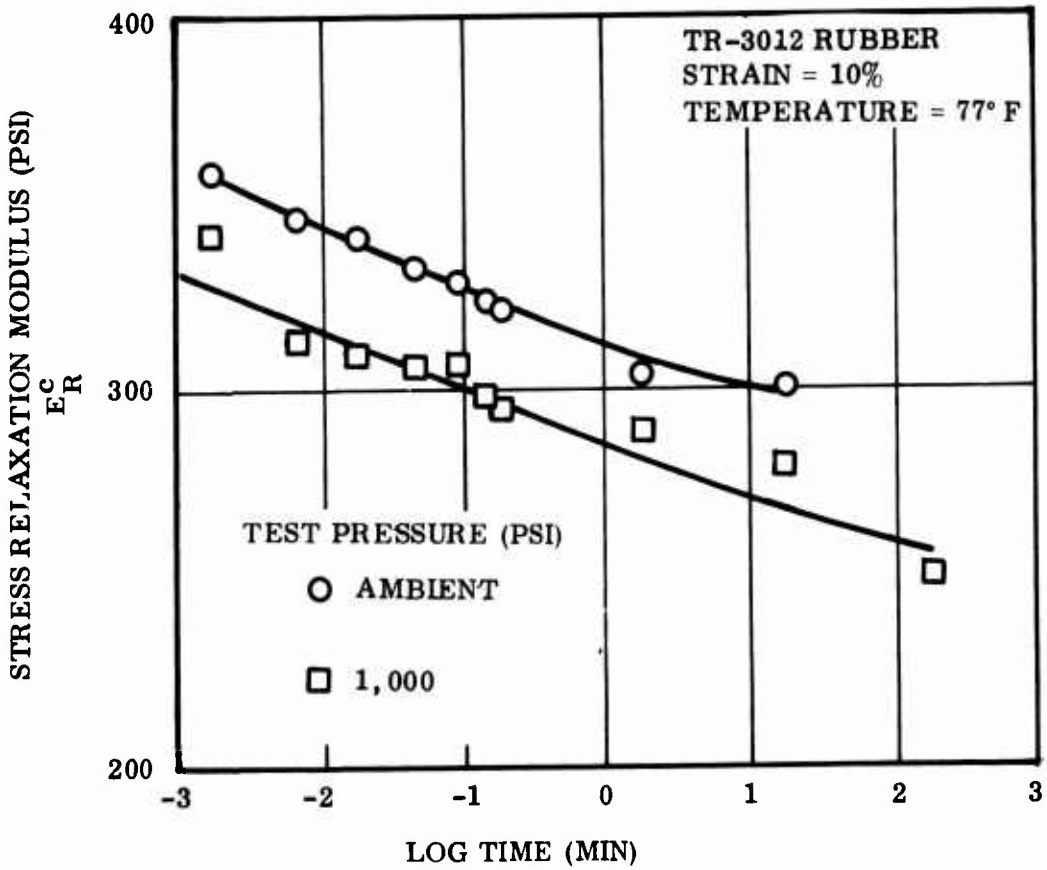

Figure 3-3. Effect of Hydrostatic Pressure on Relaxation Modulus

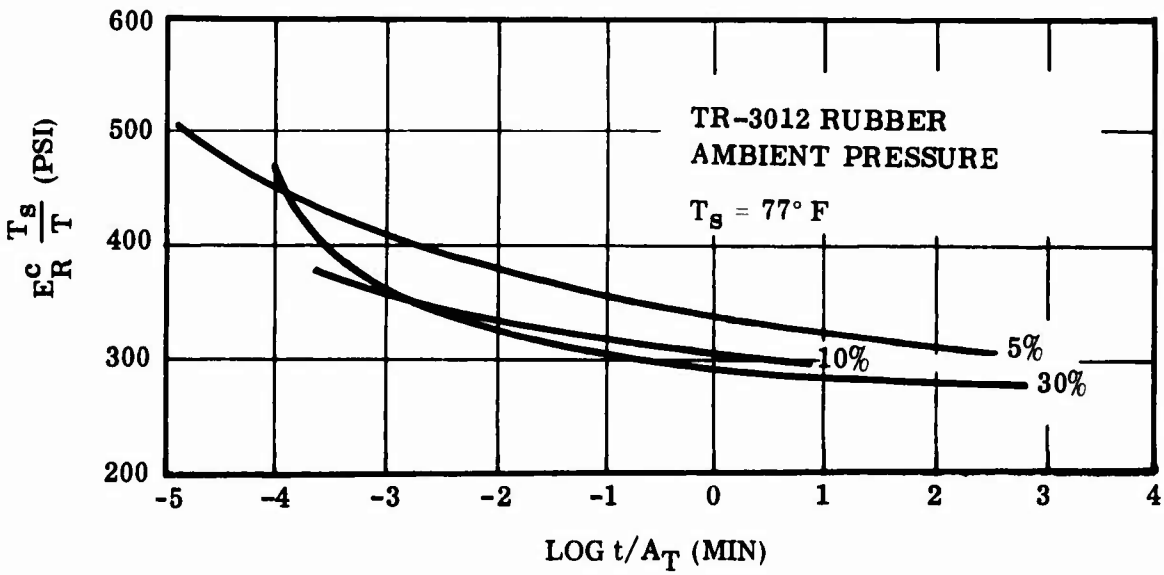

Figure 3-4. Effect of Strain on Relaxation Modulus

TABLE 3-1

STRESS RELAXATION MODULUS
(10% Strain)

Test Temp (°F)	Log Time (min)	Avg E_R (psi)	Avg E_R^c (psi)	Avg $E_R^c T_s/T$ (psi)	Avg $E_R T_s/T$ (psi)
77	-2.78	325	358	358	325
	-2.18	315	346	346	315
	-1.78	310	341	341	310
	-1.38	303	333	333	303
	-1.08	299	329	329	299
	-0.90	295	324	324	295
	-0.78	292	321	321	292
	+0.22	276	304	304	276
	+1.22	274	301	301	274
	+2.22	--	--	--	--
77 at	-2.78	311	342	342	311
1,000 psi	-2.18	285	313	313	285
	-1.78	282	310	310	282
	-1.38	279	307	307	279
	-1.08	279	307	307	279
	-0.90	271	298	298	271
	-0.78	268	295	295	268
	+0.22	263	289	289	263
	+1.22	254	279	279	254
	+2.22	227	250	250	227

TABLE 3-2

STRESS RELAXATION MODULUS
(5% Strain)

Test Temp (°F)	Log Time (min)	Sample 1 E_R^c (psi)	Sample 2 E_R^c (psi)	Avg E_R (psi)	Avg E_R^c (psi)	Avg $E_R^c T_s/T$ (psi)	Avg $E_R T_s/T$ (psi)	Log a_T (min)	Log t/a_T (min)
-20	-2.78	434	443	418	439	536	510	+2.50	-5.28
	-2.18	397	401	380	399	487	464		-4.68
	-1.78	377	478	360	378	461	439		-4.28
	-1.38	359	360	342	359	438	417		-3.88
	-1.08	359	348	337	354	432	411		-3.58
	-0.90	359	348	337	354	432	411		-3.40
	-0.78	340	348	328	344	420	400		-3.28
	+0.22	321	307	299	314	383	365		-2.28
	+1.22	302	301	288	302	369	351		-1.28
	+2.22	297	295	281	295	360	343		-0.28
77	-2.78	422	411	397	417	417	397	0.0	-2.78
	-2.18	410	397	384	403	403	384		-2.18
	-1.78	384	375	357	380	380	357		-1.78
	-1.38	370	357	347	364	364	347		-1.38
	-1.08	356	348	335	352	352	335		-1.08
	-0.90	347	339	327	343	343	327		-0.90
	-0.78	324	321	308	323	323	308		-0.78
	+0.22	324	317	306	321	321	306		+0.22
	+1.22	324	309	302	317	317	302		+1.22
120	-2.78	389		370	389	360	343	-1.75	-1.03
	-2.18	376		358	376	348	332		-0.43
	-1.78	371		353	371	343	327		-0.03
	-1.38	354		337	354	328	312		+0.37
	-1.08	354		337	354	328	312		+0.67
	-0.90	349		332	349	323	308		+0.85
	-0.78	349		332	349	323	308		+0.97
	+0.22	341		325	341	316	301		+1.97
	22	320		305	320	296	282		+2.97

TABLE 3-3

STRESS RELAXATION MODULUS
(30% Strain)

Test Temp (°F)	Log Time (Min)	Sample 1 E_R^c (psi)	Sample 2 E_R^c (psi)	Avg E_R^c (psi)	Avg $E_R^c T_s/T$ (psi)	Log a_T	Log T/a_T
-20	-2.78	375	351	363	443	+3.18	-5.96
	-2.18	327	315	321	392		-5.36
	-1.78	309	297	303	370		-4.96
	-1.38	295	254	275	335		-4.56
	-1.08	280	243	262	320		-4.26
	-0.90	274	237	256	312		-4.08
	-0.78	268	234	251	306		-3.96
	+0.22	246	211	249	304		-2.96
	+1.22	238	201	240	243		-1.96
	+2.22	223	185	234	286		-0.96
77	-2.78	339		339	339	0	-2.78
	-2.18	320		320	320		-2.18
	-1.78	316		316	316		-1.78
	-1.38	309		309	309		-1.28
	-1.08	304		304	304		-1.08
	-0.90	302		302	302		-0.90
	-0.78	300		300	300		-0.78
	+0.22	294		294	294		0.22
	+1.22	288		288	288		1.22
	+2.22	272		272	272		2.22
120	-2.78	341		341	316	-0.78	-2.0
	-2.18	331		331	306		-1.4
	-1.78	330		330	305		-1.0
	-1.38	322		322	248		-0.6
	-1.08	320		320	296		-0.3
	-0.90	320		320	296		-0.12
	-0.78	317		317	243		0.0
	+0.22	311		311	288		1.0
	+1.22	304		304	281		2.0
	+2.22	290		290	269		3.0

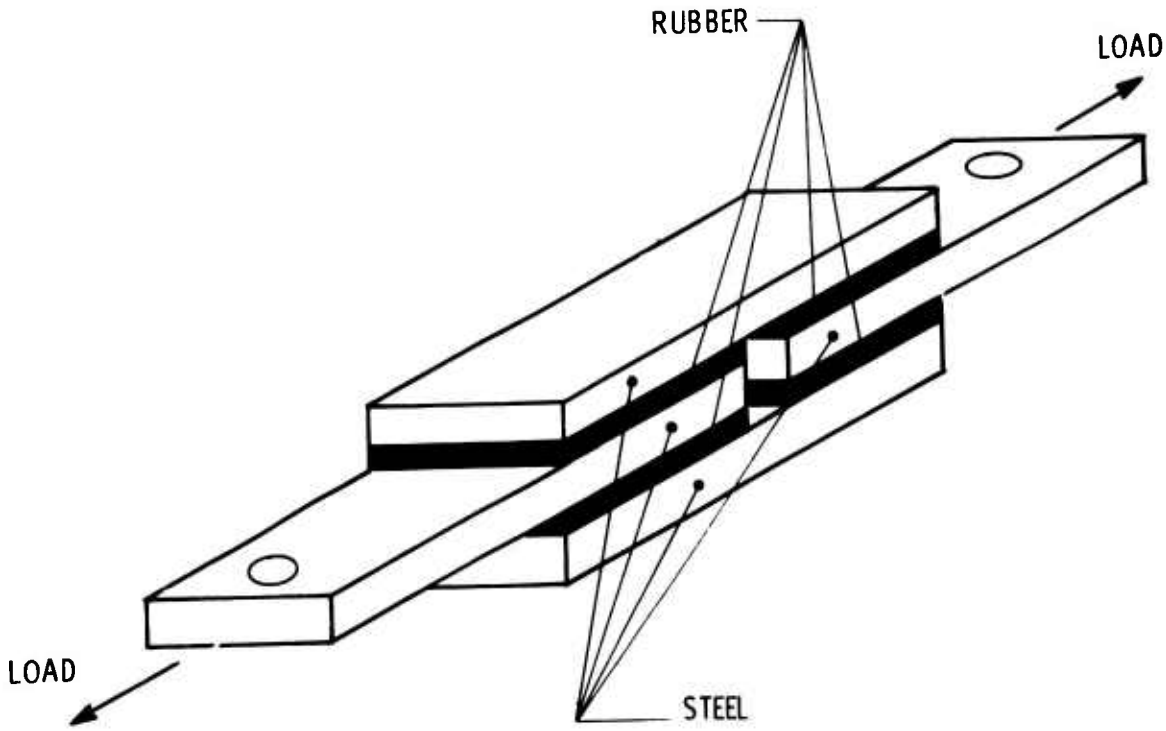

Figure 3-5. QLS Test Specimen

The following tabulation indicates the variation in test data with slight changes in laboratory test procedures. Included in this variation is the mix-to-mix variation in the rubber:

	E_R^c for Log t/AT (Range, % of Mean)	
Strain (%)	3	-4
5	327 ± 27 (8)	435 ± 27 (6)
30	292 ± 42 (14)	400 ± 80 (20)

Three methods of obtaining dynamic modulus values were examined during the program. In the first method, the real part of dynamic modulus E' was obtained from relaxation modulus using the approximate formula

$$E'(\omega) \sim E_R(t)\Big|_{t = 1/\omega}$$

In the second method, a Rheovibron at the University of Utah was used. The third method used a "Gottenberg" disc. These data are presented in Table 3-4 and plotted in Figure 3-6. The main limitation of the Gottenberg disc test is the limited frequency range available with the present Thiokol test equipment (30 Hz minimum). A comparison of data for a single point (35 Hz, T = 77° F) is given below:

Method	E' (psi)
Conversion from E_R	375
Gottenberg disc	450
Rheovibron	650

The Rheovibron data are, therefore, felt to be high. This is probably due to the limited time period for which the Rheovibron was available and the rather complex operating procedure required. We feel that the Rheovibron is a very useful tool and does produce reliable data when properly calibrated and used. The trends of the data are useful in describing the effect of temperature and frequency on dynamic modulus values.

TABLE 3-4

DYNAMIC MODULUS, TR-3012 RUBBER, GOTTENBERG DISC

Frequency (Hz)	Sample 1		Sample 2		Sample 3		Average	
	G'	G''	G'	G''	G'	G''	G'	G''
90			1,088	58.4				
85	1,008	98	989	80.5			999	89.25
80	843	106	825	88.6	867	121	845	105.20
75	691	106	688	83.7	724	110	700	99.90
70	569	112	558	79.3	593	106	573	99.10
65	456	89	449	65.7	477	86	461	80.23
60					345	92		
55	284	42	270	28.5	284	24.5	279	31.67
50			237	120.0	234	15.4	236	13.70
45	200	9	214	5.4	209	11.9	208	8.77
40	179	1.2	193	2.7	188	12.3	187	5.40
35	156	3.3	175	1.2	168	9.4	166	4.63
30	140	3.2			149	8.5	145	5.85
25	55.6	0.0			128	2.5		

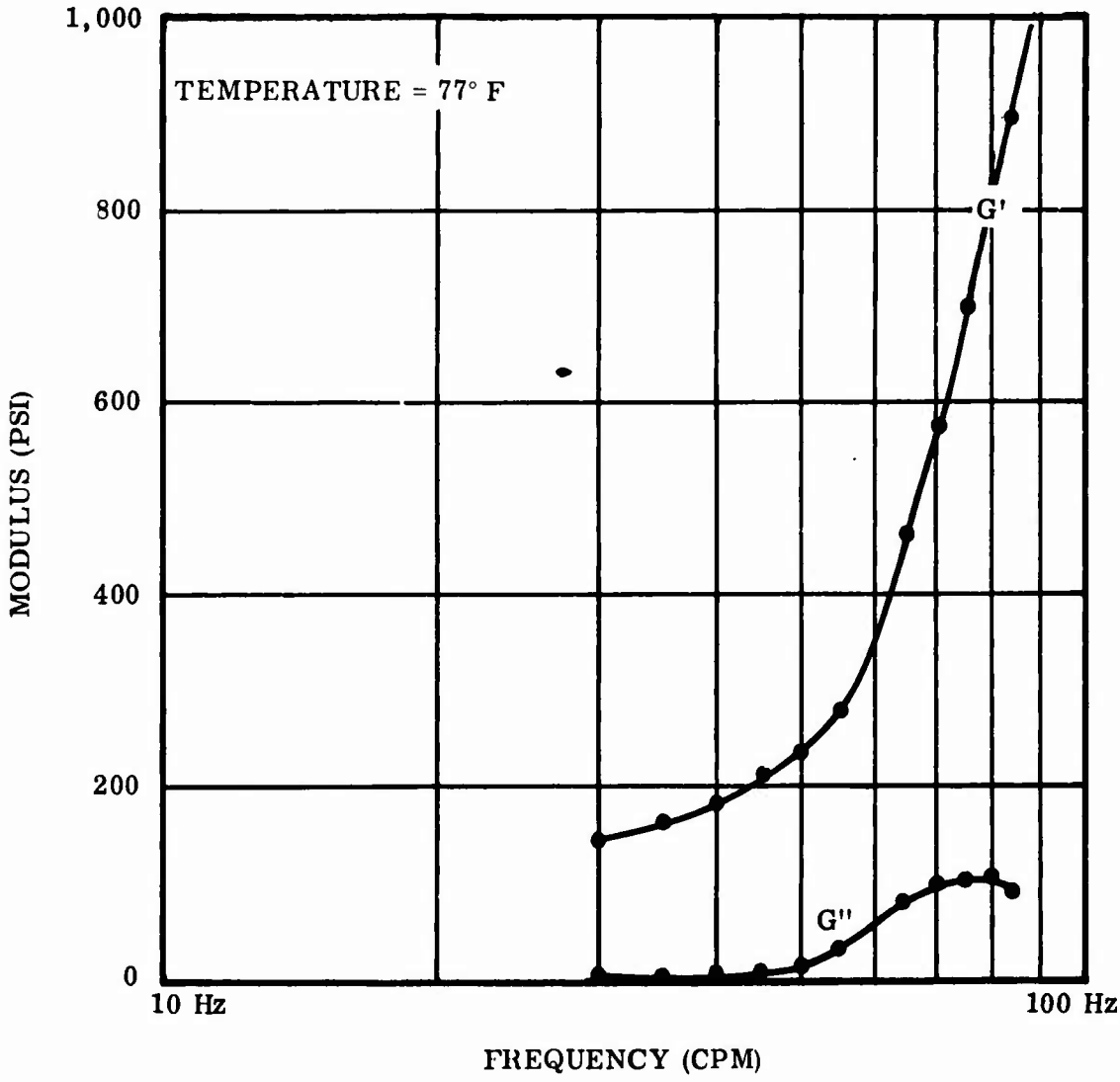

Figure 3-6. Dynamic Modulus, Gottenberg Disc

3.2 COEFFICIENT OF LINEAR THERMAL EXPANSION

The techniques used in the program to obtain coefficient of linear thermal expansion (α) were designed for similar measurements in solid propellants. The main difficulty in α evaluation for rubbers is in accurately measuring length changes without applying strains to the rubber by the measuring equipment or from rubber friction with its resting surface. Neither problem is present in high-modulus materials such as steel. Since the Thiokol equipment has been successfully used on low-modulus propellants (~100 psi) no difficulty was experienced with the rubber α measurements (E~300 psi). Figure 3-7 shows the length change of a specimen as a function of temperature. Figure 3-8 shows the specimen geometry that was used.

3.3 BULK MODULUS

Equipment developed at Thiokol for measuring bulk modulus (k) of solid propellants was used during this program to measure k for rubber. No difficulties were encountered. However, it was determined that the bulk modulus changes with applied hydrostatic pressure until a pressure of 500 psi is reached (Figure 3-9). This was interpreted to mean that small voids in the rubber matrix are being closed as the pressure increases. It is noted that the test samples were cured under pressure (200-300 psi). Therefore, the bulk modulus change may be negligible after the cure pressure is exceeded. Additional effort should probably be spent in checking this theory. However, our observations during this program are that these changes have little effect on bearing analyses. Therefore, a Poisson's ratio calculated directly from the high hydrostatic pressure value of bulk modulus is recommended for use. The formula

$$\nu = 0.5 - \frac{E}{6k}$$

is suggested.

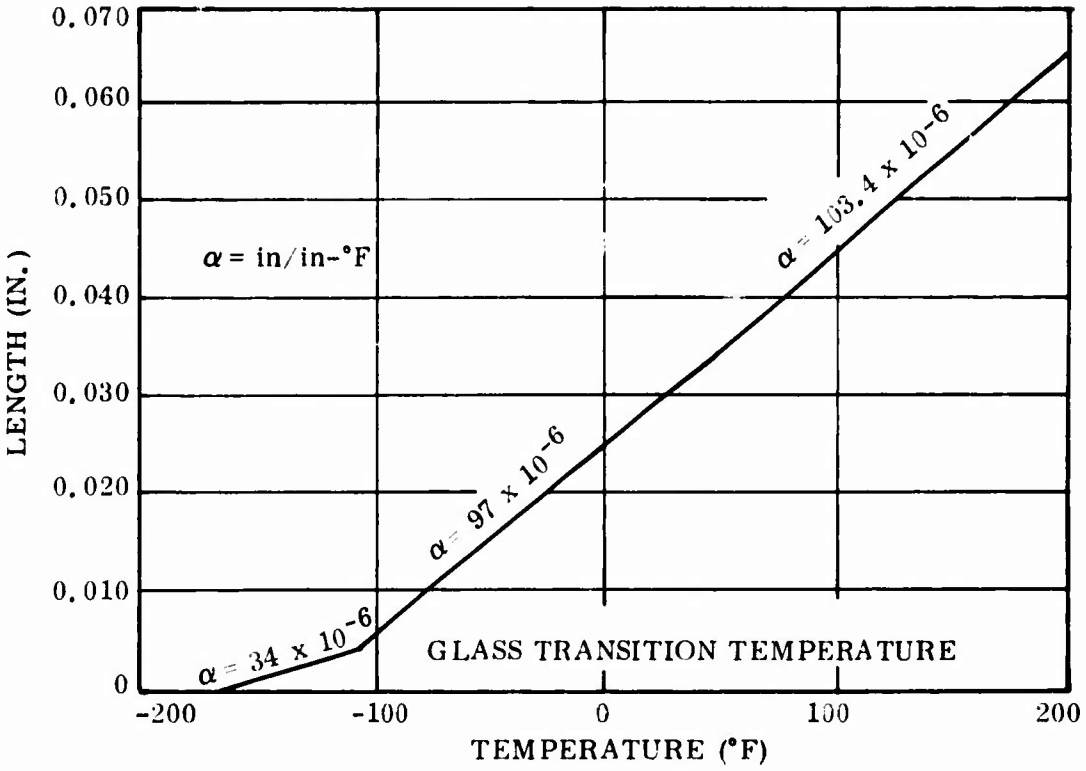

Figure 3-7. Thermal Coefficient of Linear Expansion, Natural Rubber (Formulation TR-3012)

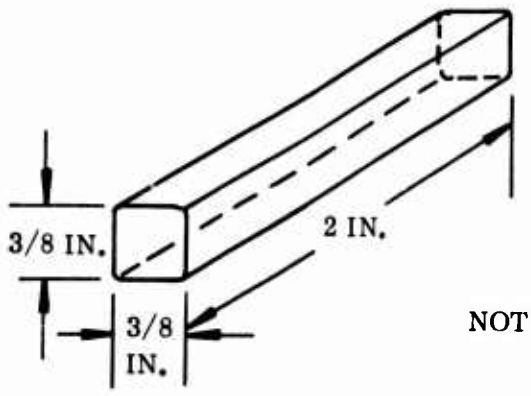

NOTES:
1. ALL EDGES AND CORNERS CURVED AT 1/16 IN. RADIUS
2. GRAPHITE COAT ALL SURFACES

Figure 3-8. TCLE Test Specimen

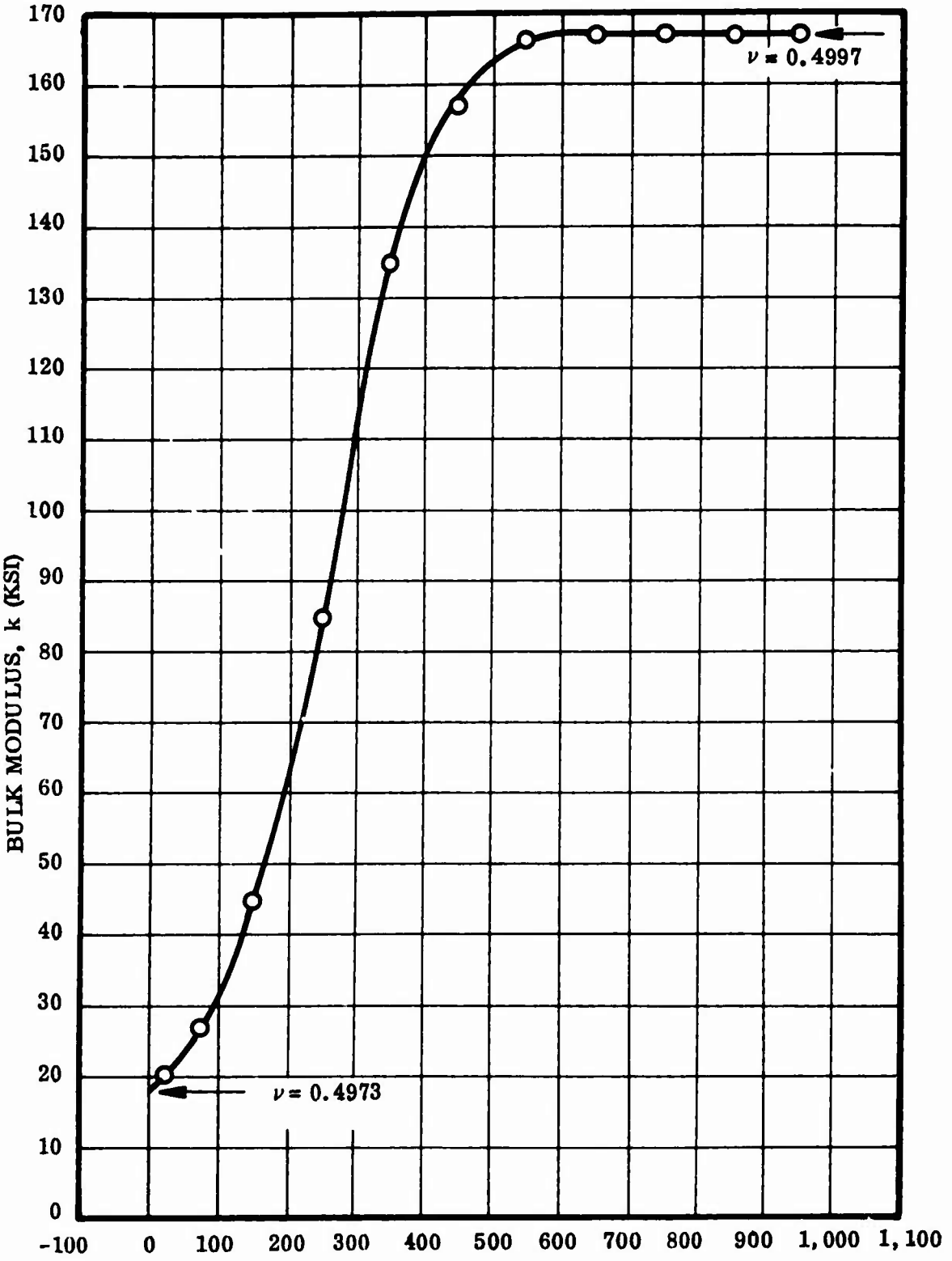

Figure 3-9. Bulk Modulus

4.0 SERVICE LIFE

The major portion of the fatigue testing completed for this program used Type 1 test specimens. Each specimen was composed of two annular laminates of elastomer bonded to steel rings as shown in Figure 4-1. Five edge conditions were examined to determine the effect of edge fillets on service life. The edge fillet conditions are sketched in Figure 4-2 with detailed dimensions in Figure 4-3. In addition, elastomer thickness was varied to determine the effect of thickness on service life (Table 4-1). The three different molds used to fabricate the five configurations are described below.

4.1 BEARING MOLD CONFIGURATIONS

4.1.1 Configurations "A" and "C" (One Mold)

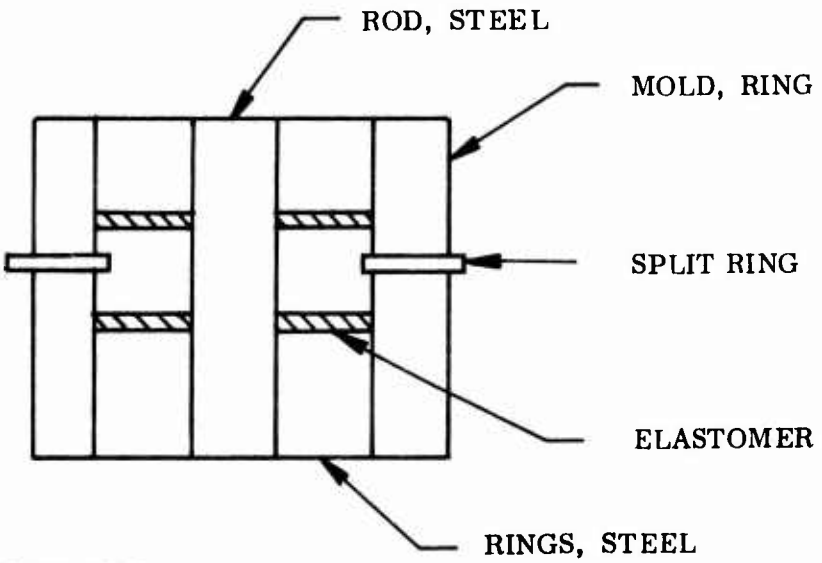

Processing Data:

1. Solvent-clean each of the three steel rings.
2. Grit-blast three steel rings on bonding surface only with silica sand.
3. Solvent-clean each of the three steel rings.
4. Obtain Chemlok 205 and stir thoroughly. Hand brush a coat of 205 on the bonding surface of each of the three steel rings. Air dry for 15 minutes.

TABLE 4-1

TYPE I SPECIMEN CONFIGURATION DIMENSIONS

Specimen Designation (No. Tested)		t_r	t_s	R	t_c	h
A1	(3)	0.075				
A2	(3)	0.100				
A3	(1)	0.125				
A4	(2)	0.150				
R2	(16)	0.100		0.050		
R4	(3)	0.150		0.075		
C1	(2)	0.075			0.125	0.150
C2	(1)	0.100			0.150	0.150
CR2	(3)	0.100		0.075	0.150	0.150
SA1A	(2)	0.075	0.037			
SA4A	(1)	0.150	0.037			
SA1B	(2)	0.075	0.063			
SA4B	(1)	0.150	0.063			

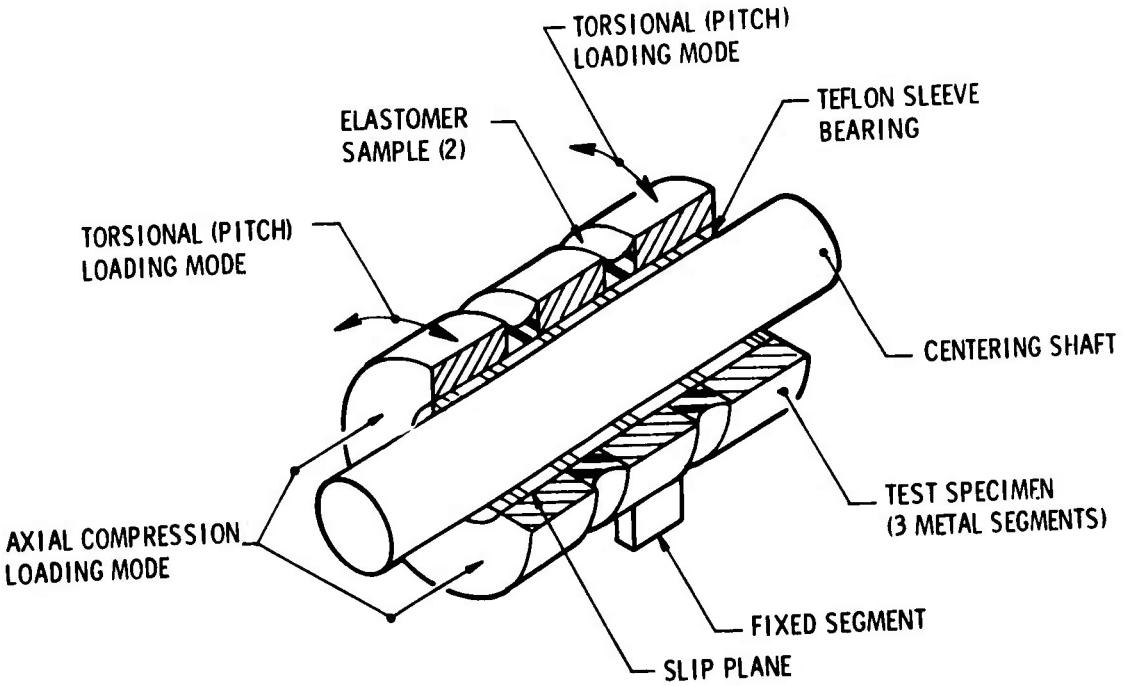

Figure 4-1. Type I Cyclic Fatigue Specimen

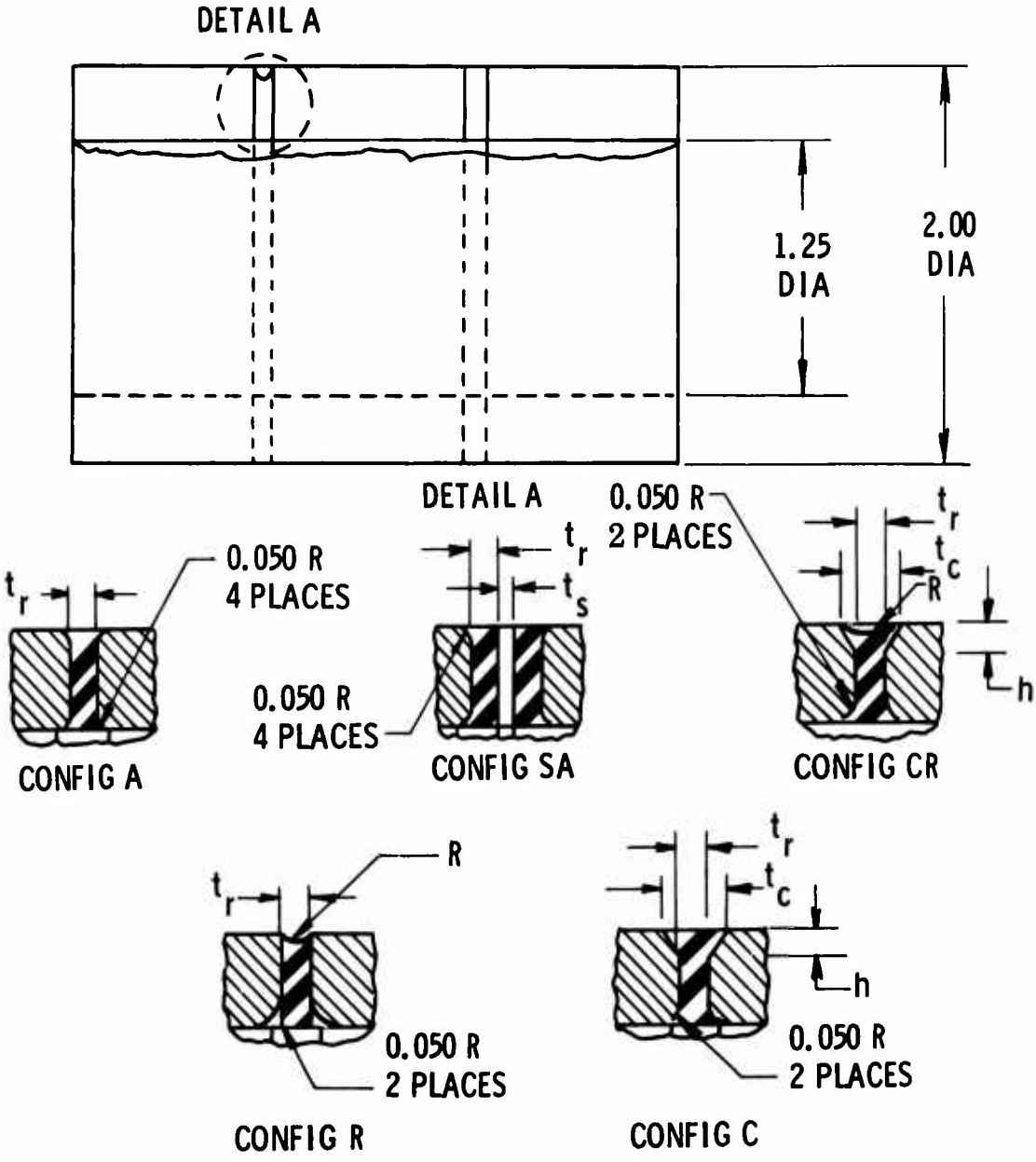

Figure 4-2. Type I Specimen Configuration

GEOMETRIES ANALYZED:

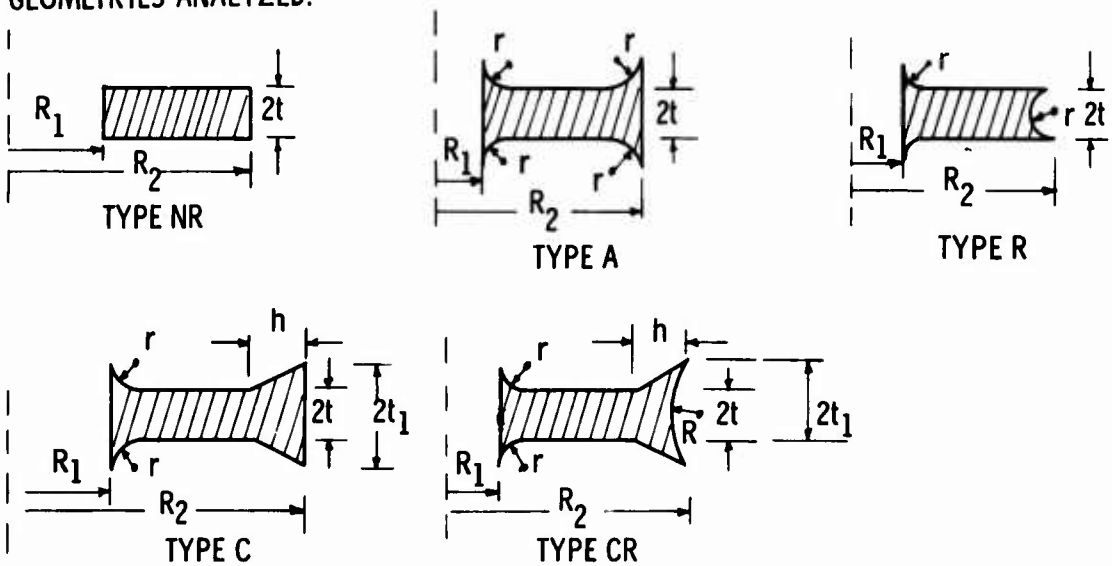

TYPE	R_1 (IN)	R_2 (IN)	2t (IN)	r (IN)	$2t_1$	h	R
NR	0.625	1.0	0.1	--	--	--	--
A	0.625	1.0	0.075, 0.1, 0.125, 0.150	0.05	--	--	--
R	0.625	1.0	0.10, 0.150	0.05, 0.075	--	--	--
C	0.625	1.0	0.075, 0.10	0.05	0.125, 0.15	0.15	--
CR	0.625	1.0	0.10	0.05	0.15	0.15	0.085

Figure 4-3. Type I Specimens

5. Obtain Chemlok 220 and stir thoroughly. Hand-brush a coat of 220 on the 205 prepared surfaces. Air-dry for 30 minutes.
6. Obtain elastomer and cut two donut-type pieces of the applicable thickness.
7. Install the steel rod in one of the steel end rings, with Chemlok painted on one end. Slide an elastomeric pad over the rod onto the Chemlok painted ring. Slide steel ring, with Chemlok on both ends, over steel rod onto the Chemlok surface of the second ring. Slide the third steel ring over steel rod, with Chemlok surface to the elastomer.
8. Slide the split rings around the center steel ring, and place this assembly into one of the steel mold rings. Place second steel mold ring on top of this assembly.
9. Place in a preheated press (300° F), apply sufficient pressure to close the mold rings onto the split rings, and cure for 1 hr.
10. Disassemble mold by removing split rings, pushing out the steel rod, and removing steel mold rings.
11. Identify test specimen with applicable identification.

4.1.2 Configurations "R" and "CR" (See Figure 4-4)

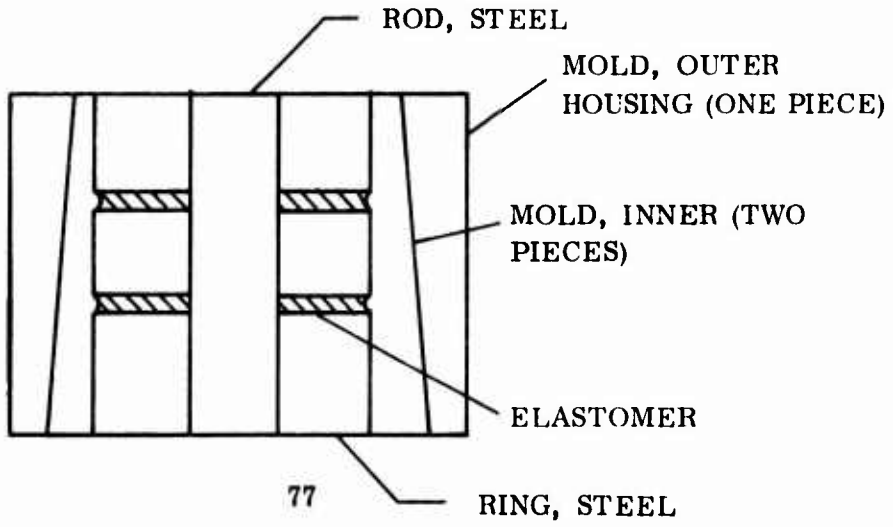

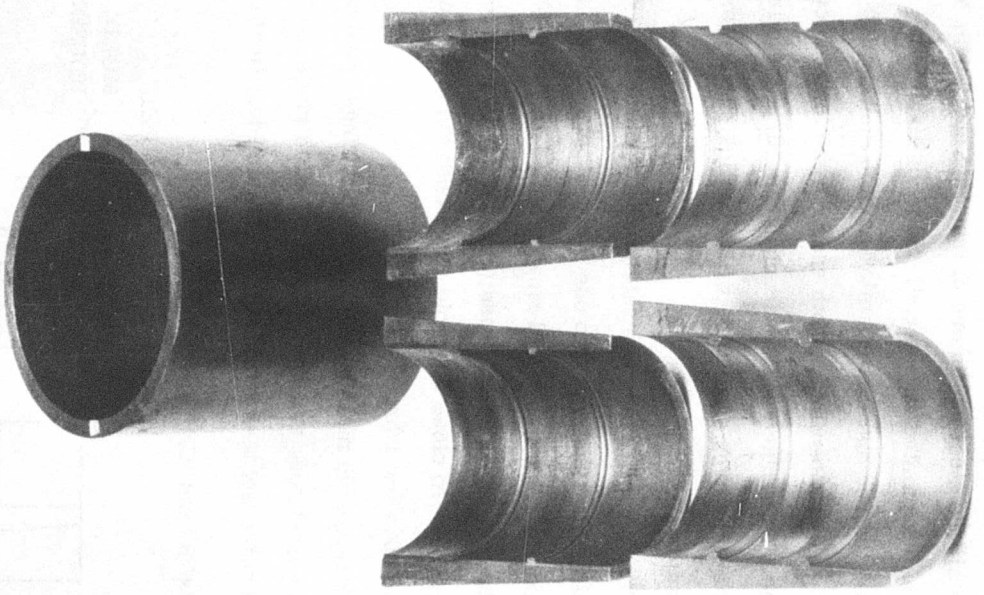

Figure 4-4. Mold Tooling for Type I R2 Service Life Bearing

Processing Data:

1. Repeat first seven processing steps of Configurations "A" and "C" (para 4.1.1).
2. Place split inner mold pieces around the specimen, and place this assembly into the mold outer housing.
3. Place mold assembly in a preheated press (300° F) and cure for 1 hr.
4. Disassemble mold by reversing assembly procedure and pushing out the steel rod.
5. Identify test specimen with applicable identification.

4.1.3 Configuration "SA" (See Figure 4-5)

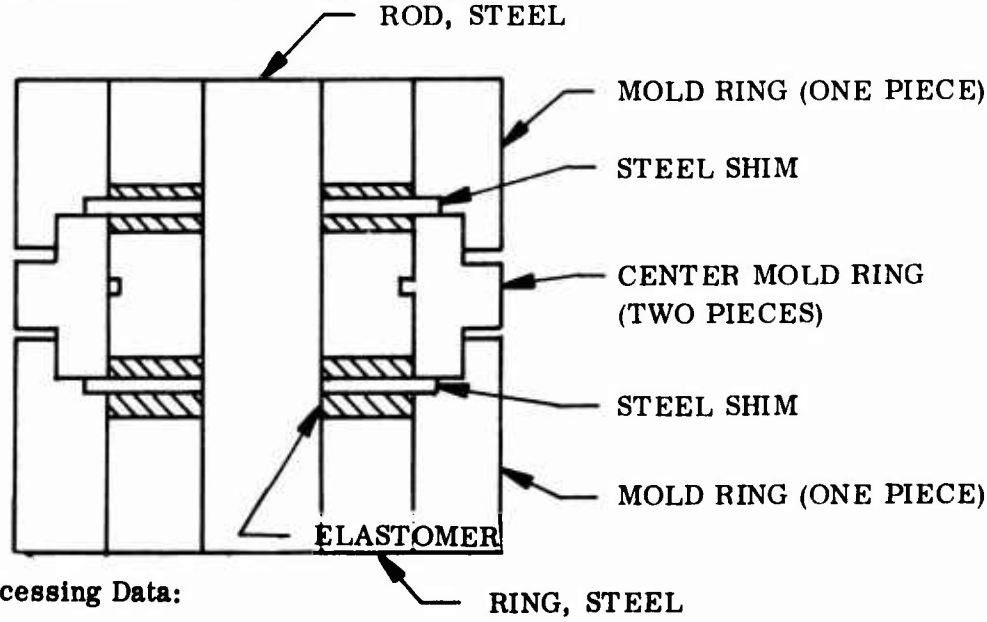

Processing Data:

1. Solvent-clean each of the three steel rings and both sides of each of the steel shims.
2. Grit-blast three steel rings and both sides of the steel shims with silica sand.
3. Solvent-clean all grit-blasted parts.
4. Obtain Chemlok 205 and stir thoroughly. Hand-brush a coat of 205 on the bonding surface of each of the three steel rings and the two steel shims. Air-dry for 15 minutes.

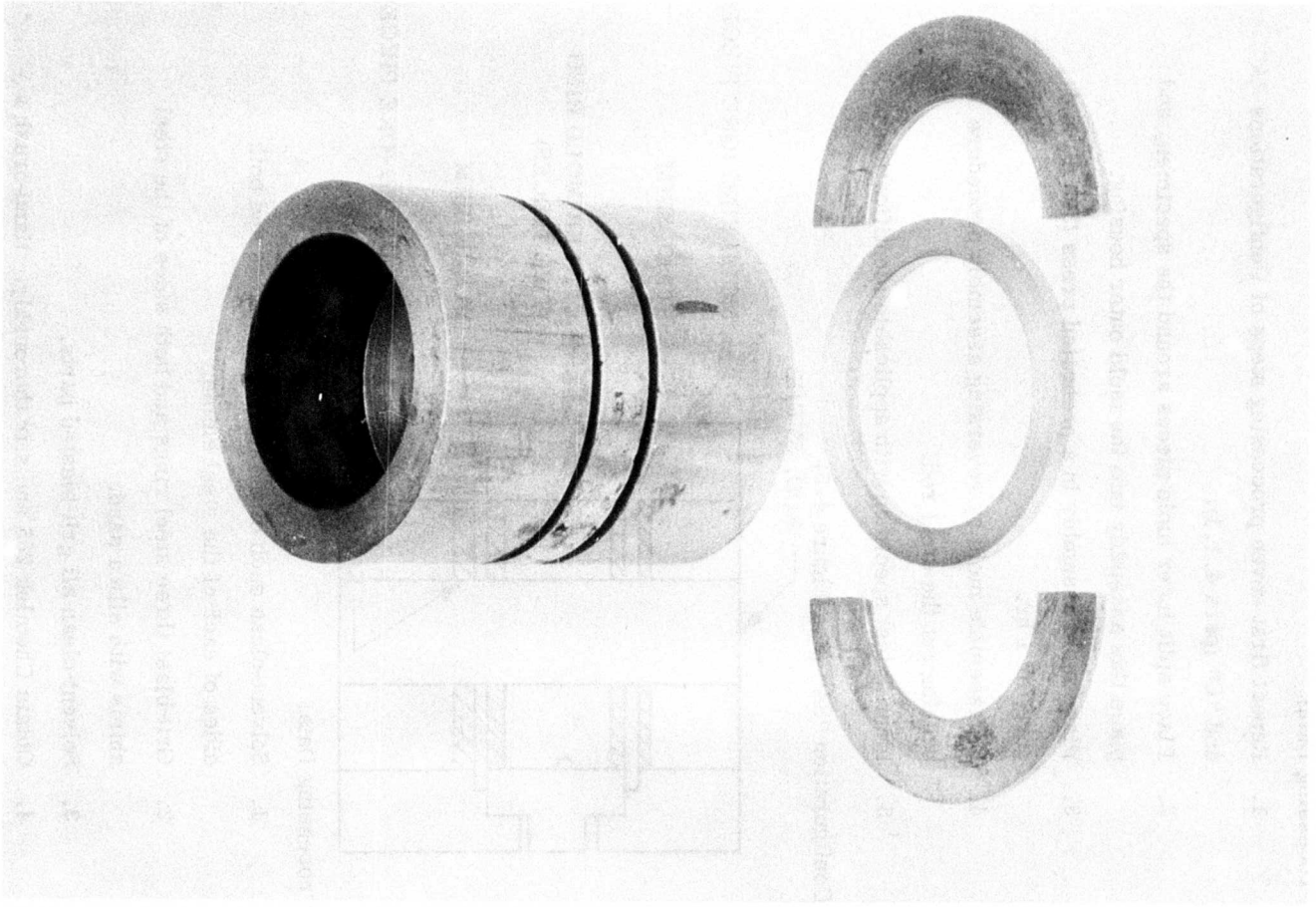

Figure 4-5. Mold Tooling for Type I SA Bearing

5. Obtain Chemlok 220 and stir thoroughly. Hand-brush a coat of 220 on the 205 prepared surfaces. Air-dry for 30 minutes.
6. Obtain elastomer and cut four donut-type pieces of the applicable thickness.
7. Install the steel rod in one of the steel end rings, with Chemlok painted on one end. Slide an elastomeric pad over the rod onto the Chemlok painted ring. Place one of the Chemlok painted shims over the steel rod onto the elastomer pad. Place the second piece of elastomer on this assembly. Follow up with the center steel ring, a third pad of elastomer, the second steel shim, and a fourth pad of elastomer; then top with the third steel ring.
8. Place the two-piece center mold rings in place.
9. Install two (one-piece) mold rings in place, and put assembly in a heated (300° F) press. Close press with sufficient pressure to close the mold, and cure for 1 hr at temperature.
10. Disassemble tooling and identify specimen with applicable number.

The bearings generally were cooled to room temperature (75° F) before being separated from the molds. However, in the case of the R, CR, and SA configurations, this cooling could induce tensile stresses in the rubber since the rubber is prevented from normal longitudinal shrinkage by the inner molds. A stress analysis of this situation showed the possibility of tensile stresses of 180 psi. Since tensile stresses on the order of 218 psi (which is 3/4 of the torque modulus) are expected before cavitation initiation, we feel that the bearings were not damaged. However, the molded parts should be removed at an elevated temperature.

4.2 FATIGUE TESTS

Before each specimen was installed on the fatigue test machine, a series of static spring rate tests was completed. These tests included a compression-deflection test (50% compressive axial strain at 0.02 in. per minute) to determine the compressive spring rate (K_c) and a torsional spring rate test to $\pm$ 150% strain. For both cases a total of five loading cycles were completed to properly scrag the specimens prior to recording data. Load and deflection were recorded on the fifth cycle.

The specimens were then installed on the fatigue test stand (Figure 4-6), and the desired axial compression was applied to each specimen. The axial compression is applied by adjusting nuts on the center shaft at the edges of the outside shims. The center shaft is given an angular sinusoidal displacement. The outer two shims are attached to the center shaft with headed set screws. A threaded shaft attached to the center shim prevents rotation of the center shim. The torsional load is then applied as a given applied sinusoidal displacement at 250 cycles per minute.

After approximately 105 hr (1.6×10^6 cycles) of fatigue testing, the bearings are removed, and the compressive and torsional static tests are repeated.

Those specimens for which the torsional spring rate was greater than 70% of that initially measured were reinstalled in the cyclic fatigue test machine and run under the same condition as originally specified for an additional 105 hr. This procedure was satisfactory for the majority of the tests with two exceptions: (1) some bearings reached the failure point before completion of the 105 hr, and (2) many bearings exceeded 30×10^6 cycles, at which time testing was normally terminated. Three specimens were cycled to 50×10^6 cycles with little reduction in torsional spring rate noted.

A special test series was conducted on specimen R2-0 wherein a load cell was mounted on the shaft attached to the center shim. This load cell measured applied torque for a given angular displacement without removing the bearing from

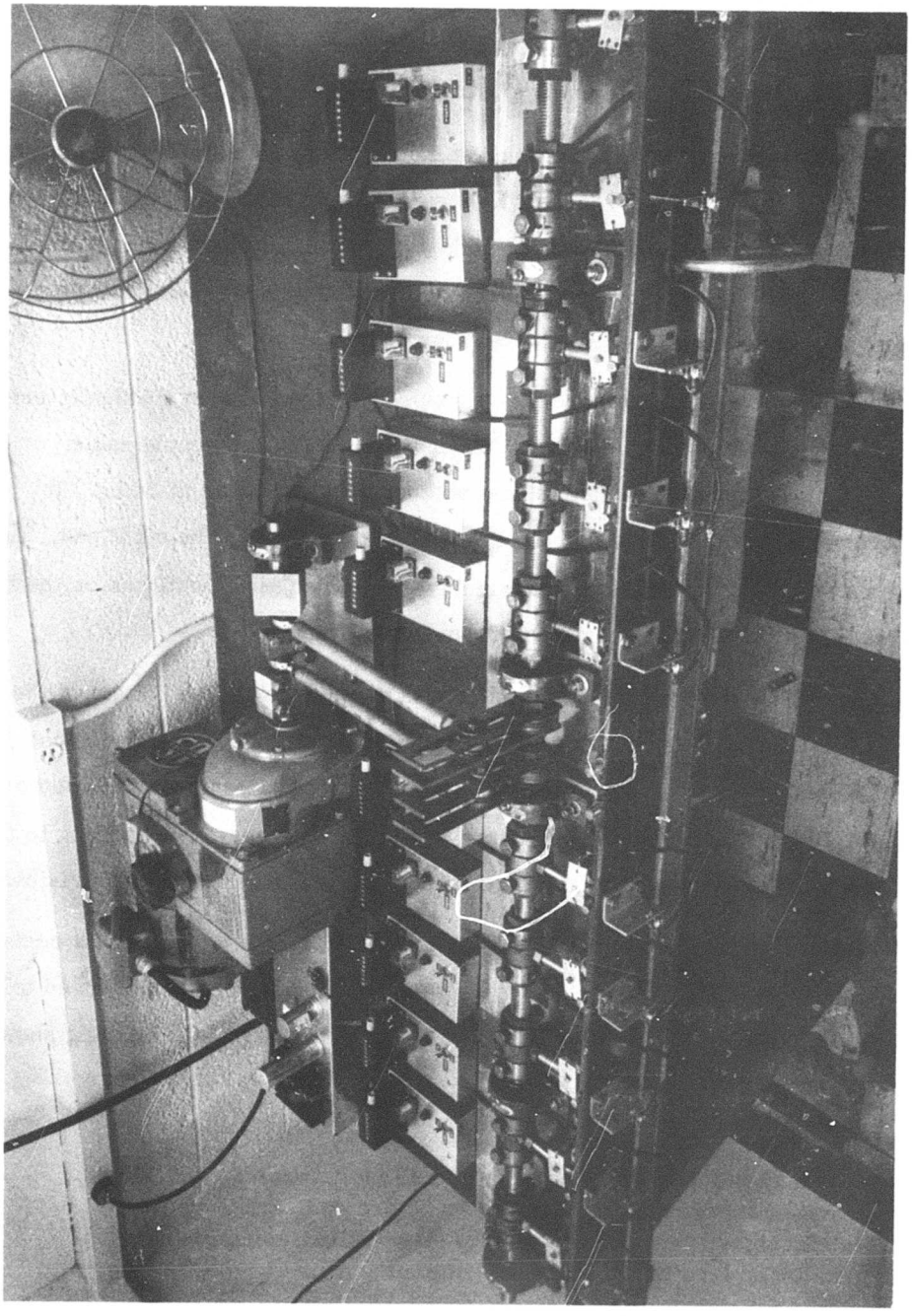

Figure 4-6. Fatigue Test Apparatus for Type I Bearings

the cyclic fatigue test machine. In addition, photographs were taken and visual inspections completed at frequent intervals during the fatigue testing. A torsional strain of $\pm$ 84% was applied with no axial strain.

The starting force on the bearing was 30 lb. This remained fairly constant for the first 17 hr (Figure 4-7), but by 18 hr, the force had dropped to 28 lb. Corresponding to this is an observation made at 15 hr that a small amount of reversion had started on the left pad. The photographs (Figure 4-8) show no reversion or any other damage at times less than 15 hr.

From the time that the force first dropped, it changed very gradually until 99 hr* had passed. There were several observations and photographs taken between these two times. The first of the photographs was taken at 34 hr. It shows reversion on the left pad with no apparent degradation of the right pad. At 38 hr it was observed that reversion spanning about 20 deg had occurred on the left pad. This is about the same length as shown in the photograph.

At 56 hr it was observed that rubber was dripping from the bottom of the bearing. Also, the reversion was noted to have grown so that it spanned about 270 deg. Some of this reversion appeared to start from the center, while some started at the edge. In the photograph taken at this time, a part of it starting in the center is shown and part of the pad where no reversion has taken place is visible.

At 88 hr the first damage to the right pad appeared in the form of a center crack of about 25 deg. The extent of the reversion on the left pad was observed to be unchanged. A photograph was taken at 94 hr, but on the part of the bearing shown, there is no crack visible on the right pad.

*The shaft holding the center shim broke sometime between 56 and 116 hr. All figures for the number of hours after 56 are an average of the two possible extremes. Therefore, each of these values could be as much as 29 greater or less than what was recorded.

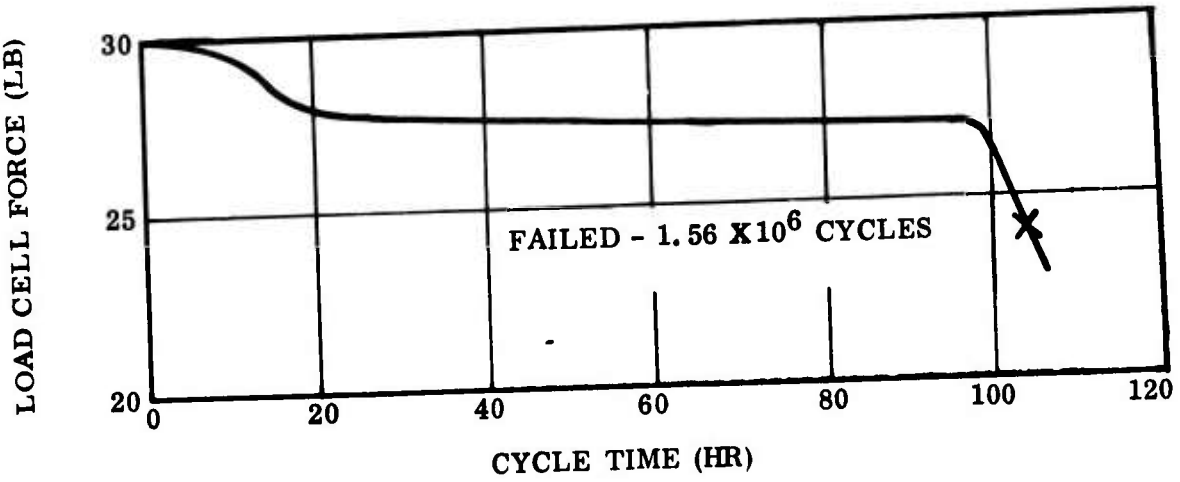

Figure 4-7. Load Drop in Bearing R2-0 With Cycle Time

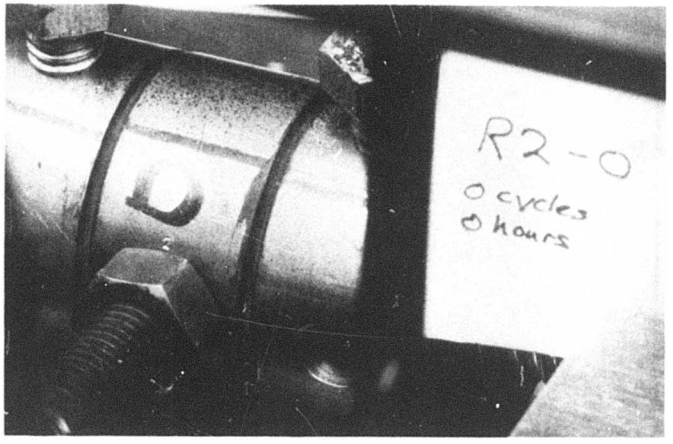

a. Pretest

b. 510,000 Cycles

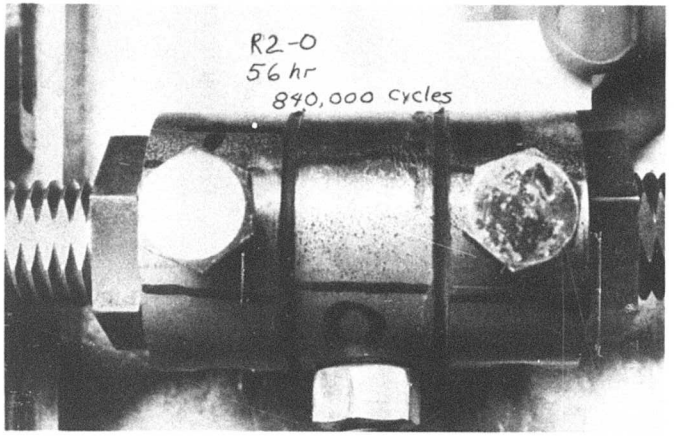

c. 840,000 Cycles

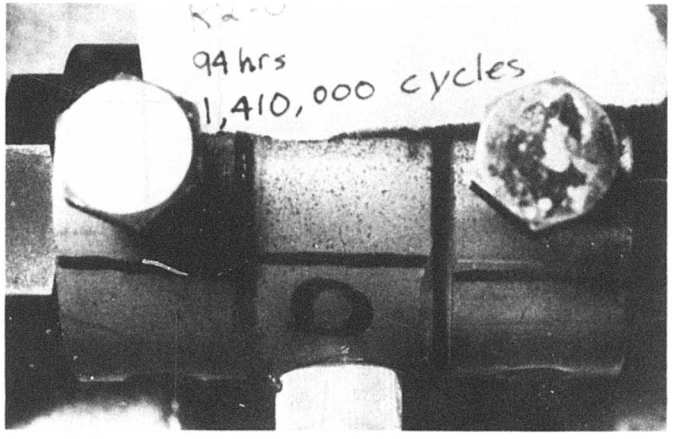

d. 1,410,000 Cycles

Figure 4-8. Bearing R2-0 During Fatigue Tests

The final observation of the state of the bearing was made at 100 hr, about the time when the force began to drop rapidly. The reversion had grown until it spanned 90 deg on the right pad and 280 deg on the left pad.

Looking at all these observations, we can conclude that no significant drop in force occurred until some reversion had occurred. However, after the first damage to a rubber pad, an increase in visible damage was not accompanied by significant decrease in the load. It is interesting to note that the bearing did not have a rapid drop in the force until both pads had considerable amounts of reversion. This was observed to have happened by the 100th hr. At 99 hr the force was 27.0 lb, but it had dropped to the failing level of 24.0 lb by the 104th hr, which corresponds to a value of 1.56 megacycles (see Table 4-2).

A failure surface was constructed using data from Type I-R2 bearings. A total of 27 R2 bearings were tested at different levels of axial strain. As can be seen from Figure 4-7, the torsional spring rate at zero axial compression drops off rapidly after a reduction of 20% is observed. We have, therefore, chosen to define the life at bearing incipient failure (20% reduction in static torsional spring rate) as the bearing fatigue life.

A summary of all test data from R2 specimens is shown in Table 4-3. The definitions of service life parameters are shown in Figure 4-9. The service in an R2 specimen is based at a point in the specimen which experiences the highest cyclic loading. A plot in log-log form is shown in Figure 4-10. The log-log form was chosen based upon observations by other researchers, such as Dr. R. A. Schapery, that the failure life is a linear function of load if plotted in log-log form.

A form of the failure surface more generally applicable to other bearing types was then desired. Failure in the Type I-R2 bearings was attributed to rubber reversion, which in turn is related to the heat generated in the pads due to viscous

TABLE 4-2

R2-0 BEARING SERVICE LIFE SUMMARY

Time (hr)	Cycles	Force (lb)	Visual Observation
0	0	30.0	No damage
18	255,000	28.0	Small reversion started on left pad
34	510,000	27.5	20-deg reversion on left pad
56	840,000	27.3	270-deg reversion on left pad. Rubber dripping from bottom
94	1,410,000	27.1	270-deg reversion still on left pad. 25-deg reversion started on right pad
100	1,500,000	26.5	280-deg reversion on left pad. 90-deg reversion on right pad
104	1,560,000	24.0	Failed

TABLE 4-3

TYPE I R2 BEARING FAILURE SUMMARY

Specimen Number	Axial Strain (%)	Torsional Strain (%)	Fatigue Life (megacycles)	Comments
1	-15	31	>38.5	
2	-15	31	>38.5	
3	-15	31	>38.5	
4	-15	31	>38.5	
5	0	31	>50	Slight reversion noted at 50 x 10^6 cycles
7	-15	31	>50	
8	-22	31	>50	
9	-45	31	9.5	
10	-30	31	>37	
11	-15	31	>39	
12	0	55	25	At 28.6 x 10^6 cycles, bearings were completely failed.
13	-15	55	25	At 28.6 x 10^6 cycles, bearings were completely failed.
14	--	--	--	Test specimen no good
15	-30	55	7.6	
16	-45	55	2.7	
0	0	84	1.5	Load cell recorded force directly
12A	-15	84	1.0	Reversion initiated at 0.36 x 10^6 cycles.
0x	0	84	--	Insufficient periodicals to detect failure (0.34 x 10^6 slight reversion)
3x	-15	84	--	Insufficient periodicals to detect failure (0.34 x 10^6 slight reversion)
4x	-22	84	--	Insufficient periodicals to detect failure (0.34 x 10^6 slight reversion)
9x	-30	84	0.3	0.075 extreme reversion
11x	-45	84	<0.09	0.015 extreme reversion
6x	0	157	--	Failed before 0.24 x 10^6 cycles (first periodical)
13x	-15	157	--	Failed before 0.24 x 10^6 cycles (first periodical)
12x	-22	157	--	Failed before 0.24 x 10^6 cycles (first periodical)
15x	-30	157	--	Failed before 0.24 x 10^6 cycles (first periodical)
14x	-45	157	--	Failed before 0.24 x 10^6 cycles (first periodical)

Pad thickness = 0.1 in.

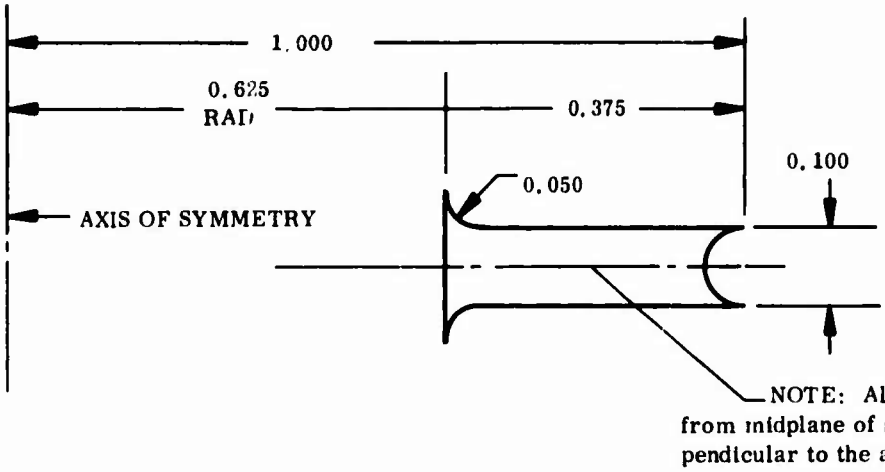

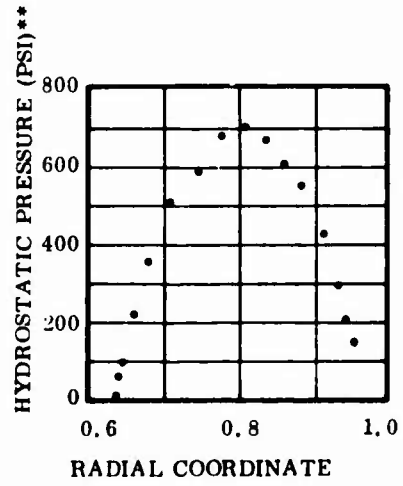

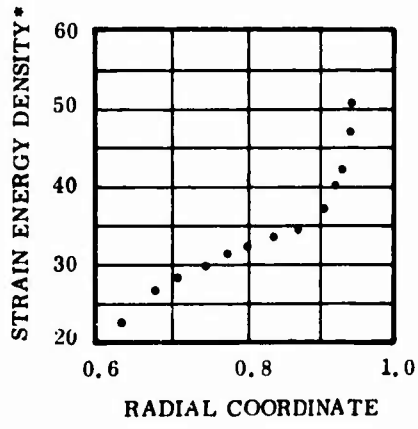

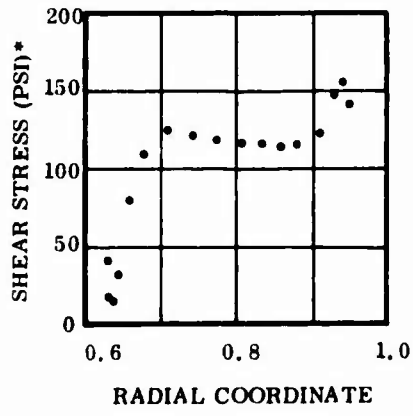

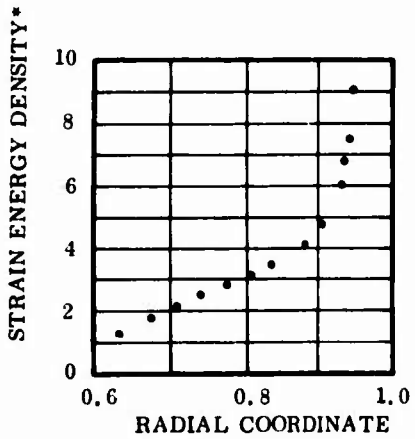

*FOR 30% TORSIONAL STRAIN
**FOR 30% AXIAL STRAIN

Figure 4-9. Service Life Parameters

dissipation during cycling. The heat generated per cycle at any point is given by the equation

$$q = 2\pi \sin \delta \int_{v_o} U \, dv_o$$

where $\delta = \tan^{-1}$ (loss modulus)

U = strain energy density

v_o = volume of interest

One possible choice for a failure parameter, therefore, is maximum strain energy density. As noted in Figure 4-10, the R2 bearing failures depend upon the amount of axial compression. Axial compression creates a large component of hydrostatic pressure within the bearings which tends to close microflows and results in a higher torsional spring rate with a higher heat generation rate. Therefore, the hydrostatic pressure was chosen as a failure parameter. The hydrostatic pressure is calculated for the same location as the maximum dynamic energy density. The resulting failure curve is plotted in Figure 4-11. It is emphasized that these curves should be used only for rough estimates of bearings with similar designs. They are conservative in that they are obtained from continuous cycling as opposed to intermittent cycling and may be nonconservative in that the thick shims used dissipate more heat than the normal thin shims.

Since no mechanical damage was noted for these specimens, the failure curve in Figure 4-10 could also be considered a lower bound for bearings which do experience mechanical damage. In this case, a more useful set of parameters is probably maximum shear stress from the cyclic load since fracture normally depends directly upon the distortional components of stress. Hydrostatic pressure exerted by the static load at the point of maximum dynamic shear stress was chosen as a parameter. A plot of the failure surface using these parameters is presented in Figure 4-12.

To get the maximum shear stress and maximum energy density failure surfaces, two computer runs were completed. The same grid which was used for

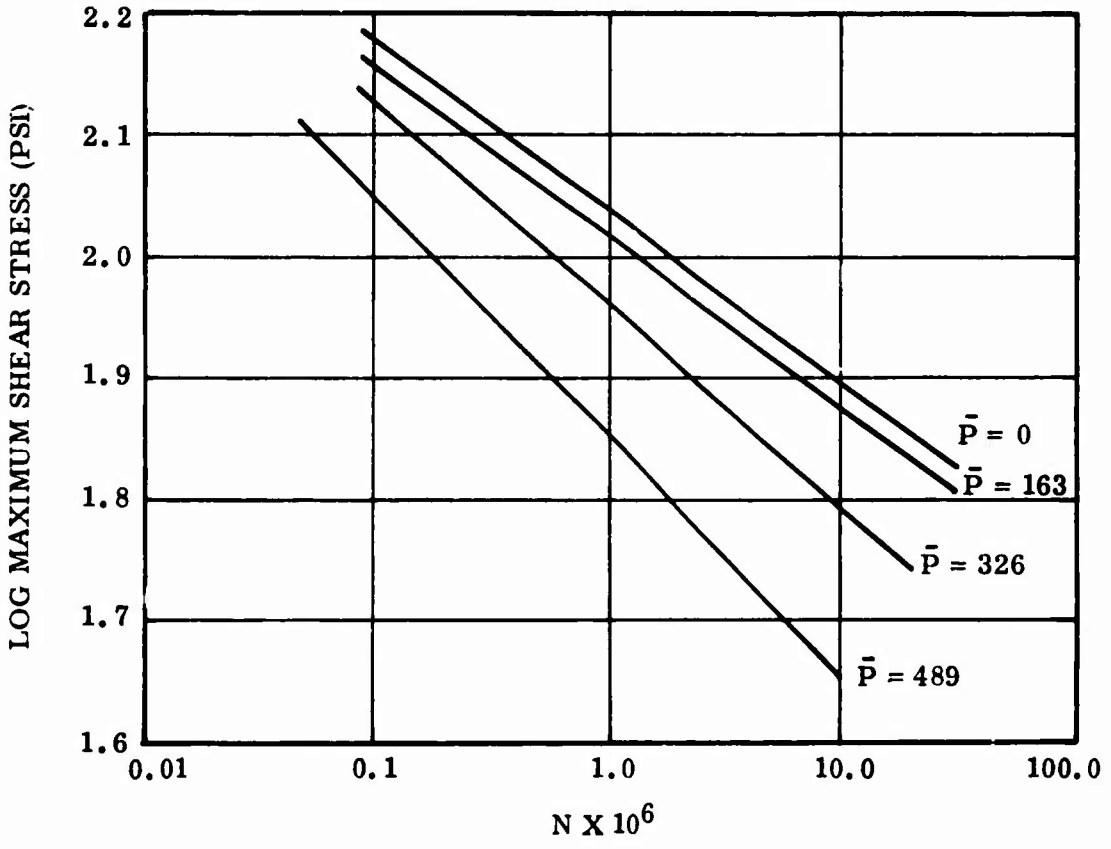

Figure 4-10. Maximum Shear Stress Failure Surface

CURVE	ϵ_z (%)	$\bar{P}$ (PSI)	τ_{ST} (PSI)
1	0	0.0	0.0
2	15	54.3	51.4
3	30	108.6	102.8
4	45	162.9	154.25

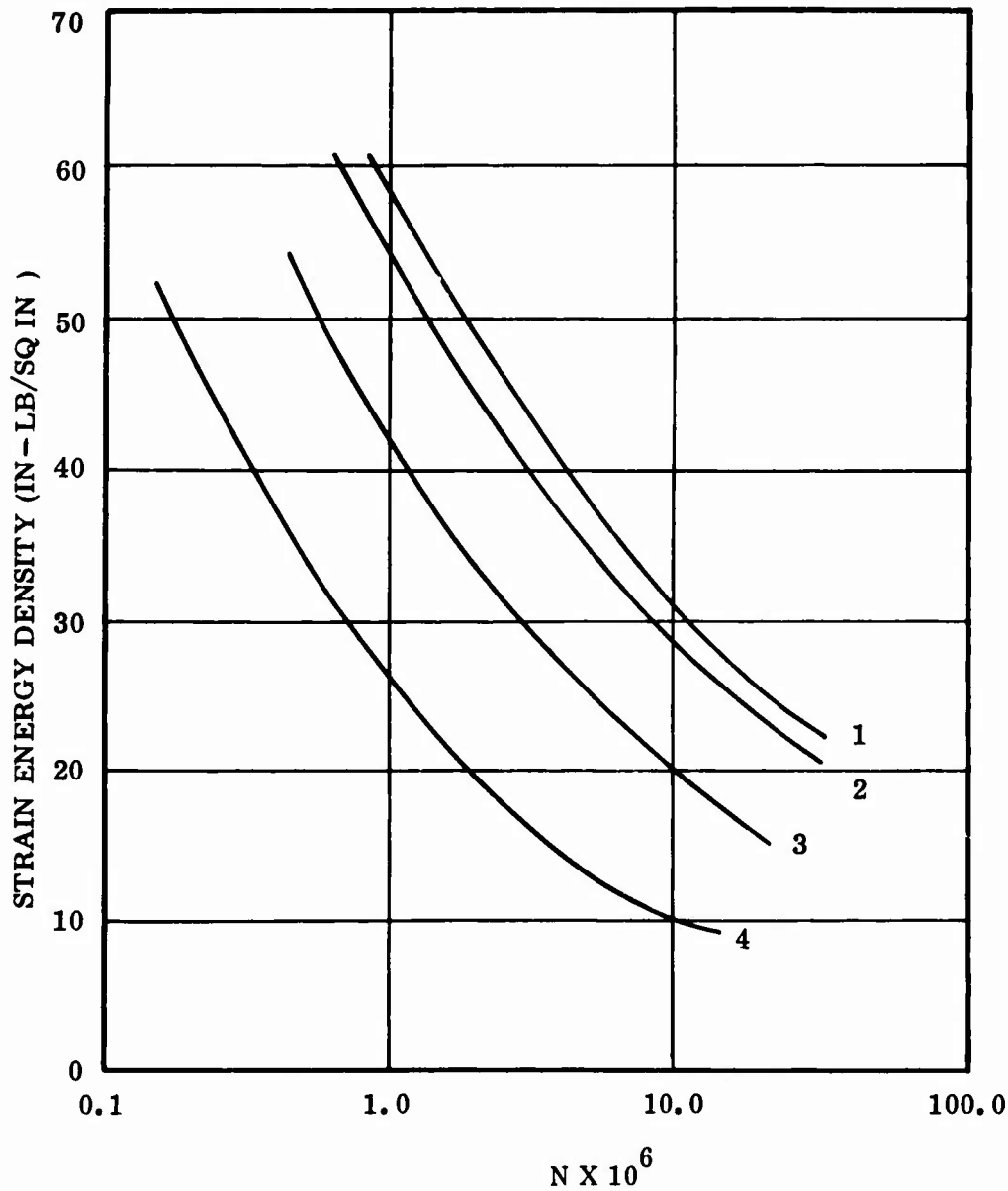

Figure 4-11. Strain Energy Density Failure Surface

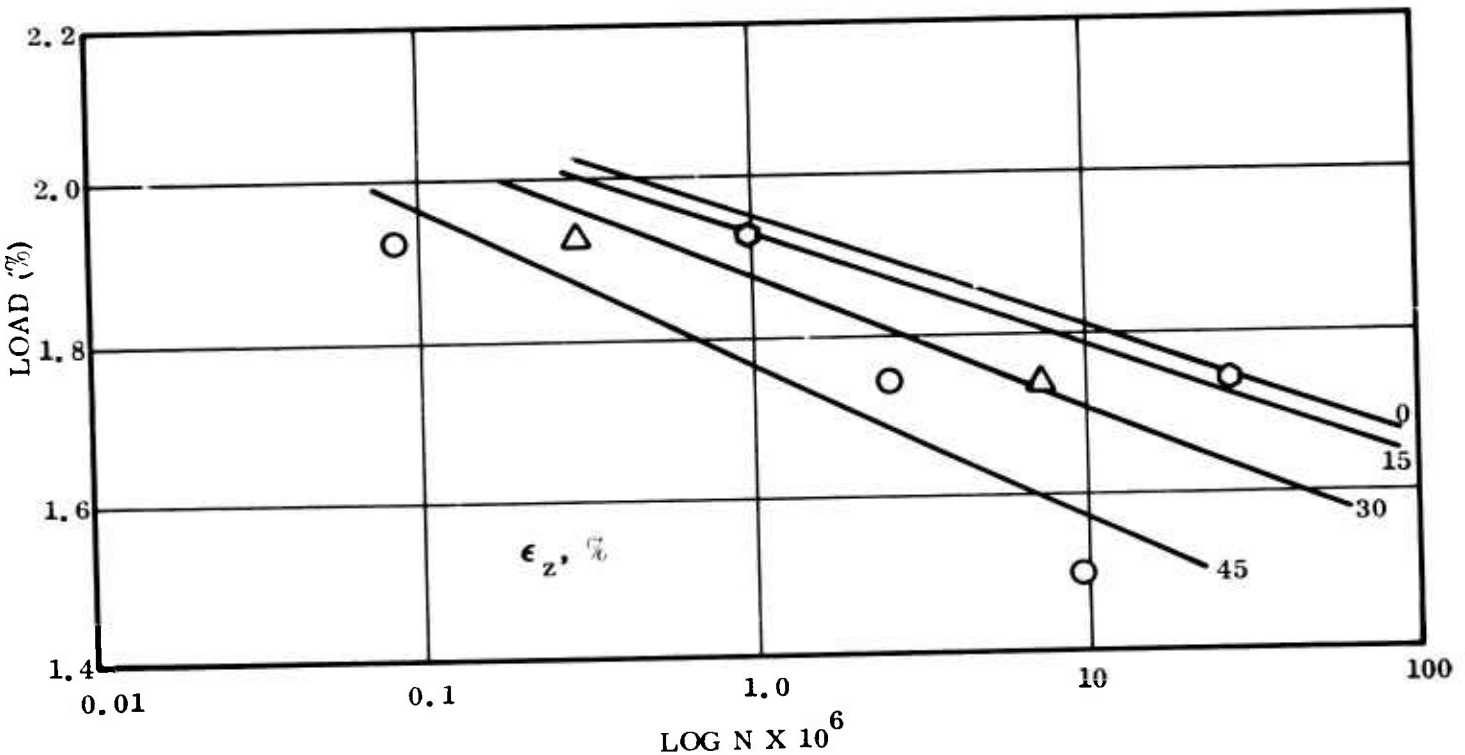

Figure 4-12. Type I R2 Bearing Failure Surface

both surfaces is shown in Figure 4-13. Because of symmetry, only the upper half of the pad was modeled. The first run was for a torsional load of 30% applied by a displacement in the theta direction of 0.86 deg along the edge of the rubber next to the steel. There was a sliding boundary in the radial direction with hoop displacement fixed along the lower edge.

The second run was completed with a static compression of 30%. An axial displacement of -0.015 in. was placed along the upper edge. As before, there was a sliding boundary condition on the lower edge.

These two computer runs, along with the R2 bearing failure surface obtained experimentally (Figure 4-10), were used to draw the new failure surfaces. From the torsion run, the maximum shear stress (τ_{max}) and strain energy density (U) could be found for a torsional load (γ) of 30%. Then the hydrostatic pressure ($\bar{P}$) for a static load (ϵ_z) of 30% was taken from the other run at the position where τ_{max} and U were largest on the torsion run. Maximum shear stress, strain energy, density, and hydrostatic pressure values for other values of torsional or static load were calculated using the following equations:

$$\tau_{max} \mid_{\gamma = x} = \left(\frac{x}{0.30}\right) \tau_{max} \mid_{\gamma = 0.30}$$

$$U \mid_{\gamma = x} = \left(\frac{x}{0.30}\right)^2 U \mid_{\gamma = 0.30}$$

$$\bar{P} \mid_{\epsilon_z = x} = \left(\frac{x}{0.30}\right) \bar{P} \mid_{\epsilon_z = 0.30}$$

Photographs were taken during the Type I bearing fatigue program to document the failure phenomenon. In Figure 4-8 the progress of reversion was traced as the specimen was fatigued. The typical rubber reversion pattern is shown in Figure 4-14 for specimen R2-12. This specimen had a torsional spring rate reduction of 20% at 25 megacycles. This figure shows its condition after 8.9 megacycles. At this time, the static spring rate was reduced by only 7% although

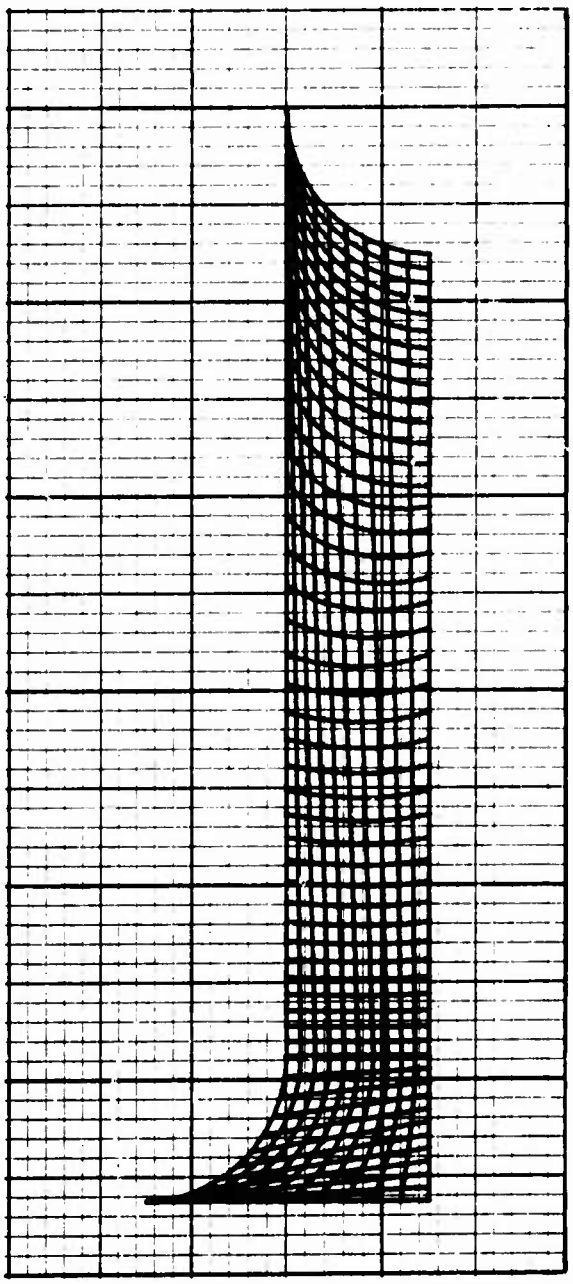

Figure 4-13. Grid Network for Upper Half of R2 Bearing

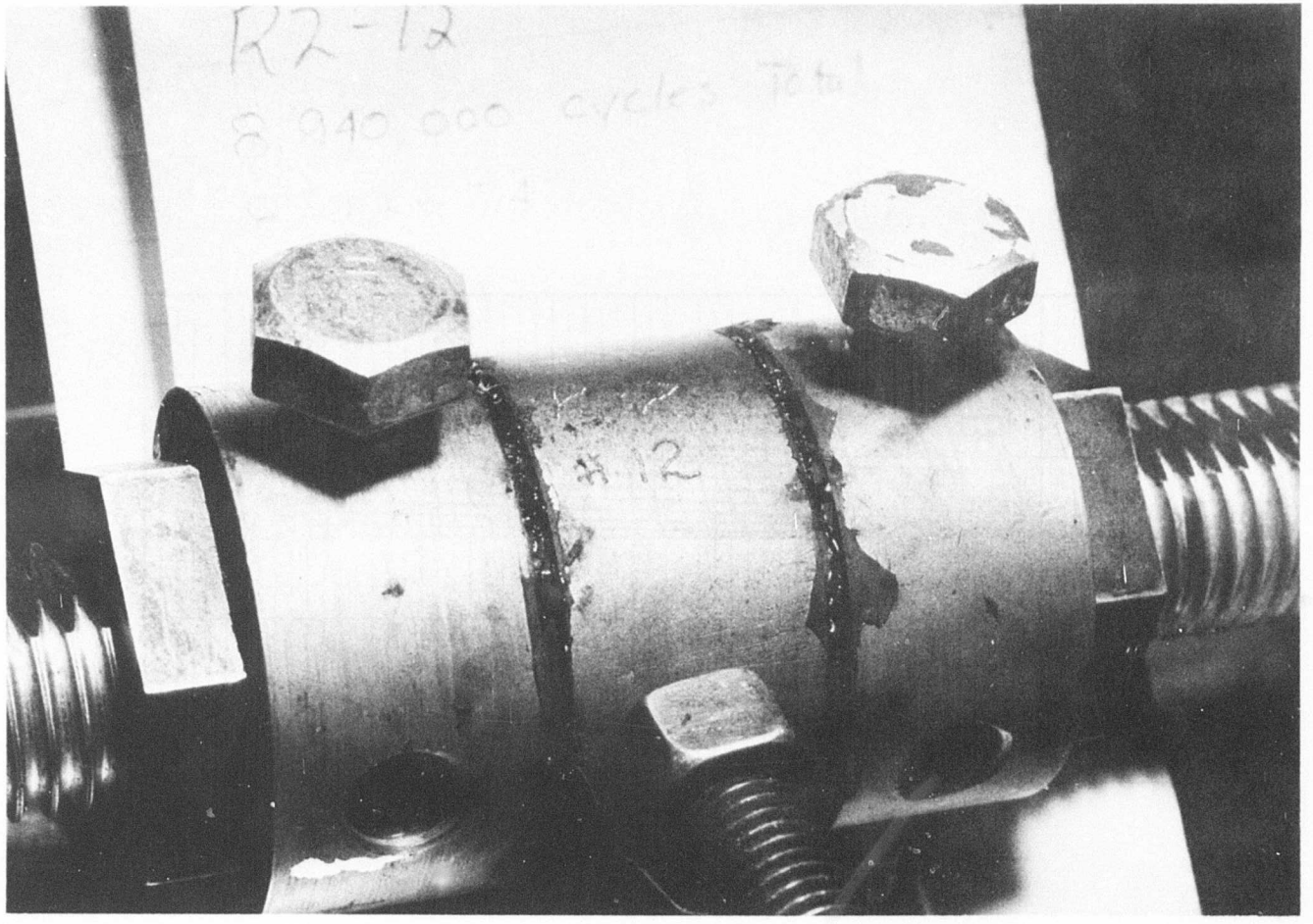

Figure 4-14. Bearing R2-12 at 8.9 Megacycles

considerable reversion is present. This amount of reversion was common in most specimens before appreciable reduction in spring rate.

Several Type I bearings were dissected after fatigue testing to study the reversion behavior. From these specimens, it appears that the reversion initiates as a small circular torus located at the axial center of a pad but near the pad outer edge (Figure 4-15). As fatigue continues, the reversion progresses toward the center of the pad as shown in Figure 4-16. In one case, reversion appeared to start at a pad-shim bondline, possibly indicating an initially weak bond (at least locally). Rubber to shim surface friction during the fatigue test may have induced local heating and therefore rubber reversion initiation at the bond failure site.

The rubber reversion is very pronounced at bearing failure. In most cases, reverted rubber drips from the bearing and forms a pile under the bearings as cycling continues. The bearing in Figures 4-17 and 4-18 shows the pad condition after bearing failure (20% reduction in torsion spring rate). Bearing R2-15 (as shown in Figure 4-17) has 8.9 megacycles with a reduction in torsional spring rate of only 31%. This bearing failed at 7.6 megacycles. Bearing R4-3 (as shown in Figure 4-18) has 1.7 megacycles with a reduction in spring rate of 33%. The reversion appears to be initiating at or near the bond in R4-3 but near the pad center in R2-15. Extreme reversion is shown for bearing R2-16 in Figure 4-19. This bearing "failed" at 2.7 megacycles with cycling continued until 6.15 megacycles. At 6.15 megacycles the torsional spring rate had dropped to 36% of the initial level, which corresponds roughly to that expected by the 0.25 in. loss of rubber (see Figure 4-19).

Most of the specimens failed by the reversion process as shown in previously referenced photographs. However, two radically different failure mechanisms were observed. The first is shown in Figure 4-20 for bearing R2-11X. This bearing was subjected to an extremely high torsional shear strain ($\pm$ 157%). At this load the outer layer of rubber shredded during initial testing. However, as testing progressed the normal reversion failure was noted. A second failure type (rubber to shim debond)

Figure 4-15. Void in R2-9 Bearing Shortly After Reversion Initiation (9.5 Megacycles)

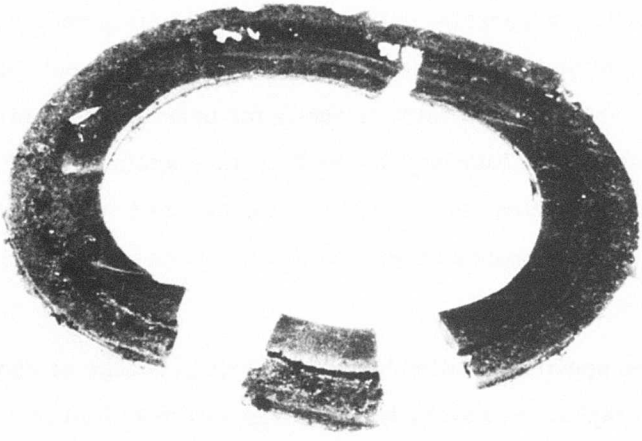

Figure 4-16. Section of R2 Bearing After Failure

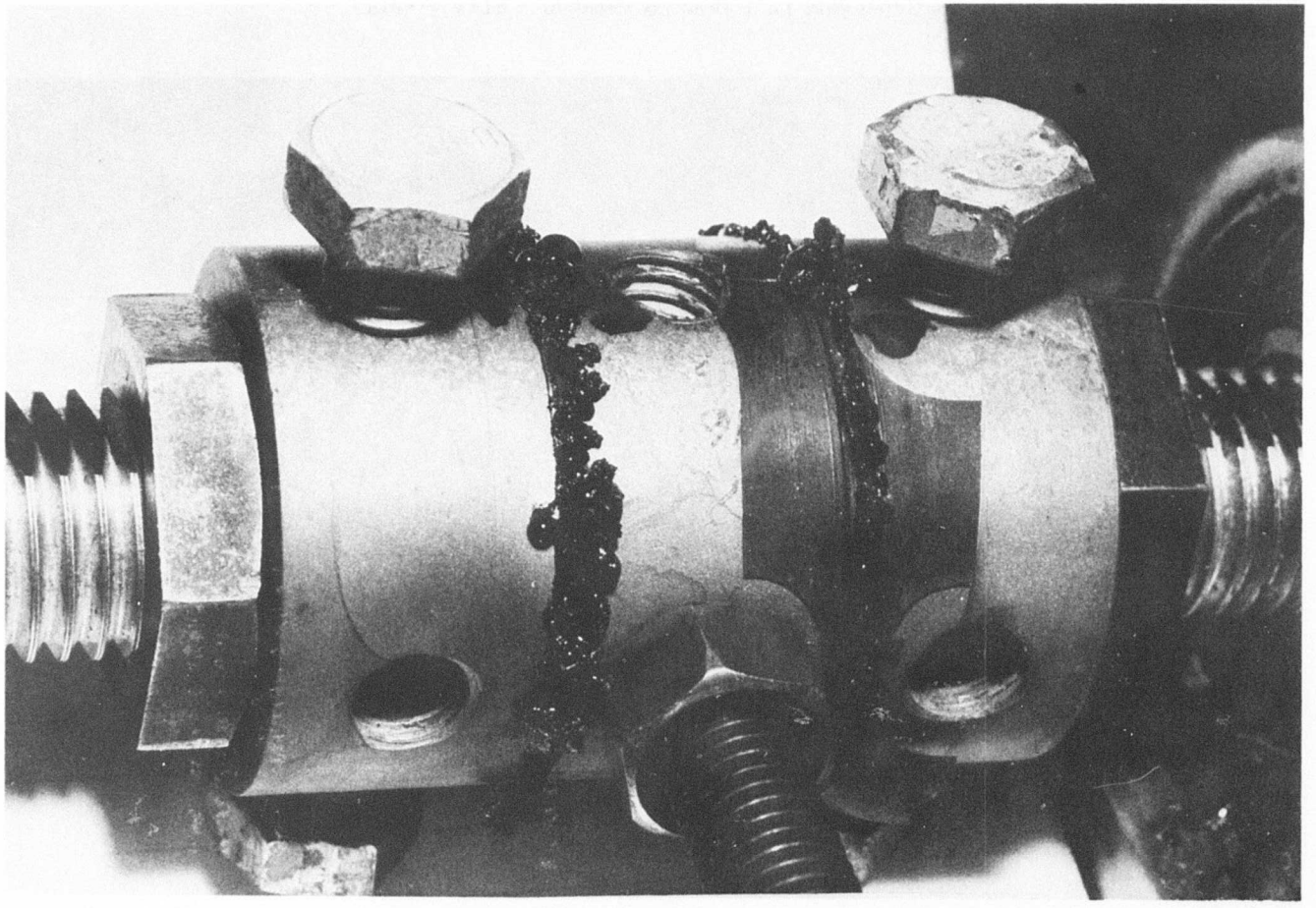

Figure 4-17. Bearing R2-15 at 8.9 Megacycles

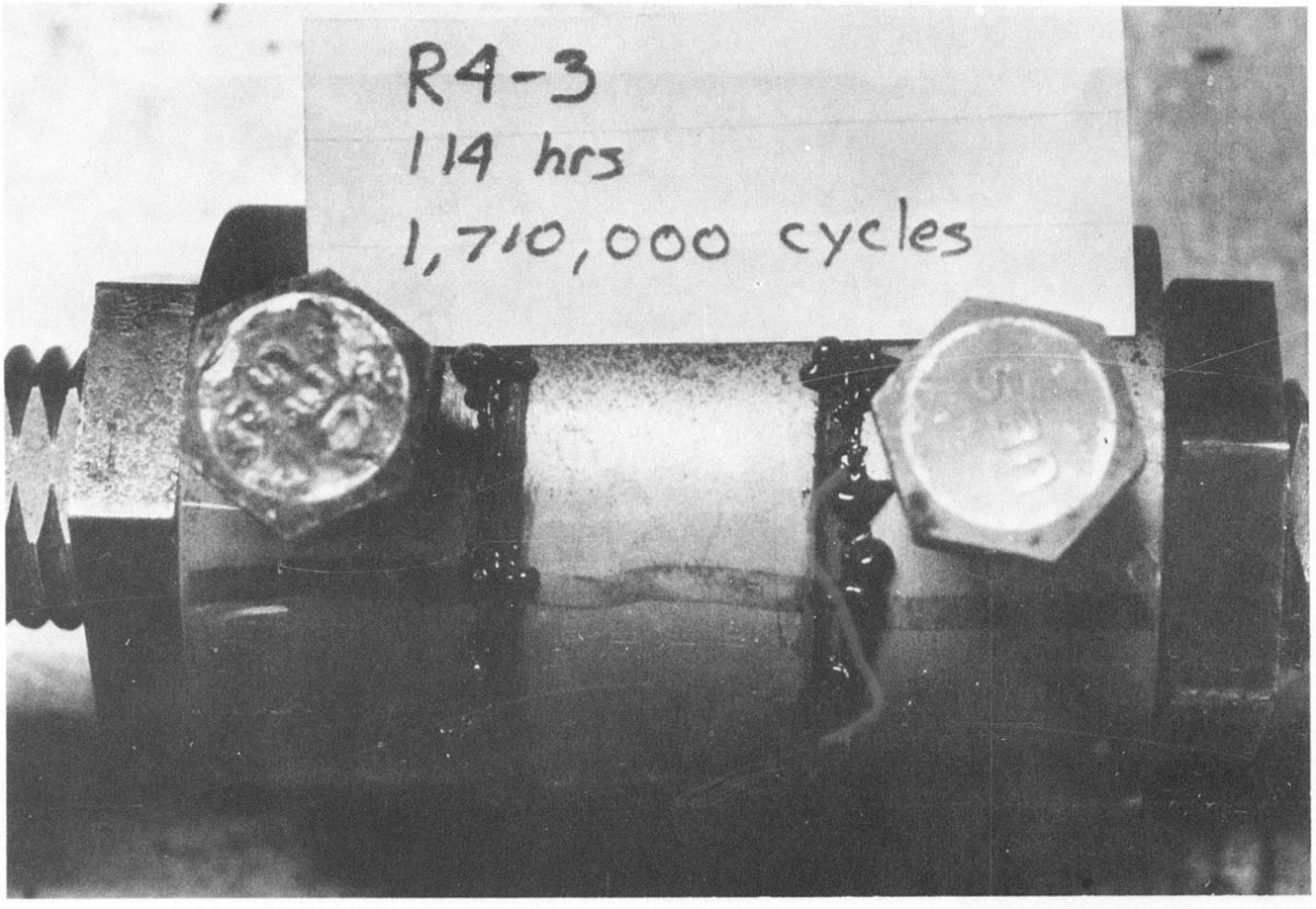

Figure 4-18. Bearing R4-3 at 1.71 Megacycles

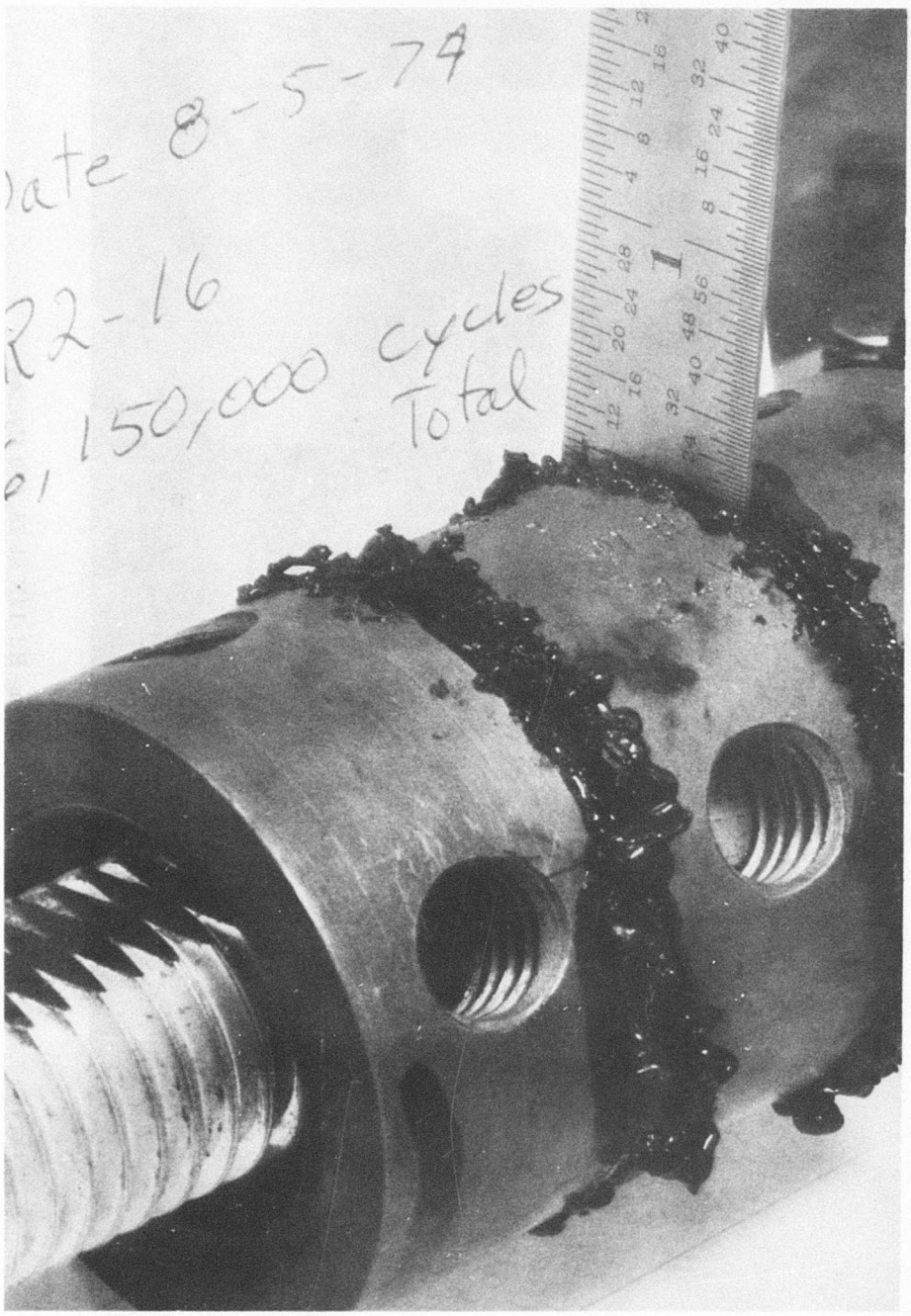

Figure 4-19. Bearing R2-16 at 6.15 Megacycles

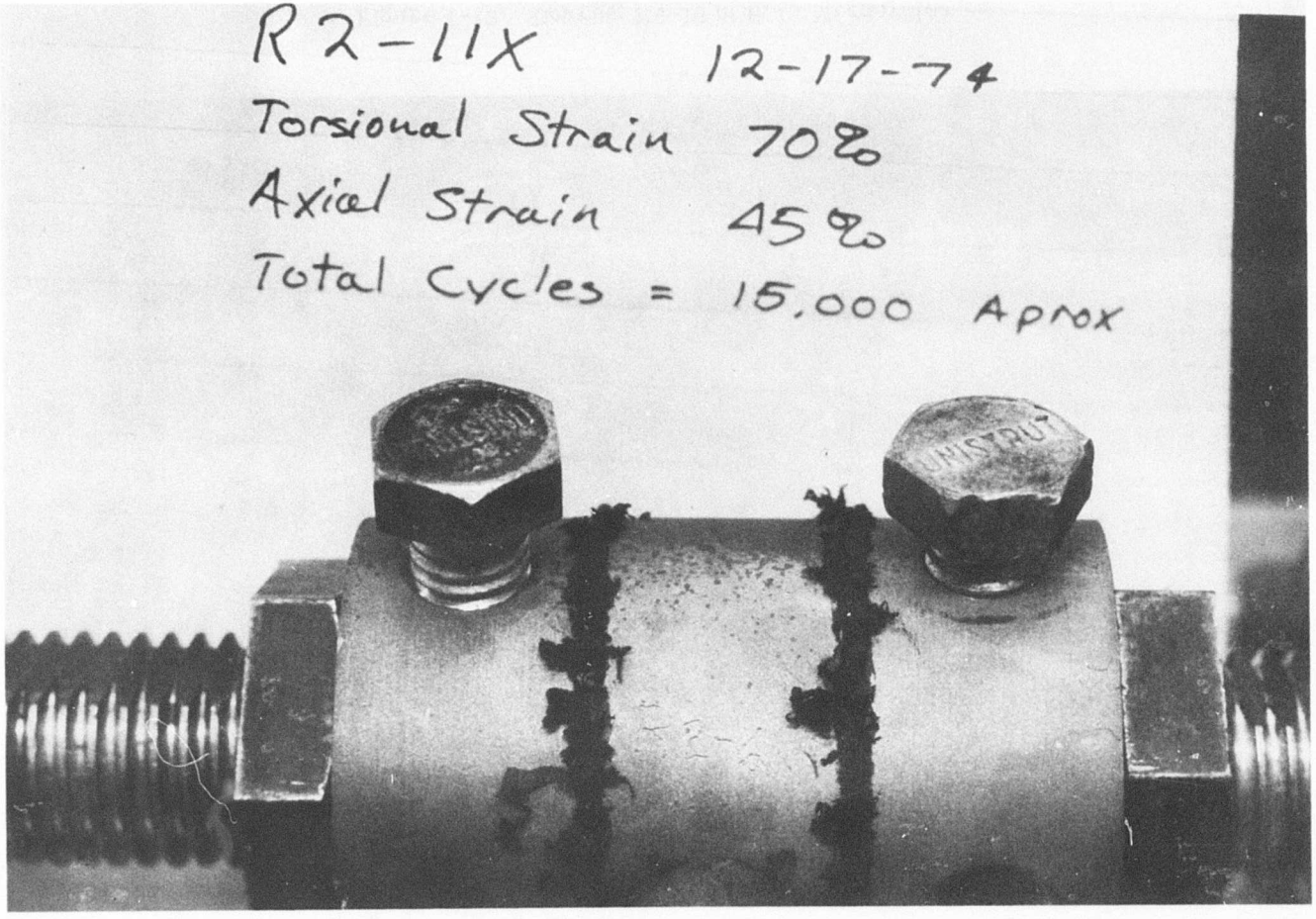

Figure 4-20. Bearing R2-11X at 15,000 Cycles

was observed in the SA series bearing as shown in Figures 4-21 and 4-22. A small amount of reversion can be seen in the vicinity of the bondlines. Analytical treatment of related fracture mechanics and crack propagation is discussed in Appendix C.

Data from the additional R2 bearing tests are presented in Table 4-4. By comparing these data with the R2 failure surface (Figure 4-10), the following observations are made:

1. The R4 specimens, which have thicker pads than the R2 specimens, failed near the failure surface but at an earlier time. This is probably due to less efficient heat transfer in the R4 specimens, thus resulting in higher temperatures.
2. The "A" series of specimens have a consistently shorter life than comparable R2 specimens. This is consistent with finite-element stress analyses, wherein a 16% lower torsional shear stress is predicted for the R2 specimens for the same angular deflection (see Appendix A).
3. A life greater than 30 million cycles was predicted for all "C" series bearings at the scheduled load levels. Testing was terminated before failure in all cases.
4. The "CR" series bearings performed as expected from the R2 bearing failure surface.
5. The SA series bearings all had center shims with no elastomer fillets. Analytically this means that linear elasticity theory would predict infinite stresses at the outer radius of the elastomer-shim interface. As explained in Appendix A , this means that for real materials, the stresses are very large at that interface. These tests verified the theory in that the SA series bearings were the only ones which had debonding before rubber reversion was noted. Therefore, we feel that the theory has been verified, and the experiments

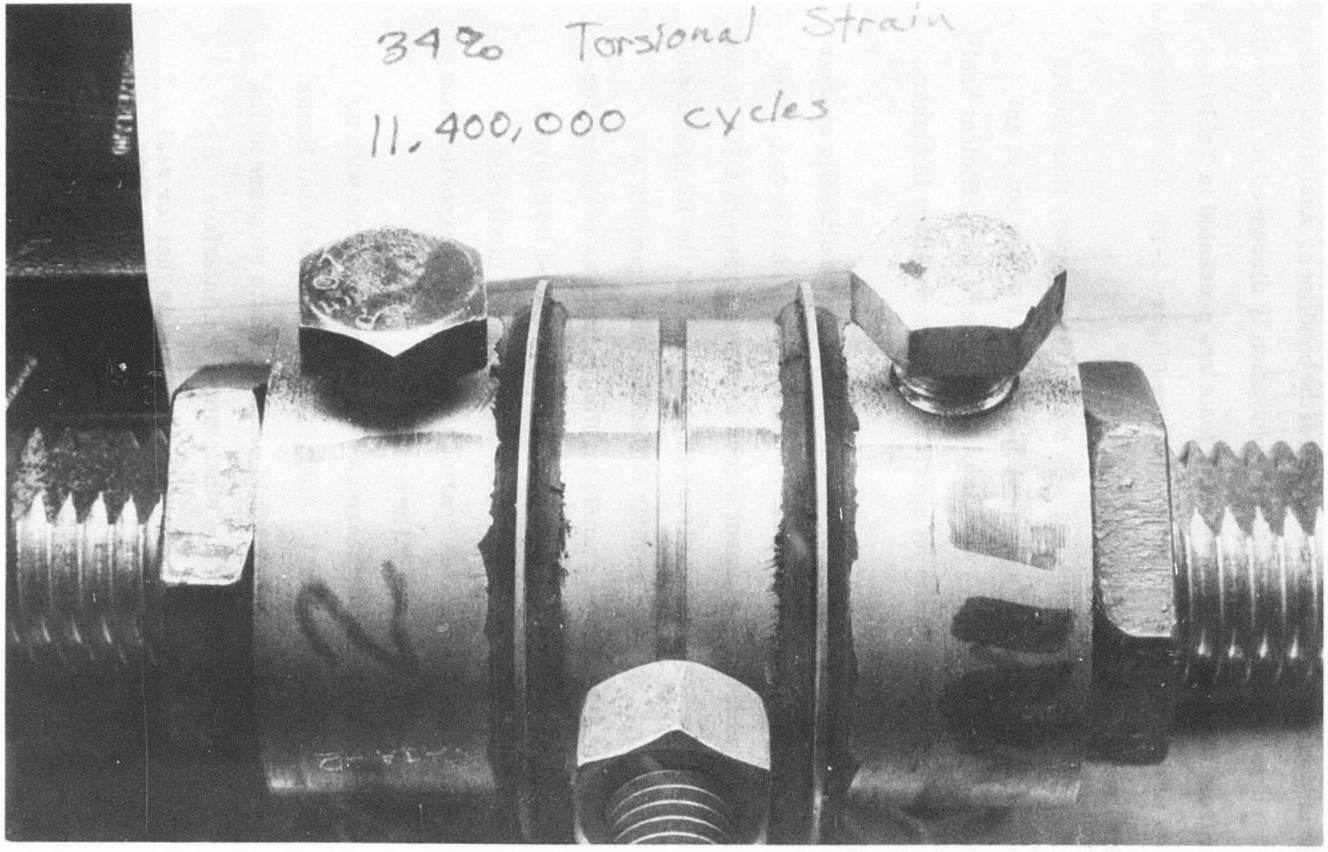

Figure 4-21. Bearing SA1A-1 at 11.4 Megacycles

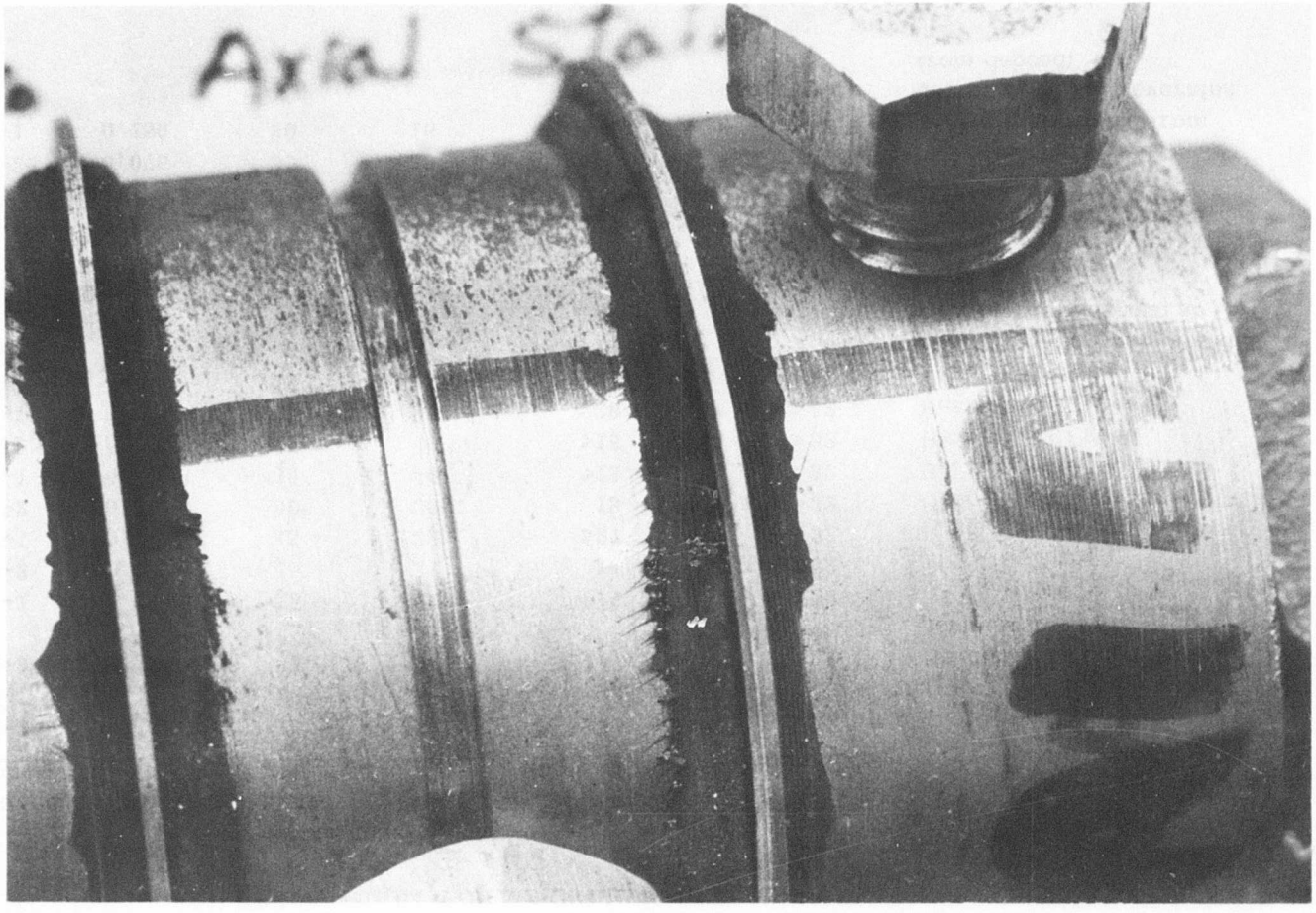

Figure 4-22. Bearing SA1A-1 at 11.4 Megacycles

TABLE 4-4

FAILURE SUMMARY FOR MISCELLANEOUS TYPE I BEARINGS

Specimen Number	Thickness (in.)	Axial Strain (%)	Torsional Strain (%)	Fatigue Life (megacycles)	R2 Life (megacycles)	Comments
R4-2	0.15	15	22	>32	>32	
R4-1	0.15	22	55	3	13	
R4-3	0.15	30	55	<1.7	7	Bond failed before first periodic
A1-1	0.075	15	41	6.7	>32	
A2-2	0.10	15	31	11	>32	
A3-1	0.125	15	22	>27	>32	
A4-2	0.15	30	36	13	>32	Debond initiated 12.6
C1-1	0.075	15	40	>13	>32	Bearing still good
C1-2	0.075	15	40	>16	>32	Bearing still good
C2-1	0.1	15	31	>26	>32	Bearing still good
CR2-1	0.1	15	31	>32	>32	
CR2-2	0.1	0	84	<2.16	1.5	Failed before first periodic
SA1A-1	0.075	30	35	17	>32	Considerable debond at 12.6
SA1A-2	0.075	30	35	13.5	>32	
SA4A-1	0.150	30	16	~22	>32	Considerable debond at 12.6
SA1B-1	0.075	30	35	14.5	>32	12.6 debond from center shim
SA1B-2	0.075	30	35	14.5	>32	
SA4B-1	0.150	30	16	~22	>32	12.6 slight debond from center shim (15 reversion from debond)

have demonstrated the reduction in service life caused by improper elastomer-to-pad bond termination edge geometry (Table 4-4).

We also noted that the bearings with thinner pads failed first. This would not have been predicted if the failure mode had been due to heat buildup in the elastomer. Therefore, the failure is attributed strictly to debond caused by improper bond terminations. The reason for the bond to be weaker for thin pads is not understood at the present time. In fact, this is opposite to the trend seen in bonding of "butt" joints loaded in tension (i.e., bond strength increases with decreasing adhesive thickness). A fracture mechanics analysis is recommended to determine if the SA series bearings' increase in fatigue life with increasing pad thickness can be predicted analytically. However, the problem is somewhat academic in that we do not recommend construction of bearings with points of singular stress.

4.3 TEST RESULTS SUMMARY

A total of 45 Type I bearings were tested with various loads and geometries. It was rather difficult to predict, at the beginning of the test program, what load levels should be tested in order to obtain bearing failure with a reasonable number of cycles (less than 50 million). For those specimens which failed at less than one million cycles, the periodic data (static spring rates) were often insufficient to determine the number of cycles for which the torsional spring rate decreased by 20%. However, by testing additional samples and adjusting loads and times for which periodic data were taken, we feel that the failure surface generated (Figure 4-10) is fairly accurate although only one test per data point was obtained. In addition, we have shown experimentally that the pad designs predicted by the finite-element computer program to have low stresses actually have greater service life.

Elastomer thickness was seen to decrease service life for those bearings in which elastomer reversion was the failure mechanism. In the SA series bearings, the failure mechanism was elastomer to shim debond, in which case the fatigue life increased with increasing pad thickness.

5.0 STABILITY

This section describes the stability tests performed on the elastomeric bearing specimens. Experiments carried out to determine the critical buckling loads of various specimens indicated good agreement with theoretical predictions.

5.1 THEORETICAL APPROACH

The theoretical approach used to predict instability is a column consisting of alternate elements of elastomer pads and shims is described in Volume II (ref 5-1). It was shown that the buckling load of the entire column is characterized by the bending and shear stiffness of a single unit in the column. The theory was developed by Haringx (ref 5-2, 5-3, 5-4) and Gent (ref 5-5), who modified the classical theory of buckling to take into account the shear deflection of column elements. Gent corrected Haringx's expression for the bending stiffness of thin pads to improve the correlation between theory and experiments for long columns.

The above theories predict a lower buckling load for short columns because of the assumption that the column is incompressible. This assumption is generally not correct for helicopter bearings which are short and compress significantly before buckling. The present method uses an iterative technique with the above theories to correct for the changing geometry of the column as it is being compressed. This procedure which improves correlation between theory and experiment has been incorporated into the computer program (ref 5-6) as a separate module.

The method used for the iterative procedure is as follows. Starting with the initial geometry, the program calculates the buckling load and the corresponding critical compression for the first iteration. The thickness of the elastomer pad is modified to account for this compression, and the buckling load and critical compression are calculated again for this modified column. These iterations continue until the percentage change in the load between two successive iterations is less

than a specified factor. Table 5-1 shows the buckling load, elastomer pad thickness, and total percentage of compression for each successive iteration for a typical stability specimen.

TABLE 5-1

COMPUTER PROGRAM OUTPUT FOR A TYPICAL TYPE I STABILITY SPECIMEN*

	Buckling Load (lb)	Elastomer Pad Thickness (in.)	Critical Compression (%)
Iteration No. 1	38,519	0.07500	9.3485
Iteration No. 2	46,967	0.06799	9.3756
Iteration No. 3	46,995	0.06797	9.3757
Iteration No. 4	46,995	0.06797	9.3757

*Column height = 1.725 in.; No. of steel shims = 15; No. of elastomer pads = 16; shim thickness = 0.035 in.; elastomer pad thickness = 0.075 in.; elastomer modulus of elasticity = 290.0 psi.

It can be seen from Table 5-1 that the predicted buckling load (46,995 lb) is 22% higher than would have been predicted had the iterative procedure not been used (38,519 lb).

5.2 STABILITY SPECIMEN FABRICATION

Per Test Plan TWR-7838 (Appendix A), specimens were fabricated for the stability test requirements. Two configurations were made.

The procedure used for fabrication is given below for the two different configurations.

5.2.1 Configuration 1

1. Solvent-wipe each of the two end steel disks and reinforcements.
2. Grit-blast, with silica sand, bonding surfaces of disks and reinforcements.
3. Solvent-wipe each of the two steel disks and reinforcements.
4. Obtain Chemlok 205, stir thoroughly, and brush a coat on grit-blast-cleaned side of each disk. Air-dry 15 minutes.
5. Obtain Chemlok 220, stir thoroughly, and brush a coat on 205 painted surface. Air-dry 30 minutes.
6. Repeat Chemlok procedures by painting both sides of the reinforcements.
7. Obtain elastomer and cut a disk the same diameter as the steel disk.
8. Layup procedure is as follows:
   a. Place steel disk in mold, Chemlok side up.
   b. Place a piano wire spacer on top of disk (Figure 5-1).
   c. Place an elastomer pad on disk.
   d. Place a reinforcement in mold.
   e. Install a piano wire spacer in mold.
   f. Place an elastomer pad in mold.
   g. Repeat process until all reinforcements are in mold.
   h. Finish off by placing steel disk on last pad of elastomer in mold.

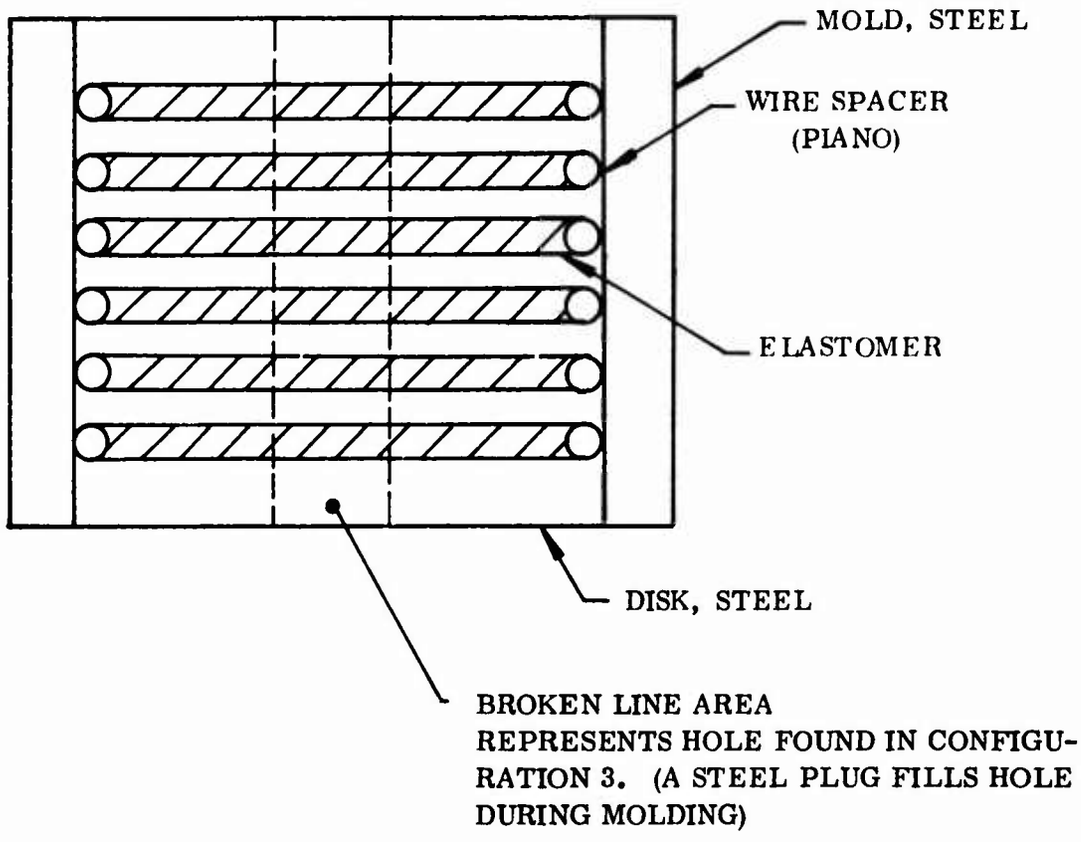

Figure 5-1. Stability Mold Configuration

9. Place mold assembly in a preheated press at 300° F for 1 hr 15 minutes.
10. Disassemble by pushing specimen out of mold and removing wire spacers.
11. Identify specimen with applicable identification.

5.2.2 Configuration 2

Repeat the process indicated for Configuration 1 except install a steel rod in center hole before curing.

5.3 STABILITY EXPERIMENTS

The primary objective of the study was to generate stability test data to verify the theoretical predictions. Stability tests were performed on flat, columnar shaped, Type I elastomeric bearing specimens. Each specimen was cylindrical in shape, 3.0 in. in diameter, and made of alternating flat layers of elastomers and steel shim reinforcements. The principal geometric variables were:

1. Thickness of elastomer pads.
2. Thickness of shim reinforcements.
3. Number of elastomer pads and shims.
4. Inside core diameter.

A total of 19 specimens utilizing two basic configurations (Figure 5-2 and Table 5-2) were built. The initial attempt at fabricating these specimens showed shim spacing and concentricity problems. This attempt gave a better insight into fabrication problems and methods to keep such problems from recurring. With this added experience, some of the stability specimens that showed serious defects were rebuilt. Each specimen was inspected to determine end-to-end plate parallelism and specimen height. The thickness of each elastomer pad was also measured.

TABLE 5-2

SPECIMEN DIMENSIONS

Specimen Designation	t_s	N_s	t_e	N_e	h_c	D_o	D_i	D_o/D_i
SL3 and SL4	0.063	21	0.075	22	2.97	3.0		
SL5 and SL6	0.063	21	0.045	22	2.31	3.0		
SL7 and SL8	0.063	15	0.125	16	2.95	3.0		
SL9 and SL10	0.063	15	0.075	16	2.15	3.0		
SL11 and SL12	0.063	15	0.045	16	1.67	3.0		
SL13 and SL14	0.063	11	0.125	12	2.19	3.0		
SL15 and SL16	0.063	11	0.075	12	1.59	3.0		
SL17 and SL18	0.063	11	0.045	12	1.23	3.0		
SS2	0.035	15	0.075	16	1.73	3.0		
SD1	0.063	15	0.075	16	2.15	3.0	1.00	3.0
SD2	0.063	15	0.075	16	2.15	3.0	2.00	1.5

Where: t_s = shim thickness
N_s = number of shims
t_e = elastomer thickness
N_e = number of elastomeric layers
h_c = height of laminate composite
D_o = outside diameter
D_i = inside diameter

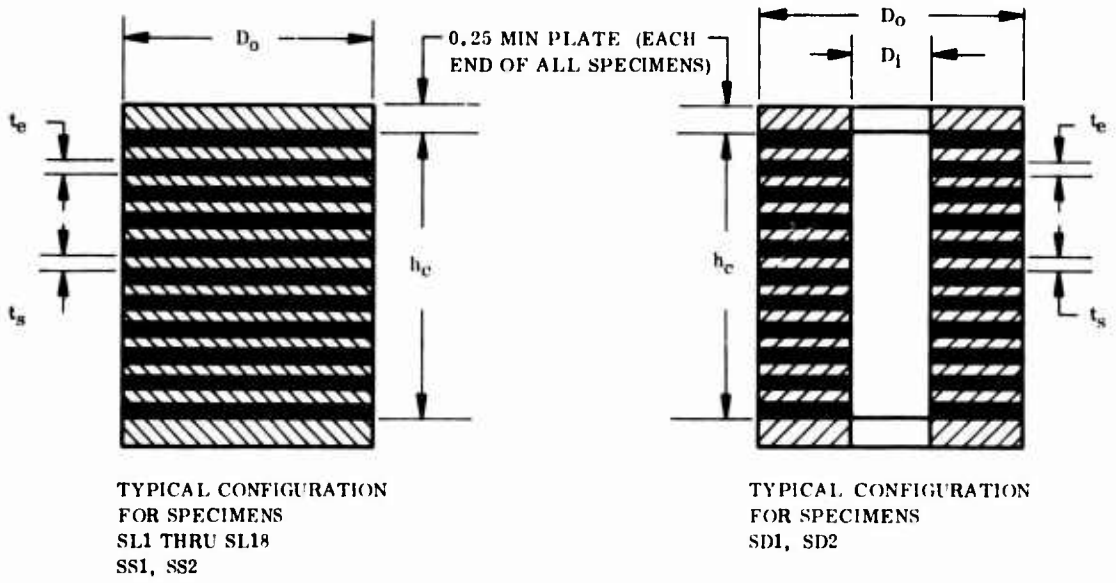

Figure 5-2. Typical Specimen Configurations

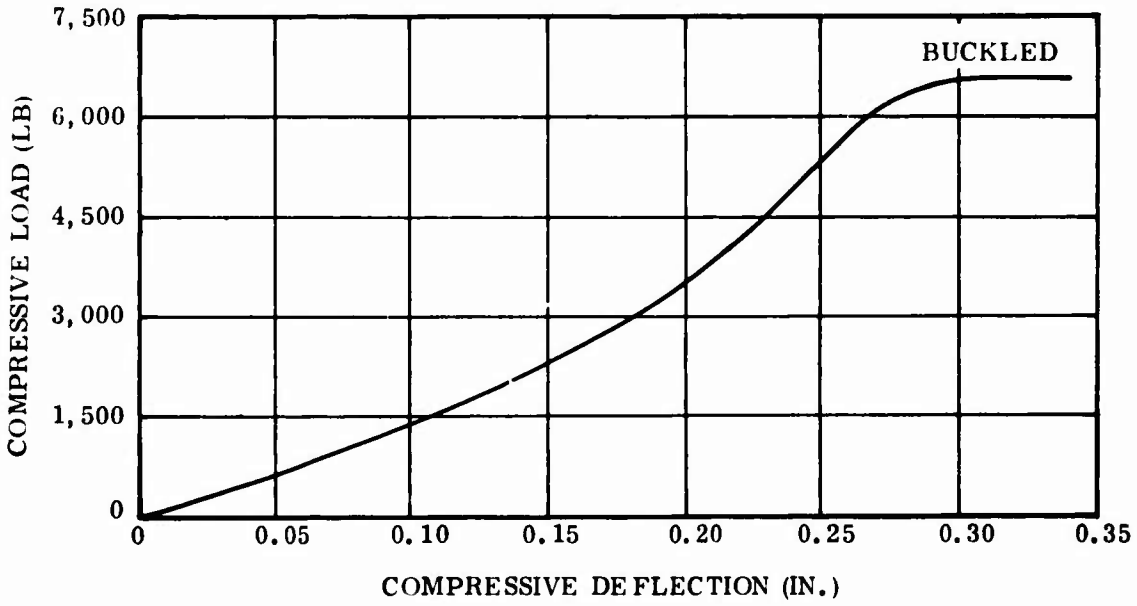

Figure 5-3. Experimental Load-Deflection Relation for SD2 Specimen

Prior to stability testing, each specimen was initially subjected to five cycles of "stress softening" under an axial load. Loading was applied at the rate of 0.02 in./min from 0 to 6% strain and back to 0% strain, completing one cycle. A load deflection plot of each cycle was continuously recorded. If there was any significant change of the load-deflection plot between the last two cycles, stress softening was continued until the change disappeared.

5.3.1 Buckling Load Determination

The well-known approach to determine the onset of buckling is to load the column until there is a marked increase in deflection for a slight change in the axial load. Figure 5-3 shows the load deflection curve for a typical stability specimen.

The relation between the axial load and the compression is very sensitive to the straightness of the column and the accuracy with which the load is centrally applied. All actual columns are more or less imperfect, so the above method will yield approximate values for the buckling load.

Southwell's (ref 5-7) method, however, provides a reliable approach for analyzing experimental data. The power and versatility of this method has great significance in the correlation of experimental data with theory in all linear instability problems (ref 5-8). By this method, the test results of an imperfect column can be used to predict the buckling load of the corresponding perfect column. According to this method (Figure 5-4), the lateral deflection y at the center of the column is measured as the compression load P is increased. If y/P is plotted against y, the test results will be approximately a straight line, and the inverse of the slope of this line is the critical buckling load P_c. The intercept with the y axis gives the initial imperfection.

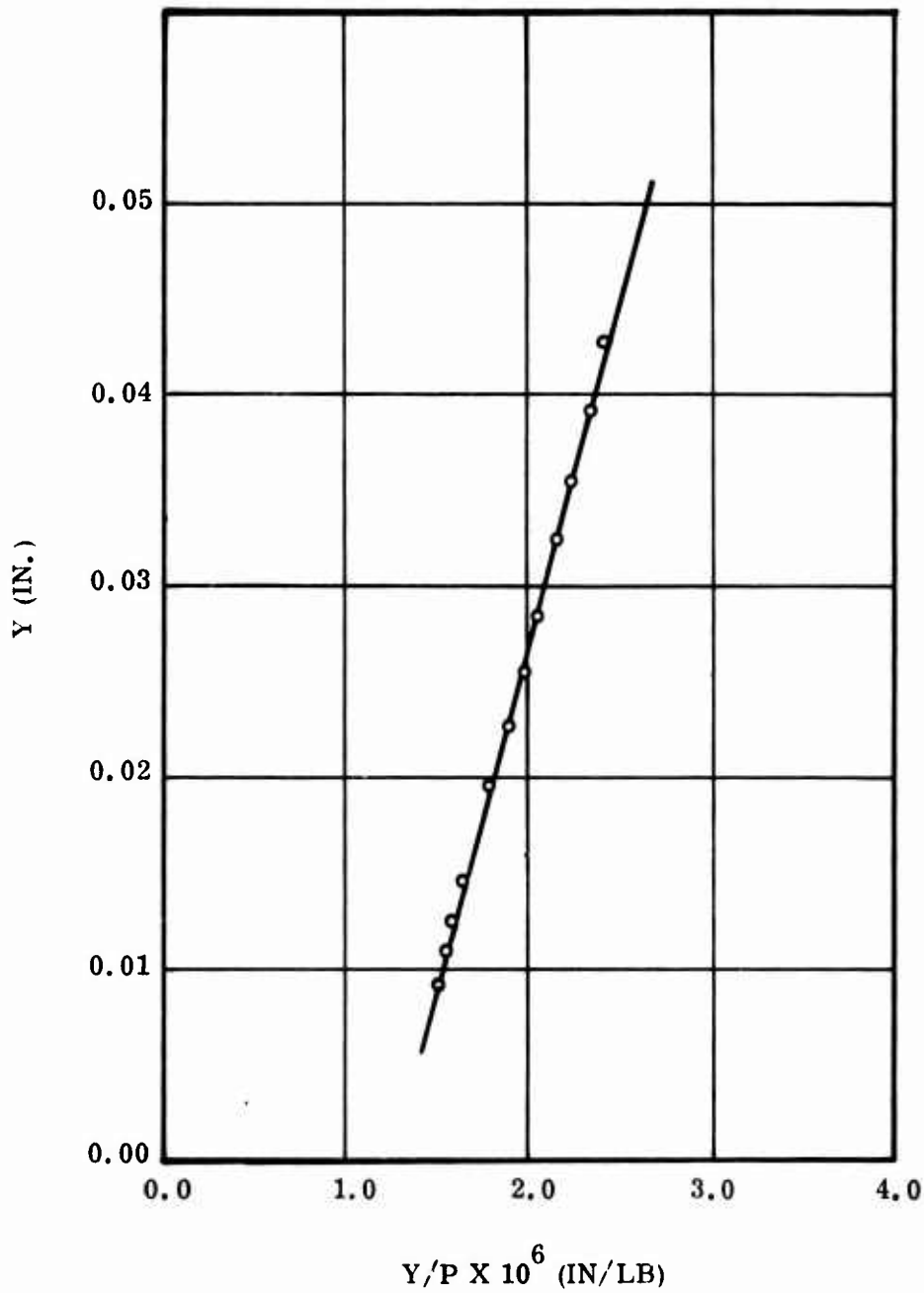

Figure 5-4. Southwell Plot for SL4 Specimen

Southwell's procedure for experimentally predicting the buckling load of a column is accurate if the maximum lateral deflection occurs at its center. Since actual columns are not perfect, the maximum lateral displacement is normally observed away from the center. This imperfect behavior was noticed in some of our stability specimens even after care was taken to manufacture the specimens to close tolerances. Since Southwell's procedure is not invalidated even by large eccentricities, the specimens were loaded in the machine using a 1-deg wedge plate (Figure 5-5). The wedge plate gave the specimen a slight tilt, causing the maximum transverse deflection to occur at the center.

To compare results as given by the theory, experiment, and Southwell's method, four specimens were tested to failure. Table 5-3 shows the results to be in good agreement, thereby indicating that the Southwell method is a reliable approach in determining the buckling load of elastomeric bearings without testing them to failure.

After the validity of Southwell's method was established, the stability tests on the remaining specimens were carried out. Table 5-4 shows the correlation. Figure 5-6 shows a photograph of a stability specimen under axial load. The dial indicator was used to measure the lateral deflections.

It was found that better correlation was obtained for the SD1 and SD2 specimens if the first iteration loads were compared with the experimental results. These specimens showed extremely large compressions (about 35%) according to the theory. Since all the equations are derived under the assumption of Hooke's law, the validity of its application to such large compressions is questionable. Also, the expressions for bending and shear stiffness for an annular pad are not exact, and these stiffnesses should be determined experimentally.

5.4 BUCKLING OF TYPE III SPECIMENS

The buckling equation presented in Volume II was used to predict the buckling loads for the Type III specimens. Experimental data for the Type III

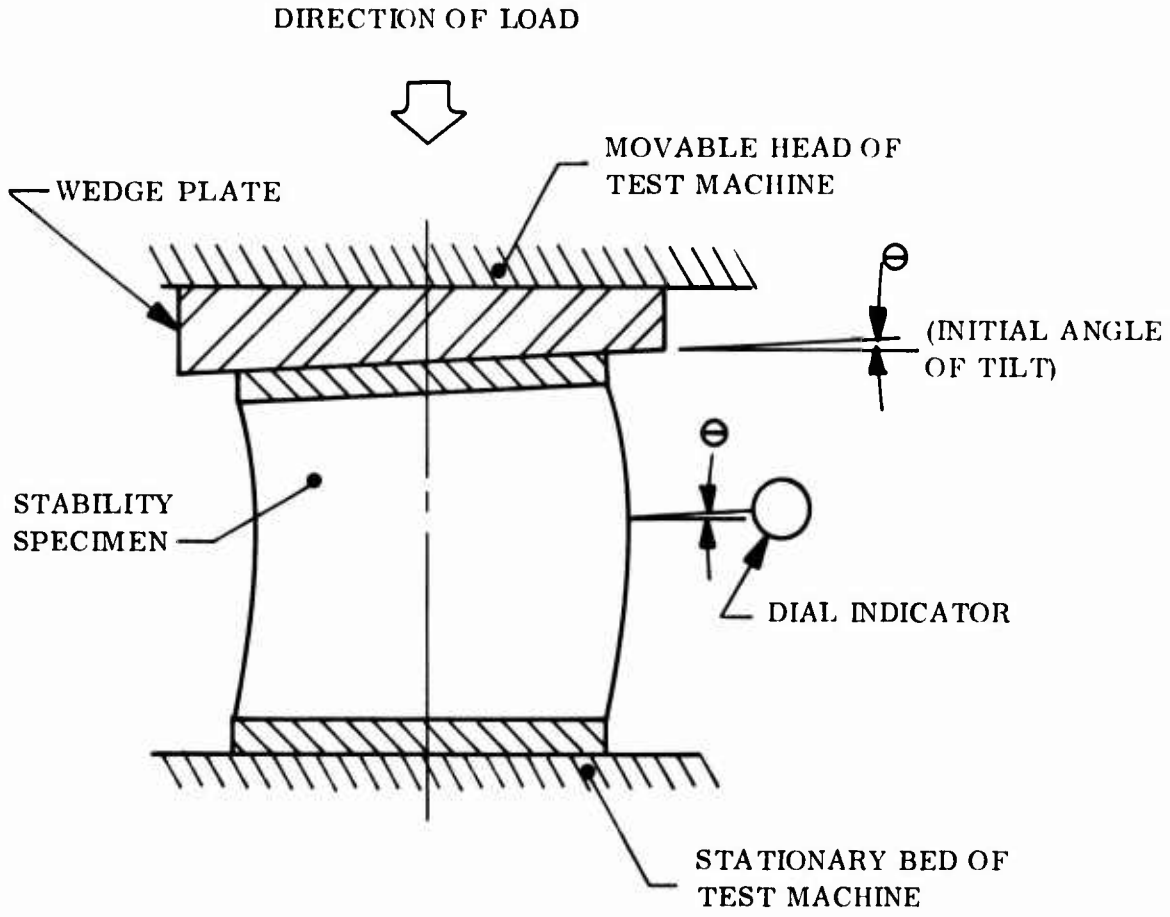

Figure 5-5. Installation of Wedge Plate and Stability Test Specimen in Test Machine

TABLE 5-3

COMPARISON OF THEORY, EXPERIMENT, AND SOUTHWELL'S METHOD

Specimen Designation	No. of Elastomer Pads	No. of Steel Shims	Elastomer Pad Thickness (in.)		Column Height (in.)		Buckling Load (lb)		
			Design	Actual	Design	Actual	Predicted*	Experiment	Southwell's Method
SL5	22	21	0.045	0.0388	2.313	2.1766	121,780	142,500**	142,000
SL6	22	21	0.045	0.0385	2.313	2.1700	123,705	120,750	Bad data
SL7	16	15	0.125	0.1218	2.945	2.8548	17,636	16,200	14,535
SL14	12	11	0.125	0.1261	2.193	2.2062	23,981	24,000	22,830

*Based on actual pad thickness.

**The specimen had metal-to-metal contact between two shims after the axial load was applied. This reduced the effective height of the column, resulting in a higher buckling load.

TABLE 5-4

CORRELATION BETWEEN THEORY AND SOUTHWELL'S METHOD

Specimen Designation	Elastomer Pad Thickness (in.) Design	Actual	Column Height (in.) Design	Actual	Buckling Load (lb) Predicted*	Southwell's Method	Remarks
SL3	0.075	0.0704	2.973	2.8298	36,415	37,500	
SL4	0.075	0.0705	2.973	2.8173	36,308	36,585	
SL8	0.125	0.1224	2.950	2.8810	17,641	--	Showed excessive lateral deflection, indicating presence of voids.
SL9	0.075	0.0696	2.145	2.0580	55,111	58,333	
SL10	0.075	0.0734	2.145	2.0550	49,428	57,692	
SL11	0.045	0.0418	1.670	1.6140	154,942	--	Unequal shim spacing. Experimental data showed significant variation for each load increment.
SL12	0.045	0.0431	1.670	1.6350	145,627	--	Shims not parallel.
SL13	0.125	0.1164	2.190	2.0840	28,225	--	Unequal shim spacing. Specimen did not show maximum deflection in center.
SL15	0.075	0.0653	1.590	1.4250	91,391	--	Data for Southwell plot was not reliable.
SL16	0.075	0.0656	1.590	1.4310	90,550	100,840	
SL17	0.045	0.0418	1.230	1.1940	226,889	--	Specimens were short and had thin elastomer pads. Metal-to-metal contact occurred after a small load was applied.
SL18	0.045	0.0437	1.230	1.2090	214,314	--	Same as for SL17.
SS2	0.075	0.0653	1.730	1.5890	62,249	--	Specimen was loaded up to 30,000 lb and did not indicate any instability.
SD1	0.075	0.0725	2.150	2.0600	25,971**	24,000	The 24,000 lb was obtained by testing specimen to failure.
SD2	0.075	0.0739	2.150	2.0820	9,182**	6,600	The 6,600 lb was obtained by testing specimen to failure.

*Based on actual pad thickness.
**First iteration loads.

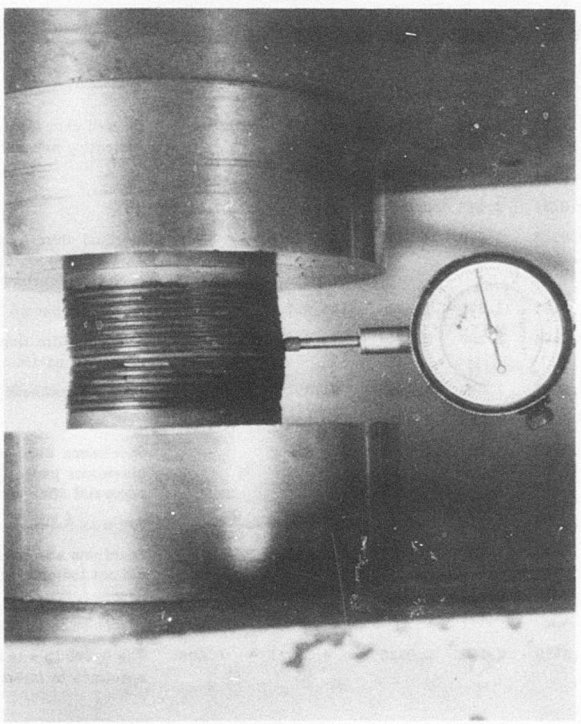

Figure 5-6. Stability Test on a Type I Specimen

specimens (Figure 5-7) show that the "B" geometry buckled because of excessive lateral deflections at 52,000 lb. The "A" geometry did not indicate any instability at this load. Using the equation for bending and shear stiffness as presented in Volume II, the theoretical buckling load was determined as follows:

Type III B: Theoretical buckling load = 41,919 lb

The above load is based on using the dimensions of the center pad and is the first iteration load. It was not modified to allow for the compression of the column. It was felt that the predictions are accurate enough considering all the approximations involved in the analysis. Further effort is required before a complete tested analysis is available.

5.5 CONCLUSIONS

Good agreement was obtained between theory and experiment for columns of Type I pads. The buckling load of a column is related to the bending and shear stiffness of a single pad, and these can easily be calculated from pad dimensions.

The analysis was also used to determine the buckling load of Type III bearings. The predictions are conservative, but additional work is required before the buckling equation can be used with confidence.

Southwell's method was found to be a reliable approach to experimentally determine the buckling load of a column without testing to failure.

5.6 RECOMMENDATIONS

Buckling experiments call for diligence in the setup and in the manufacture of specimens. An imperfect column differs considerably from that of a perfectly straight column. In reality, a perfectly straight column does not exist in engineering structures. The Southwell method is useful in estimating the magnitude of any imperfections.

Every care should be exercised to improve the accuracy of the column tests. Sometimes this may require a few simple adjustments in the testing machine.

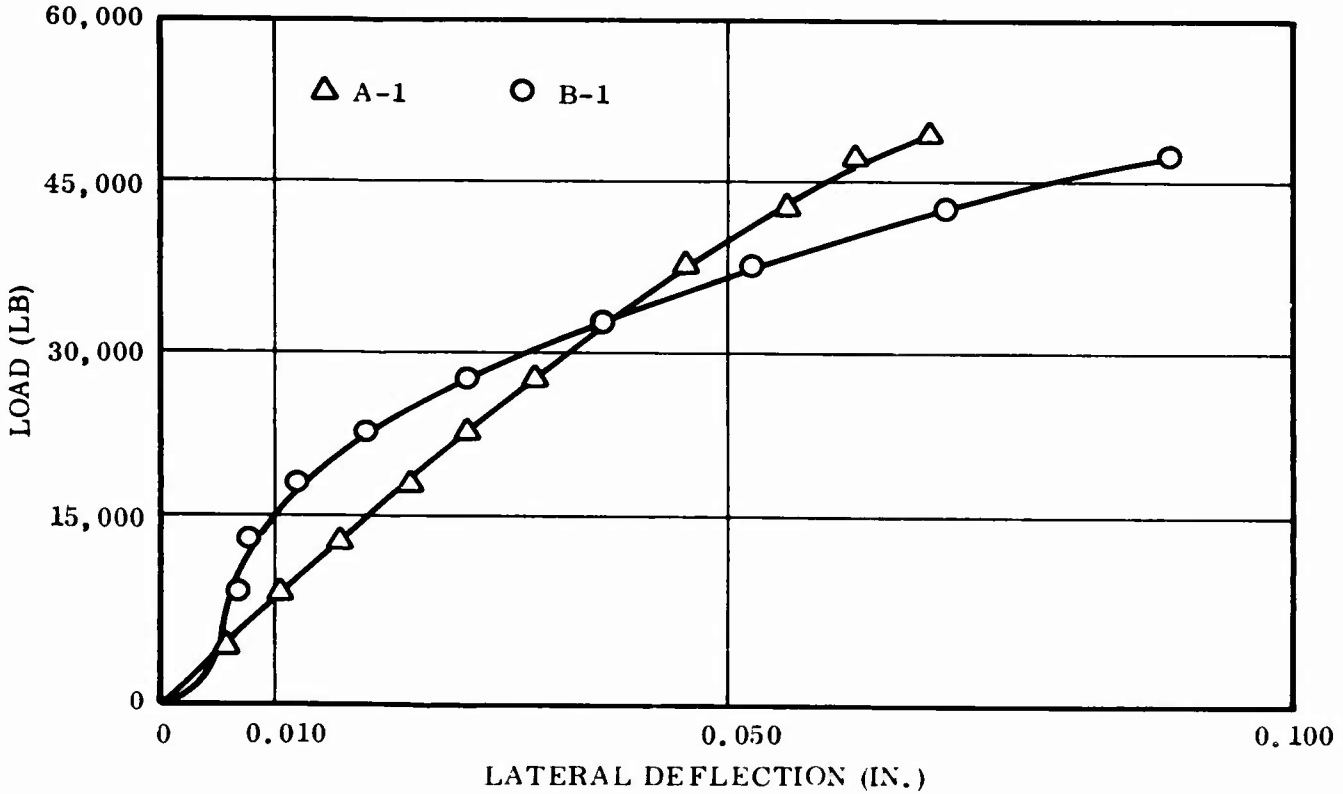

Figure 5-7. Lateral Deflection vs Load for Type III Elastomeric Bearings

Other times, it may be necessary to completely rebuild the specimen. The effect of the presence of voids will be to reduce the bending and shear stiffness and hence reduce the buckling load.

There is another method in addition to Southwell's to determine the buckling load of specimens without testing them to failure. The procedure for this method is as follows.

With the specimen subjected to a constant compressive load, shear loads could be applied to the center of the specimen and the lateral deflection measured for each value of the shear load. As the compressive load is increased, the slope of the shear load-deflection line will decrease (Figure 5-8). Theoretically, buckling occurs when the shear load required to cause a large lateral deflection is negligible. If the shear stiffness (i.e., slope of the relation between shear load and deflection) is plotted against compressive load, a plot of the type shown in Figure 5-9 should be obtained. The curve can be extrapolated to intersect the abscissa at P_{cr}, which is the critical buckling load at which shear stiffness is zero. However, this method has not been used in the present tests.

5.7 LIMITATIONS OF THE ANALYSIS

The analysis is applicable to specimens with a pad geometry that has constant bending and shear stiffness through the entire column (i.e., Type I). The bending stiffness can easily be calculated for some of the simple pad geometries (circular, rectangular, etc.). For other geometries, such as annular, they should be determined either experimentally or with the finite-element computer program.

The analysis should be used with caution for Type III bearings which have variable stiffnesses in the column. The buckling phenomenon in these bearings is not well known, and further effort is required to analyze such bearings. It may be possible that instability in these bearings is controlled by a single critical pad.

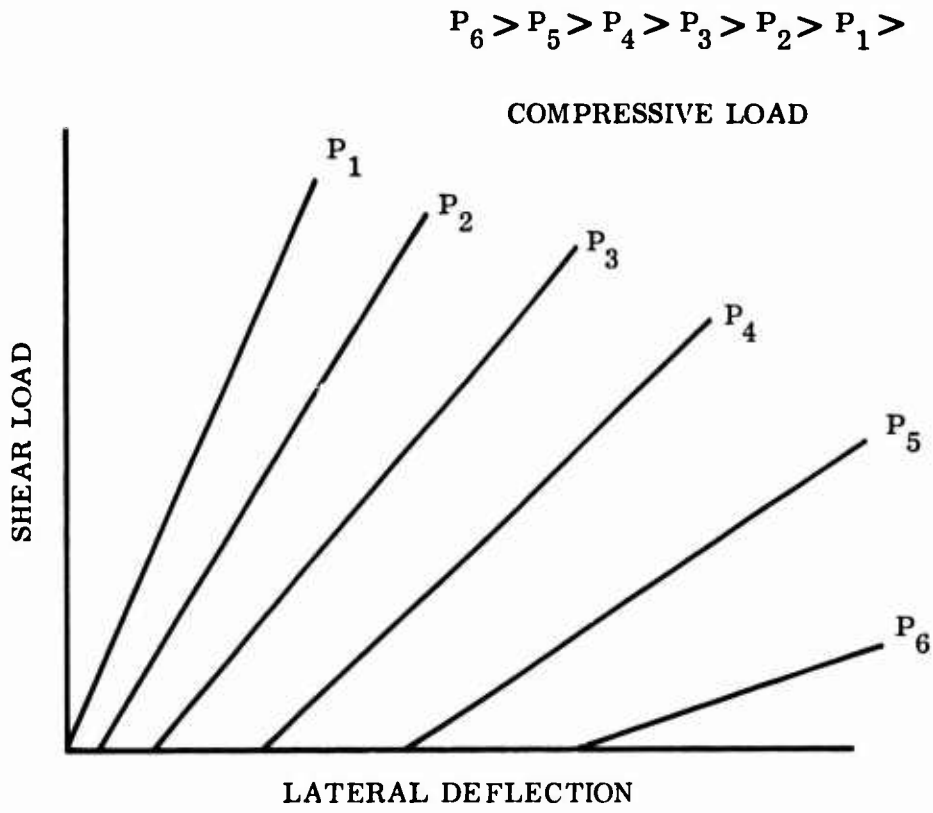

Figure 5-8. Relation Between Shear Load and Lateral Deflection at Center of Column for Various Compressive Loads

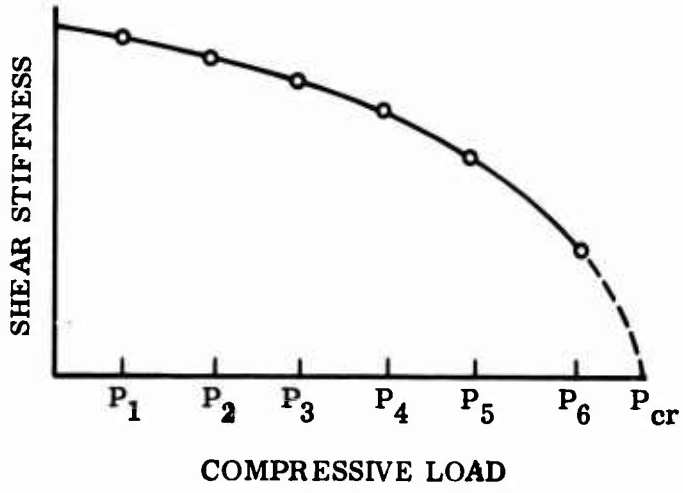

Figure 5-9. Shear Stiffness vs Compressive Load To Determine Critical Buckling Load

6.0 VERIFICATION OF TECHNIQUES

Having developed closed-form equations, design curves, and computer capability, the next item is to verify the usefulness of these calculations. The specimens will be identified and the results compared with predictions. Three types of bearings will be considered:

1. Type I--Flat Laminated Columns
    a. Axial loading
    b. Torsional loading
2. Type II--Radial Concentric Shim Structures
    a. Axial loading
    b. Torsional loading
    c. Lateral loading
3. Type III--Spherical Bearings
    a. Axial loading
    b. Torsional loading
    c. Bending loading

6.1 TYPE I ANALYTICAL VERIFICATION

Three portions of the experimental programs are applicable to Type I verification: (1) compressive specimens, (2) stability specimens, and (3) service life specimens. The complete test matrix and geometry are included in Appendix A. The service life specimens were tested axially and torsionally. The stability and compression specimens were axially tested only. The range of shape factor is 2 to 17. Analyses of these geometries for appropriate loading conditions were compared with measured deflections. Figure 6-1 gives the loading possibilities of a Type I bearing.

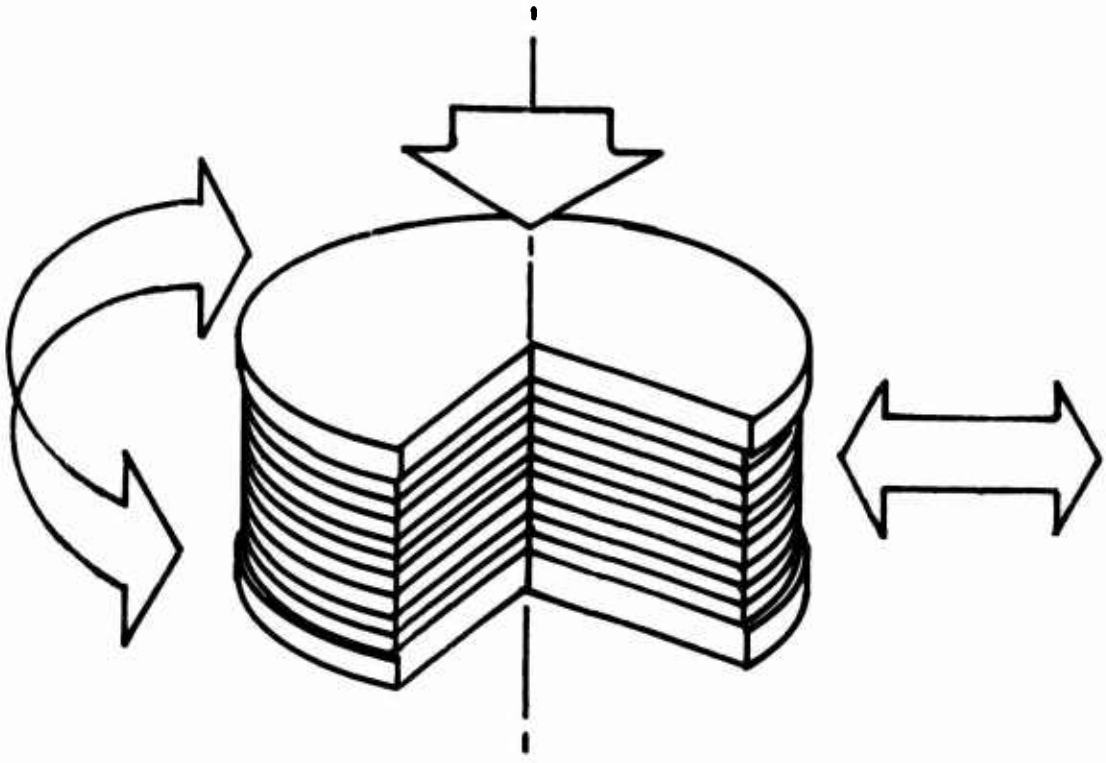

Figure 6-1. Type I Flat Laminated Bearing

6.1.1 Compressive Specimens

The prime purpose of these Type I specimens was to measure the radial deflection and the shape of bulge. The secondary interest was the axial deflection of the single pad geometry. The two specimens are shown in Figure 2-8. The 3-in.-diameter tooling was 0.120 in. and 0.400 in. thick. After the molding, the thickness reduced to 0.100 in. and 0.381 in. Calculations using a thermal coefficient of linear expansion (TCLE) of 10.3×10^{-5} in./in.-°F were within 1% for radial and axial deflections. Figures 6-2 and 6-3 show the undeformed and the deformed grid used to make these calculations.

Axial loads were imposed at temperatures of -40°, 75°, and 160° F. Load rates of 0.01 and 0.1 in./min were used in conjunction with these temperatures. A pronounced bulge can be seen in the 0.381-in.-thick specimens at 50% strain and room temperature (Figure 6-4). Room-temperature measurements of the radial deflection using both calipers and an optical cathetometer are shown in Figure 6-5. The prediction of this radial deflection versus percentage of axial strain is plotted along with the measured values for comparison (Figure 6-6). Predictions of axial and radial deflections were made using finite-element techniques and are compared with measured results in Figure 6-7 for the 0.381-in. thickness. The predictions appear to be within 3% at an axial strain of 10%.

6.1.2 Stability Specimens

The stability test matrix and geometry identification are shown in Appendix A, TWR-7838. These specimens were principally designed for stability tests; however, good use can be made of the axial load data for Type I verification. Specimens of various pad thicknesses and shape factors were tested. Specimens with both solid and annular pads had shape factors (loaded area/free area) of 3 to 33. This provides a good cross section for helicopter application. The fabrication of these specimens is described in Section 5.0.

Selected formulas for computing stress distribution in Type I bearings can be made from a number of authors. Two of the more prominent analyses were Messner's numerical analysis (ref 6-1) and Schapery's closed-form analysis (ref 6-2). These analyses modeled the elastomeric material as linear elastic and slightly compressible, that is, with stress proportional to strain and Poisson's ratio not equal to 1/2. Several simplified derivations assume an incompressible material, then empirically correct the axial stiffness calculations for the effects of compressibility (ref 6-3, 6-4, 6-6 and 6-7). The stress distribution under axial compression will be parabolic if compressibility is not considered. The compressibility greatly changes this distribution, as shown in Figure 6-8.

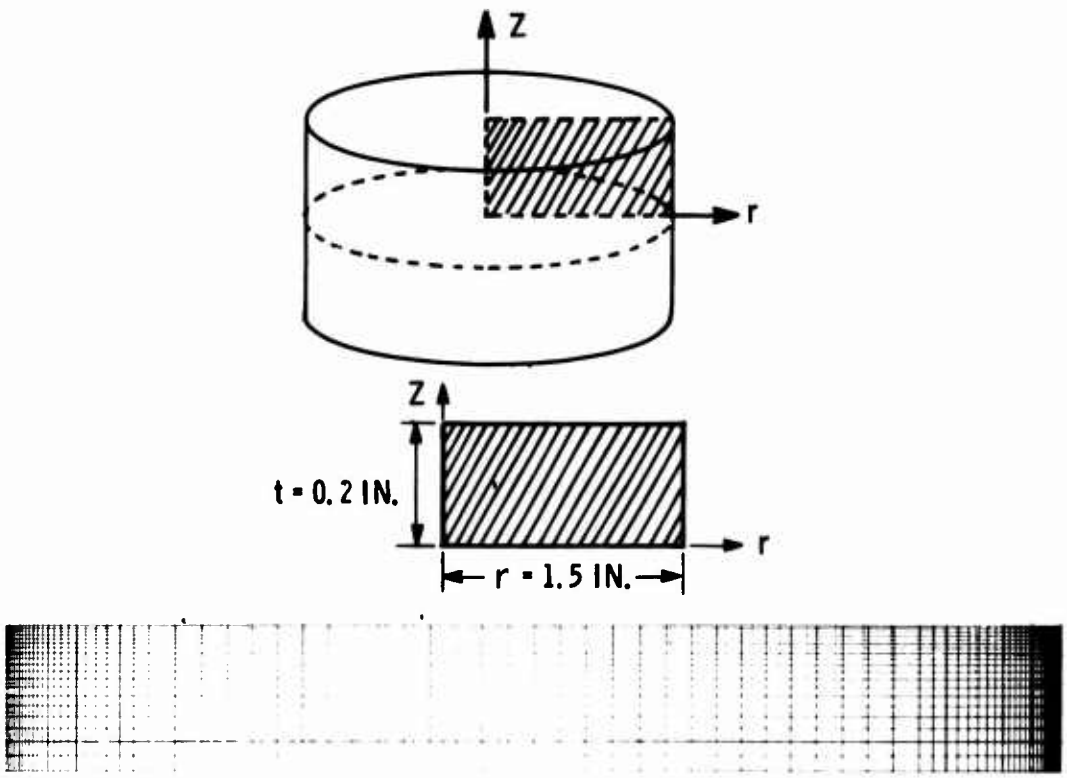

Figure 6-2. Finite-Element Model for Compression Specimen

Initial Temp (°F)	300
Final Temp (°F)	70
α (in./in./°F)	10.3×10^{-5}
E (psi)	290
μ	0.4995

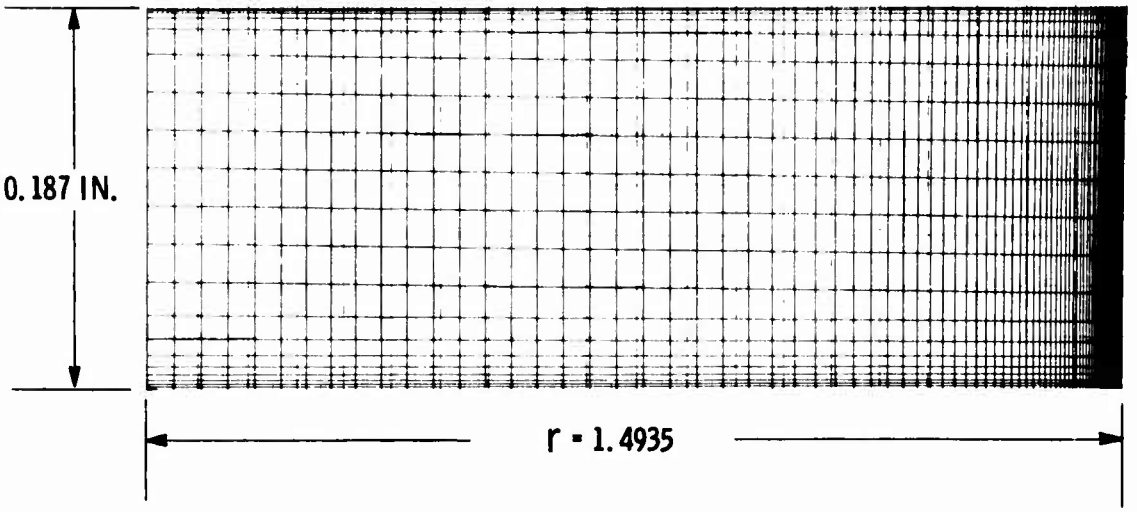

		Final		
	Initial	Prediction	Experimental	Ratio of Observed to Predicted
Thickness (in.)	0.400	0.187	0.19	1.016
Minimum Radius (in.)	1.500	1.4935	1.4935	1.000

Figure 6-3. Finite-Element Model After Thermal Run

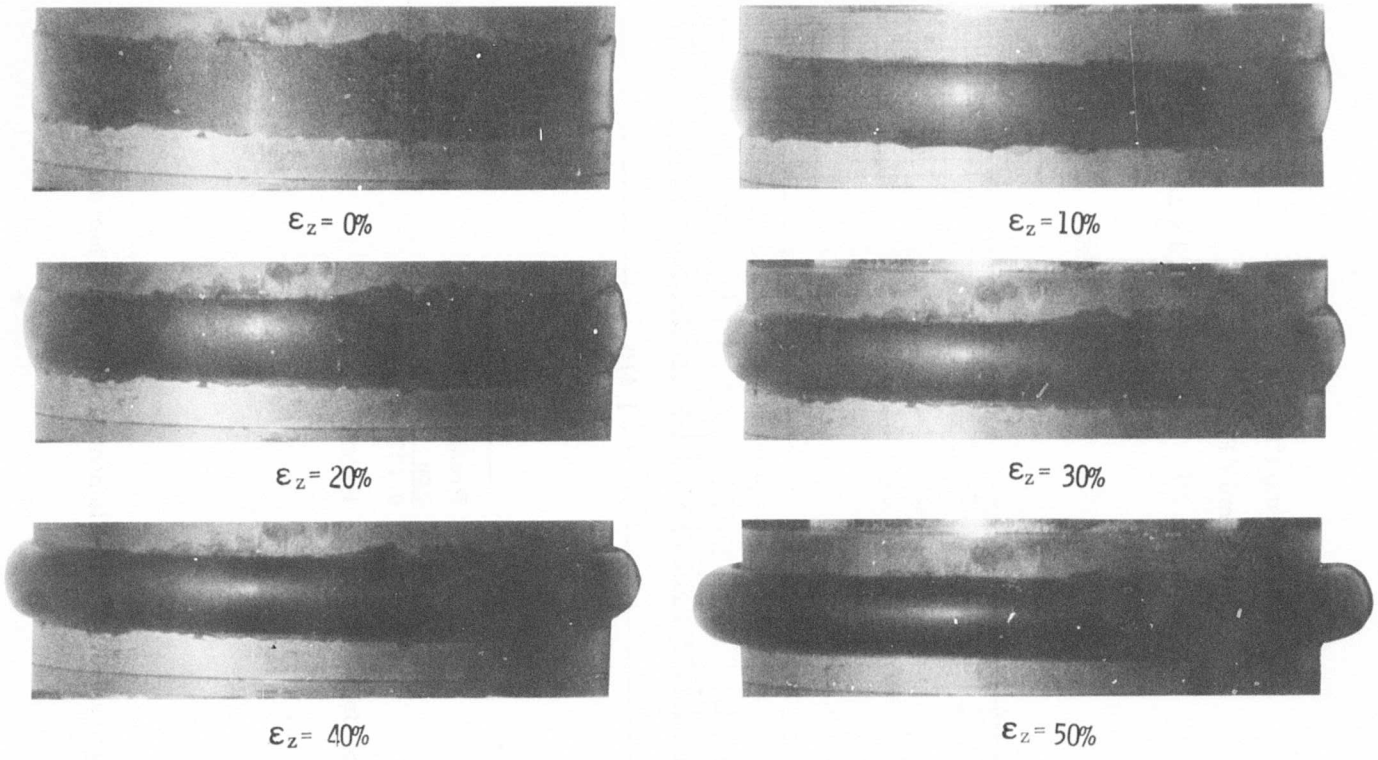

ε_z = AXIAL STRAIN; THICKNESS = 0.381 IN.; AMBIENT TEMPERATURE

Figure 6-4. Compression Tests

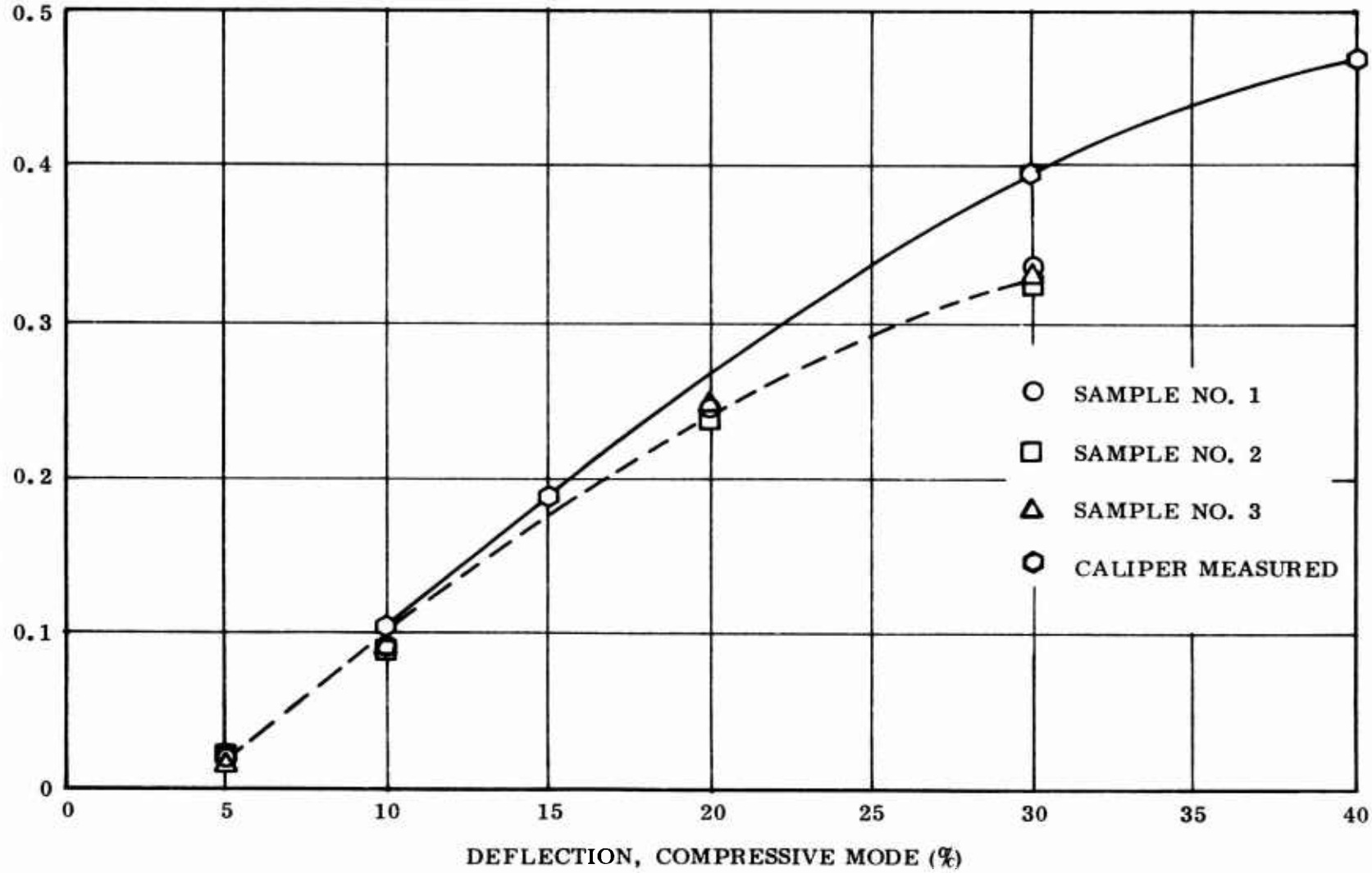

Figure 6-5. Flexible Bearing Materials Service Life Screening Tests (Compression Specimen Measurements - Cathetometer Displacement)

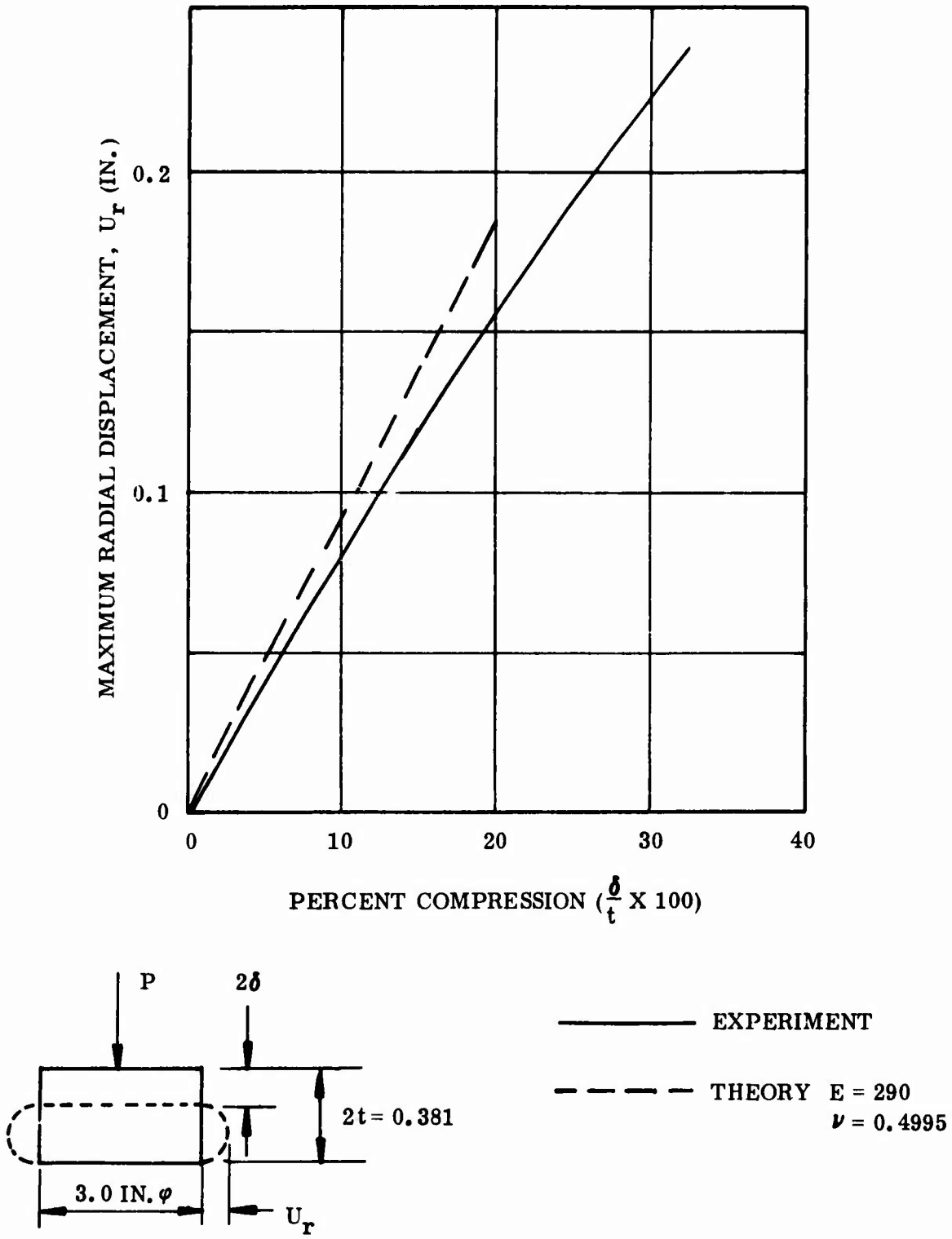

Figure 6-6. Comparison of Theory and Experiment (Compression Specimen)

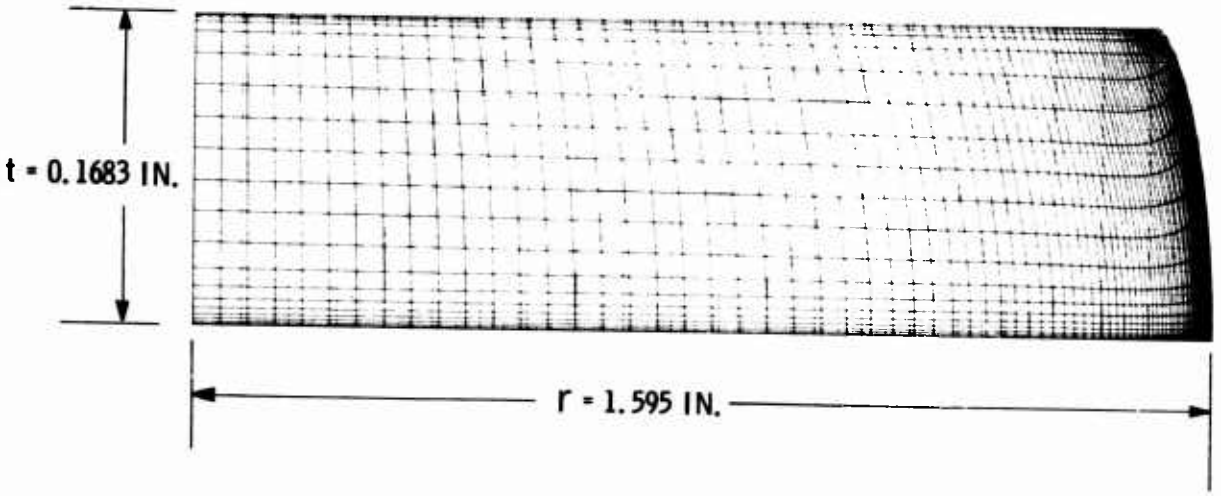

	Predicted	Observed	Ratio of Observed to Predicted
Maximum Radial Displacement (u)	0.0946	0.093	0.983
Axial Load (P)	1,645	1,600	0.973

Figure 6-7. Finite-Element Model After 10% Compression and Cooling Deformation

The figure shows the large effect of the assumption of material properties and the variation due to geometry (shape/factor). Another interesting method of understanding this phenomenon is to use the effective compressive modulus concept versus shape factor. Figure 6-9 shows this relationship. On a log scale, this results in an S-shape curve. Thick pads (low shape factors) respond according to the actual tensile modulus. However, as the shape factor increases, a much higher modulus must be used to express measured stiffness of the pad. The limit is the bulk compression modulus of the elastomer. Thus, for TR-3012 rubber, this variation would be 290 psi to 150,000 psi, or a factor of about 500.

To rapidly compute axial stiffness, the format of the empirically modified equations was selected for preliminary design. The compressible solution and the modified incompressible derivations were made to match by selecting one appropriate constant with the resulting relationships:

$$\frac{1}{E_A} = \frac{1}{E + 6GS^2} + \frac{1.25}{k} \quad \text{(for solid pads } a = 0\text{)}$$

$$\frac{1}{E_A} = \frac{1}{E + 4GS^2} + \frac{1.25}{k} \quad \text{(for annular pads } a \neq 0\text{)}$$

The comparison of measured and predicted data using equation (1) is shown in Figure 6-10. The correlation is very good for thick specimens (low shape factors), but the data scatter for thinner (high shape factors) specimens is noticeable.

6.1.3 Service Life Specimens

The primary interest in this group of specimens was to provide service life data. However, they are particularly useful for Type I verification because they were loaded both axially and torsionally. In fact, the effect of torsional stiffening due to axial loading was measured. The full description of the fabricating process is contained in Section 4.0. Test Plan TWR-7468 (Appendix A) shows the test matrix and the geometric properties of the specimens.

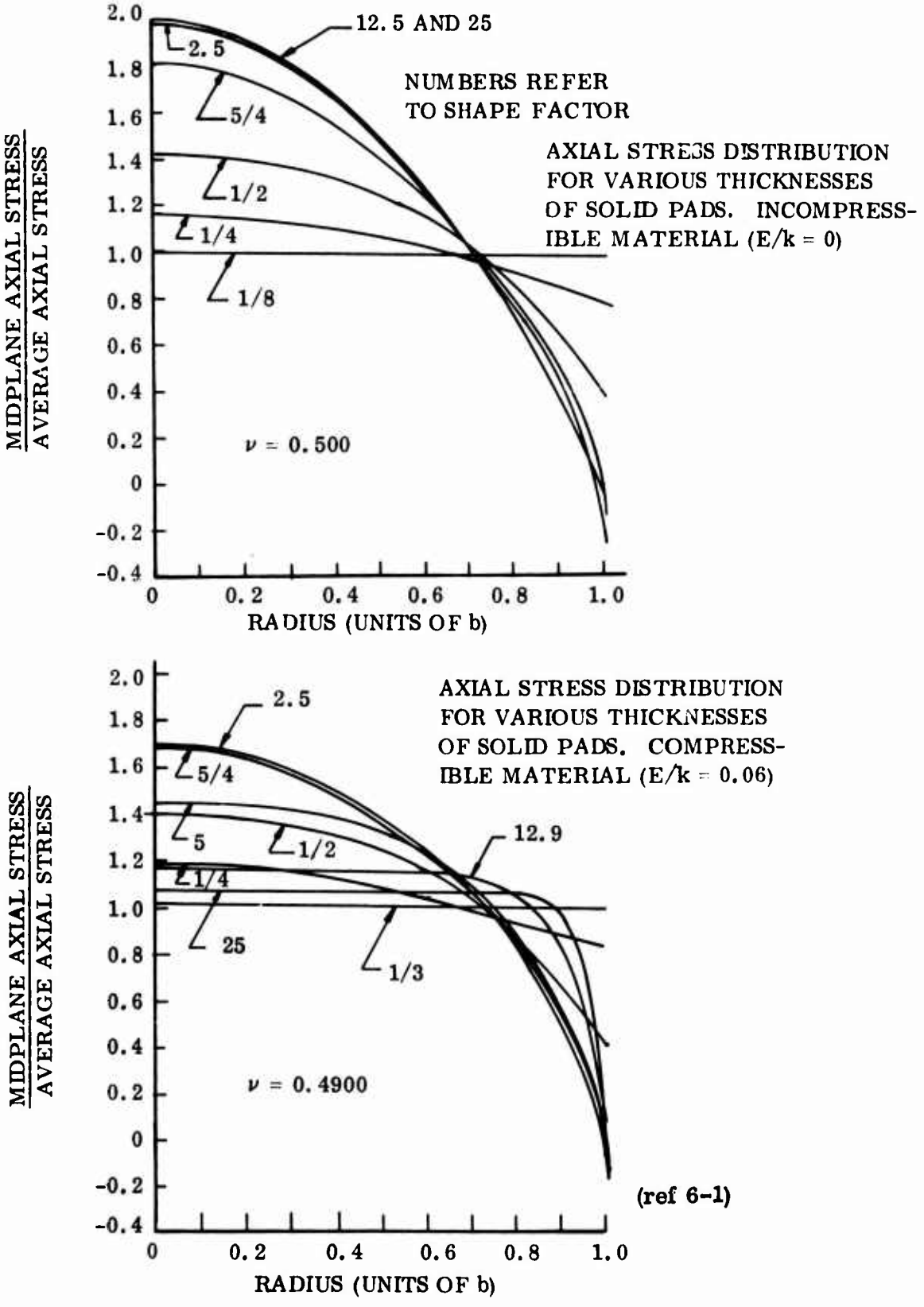

Figure 6-8. Normal Stress Distribution on a Circular Pad

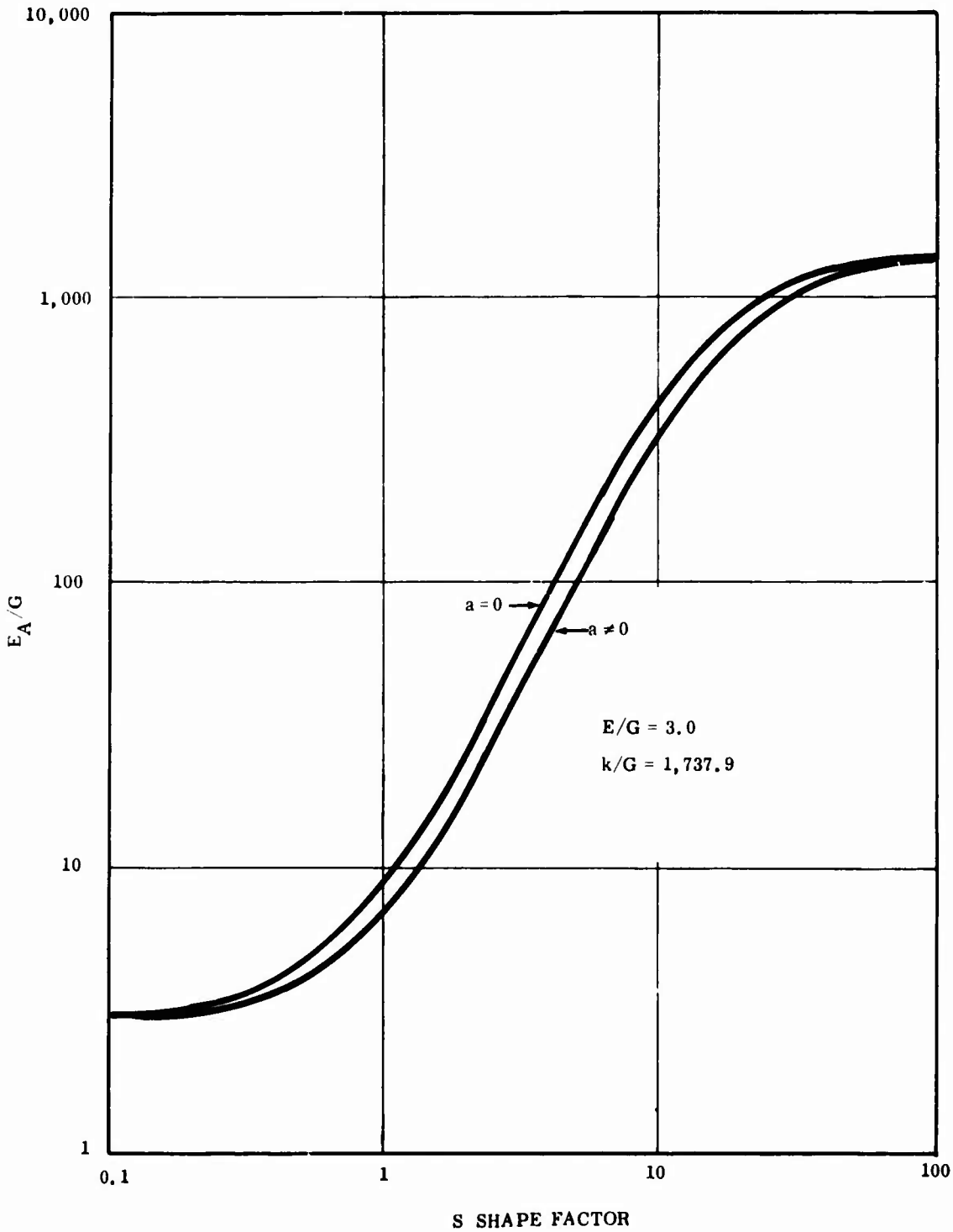

Figure 6-9. Typical Design Curve for Compressive Stiffness Calculation

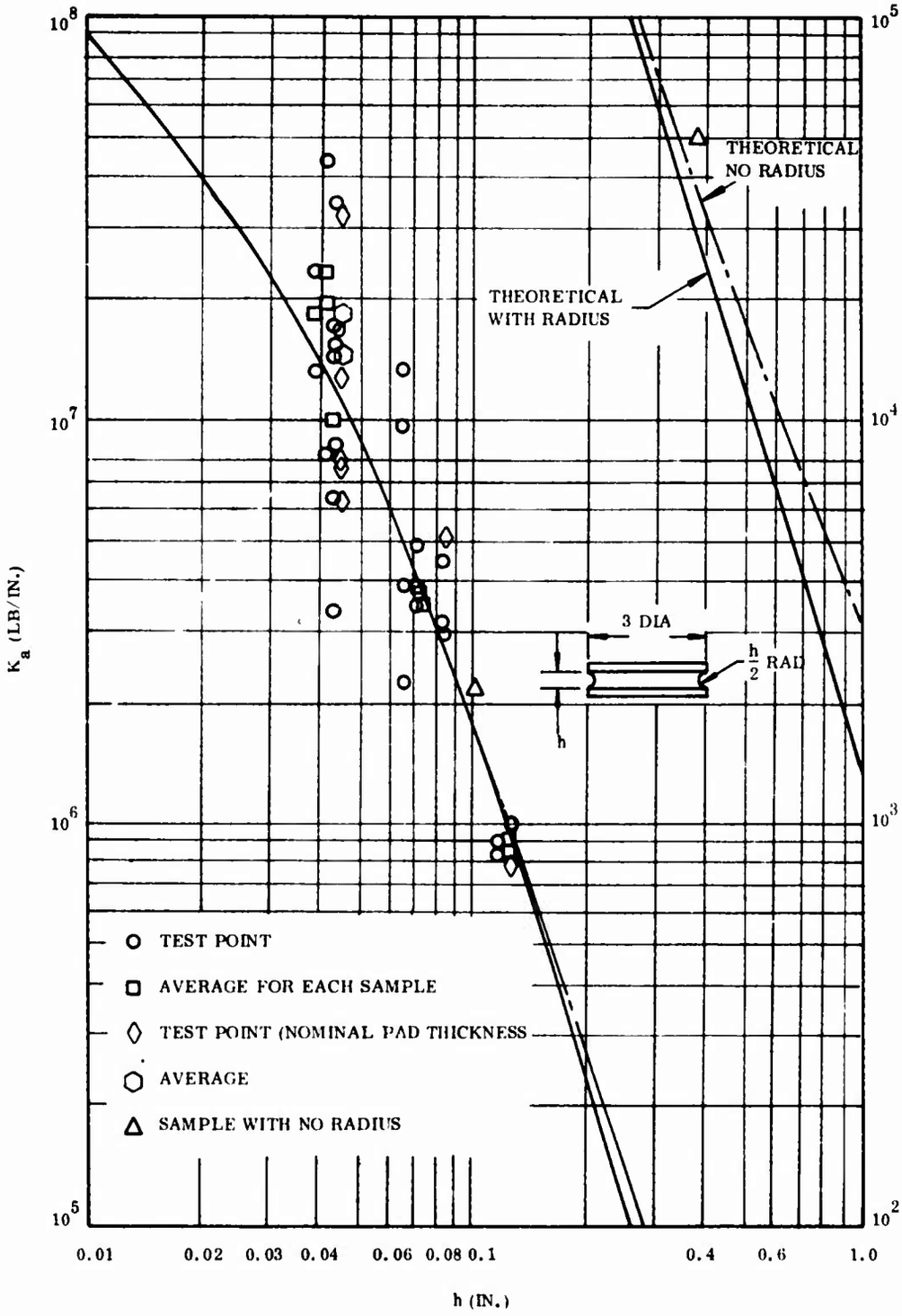

Figure 6-10. Comparison of Calculated and Experimental Spring Rates for Stability Samples

Summarizing the geometry differences which are detailed in the test plan, Figure 6-11 shows the difference in configurations A, SA, CR, R, and C. Detailed finite-element analysis and engineering judgment show that stress discontinuities occur at sharp edges. Thus, a variety of edge conditions were tested. The maximum induced shear stress due to an axial load is shown in Figure 6-12 based on finite-element computer analysis.

The closed-form equation is very useful in preliminary design because of the rapid iteration time between design comparisons. Also, the effect of design and material parameters can be determined by equation inspection. The closed forms do not yield the effects of pad or shim edge conditions but do give accurate axial and torsional spring constants.

The predicted vs measured axial spring constants are presented in Figure 6-13 for an R2 specimen. Excellent agreement is obtained up to 15% axial strain. Table 6-1 gives the axial stiffness comparison for all geometries in the service life matrix. Predictions based on computer and closed-form equations are included.

The torsion response of an R2 geometry is shown in Figure 6-14. The secant slope approximations (1) taken at 10 deg twist and the initial tangent scope (2) are compared with the predicted slope (3). If (1) and (2) are averaged, the agreement is excellent. Notice the nonlinearity of the torque versus angle of twist. This is at 100% torsional strain, which is far above that which service life would allow for reasonable helicopter service.

The torsional stiffness comparison for the variety of service life specimens is shown on Table 6-2. Again, both computer and closed form are compared. The torsional measurements were quite variable. The torsional measuring and manufacturing variable plotted out a better verification. The predictions are generally high compared with measured results.

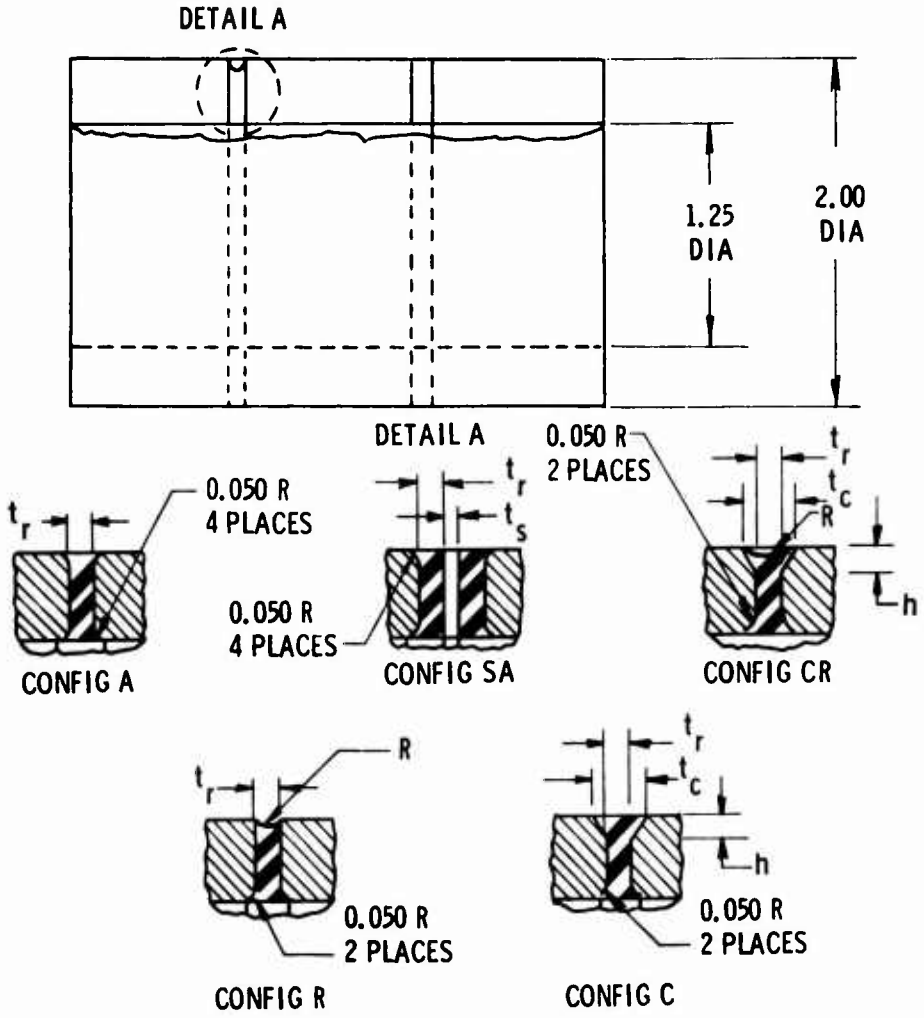

Figure 6-11. Type I Specimen Configurations

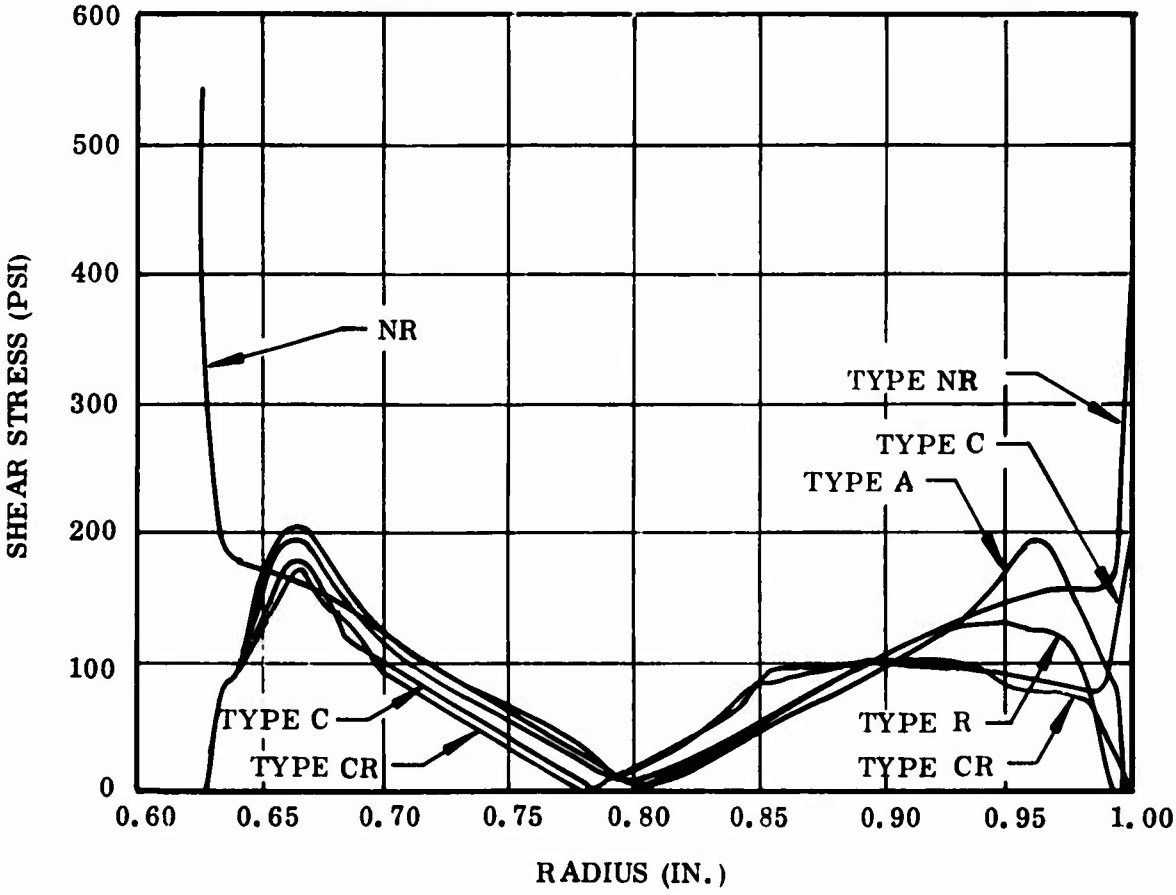

Figure 6-12. Comparison of Shear Stress Distribution at Top Surface in Service Life Specimen for 10% Axial Compression

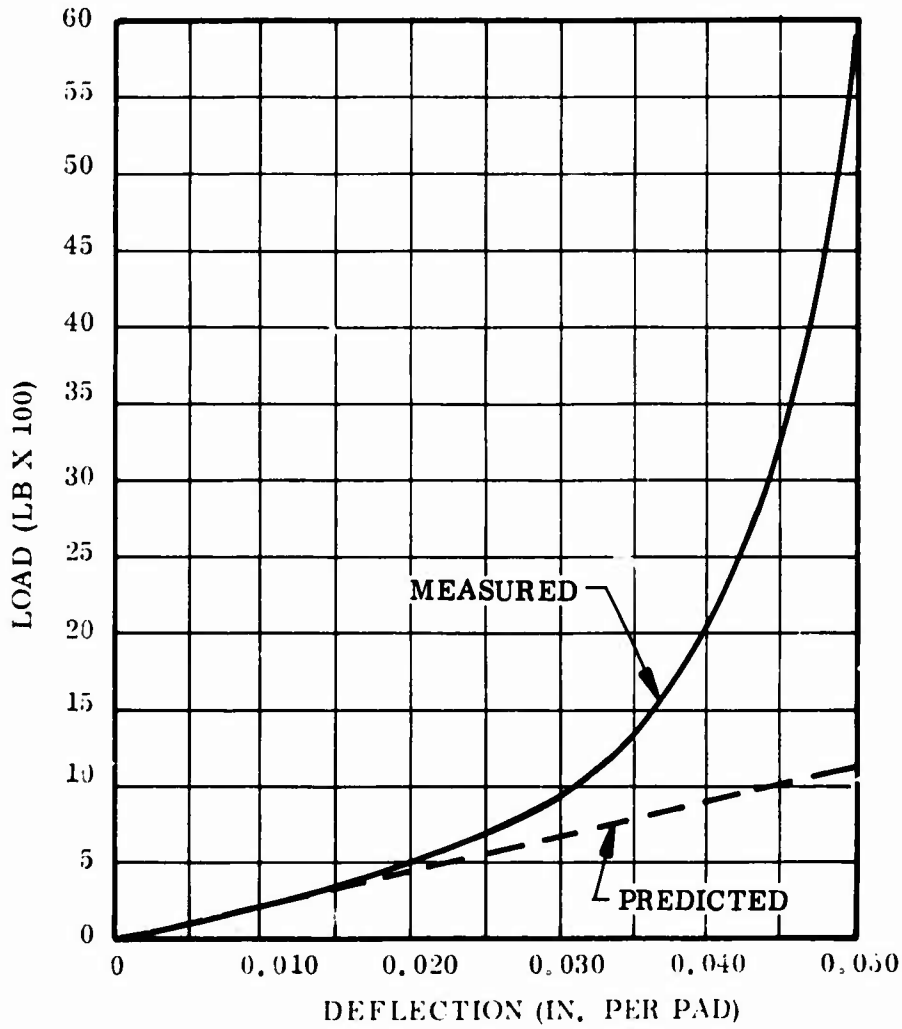

Figure 6-13. R2 Specimen Predicted vs Measured Axial Spring Constant

SAMPLE R2-3
NO AXIAL
COMPRESSION

TORSIONAL STIFFNESS

① SECANT $1/2 \times \frac{293 \text{ IN.-LB}}{9 \text{ DEG}} = 16.3 \frac{\text{IN.-LB}}{\text{DEG}}$

② INITIAL $1/2 \times \frac{370 \text{ IN.-LB}}{10 \text{ DEG}} = 18.5 \frac{\text{IN.-LB}}{\text{DEG}}$

③ PREDICTED $17.5 \frac{\text{IN.-LB}}{\text{DEG}}$

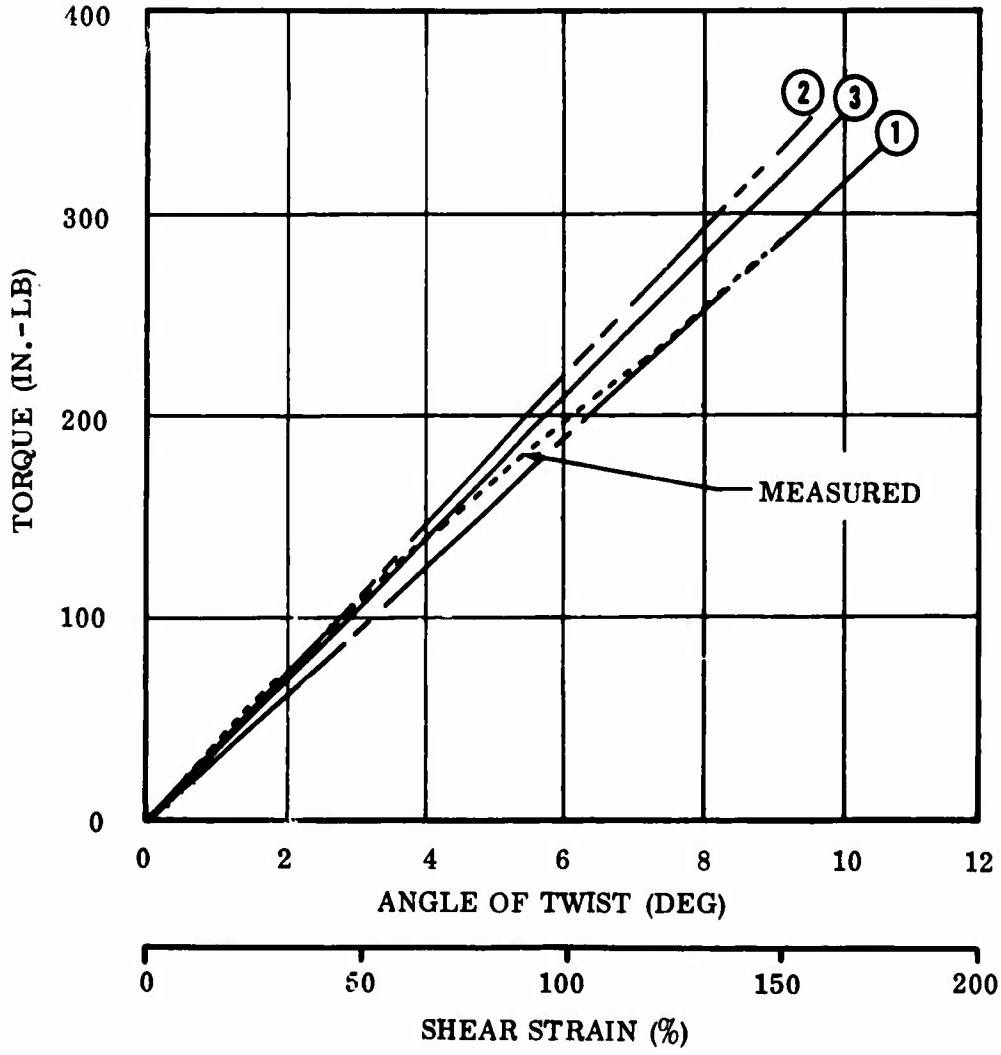

Figure 6-14. Data Interpretation for Torsional Testing

In conclusion, the prediction techniques are of sufficient accuracy to be useful in design application. Closed-form equations for annular pads (with hole in the center) are a degenerate form of a Type III spherical bearing and will be discussed later.

TABLE 6-1

AXIAL STIFFNESS COMPARISON FOR SINGLE PAD
(Service Life Specimens)

Sample Type	No. of Samples	Stiffness (lb/in.)				
		K_a	K_a Maximum	K_a Minimum	Computer	Closed Form
A1	3	34,680	54,000	17,000	--	67,000
A2	3	26,600	30,000	23,200	22,640	31,645
A3	1	43,000	--	--	--	17,920
A4	--	11,000	12,000	10,000	8,467	11,601
C2	3	17,600	20,400	14,800	--	31,645
R2	13	23,800	31,000	19,000	22,640	21,297
R4	3	15,400	20,000	10,000	8,467	6,590
SA-1A	2	50,600	56,400	44,800	--	67,000
SA-1B	2	62,800	62,800	62,800	--	67,000
SA-4A	1	12,200	--	--	--	11,601
SA-4B	1	12,000	--	--	--	11,601

TABLE 6-2

TORSIONAL STIFFNESS COMPARISON
(Service Life Specimens)

Sample Type	No. of Samples	Stiffness (in.-lb/deg)				
		Average	Maximum	Minimum	Computer	Closed Form
A1	3	17.5	21.1	13.9	--	29.5
A2	3	15.9	18.7	14.2	20.6	22.1
A3	1	13.2	--	--	--	17.7
A4	2	11.9	11.9	11.8	--	14.8
C2	3	14.9	15.8	13.9	--	22.1
R2	13	13.8	15.6	8.3	17.7	17.3
R4	3	8.6	9.4	8.6	--	12.3
SA-1A	2	20.4	20.4	20.4	--	29.5
SA-1B	2	22.3	22.3	22.3	--	29.5
SA-4A	1	11.8	--	--	--	14.8
SA-4B	1	12.1	--	--	--	14.8

6.2 TYPE II VERIFICATION

Type II bearing specimens are difficult to build because of their inherent thermal stress field. The pad is surrounded both inside and outside by rigid cylinders. Depending on length and pad cylindrical wall thickness, the thermal stress developed on cool-down from molding (300° F) temperature to room temperature, or even worse, to service temperatures (-65° F), induce a hydrostatic tensile stress field that can fail. An additional complication is added when radial loads are applied. The side opposite the radial load tends to go into a tensile stress field. Dr. A. Gent has shown that the magnitude of hydrostatic tensile stress field capability is on the order of 3/4 the tensile modulus. To offset this tensile tendency, the bearing must be molded at high pressures to give an initial compression. Prediction verifications will be made on single-pad and multipad specimens.

6.2.1 Selection Type

A Type II bearing consists of a cylindrical elastomer annulus with rigid metal cylinders bonded to the inner and outer surfaces. Such a configuration allows the displacement of two nearly rigid cylinders relative to each other, in both axisymmetric and asymmetric modes. A typical bearing for helicopter application is made up of multiple elastomeric cylinders (pads) and metal shims as shown in Figure 6-15. This type of configuration has received use as teetering or flapping bearings on semiarticulated rotors as shown in Figure 6-16. Degeneration to one or a few pads is typical of dampers (Figure 6-17).

Specimens of multiple pad geometry and the single pad geometry have received attention in testing conditions. Results of these studies will be reported and compared in following sections.

6.2.2 Specimen Design

Some guidelines need to be specified to aid in selecting parameters such as pad and shim thickness and in avoiding possible manufacturing problems.

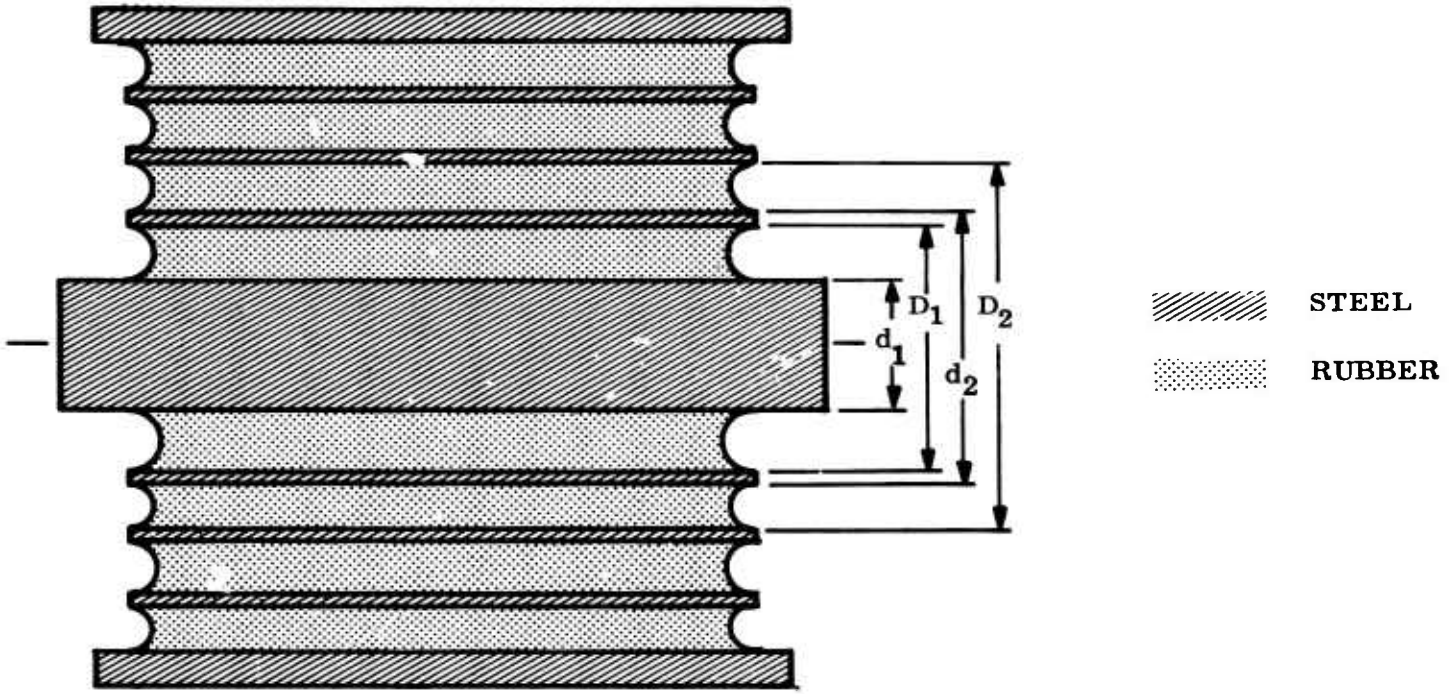

Figure 6-15. Compound Type II Bearing

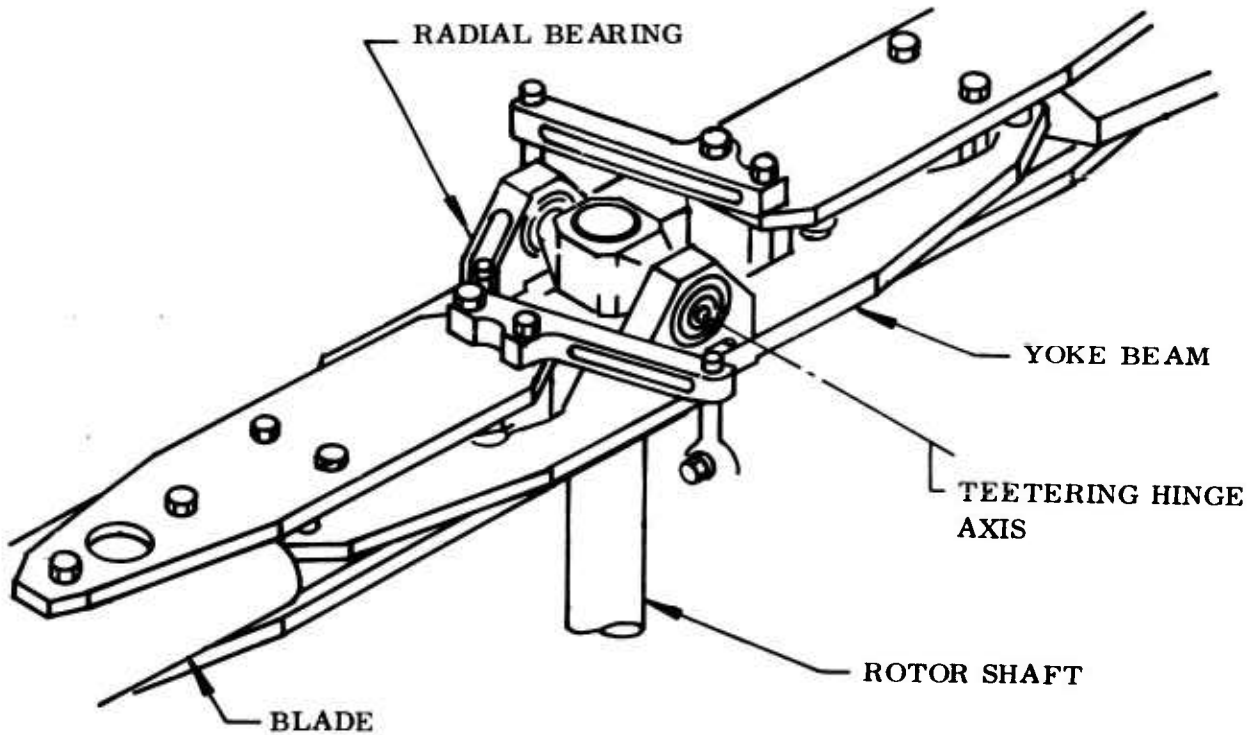

Figure 6-16. Type II Radial Bearing

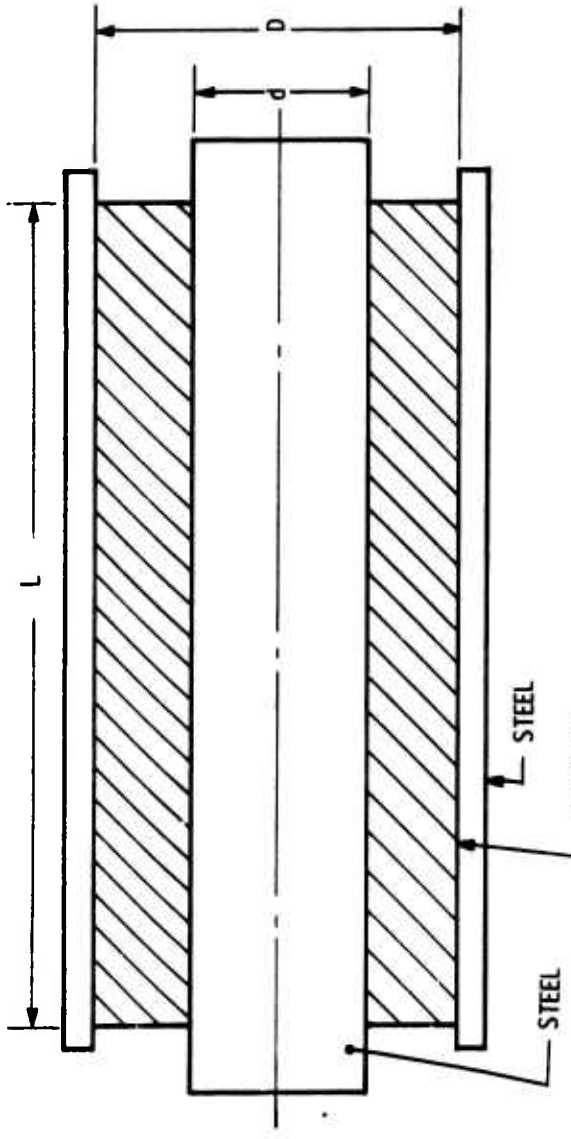

Figure 6-17. Type II Elastomeric Bearing

Variations are possible in selecting shim thickness; however, three methods seem to be widely used:

1. Shim thickness equal to pad thickness.
2. All shims as thick as the second pad.
3. Variable shim thickness.

At present, no recommendation is made relative to any of these methods. Additional effort is needed to evaluate and select a suitable criterion for selecting shim thickness distribution and determining stress/strain levels in the shims. It is recommended that shim stresses and strains be considered in the final design using finite-element analyses until preliminary design curves are available in this area.

A linearly increasing pad thickness with radius has been used as a method of elastomeric material distribution. The thickness of the first pad is primarily influenced by manufacturing considerations and in most cases has a minimum thickness of 0.02 inch. The formula

$$Y_i = m(i-1) + Y_i$$

has been used previously to determine pad thickness,

where Y_i = thickness of pad i

m = slope of the line representing the increase of pad thickness with pad number

The linear variation of pad thickness is determined from the factor m, defined above and determined by use of the formula

$$m = \frac{T_R - (n+1)\, Y_1}{\sum_{1}^{n} n}$$

where T_R = total rubber thickness of bearing

n = number of shims

Y_1 = thickness of the first pad

As a general rule, the shear strain in the elastomeric material should be limited to a maximum value of 40%. Because of the geometry in a Type II bearing, the maximum average shear strain will occur at the inner surface of the innermost pad. Using this general rule, the outside diameter of the innermost pad can be determined using the preliminary design curves presented in this manual, as will be illustrated in the next section.

Another consideration in pad design is that the inner pads are more highly stressed. Use of a stiffer elastomer in the first few pads may be considered worthwhile if necessary to meet the requirements.

Keeping with generally accepted stress relieving practices, it is recommended that a full radius be applied to the free surface of the elastomeric material.

6.2.3 Type II Bearing Specimen Preparation

Three bearing configurations were fabricated of the type described in this section. These are described as multiple pad bearings. Figure 6-18 shows a sample of the bearing. Fabrication is accomplished by means of the mold shown in the accompanying sketch and in Figure 6-19.

6.2.3.1 Configuration 1

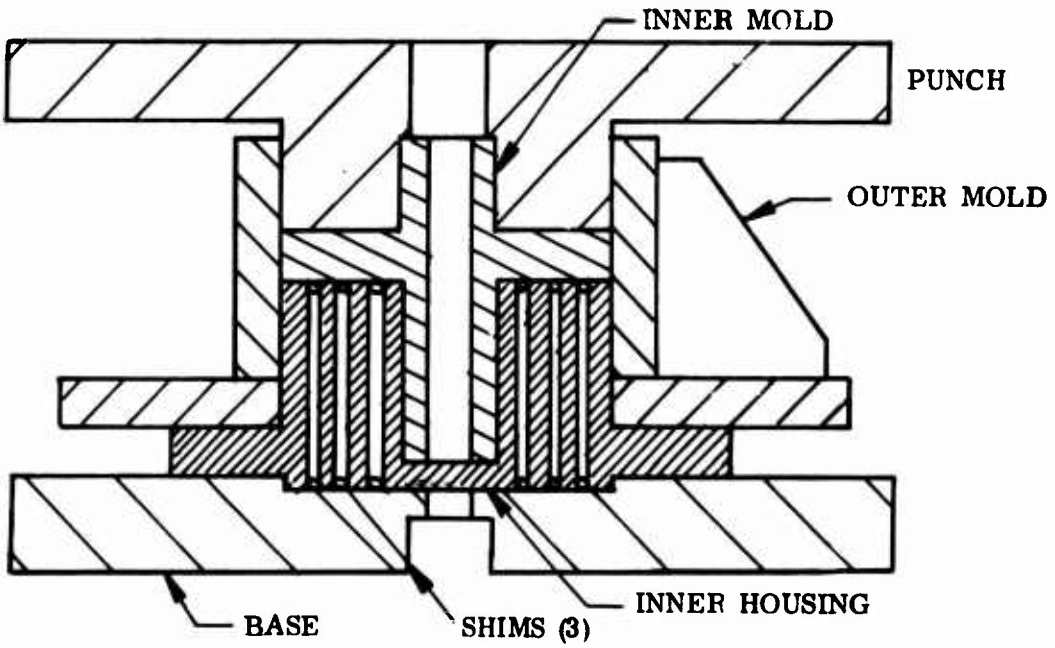

Processing Data:

1. Solvent-clean the inner and outer housings and each of the shims.
2. Grit-blast, with silica sand, the OD of the inner housing (cylindrical section), both the ID and OD of the shims, and the ID of the outer housing.
3. Solvent-clean both housings and all the shims.

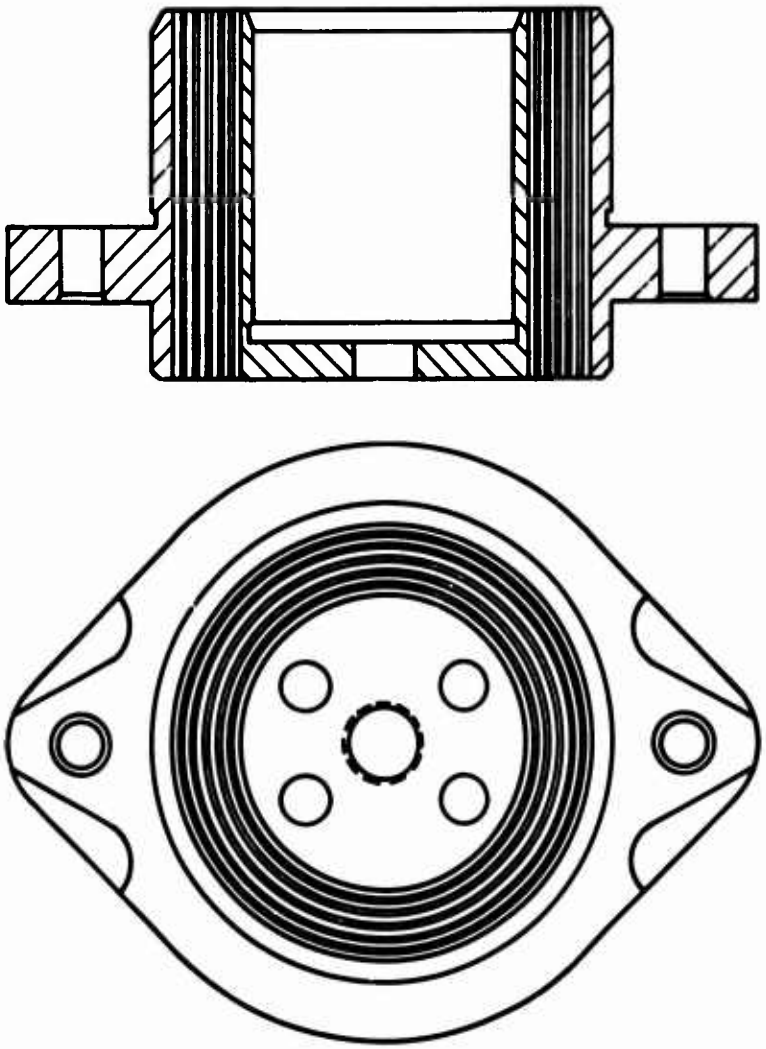

Figure 6-18. Typical Type II Multiple Shim Bearing

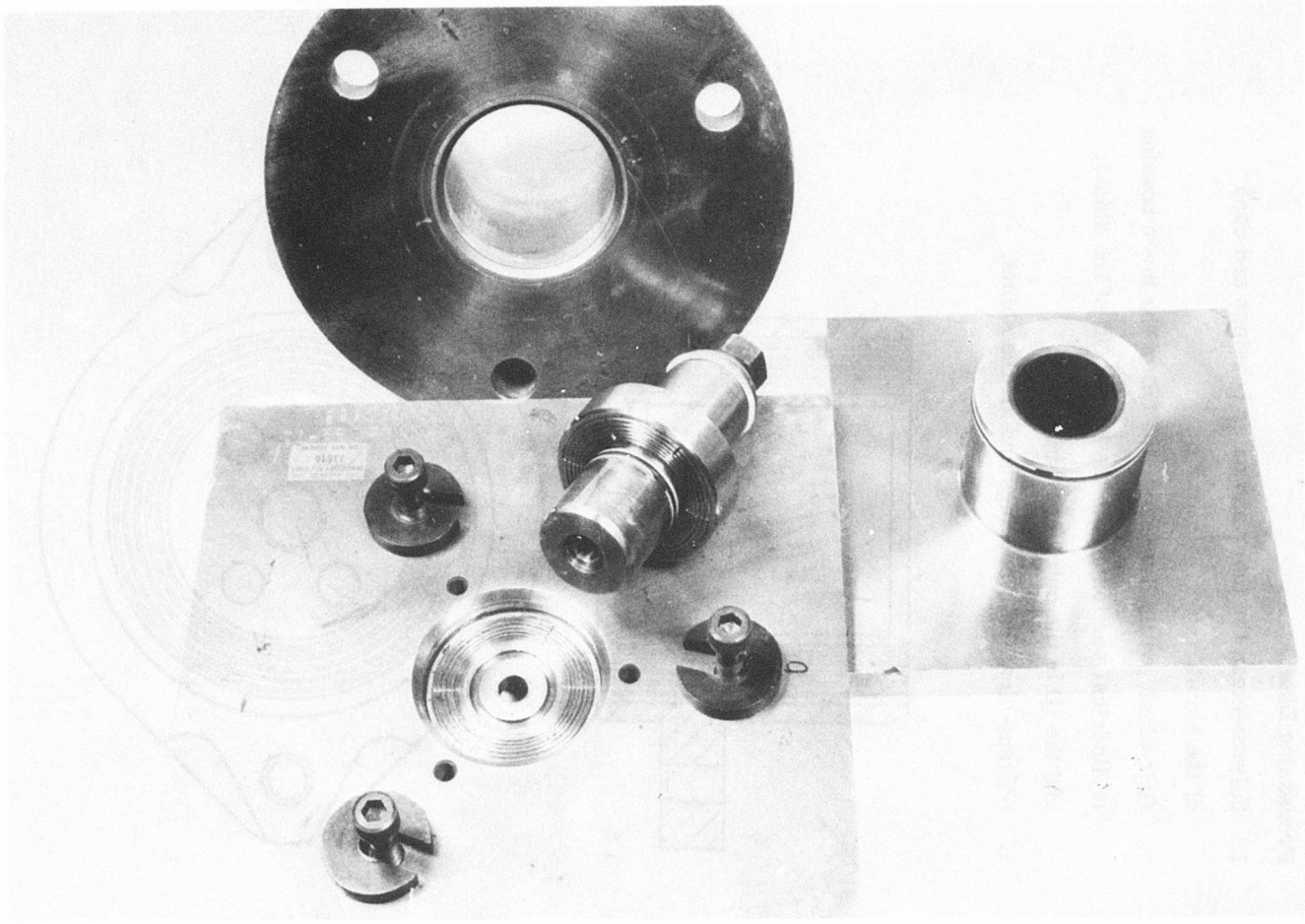

Figure 6-19. Bearing Mold

4. Obtain Chemlok 205, stir thoroughly, and paint the OD, cylindrical section of the inner housing, the OD and ID of the shims, and the ID of the outer housing. Air-dry 15 minutes.
5. Obtain Chemlok 220, stir thoroughly, and paint each of the 205 painted surfaces of each component. Air-dry for 30 minutes.
6. Solvent-clean each of the mold components.
7. Install new O-rings and backups as required.
8. Place inner housing on base of mold and secure with high-strength bolt. Place each of the shims on base of mold, followed by the outer housing. Install inner mold by inserting base of inner mold into the inner housing until contact is made with the bearing components. Insert long tiedown bolt through the inner mold and screw onto high-strength bolt which fastens the inner housing to the base of the mold, do not tighten at this time. Install the outer top portion of the mold and bolt to base. Tighten the tiebolt of the inner mold.
9. Obtain elastomer and cut into donut type pieces.
10. Remove plastic film from elastomer and stack into cavity of mold.
11. Install punch portion of the mold in mold.
12. Place mold assembly in a press preheated to 200° F and allow to soak for 1 hr with approximately 20,000 lb gage pressure.
13. After 1 hr soak time, raise ram pressure very slowly until a maximum pressure of 72,000 lb gage pressure is reached.

14. When maximum pressure is obtained, turn heat controls to 300° F and cure bearing for 1 hr and 15 minutes.
15. Cool to handling temperature and disassemble the mold.
16. Identify the bearing with applicable identification.

6.2.3.2 Configurations 2 and 3

These bearings are of the same general description, except for the length. Therefore, the processing is identical:

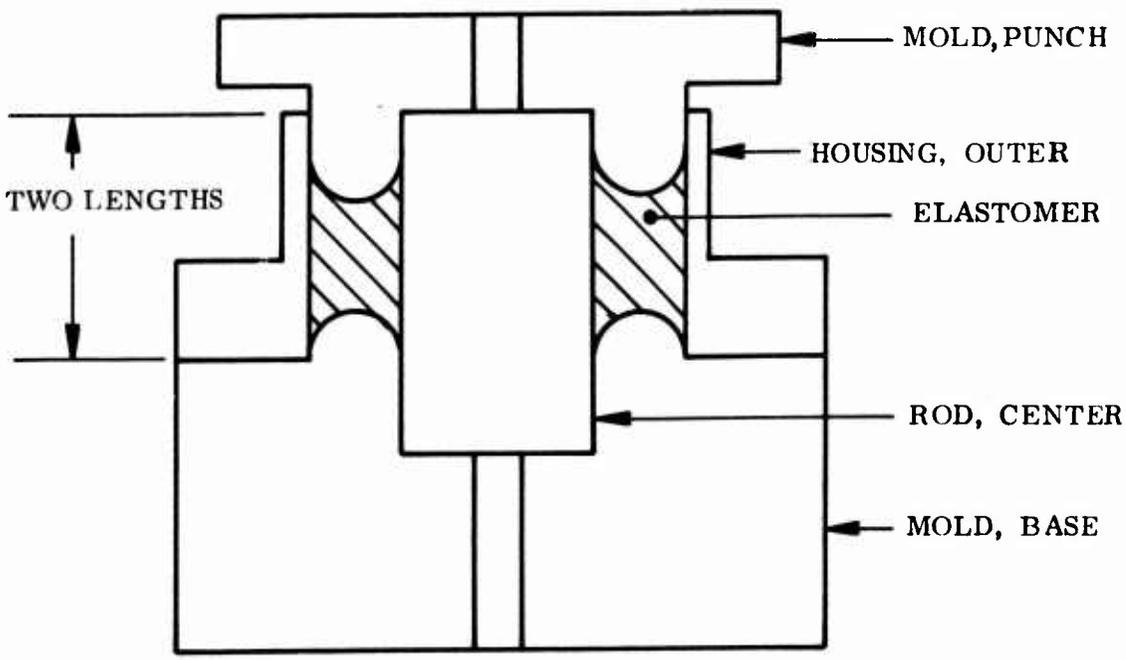

Processing Data:

1. Solvent-clean all components (metal).
2. Grit-blast, with silica sand, the center rod in the elastomer bonding area only and also the ID of the housing.
3. Solvent clean the rod and housing.
4. Obtain Chemlok 205, stir thoroughly, and paint the rod and the ID of the housing on bond area only. Air-dry for 15 minutes.

5. Obtain Chemlok 220, stir thoroughly, and paint the rod and housing areas previously painted with the 205. Air-dry for 30 minutes.
6. Cut a strip of elastomer the same width as the Chemlok painted area, and of sufficient length so that the elastomer can be stretched around the center rod. The OD of the elastomer should be small enough to allow this rod to be inserted into the housing.
7. Wrap elastomer on rod and insert into the housing.
8. Cut several elastomer donuts that have small enough OD to fit into the housing and large enough ID to slip over the rod, and exceed the finish elastomer length by 0.25 inch.
9. Insert elastomer donuts into mold.
10. Install mold punch.
11. Place in a press heated to 200° F. Apply 5,000 lb gage pressure.
12. Allow the short bearing to soak at 200° F for 30 minutes, apply sufficient pressure to close mold, and turn temperature up to 300° F for 1 hr and 15 minutes.
13. Allow the long bearing to soak at 200° F with the aid of a hot air gun blowing on center of housing, for 45 minutes; apply sufficient pressure to close the mold, and turn temperature up to 300° F for 1 hr and 30 minutes.
14. Cool mold to handling temperature and remove the punch and base. Identify specimen with applicable numbering, and deliver to machine shop to be machined to desired length.

6.2.4 Analysis of Stress and Strain Field Service Life Prediction

Presently only limited data are available for verifying the service life of elastomeric bearings. Section 4.0 details the important factors and parameters

necessary to predict a preliminary service life. One of the methods outlined makes use of the maximum shear stress and the hydrostatic pressure existing in the elastomer. Figure 6-20 shows that for given values of maximum shear stress and hydrostatic pressure it is possible to estimate service life-cycle limitations.

A multiple pad radial bearing manufactured by Thiokol was tested and subjected to the loading outlined in Figure 6-21. A radial load of 27,000-lb was applied for a duration of 1 minute. Over the next one-half minute, the load was reduced to 3,200 lb and again loaded to the 27,000-lb level. This load was cycled 40 times per hour. Simultaneously a feathering load of ± 6 deg was applied at a rate of 325 cycles per minute. This bearing has survived 364 hr of continuous testing. It is expected that the bearing would survive up to 4,000 hr intermittent loading in actual helicopter applications.

There are basically two types of failure mechanisms. The maximum shear stress method considers mechanical failures, while strain energy density applies to bulk degradation of the elastomer due to the reversion phenomenon. Both methods consider values of hydrostatic pressure ($\bar{P}$). Laboratory tests were conducted and values of service life measured for $\bar{P}$ up to 489 psi.

Finite-element computer analyses have been conducted on the multiple pad bearing. A comparison of predicted and measured service life has been made using these results. Two points of interest have been considered: (1) the area of maximum shear stress due to torsional load (inner pad) and (2) that due to radial loading (outer pad). Miner's rule states that failure will occur when the sum of the ratio of the number of cycles at the ith stress level, n_i, to the constant amplitude life time at that level, N_i, summed over all i stress levels is equal to unity or

$$\sum_{i=i}^{i=i} \frac{n_i}{N_i} = 1$$

This guide has been applied to the variable amplitude loading detailed in Figure 6-21 for the two cases outlined above.

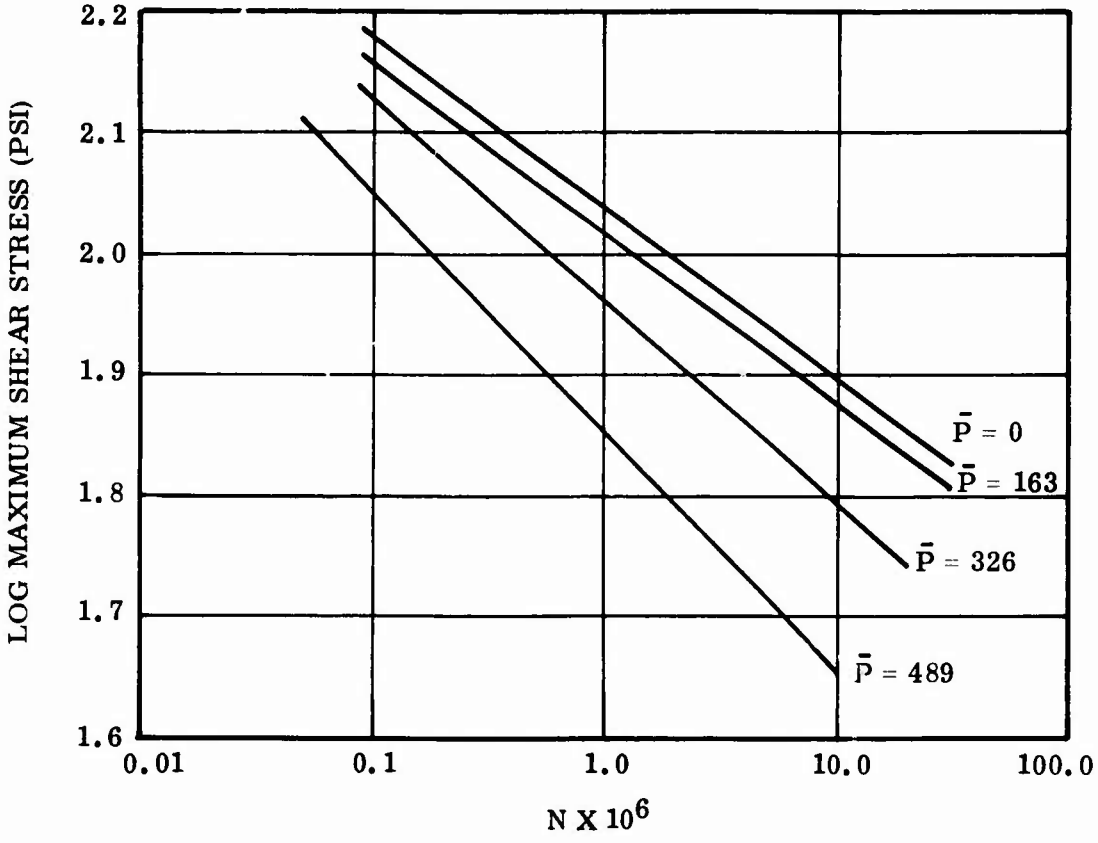

Figure 6-20. Maximum Shear Stress Failure Surface

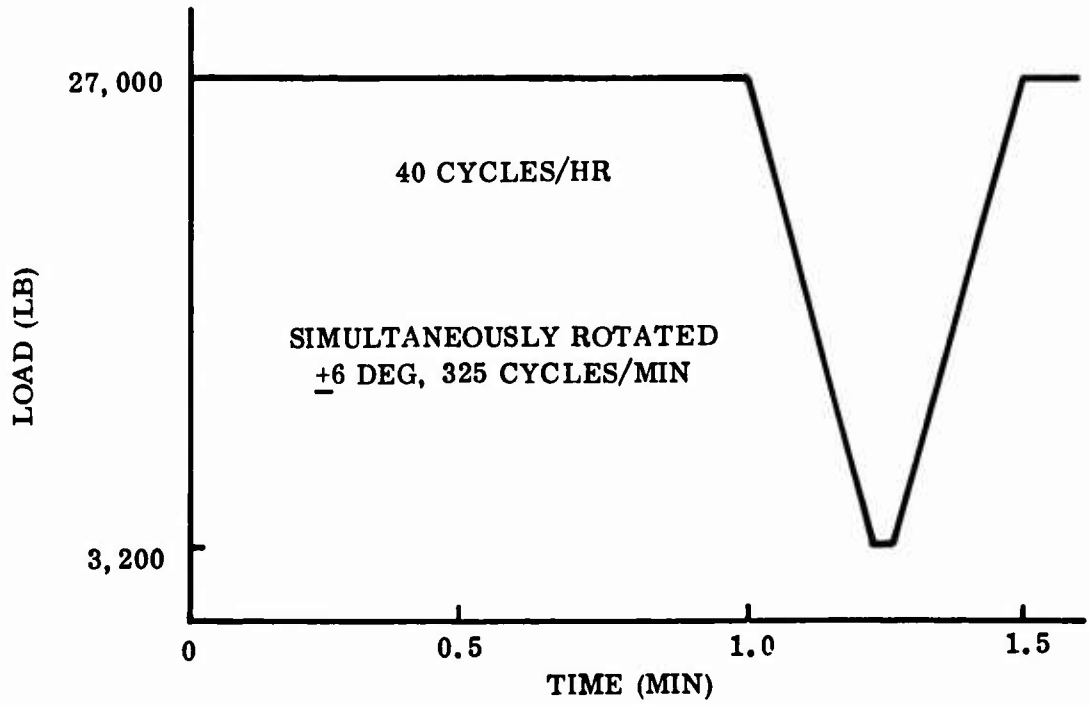

Figure 6-21. Loading Cycle Test on Multiple Pad Radial Bearing

6.2.4.1 Case No. 1 (outermost pad)

	psi
τ_{max} due to torsional load	27.5
Hydrostatic compression ($\bar{P}$)	0
τ_{max} (at point of τ_{max} due to torsion) due to radial load	175
Hydrostatic compression	-314

Because of the cycling of the radial load, the hydrostatic compression value was divided by two. Applying these values to the curves of Figure 6-20, the following values of service life are predicted for the loads applied individually.

$\log 27.5 = 1.44$

$\log 175 = 2.24$

$N_{torsion} \cong 1 \times 10^9$ cycles

$N_{radial} = 30,000$ cycles

Applying Miner's rule based to the higher frequency,

$$N = \left[\frac{1}{1 \times 10^9} + \frac{40}{(325)\ (60)\ (30,000)} \right]^{-1}$$

$$= 14.4 \times 10^6 \text{ cycles}$$

Thus, failure is predicted to occur in the outermost pad after 14.4×10^6 cycles or 738 hr of testing.

6.2.4.2 Case No. 2 (innermost pad)

	psi
τ_{max} due to torsional load	66
Hydrostatic compression ($\bar{P}$)	0
τ_{max} (at point of τ_{max} due to torsion) due to radial load	106
Hydrostatic compression ($\bar{P}$)	1,811

Again, using $\bar{P}/2$, because of the cycling effect, gives the following values:

$\log 66 = 1.82$; $\log 106 = 2.03$

$$N_{torsion} = 35 \times 10^6 \text{ cycles}$$

$$N_{radial} = 17,000 \text{ cycles}$$

$$N = \left[\frac{1}{35 \times 10^6} + \frac{40}{(325)(60)(17,000)} \right]^{-1}$$

$$= 6.7 \times 10^6 \text{ cycles}$$

Thus, failure is expected to occur in the innermost pad after 6.7×10^6 cycles or 344 hr of testing, long before the outermost pad will fail.

Testing experience has produced failure in the innermost pad of a multiple pad bearing after 7.1×10^6 cycles or 364 hr, showing that our predictive techniques and the assumption of $\overline{P}/2$ give good correlation.

6.2.5 Specimen Testing

Several specimens of the multiple pad flapping elastomeric bearing have been manufactured using various formulations for the elastomer. In the process of manufacturing these specimens, several different molding pressures (5,000, 10,000, and 15,000 psi) were used to investigate the effect on stiffness.

The axial stiffness was measured using a standard Riehle testing machine. A special test apparatus (Figure 6-22) was constructed to measure radial and torsional stiffness. The apparatus has been designed such that the radial and torsional loads can be applied separately or in combination to measure the combined effects.

The spring constants for the various elastomer formulations and molding pressures are shown in Table 6-3. The required spring constants are also shown in this table, and the measured results are compared to predicted values.

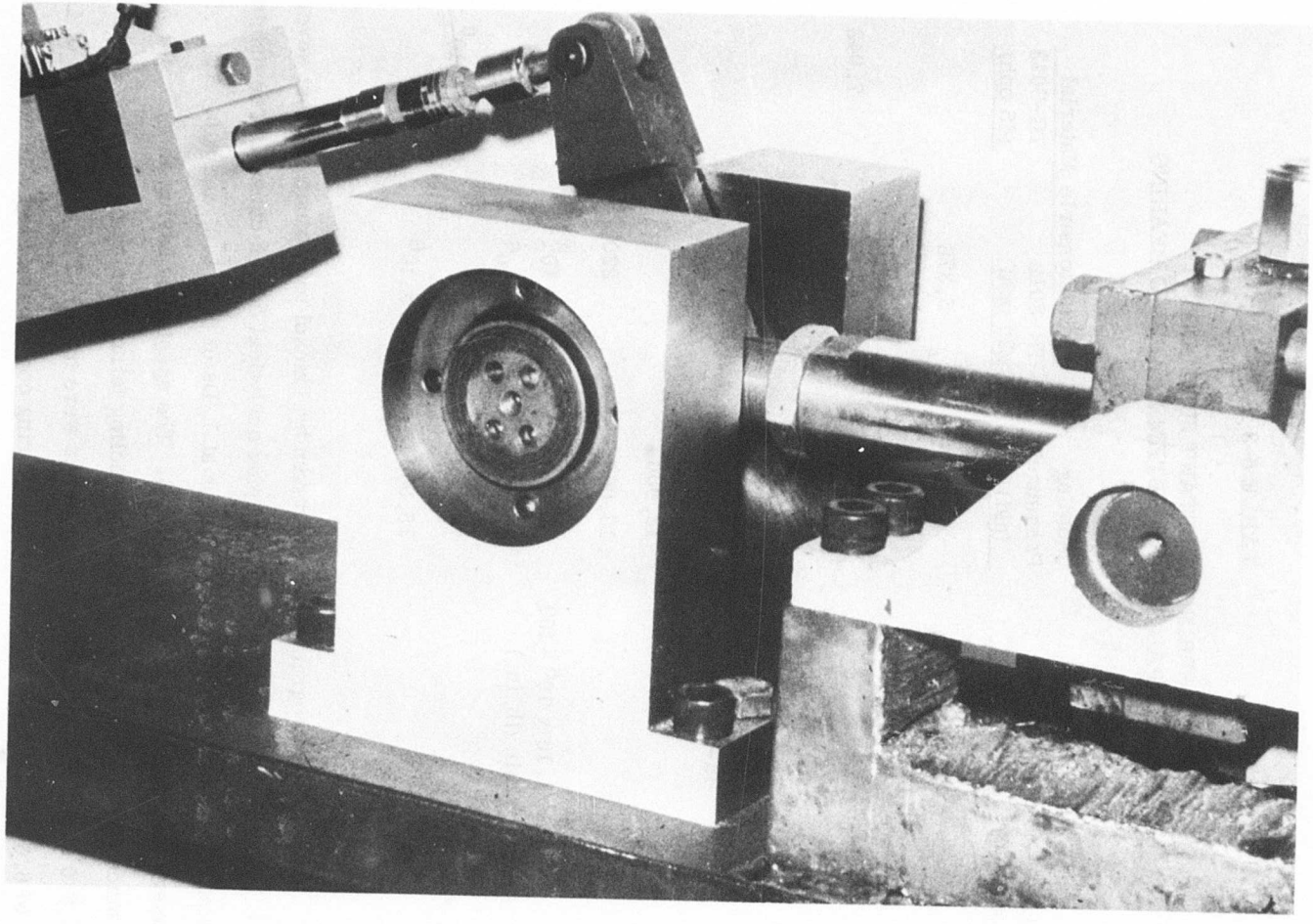

Figure 6-22. Type II Testing Machine (Radial and Torsional Loads)

TABLE 6-3

SPRING CONSTANT SUMMARY
MULTIPLE PAD ROTOR SYSTEM FLAPPING BEARING

Spring Constant	Design Goal	Molding Pressure (psi)	Elastomeric Material TR-3012 (30 pph)	Elastomeric Material IR-3013 (45 pph)
K_A	11,000 ± 12% (lb/in.)	5,000	5,376	
		10,000		
		13,000		7,042
		15,000		
K_T	230 ± 12% (in-lb/deg)	5,000	139	
		10,000	250	
		13,000		200
		15,000	220	
K_R	1.16×10^6 -10% min (lb/in.)	5,000	0.757×10^6	
		10,000	0.757×10^6	
		13,000		0.819×10^6
		15,000	0.735×10^6	

A small test program was undertaken by Thiokol to produce and test several Type II bearings for the purpose of verifying analytical design curves. The original intent was to fabricate two specimens each at L/Ds of 0.5, 6.0, and 8.0. All specimens were to have a d/D ratio of 0.6. The specimens having an L/D of 0.5 were made and tested; however, due to a tooling failure during fabrication of the L/D = 6.0 specimens, no other test bearings were made. The one specimen of L/D equal to 6.0 that was manufactured failed during cool-down of the elastomeric

material after vulcanization. Radial and axial stiffness of the specimen having an L/D = 0.5 were measured, giving the following results:

$$K_R = 4,667 \text{ lb/in.}$$

$$K_A = 777 \text{ lb/in.}$$

These results are compared to closed-form and computer-generated solutions in para 6.2.6.

Adkins and Gent (ref 6-9) investigated the effects of elastomer length on stiffness by considering the load-deflection relations of eight bearings of different lengths but constant d/D ratios. The four principal modes of loading were considered: (1) torsional, (2) axial, (3) radial and (4) bending (also referred to as tilting). As a means of verifying their predictive techniques, a bearing having a d/D ratio considerably different from the constant value mentioned previously was also included.

The torque necessary to rotate the inner elastomer surface about its axis in torsional loading through an angle (H) for a single pad is given by Stevenson (ref 6-12) and Rivlin (ref 6-13) as

$$T = \frac{\pi G D^2 L}{(D/d)^2 - 1} \quad (H)$$

Adkins and Gent used this relationship and measured torsional data to calculate the shear modulus of the elastomeric material used in their experimental bearings. The torsional loading mode was used since the end effects would be negligible if the angle of twist were kept small.

The results of this experimental work is shown in Table 6-4. A comparison of predicted and measured data is made in para 6.2.6.

6.2.6 Comparison of Prediction With Measured Data

Several comparisons of predicted and measured data are available. These will be summarized as follows:

1. Computer design curves, Lindley (ref 6-3) and Bakken (ref 6-12).

TABLE 6-4

MEASURED STIFFNESS (ADKINS AND GENT)

Bearing No.	L (in.)	d (in.)	D (in.)	d/D	L/D	G (psi)	K_T (in.-lb/deg)	K_A (lb/in.)	K_R (lb/in.)	K_B (in.-lb/deg)
1	0.25	0.490	1.016	0.48	0.25	52	0.224	88	288	0.141
2	0.50	0.490	1.016	0.48	0.49	66	0.565	257	1,114	0.608
3	0.75	0.490	1.016	0.48	0.74	49	0.631	293	1,448	1.148
4	1.00	0.490	1.016	0.48	0.98	64	1.096	551	3,259	3.405
5	1.25	0.490	1.016	0.48	1.23	49	1.049	501	3,220	5.244
6	1.50	0.490	1.016	0.48	1.48	53	1.359	698	4,698	11.552
7	1.75	0.490	1.016	0.48	1.72	47	1.418	689	5,057	16.872
8	2.00	0.490	1.016	0.48	1.97	53	1.809	863	6,266	28.576
9	3.80	0.559	2.625	0.21	1.45	68	4.712	997	3,472	60.192

2. Figure 6-18, Multiple Pad Bearing: Measured Computer Design Curves and Finite-Element Analysis.
3. Single pad (L/D = 0.5, d/D = 0.6) and computer design curves.
4. Tilting: Adkins-Gent (ref 6-9) and Bakken (ref 6-12).

Figure 6-23 shows the plane stress solution (very low values of L/D) of Lindley to be lower than the computer values while the plane strain solution (large L/D) is higher. These results would be expected and show the need for the design curves. The closed-form solution by Bakken shows good agreement for values of d/D equal to and greater than 9.0.

Reasonably good agreement is seen between predicted and measured values of axial and torsional stiffness for the multiple pad bearing.

	Stiffness (lb/in.)	
	Measured	Predicted
Axial	5,378	6,180
Torsional	139	167
Radial	0.757×10^6	1.76×10^6

At first the predicted radial stiffness appears to be double the measured value; however, finite-element analysis of the multiple pad bearing indicates that for the applied testing loads, the tensile side of the elastomer was subjected to a state of hydrostatic tension greater than 3/4 of the material tensile modulus. As pointed out in Volume II, this condition results in cavitation of the elastomer and that portion adds no structural capability to the bearing.

The computer design curves and present computer codes do not reflect this phenomenon, and thus the predicted radial stiffness could be as much as half the amount shown and good agreement is seen.

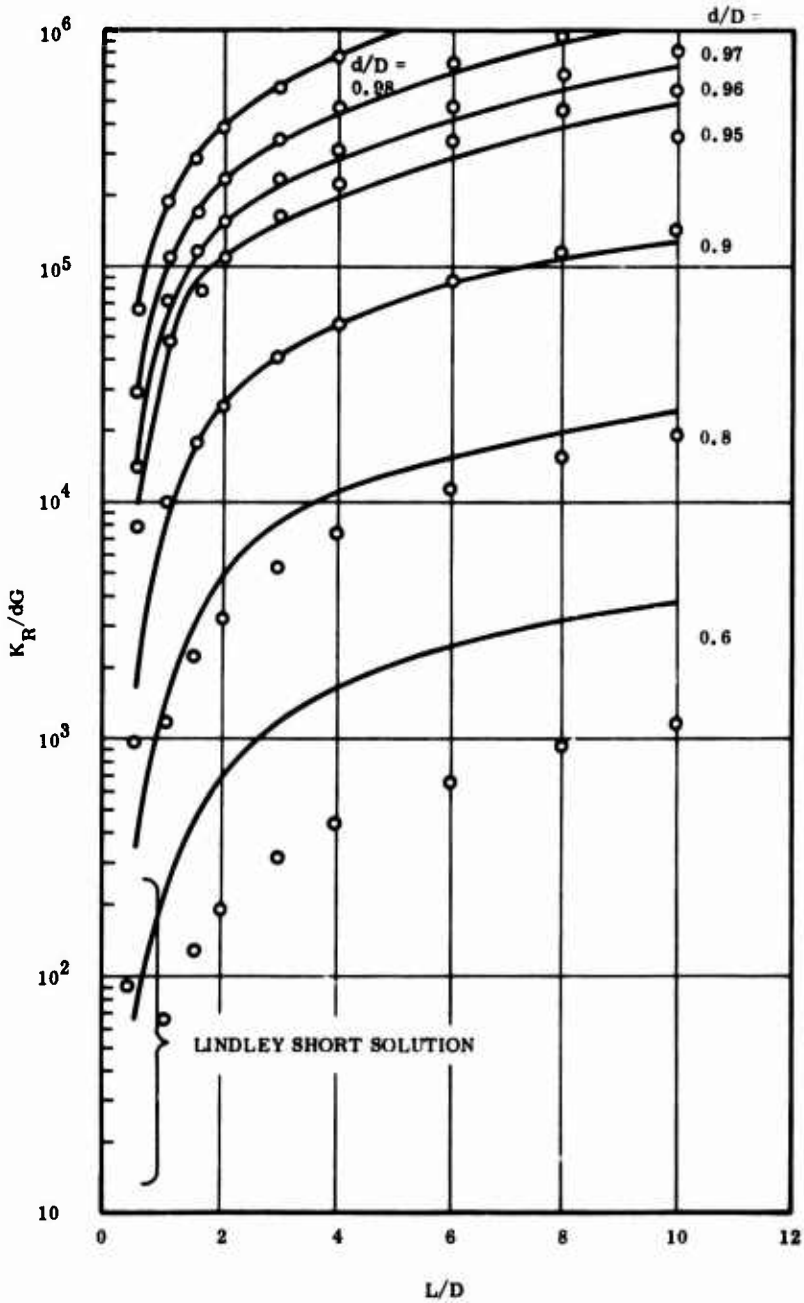

Figure 6-23. Comparison of Computer Design Curves (Lindley and Bakken) for Radial Stiffness

Comparison of the single pad bearing resulting from the Thiokol test program shows:

	Stiffness (lb/in.)	
	Predicted	Measured
Radial	6,305	4,667
Axial	931	777

The predicted values are somewhat higher than the measured. This difference is greater than the difference for the multiple shim bearing and could be the result of partial failure of the specimen during the manufacturing cool-down period. The specimen was not dissected, and this speculation is not as yet definitely confirmed.

An equation has been derived to enable the calculation of the tilting stiffness from the radial and axial stiffnesses. This is in the form of

$$K_\beta = r^2 K_a + \sum_{m=1}^{m=\infty} \frac{L^2}{4} + \frac{K_m}{2^m}$$

where $r = \frac{D+d}{4}$

K_m = radial stiffness (K_r) for a pad of length $l = \frac{L}{2^m}$

K_a = axial stiffness of pad of length L

Usually four terms in the series are sufficient. A comparison using measured data of Adkins and Gent (ref 6-9) has been made:

	Bending Stiffness (in.-lb/deg)	
L/D	Measured	Calculated
0.49	0.608	0.502
0.98	3.405	3.860
1.48	11.552	11.263
1.97	28.576	28.834

All of the above bearings had a d/D value of 0.6.

It is seen from the above that the calculated values using the radial and axial stiffnesses are in reasonably good agreement with measured data for preliminary design purposes.

6.3 TYPE III VERIFICATION

6.3.1 Selection of Type

A Type III bearing consists of alternate spherically shaped layers of rubber pads and metal shims. It is designed to allow rotation about all three axes - like a ball and socket - and yet support a high load along its axis and a moderate load transverse to its axis. It is used as a main rotor blade bearing, as it would allow lead-lag, flapping and feathering, and yet would support the blade centrifugal load while transferring the rotor torque to the blade.

Two types of spherical bearings, IIIA and IIIB, were tested to verify the analytical procedures given in the Design Manual, Volume II (ref 5-1). Comparisons of service life and stiffness tests with predictions are made in this section. Buckling results are discussed in Section 5.0.

6.3.2 Specimen Design

The specimens were fabricated using shims available from a rocket nozzle vectoring program, and although they are valid test bearings, they do not necessarily represent optimum helicopter rotor designs.

Originally, the shims were designed for one long bearing. As a result, the included half angle, B', for the Type IIIA bearing ranges from 31 deg for the first shim to 21 deg for the last shim, and the Type IIIB bearing ranges from 20 deg for the first shim to 15 deg for the last shim.

The shims for Type IIIA were formed with radii on their inside diameters, and all the pads were molded with radii on their outside diameters to eliminate stress concentrations in the pads.

Cross-sectional sketches of the two types of bearing are shown in Figures 6-24 and 6-25.

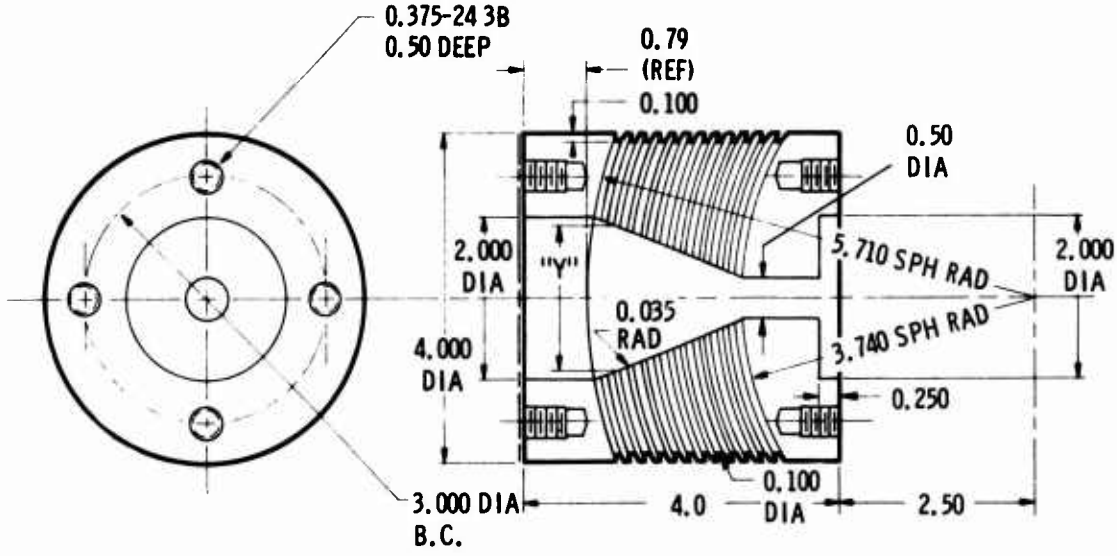

Figure 6-24. Type IIIA Elastomeric Bearing

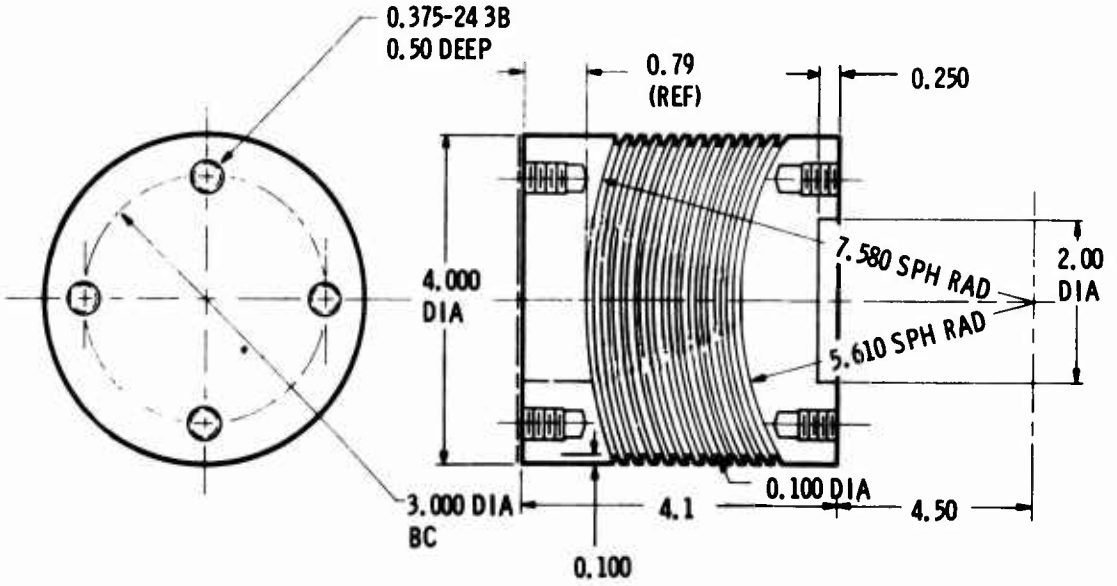

Figure 6-25. Type IIIB Elastomeric Bearing

6.3.3 Fabrication of Specimen

The Type IIIA bearing was fabricated to Thiokol Drawing 7U46959 and the Type IIIB to Thiokol Drawing 7U46960. The mold tool for the Type IIIA bearing is shown in Figure 6-26. The mold tool for the Type IIIB configuration is the housing for the Type IIIA configuration, without the center plug.

6.3.3.1 Processing Data Type IIIA

1. Solvent-clean all bearing components and the mold tool.
2. Grit-blast,with silica sand, the bonding surfaces of each of the end plates and both surfaces of the steel shims.
3. Solvent-clean each of the grit-blasted pieces.
4. Obtain Chemlok 205, stir thoroughly, and paint the bond areas of both end plates and each of the shims. Air-dry for 15 minutes.
5. Obtain Chemlok 220, stir thoroughly, and paint the areas of end plates and shims painted with 205. Air-dry for 30 minutes.
6. Cut an elastomer pad for each shim with corresponding ID and OD.
7. Place end plate with largest ID in the mold housing. Insert the center plug.
8. Insert corresponding elastomer pad on end plate in the mold. Insert a piano wire spacer in the mold housing to form outside radius. Insert the first shim into housing, and place an elastomer pad and wire spacer into housing. Repeat this operation until stackup is complete and second end plate is installed.
9. Place this mold assembly in a press preheated to 300° F, apply sufficient pressure to close the press platens on the mold housing, and cure for 1 hr and 15 minutes.

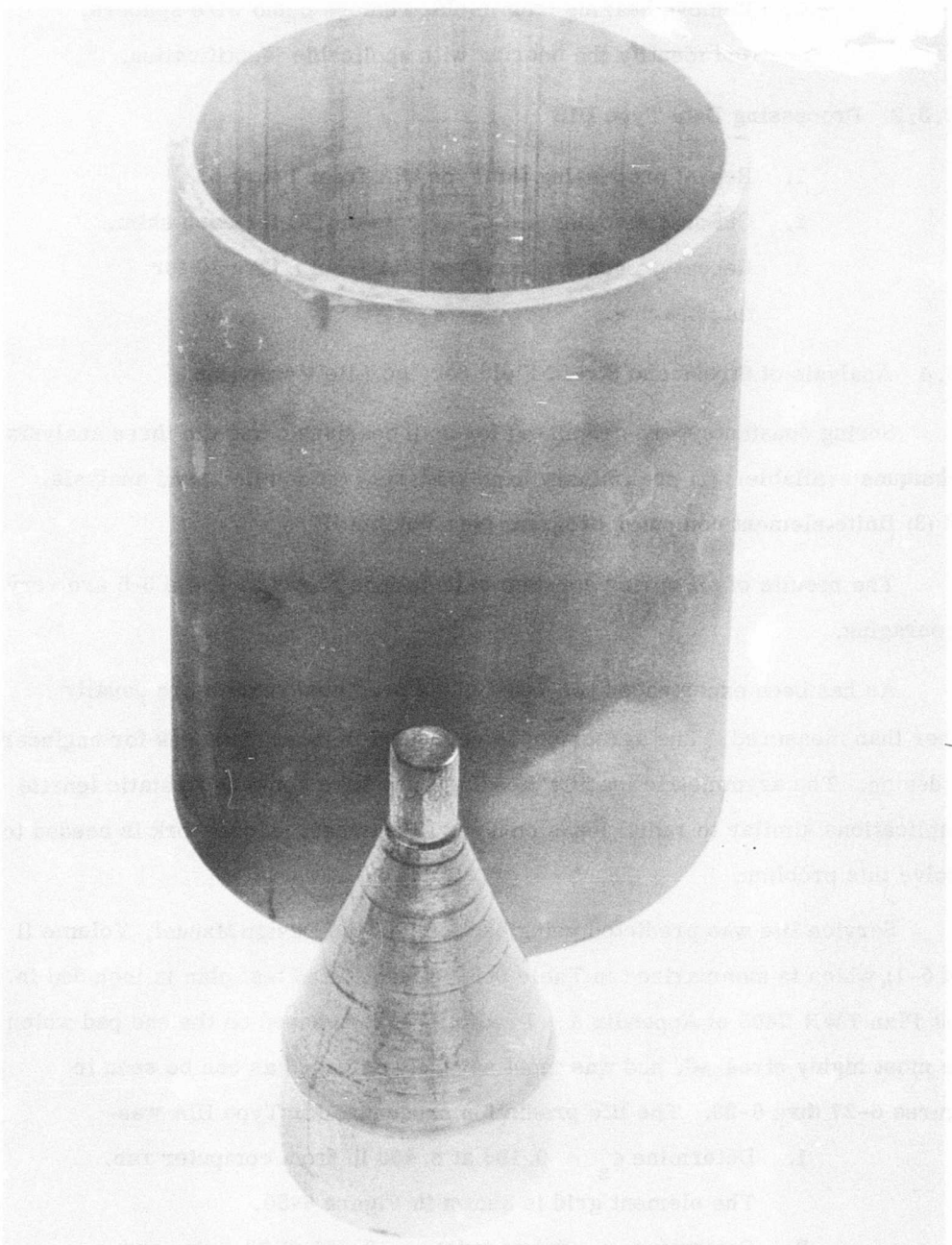

Figure 6-26. Mold Tool

10. Remove bearing from mold, remove piano wire spacers, and identify the bearing with applicable identification.

6.3.3.2 Processing Data Type IIIB

1. Repeat processing for Type IIIA from 1 thru 5.
2. Cut an elastomer pad of the current OD for each shim.
3. Repeat processing for Type IIIA from 8 thru 10 for this bearing.

6.3.4 Analysis of Stress and Strain Field Service Life Prediction

Spring constants were calculated for both bearings using the three analysis techniques available: (1) preliminary hand analysis, (2) detailed hand analysis, and (3) finite-element computer program (see Volume II).

The results of all spring constant calculations shown in Table 6-5 are very encouraging.

As has been experienced previously, the predicted results are usually higher than measured. The agreement is very good in most instances for engineering design. The asymmetric loading (bending) may have some hydrostatic tensile complications similar to radial loads on Type II bearings. More work is needed to resolve this problem.

Service life was predicted using Section 9 of the Design Manual, Volume II (ref 5-1), which is summarized in Table 6-6. The detailed test plan is included in Test Plan TWR-7405 of Appendix A. Predictions were based on the end pad which was most highly stressed, and was most severely damaged as can be seen in Figures 6-27 thru 6-29. The life prediction procedure for Type IIIA was:

1. Determine ϵ_z = 0.106 at 8,400 lb from computer run. The element grid is shown in Figure 6-30.
2. Determine γ_θ (due to twist) = 0.066 at 22.5 deg and 0.37 at 12.5 deg from computer run.

TABLE 6-5

SPRING CONSTANT COMPARISON
(TYPE IIIA AND IIIB SPECIMENS)

	Preliminary Equations	Detailed Equations	Computer Analysis	Wyle Test
TYPE IIIA				
Axial K_A (lb/in.)	156,000	134,000	138,000	100,000 to 130,000
Static Torsional K_T (lb/in./deg)	34.60	37.02	33.50	26.60 to 28.30
Dynamic Torsional K_T (lb/in./deg)	40.30	43.30	39.00	40.00 to 46.70
Bending (lb/in.)	--	7,150	6,620	5,000
TYPE IIIB				
Axial K_A (lb/in.)	505,000	424,000	411,000	360,000 to 400,000
Static Torsional K_T (lb/in./deg)	34.90	35.98	32.90	27.10
Dynamic Torsional K_T (lb/in./deg)	40.70	41.80	38.30	41.70 to 45.00
Bending (lb/in.)	--	--	--	--

TABLE 6-6

TYPE IIIA AND IIIB SPECIMEN TEST SUMMARY

Specimen	Hours	Total Hours	Load P (lb)	Load F (lb)	Twist θ (deg)	Hours to Buckle	Hours to Failure	Predicted Life
IIIA-1	1,200	(1,200)	8,400	±500	2.5 ± 10	--	--	244
IIIA-2	850	(850)	8,400	±500	2.5 ± 10	--	600-800	244
IIIA-3	176	(176)	8,400	±500	12.5 ± 10	--	65-176	100
IIIA-4	732	(732)	8,400	±500	12.5 ± 10	--	132-532	100
IIIA-5	127	(127)	8,400	±500	12.5 ± 10	--	0-127	100
IIIB-1	45	(45)	36,000	±1,000	0 ± 10	45	--	--
	200	(245)	8,400	0	12.5 ± 10	--	--	--
IIIB-2	54	(54)	36,000	±1,000	0 ± 10	54	--	--
IIIB-3	8	(8)	36,000	±1,000	0 ± 10	--	--	--
	14	(22)	16,800	±1,000	0 ± 10	22	--	--
IIIB-4	0	(0)	20,000	0	0	0	--	--
IIIB-5	14	(14)	16,800	±1,000	0 ± 10	--	--	--
	48	(62)	8,400	±500	12.5 ± 10	62	--	--
	531	(593)	8,400	0	2.5 ± 10	--	--	--
IIIB-6	19	(19)	15,000	±1,000	2.5 ± 10	19	--	--
	381	(400)	15,000	±500	2.5 ± 10	--	--	--
IIIB-7	19	(19)	15,000	±1,000	2.5 ± 10	--	--	--
	381	(400)	15,000	±500	2.5 ± 10	--	--	--

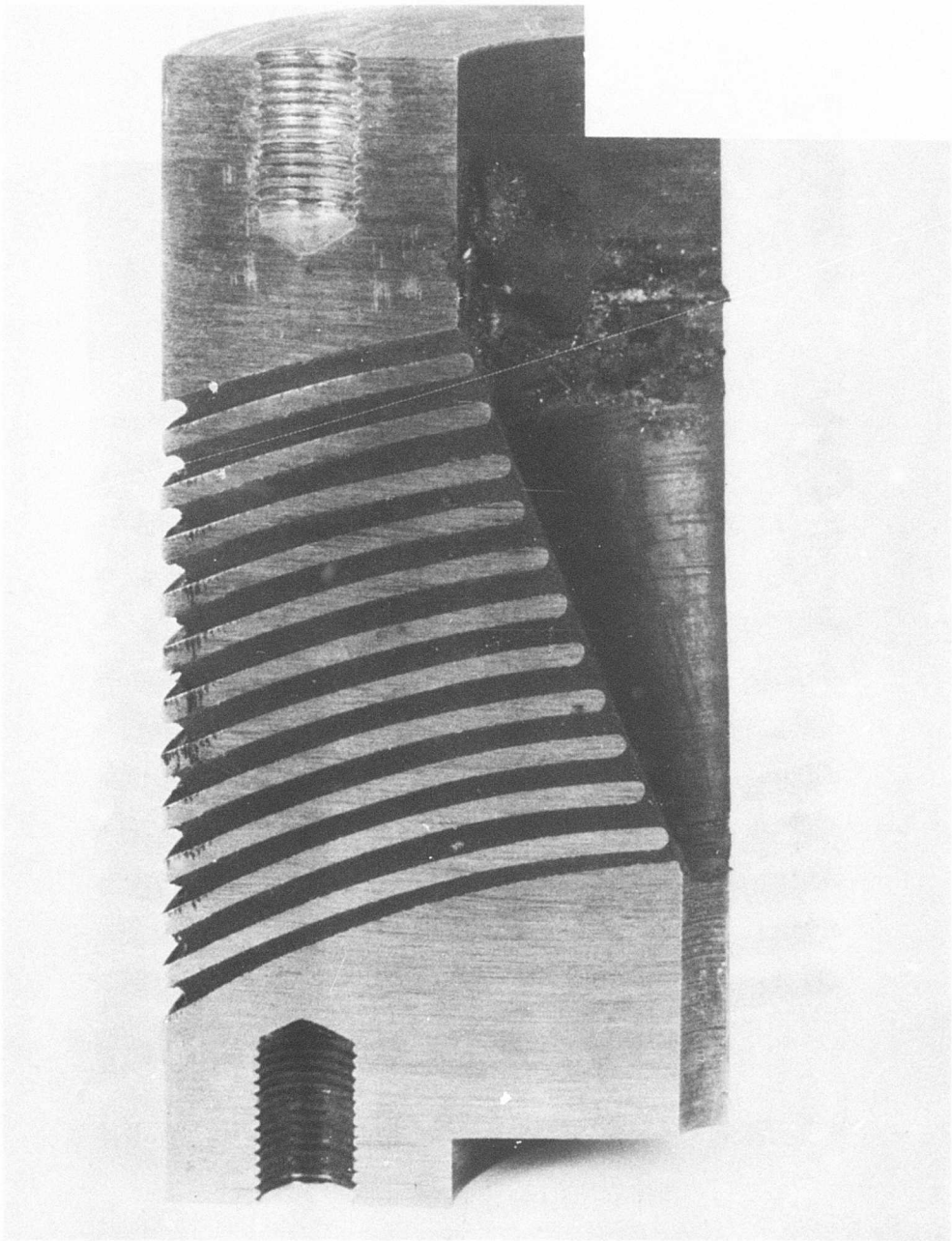

Figure 6-27. Failed Specimen Type IIIA (View 1)

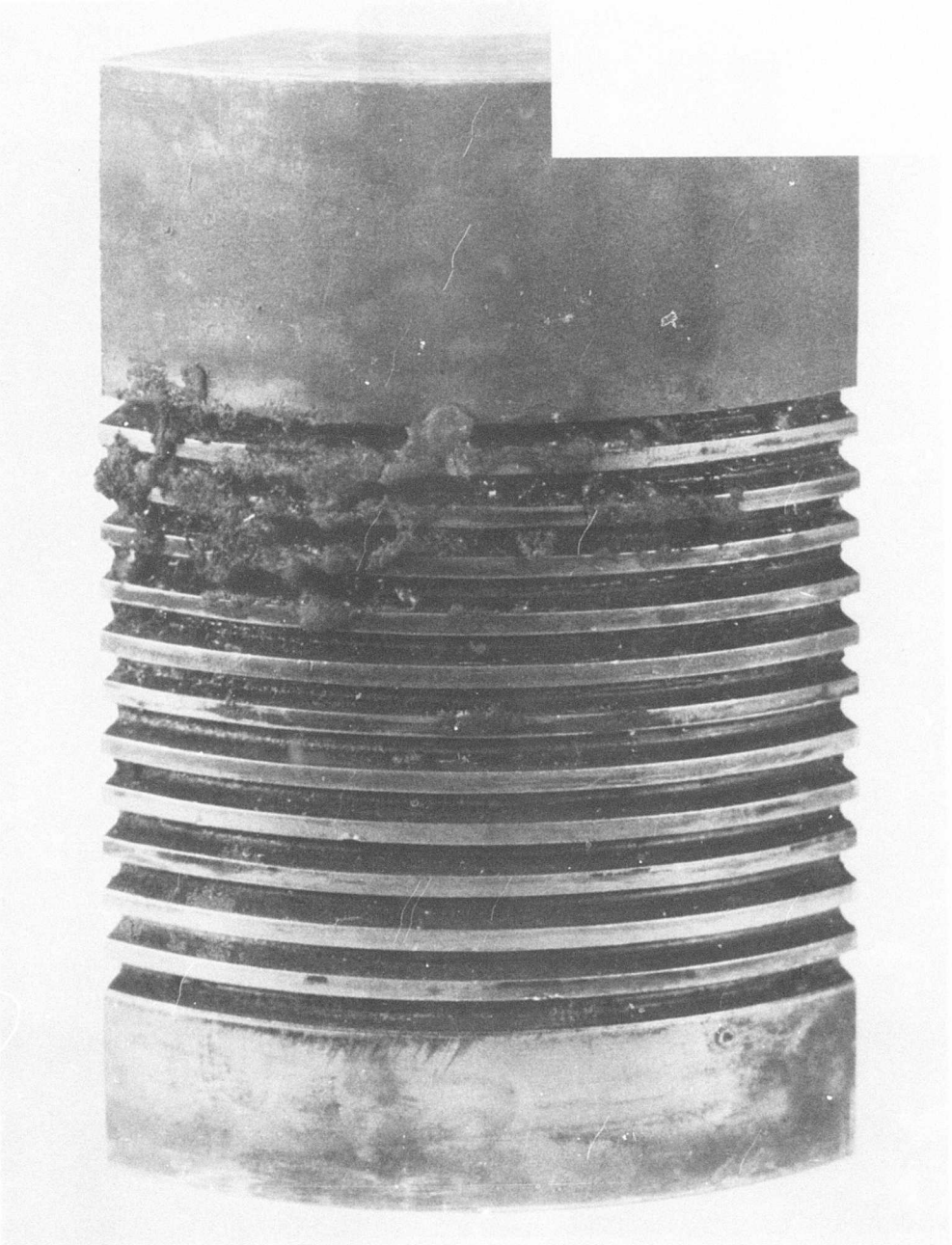

Figure 6-28. Failed Specimen Type IIIA (View 2)

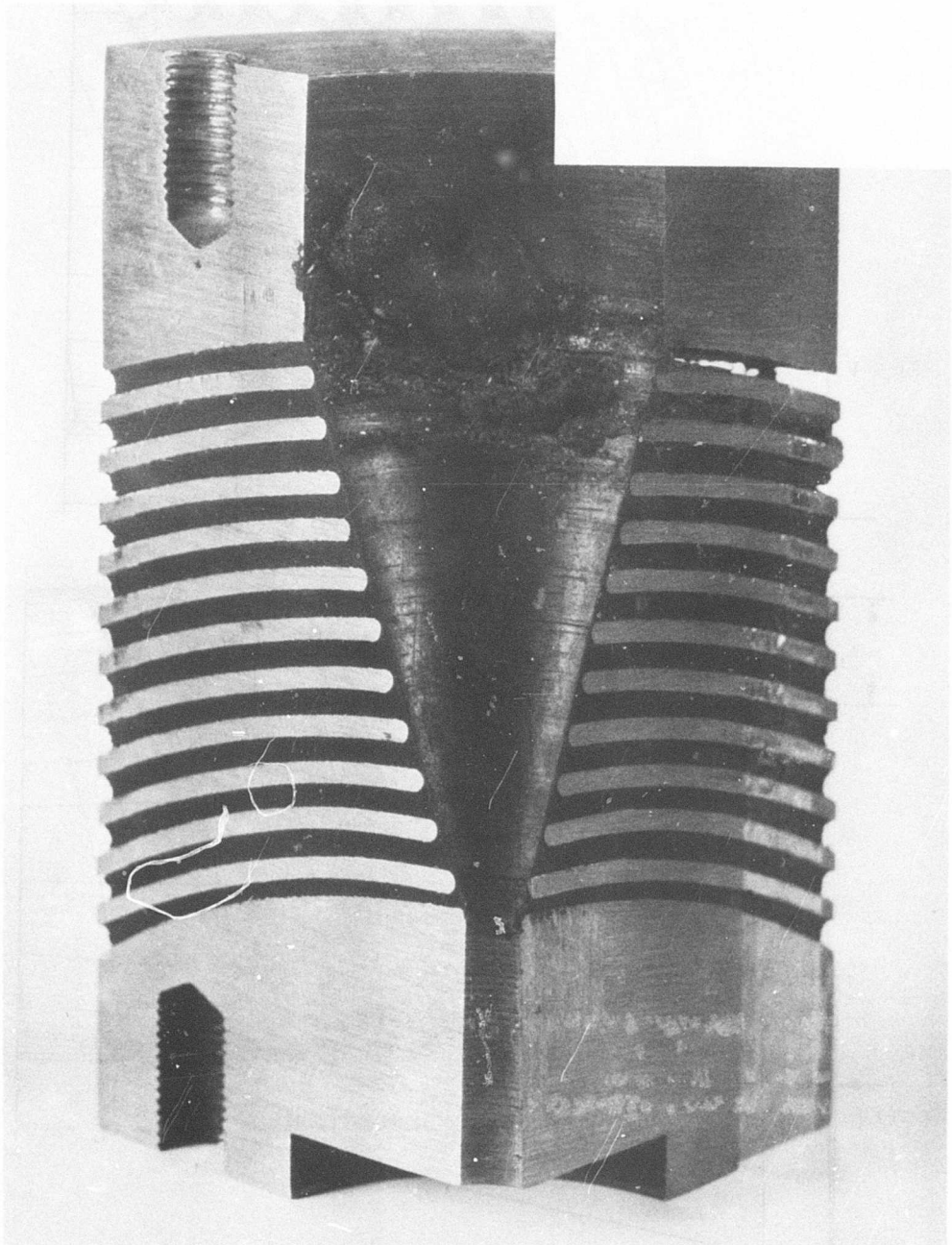

Figure 6-29. Failed Specimen Type IIIA (View 3)

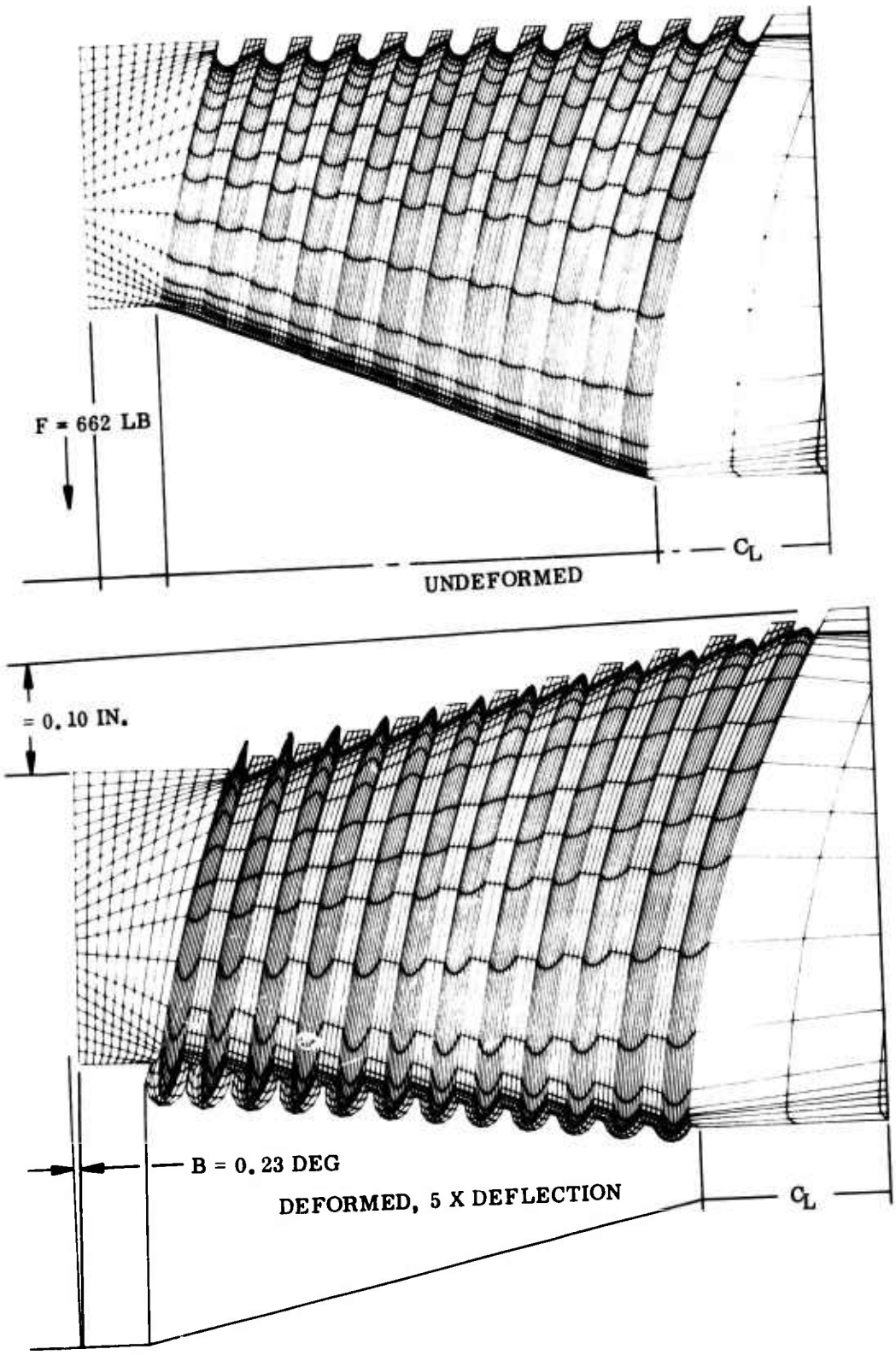

Figure 6-30. Type III Finite-Element Grids (Asymmetric Bending Load)

3. Determine γ_B (due to bending) = 0.92 with a 500 lb side load from computer run.
4. Calculate $\gamma_{eff} = (\gamma_\theta^2 + \gamma_B^2)^{1/2}$ = 1.135 at 22.5 deg and 0.992 at 12.5 deg.
5. Calculate $\tau_{eff} = G\gamma$ = 100 x 1.135 and 100 x 0.992 = 113.5 psi and 99.2 psi.
6. Find life, N = 0.9×10^6 and 2.2×10^6 from Figure 4-10.
7. Calculate life in hours, H = $\frac{N \times 2}{60 \times 300}$ = 100 and 244 hr. Test frequency was 300 cycles/minute. N is multiplied by 2 since the peak was reached only once per cycle.

Predicted and test service life are shown in Table 6-6. None of the Type IVB specimens were tested to failure, while all but one of the Type IIIA failed. The predicted life is within the data scatter for high torsional strains, but below test results for the low strain specimens.

6.3.5 Specimen Testing

The Type III testing program was subcontracted to Wyle Laboratories, Huntsville, Alabama. Five Type IIIA and seven Type IIIB specimens were included in the test program.

Figures 6-31 and 6-32 show the test setup. The specimens were to be simultaneously loaded with (1) a constant axial load, P, (2) a cyclic torsional displacement, θ, and (3) a cyclic transverse force, F.

Properties to be determined were: (1) static axial spring rate, (2) static torsional spring rate, (3) dynamic torsional spring rate at 300 cpm, (4) combined transverse-bending spring rate, and (5) bearing life, defined as service hours required to reduce torsional stiffness by 40%.

Torsional loading was always $\pm$ 10 deg, with a nominal pretwist of 0, 2.5, or 12.5 deg. Axial and side loads were varied as shown in Table 6-6. Considerable difficulty was encountered during the test with buckling of the IIIB type, and

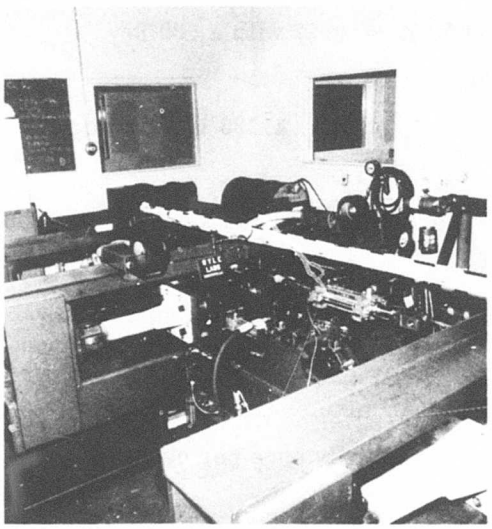

Fatigue Test Stand

Fatigue Test Stand

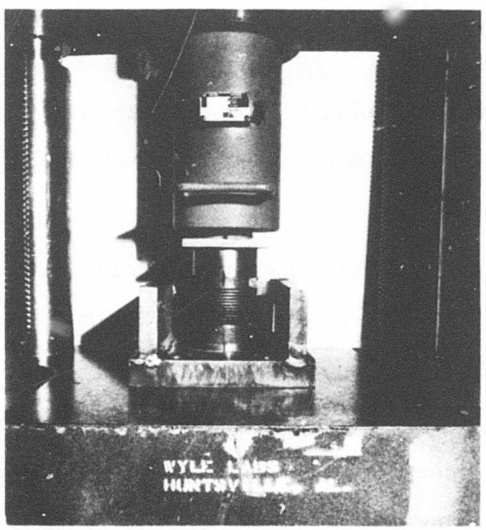

Static Compression Test Setup

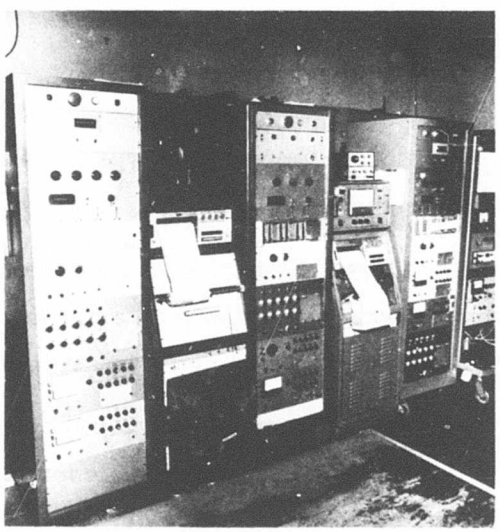

Electronic Control Consoles

Figure 6-31. Test Setup

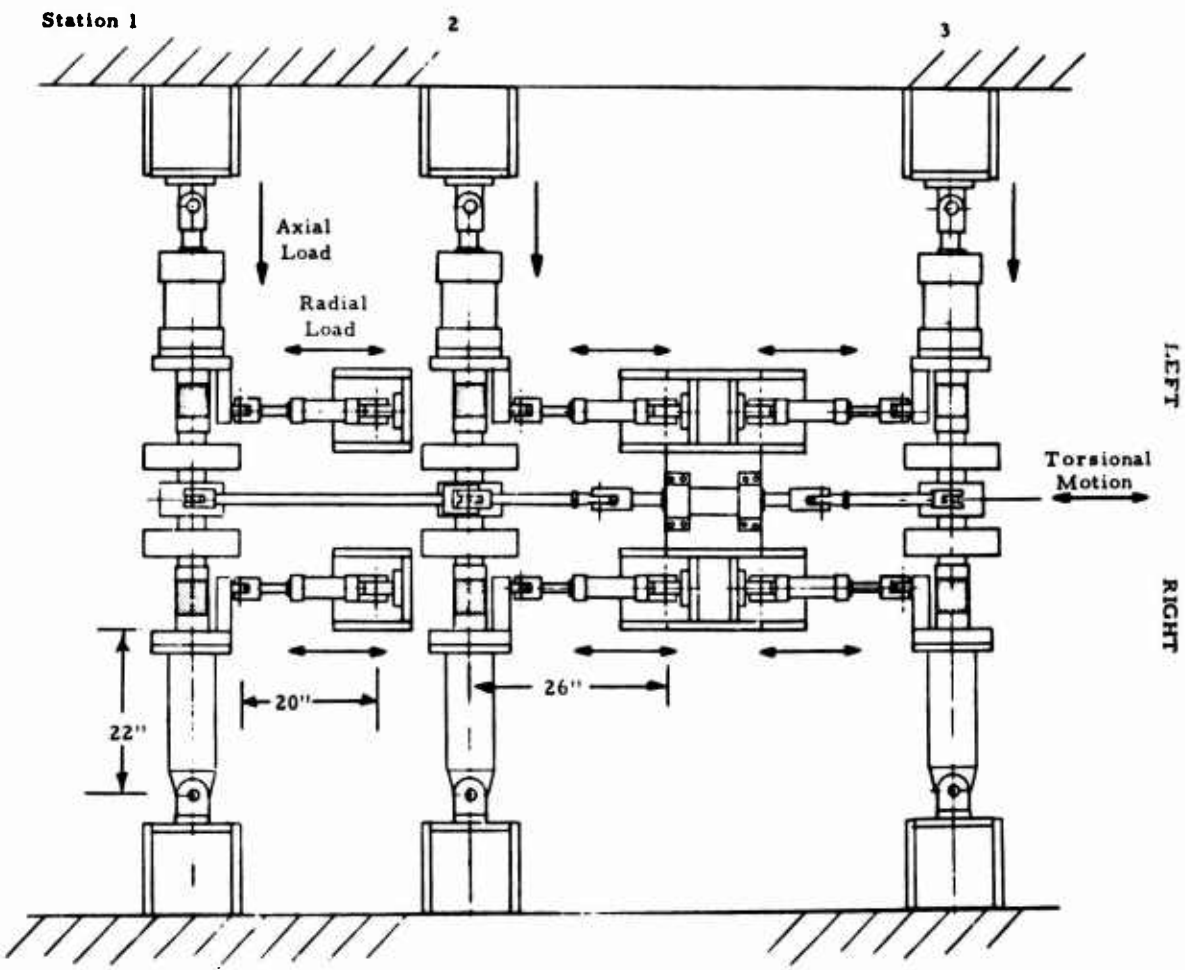

Figure 6-32. Test Setup Schematic

for most of the specimens, both the side load and axial load had to be reduced to continue testing.

Test life (Table 6-6) is shown as a range, meaning that at one check time the stiffness was all right, and at the next check time the stiffness had dropped below the 40% allowed. The exact time of failure is not known.

Failure was caused by a structural breakdown of the elastomer, which gave the appearance of reverting to unvulcanized rubber. Figures 6-27 through 6-29 show a section of a failed specimen. The onset of failure could be visually observed long before the bearing had "failed" by the arbitrary definition of a 40% reduction in torsional stiffness. Actually only four bearings, all Type IIIA, "failed" by the stiffness definition.

Spring constant results (summarized on Table 6-5) show that 4,800 specimen test hours were accumulated at 300 cycles/min (86×10^6 cycles total on various specimens).

7.0 CONCLUSIONS AND RECOMMENDATIONS

At the completion of this contract, several conclusions can be made:

1. The low sulfur content formulation (TR-3012) appears to give good service life and provides adequate mechanical properties for rotor design.
2. Material properties such as shear relaxation modulus, bulk modulus, and thermal coefficient of linear expansion are necessary for design purposes.
3. The three levels of design appear to be an efficient approach to bearing definition.
4. The rubber reversion due to internal heating appears to be the principal cause of bearing failure.
5. Proper design of pad edge conditions eliminates harmful stress discontinuities.
6. Linear analysis is usually sufficient for design because of the restraints imposed by stability requirements.
7. Excellent agreement exists between predicted and measured critical buckling loads.

Several areas requiring additional effort have been identified.

1. Evaluate the factors that control the elastomer reversion process.
2. Provide the helicopter industry with a code to make elastomeric bearing temperature prediction profiles as a function of loading time. This will aid in correlating bench tests with flight tests.
3. Expand service life data for Type II and Type IV bearings. Strain energy density concepts may be useful for correlating data.

4. Develop parametric design curves for both metallic and fiber-reinforced composites shim materials.
5. Study elastomeric bearing tolerances to determine the performance sensitivity to manufacturing tolerance variations.
6. Study the bending compliance to various geometric shapes and configurations.
7. Increase the material repertoire by studying various candidate materials and formulations.
8. Complete the analysis of the Type IV bearing and provide parametric design curves.
9. Extend stability analysis and verification to Type III and Type IV bearings.
10. Update parametric design curves and computer code to reflect feedback from users.

REFERENCES

2-1 Natural Rubber Compounds for Low Creep and Improved Dynamic Performance, J. I. Smith, NRPRA, 3rd Rubber in Engineering Conference, 1973.

2-2 Improved Method of Vulcanizing Natural Rubber, M. Porter, NR Technology, Vol 4, Part 4, 1973.

2-3 Carbon Black Effects on Engine Mount Compounds, T. A. Knurek, R. P. Salisbury, Rubber World, August 1964.

2-4 Natural Rubber Formulations for Engineering Applications, D. J. Elliott, NR Technology, 1972, Part 3.

2-5 Private Communication with Dr. P. B. Lindley, Malaysia Rubber Products Research Associates, Brickendonbury, Hertford, S. G. 13, 8 NP, England.

5-1 Design Criteria for Elastomeric Bearings, Vol II, Design Manual, Thiokol Corp, June 1975.

5-2 Haringx, J. A., On Highly Compressible Helical Springs and Rubber Rods and Their Application for Vibration Free Mountings I, Philips Res. Rep. 3, pp 401-449, 1948.

5-3 Haringx, J. A., On Highly Compressible Helical Springs and Rubber Rods and Their Application for Vibration Free Mounting II, Philips Res. Rep. 4, pp 49-80, 1949.

5-4 Haringx, J. A., On Highly Compressible Helical Springs and Rubber Rods and Their Application for Vibration Free Mountings III, Philips Res. Rep. 4, pp 206-220, 1949.

5-5 Gent, A. N., Elastic Stability of Rubber Compression Springs, Journal of Mechanical Engineering Science, V6, N4, pp 3-18-326 1964.

5-6 Design Criteria for Elastomeric Bearings, Vol III, Program Users Manual, Thiokol Corp, 6 Mar 1975.

REFERENCES (Cont)

5-7 Southwell, R. V., On the Analysis of Experimental Observations in Problems of Elastic Stability, Proc. Roy. Soc. London, Ser. A, V135, pp 601-616, 1932.

5-8 Horton, W. H., Cundari, F. L., and Johnson, R. W., The Analysis of Experimental Data Obtained From Stability Studies on Elastic Column and Plate Structures, Israel Journal of Technology, V5, N1-2, pp 104-113, February 1967.

6-1 Messner, A. M., Stress Distributions in Poker Chip Tensile Specimens.

6-2 Schapery, R. A., The Poker Chip Test, ICRPG Solid Propellant Mechanical Behavior Manual, June 1963.

6-3 Lindley, P. B., Engineering Design With Natural Rubber, N.R. Technical Bulletin, Producers' Research Association.

6-4 Gent, A. N., and Meinecke, E. A., Compression Bending and Shear of Bonded Rubber Blocks, Polymer Engineering and Science, January 1970, Vol 10, Number 1, pp 48-53.

6-5 Moghe, S. R., Neff, H. F., Elastic Deformations of Constrained Cylinders, Journal of Applied Mechanics, June 1971, pp 393-399.

6-6 Gent, A. M., Henry, R. L., and Roxbury, M. L., Interfacial Stresses for Bonded Rubber Blocks in Compression and Shear, Journal of Applied Mechanics (to be published).

6-7 Payne, A. R., and Scott, J. R., Engineering Design With Rubber, London and New York, 1960.

6-8 Bulletin of 2nd Meeting of ICRPG Mechanical Behavior Working Group, November 1963.

6-9 Adkins, J. E. and Gent, A. N., Load Deflection Relations of Rubber Bush Mountings, Br. J. Appl. Phys., 1954, pp 354-358.

REFERENCES (Cont)

6-10 Stevenson, A. C., Phil. Mag., p 766 (1943).

6-11 Rivlin, R. S., Phil. Trans. A., p 173 (1949).

6-12 Private Communication With Gordon Bakken, Thiokol/Wasatch.

APPENDIX A

TEST PLANS

DOC NO. TWR-7405 VOL REV
TITLE AS-015
Contract DAAJ02-73-C-0091

TEST PLAN FOR MATERIAL CHARACTERIZATION TESTS

Project No. CR101-01-01
CR102-01-01
CR103-01-01

August 1973

1.0 SCOPE

This document defines the mechanical tests to be performed on a natural rubber compound for the purposes of characterizing the material. These tests shall define the following mechanical properties:

1. Tensile strength and elongation
2. Tensile modulus
3. Shear strength and elongation
4. Shear modulus
5. Compression modulus
6. Compression set
7. Hardness
8. Adhesion
9. Ozone environment
10. Aging

2.0 APPLICABLE DOCUMENTS

2.1 ASTM Standards

D412 Tension Testing of Vulcanized Rubber

D395 Compression Set of Vulcanized Rubber

D429 Adhesion of Vulcanized Rubber to Metal

D1149 Accelerated Ozone Cracking of Vulcanized Rubber

D573 Accelerated Aging of Vulcanized Rubber by the Oven Method

2.2 Thiokol/Wasatch Standard Laboratory Procedures

SLP 668 Testing of Natural Rubber Compound

3.0 TEST PROCEDURE

3.1 Tensile Tests

3.1.1 General

Tensile testing shall be performed in accordance with ASTM D412 test method to obtain tensile strength and deflection characteristics of the natural rubber material.

3.1.2 Specimen

The specimen shall be a "dog bone" or "dumb bell" type cut from sheet stock of approximately 0.10 inches thick.

3.1.3 Requirements

Testing shall be done at three temperature environments, -40, +70, and +160^{o} F, with the load-deflection trace continuously recorded. The testing variables and specimen configurations are depicted in Table I and all specimens shall be pulled at 0.5 inches/minute.

3.1.4 Data

Load-deflection plots shall be recorded for each test from which the following data will be obtained:

1. Tensile modulus at 10, 30, 100, and 300% elongation.
2. Tensile strength at failure.
3. Tensile elongation at failure.

3.2 Shear Tests

3.2.1 General

Shear testing shall be performed with Quadruple Lap Shear (QLS) specimens in accordance with the Thiokol/Wasatch laboratory procedure SLP 668 to obtain lap shear strength and deflection characteristics of the natural rubber material.

3.2.2 Specimen

The specimen shall be a lap-shear type fabricated in accordance with SLP 668. The rubber thickness will be treated as a variable.

3.2.3 Requirements

Testing will be performed at a load rate of 0.5 in/min. The specimen variables are defined in Table II and include:

1. temperature
2. lateral pressure
3. rubber laminate thickness

3.2.4 Data

Load deflection plots shall be recorded for each test from which the following data will be obtained:

1. Shear modulus at 10, 30, 100, and 300% elongation
2. Shear strength at failure
3. Tensile elongation at failure

3.3 Compression Modulus

3.3.1 General

The compression modulus of natural rubber with plates bonded to the opposing planar surfaces shall be obtained from round disk specimens.

3.3.2 Specimen

The test specimen shall be cylindrical in shape, 3.0 inches in diameter, with 0.25 inch thick plates bonded to the surfaces of the rubber stock.

The specimen shall be compressive molded with the surfaces of the steel plates, in contact with the elastomer, cleaned, primed, and with adhesive applied in accordance with the manufacturers specifications. The thickness of the rubber laminate will be treated as a variable.

3.3.3 Requirements

Axial compressive loading shall be applied normal to the surface of the plates at a rate of 0.5 inches per minute. The load shall be continuously applied, stopping only for photo and deflection measurements, to an average axial strain of 100 percent at which time loading shall be terminated. Loading shall be intermittently stopped at designated strain levels for deformation measurements.

The test variables shall consist of rubber laminate thicknesses and temperatures as specified in Table III.

3.3.4 Data

Load-deflection plots shall be continuously recorded for each test and the following data will be obtained from these plots:

1. Compression modulus at 10, 30, 50, and 100 percent deflection

For the room temperature tests, a still photo capable of being magnified shall be taken of the deflected specimen at each of the following strain levels: 10, 30, 50, and 100%. A back-ground grid (10 x 10 to the 0.50 inch) shall be employed to facilitate the post test configuration analysis of the deflected shape.

A measurement of the diameter of the deflected rubber shape using a micrometer shall also be taken at each of the designated strain levels and correlated with the photo.

3.3 5 Reports

The reports shall include the following:

1. Date of test
2. Test temperature
3. Description of test apparatus
4. Physical dimensions of specimens
5. Load rate
6. Load-deflection plots
7. Photos
8. Physical dimensional measurements performed during test

3.4 Compression Set

3.4 1 General

The compression set of the vulcanized natural rubber material shall be performed in accordance with ASTM specification ASTM D395, Method B, at room and elevated temperatures.

3.4.2 Specimen

The specimen shall be of a disk shape and sized, diameter and thickness, within the intent of specification D395. Fabrication technique is optional.

3.4.3 Requirements

Method B (Compression Set Under Constant Deflection) shall be utilized and the 25 percent compression mode will be employed for all specimens with the type of loading device optional. The test configurations are as follows:

Specimen	Temp (^{o}F)	Qty
CSR	+ 20	3 min
CSH	+160	3 min

3.4.4 Data

Reporting of data shall be in accordance with ASTM D395.

3.5 Hardness

3.5.1 General

The Shore A hardness test on the vulcanized natural rubber shall be performed in accordance with the Thiokol/Wasatch SLP 668. The test specimen configuration, test requirements, and data will be per referenced specification.

3.6 Adhesion

3.6.1 General

The adhesion of the natural rubber bonded to a steel plate will be evaluated by Method B of the ASTM specification D429 which depicts a 90 degree stripping configuration.

3.6.2 Specimen

The specimen shall be in a basic agreement with the D429, Method B, configuration which depicts a 1.0 inch x 1.0 inch bond test area and a 0.25 inch thick strip of rubber.

3.6.3 Requirements

Testing shall be done at three temperature environments: -40, +70, and +160^{o} F. Five (5) specimens per temperature environment shall constitute a test when the failure exhibits some form of adhesive mode. However, if failures are cohesive (strap breakage) only three (3) specimens per test will be required. All specimens will be pulled at a uniform rate of 2.0 inches/minute.

3.6.4 Data

The description of failure relative to the cohesive-adhesive behavior including loads shall be recorded in accordance with D429.

3.7 Ozone

3.7.1 General

The effect of ozone of the mechanical shear properties of vulcanized rubber sandwiched between steel plates shall be qualitatively evaluated by QLS specimens conditioned in an ozone chamber. The general testing procedures and apparatus will be in accordance with ASTM specifications D1149.

3.7.2 Specimen

The QLS specimen defined in Section 3.2 having a rubber thickness of 0.090 inches shall be employed in place of the strip type depicted in D1149. All exposed edges of the elastomer in the QLS specimen must be free of foreign material.

3.7.3 Requirements

3.7.3.1 Exposure

The specimen shall be placed in the ozone chamber having an internal temperature of 70^{o} F with the specimen in a strained condition. The strain level and the time duration of exposure will be the primary variables as defined in Table IV.

3.7.3.2 Mechanical Testing

After exposure to the environments depicted in Table IV, the specimens will be mechanically tested in accordance with Section 3.2

3.7 4 Data

The data requirements for the mechanical testing are the same as those depicted in Section 3.2. The data associated with ozone conditioning shall be in accordance with ASTM D1149.

3.8 Aging

3 8.1 General

The effect of aging on the apparent shear properties of natural rubber will be evaluated using QLS specimens in conjunction with the requirements of ASTM standard D573. The results of these tests will be compared against the data acquired from tests depicted in Sections 3.2 and 3.7.

3.8.2 Specimen

The QLS specimen defined in Section 3.2 will be employed in place of the tensile type designated in D573. A rubber laminated thickness of 0.090 inches shall be employed.

3.8.3 Requirements

3 8.3.1 Exposure

The specimen shall be subjected to an oven environment in accordance with D573 with the specimen in a relaxed (no load) condition. The temperature and aging interval shall be treated as the primary variables defined in Table V.

3.8.3.2 Mechanical Testing

After exposure to the environment depicted in Table V, the specimen will be mechanically tested in accordance with Section 3.2. Testing will be performed at room temperature.

3.8.4 Data

The data requirements for the mechanical testing are the same as those depicted in Section 3.2 The conditioning environments shall be defined in accordance with D573.

4.0 REPORTS

The test reports shall consist of individual test summaries containing a description of the tests and data in accordance with the respective test standards or specified within this document. In general, the following information shall be included:

1. Description of the specimen including dimensions and date of fabrication.
2. Description of the test apparatus.
3. Temperature of environments (Conditioning and testing).
4. Details of load-deflection data
5. Observations pertinent to test and results
6. Failure definitions
7. Anomalies and/or deviations relative to prescribed procedures.
8. Date of test

TABLE I

TENSILE TESTS

Specimen	Temp (°F)	Qty
TL	- 40	5
TM	+ 70	5
TH	+160	5

TABLE II

QLS TEST CONFIGURATIONS

Specimen	Test Temp °F	Lateral Press° (% strain)	Rubber * Thickness (inches)	Qty
SPO	70	0	.09	5
SPZ	70	20	.09	5
SP5	70	50	.09	5
SP10	70	100	.09	5
SH	+160	0	.09	3
SC	- 40	0	.09	3
STO	+ 70	0	.05	5
ST5	+ 70	50	.05	5
ST10	+ 70	100	.05	5

* Approximate targeted configuration

° % strain = $\frac{\text{lateral deflection}}{\text{rubber thickness}}$ x 100

TABLE III

COMPRESSION MODULUS TESTING

Specimen	Temp (°F)	Rubber Thickness (inches)	Qty
CRN	70	0.075	5
CRK	70	0.40	5
CHN	+160	0.075	3
CHK	+160	0.40	3
CLN	- 40	0.075	3
CLK	- 40	0.40	3

TABLE IV

QLS OZONE EXPOSURE CONDITIONING

Specimen	Shear Strain (%)	Time of Exposure (weeks)	Qty
OLS	10	4	3
OMS	25	4	3
OHS	50	4	3
OLM	10	12	3
OLM	25	12	3
OHM	50	12	3
OLL	10	24	3
OML	25	24	3
OHL	50	24	3

TABLE V

QLS AGE CONDITIONING

Specimen	Temp (°F)	Time of Exposure (weeks)	Qty
AH1	160	1	3
AH2	160	2	3
AH4	160	4	3
AM2	120	2	3
AM8	120	8	5
AL12	70	12	5
AL16	70	24	5
AL20	70	48	5

TEST PLAN
FOR
STABILITY TESTING
OF
TYPE I SPECIMENS

PROJECT NOS. CR101-02-01
CR102-01-01
CR103-01-01

1.0 INTRODUCTION

This test plan defines the stability test requirements to be performed on flat, laminate, columnar shaped Type I elastomeric bearing specimens designed and built by Thiokol Corporation. The tests will be conducted at the Thiokol Corporation Development Laboratory.

2.0 TEST OBJECTIVE

The primary objective is to generate stability data relative to the axial bending and shear stiffness of a Type I specimen with strain level and geometry treated as variables.

3.0 TEST ITEM DESCRIPTION

For the stability test each specimen shall be cylindrical in shape, 3.0 inches in diameter and made of alternating flat layers of elastomer and steel shim reinforcements. The principal geometric variables shall be:

1) Height of laminate composites
2) Thickness of steel shim reinforcements
3) Inside core diameter

A total of twenty two specimens utilizing two basic configurations as presented in Figure 1 and Table I shall be tested.

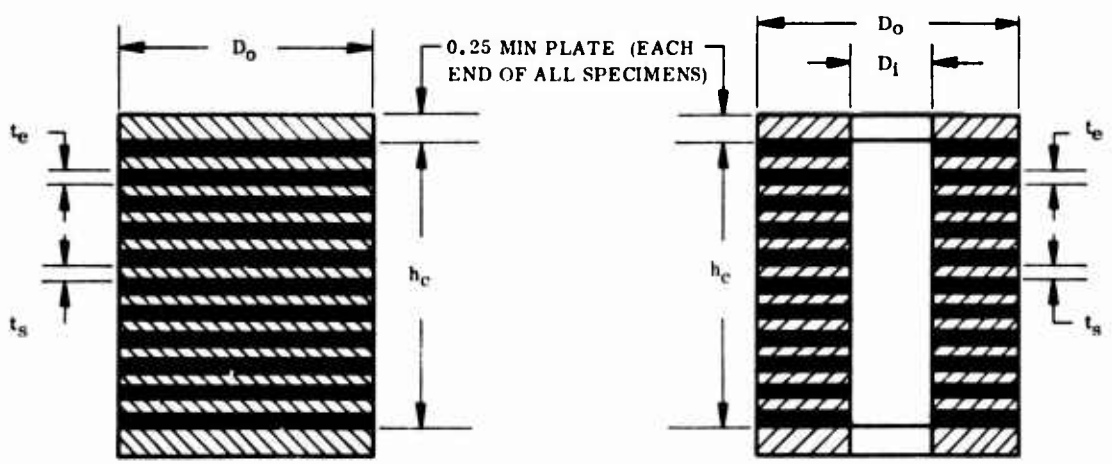

Figure 1. Typical Specimen Configurations

TABLE I

SPECIMEN DIMENSIONS

Specimen Designation	t_s	N_s	t_e	N_e	h_c	D_o	D_i	D_o/D_i
SL1 & SL2	.063	21	.125	22	4.07	3.0		
SL3 & SL4	.063	21	.075	22	2.97	3.0		
SL5 & SL6	.063	21	.045	22	2.31	3.0		
SL7 & SL8	.063	15	.125	16	2.95	3.0		
SL9 & SL10	.063	15	.075	16	2.15	3.0		
SL11 & SL12	.063	15	.045	16	1.67	3.0		
SL13 & SL14	.063	11	.125	12	2.19	3.0		
SL15 & SL16	.063	11	.075	12	1.59	3.0		
SL17 & SL18	.063	11	.045	12	1.23	3.0		
SS1	.125	15	.075	16	3.08	3.0		
SS2	.035	15	.075	16	1.73	3.0		
SD1	.063	15	.075	16	2.15	3.0	1.00	3.0
SD2	.063	15	.075	16	2.15	3.0	2.00	1.5

WHERE: t_s = Shim Thickness

N_s = Number of Shims

t_e = Elastomer Thickness

N_e = Number of Elastomeric Layers

h_c = Height of Laminate Composite

D_o = Outside Diameter

D_i = Inside Diameter

4.0 PRETEST REQUIREMENTS

4.1 Static Tests

Prior to stability testing, each specimen shall undergo three static tests at room temperature. The static test shall consist of a "stress softening" test, an axial compression test to determine the compressive spring rate (CSR), and a transverse shear test to determine the transverse spring rate (TSR). These tests will produce the data points for monitoring the change in specimen stiffness as a result of the elastomeric material's mechanical integrity decay.

4.1.1 "Stress Softening"

Each specimen shall be initially subjected to five (5) cycles of "stress softening" in an axial compressive mode of loading. Loading shall be applied at a rate of 0.02 inches per minute from zero strain to 15 percent strain and back to zero strain, completing one cycle. The maximum strain level of each specimen for "stress softening" is presented in Table II. A load-deflection plot of each cycle shall be continuously recorded.

TABLE II
15% STRAIN LIMIT VALUES FOR
STRESS SOFTENING

Specimen Designation	Axial Deflection (in.)
SL1 & SL2	.413
SL3 & SL4	.248
SL5 & SL6	.149
SL7 & SL8	.300
SL9 & SL10	.180
SL11 & SL12	.108
SL13 & SL14	.225
SL15 & SL16	.135
SL17 & SL18	.081
SS1	.180
SS2	.180
SD1	.180
SD2	.180

4.1.2 Compressive Spring Rate Test

Subsequent to the "stress softening" of each specimen (sec. 4.1.1) the CSR in the axial direction shall be determined. Loading shall be applied at a rate of 0.02 inches per minute from zero strain to 30% strain and back to zero strain, completing one cycle. Each specimen shall be subjected to two (2) cycles of loading with a load deflection plot being continuously recorded for each cycle. The maximum strain limit values of each specimen for the CSR Test are presented in Table III. Upon reaching the maximum strain limit value during the last cycle for each specimen, still photographs shall be taken as specified in section 7.1.

4.1.3 Transverse Spring Rate Test

The TSR of specimens SL1 thru SL18 shall be determined as a function of an imposed steady state axial compressive load. Each of the similar specimens (i.e. SL1 & SL2) shall be clamped together end to end by a ring fixture and placed in the test fixture with a steady state axial load applied at either end of the coupled specimens. The coupled specimens shall then be loaded normal to their axes through the ring fixture (ref Figure 2). The transverse loads shall be applied at a rate of 0.02 inches

TABLE III

30% STRAIN LIMIT VALUES FOR THE

COMPRESSIVE SPRING RATE TEST

Specimen Designation	Axial Deflection (in)
SL1 & SL2	.825
SL3 & SL4	.495
SL5 & SL6	.297
SL7 & SL8	.600
SL9 & SL10	.360
SL11 & SL12	.216
SL13 & SL14	.450
SL15 & SL16	.270
SL17 & SL18	.162
SS1	.360
SS2	.360
SD1	.360
SD2	.360

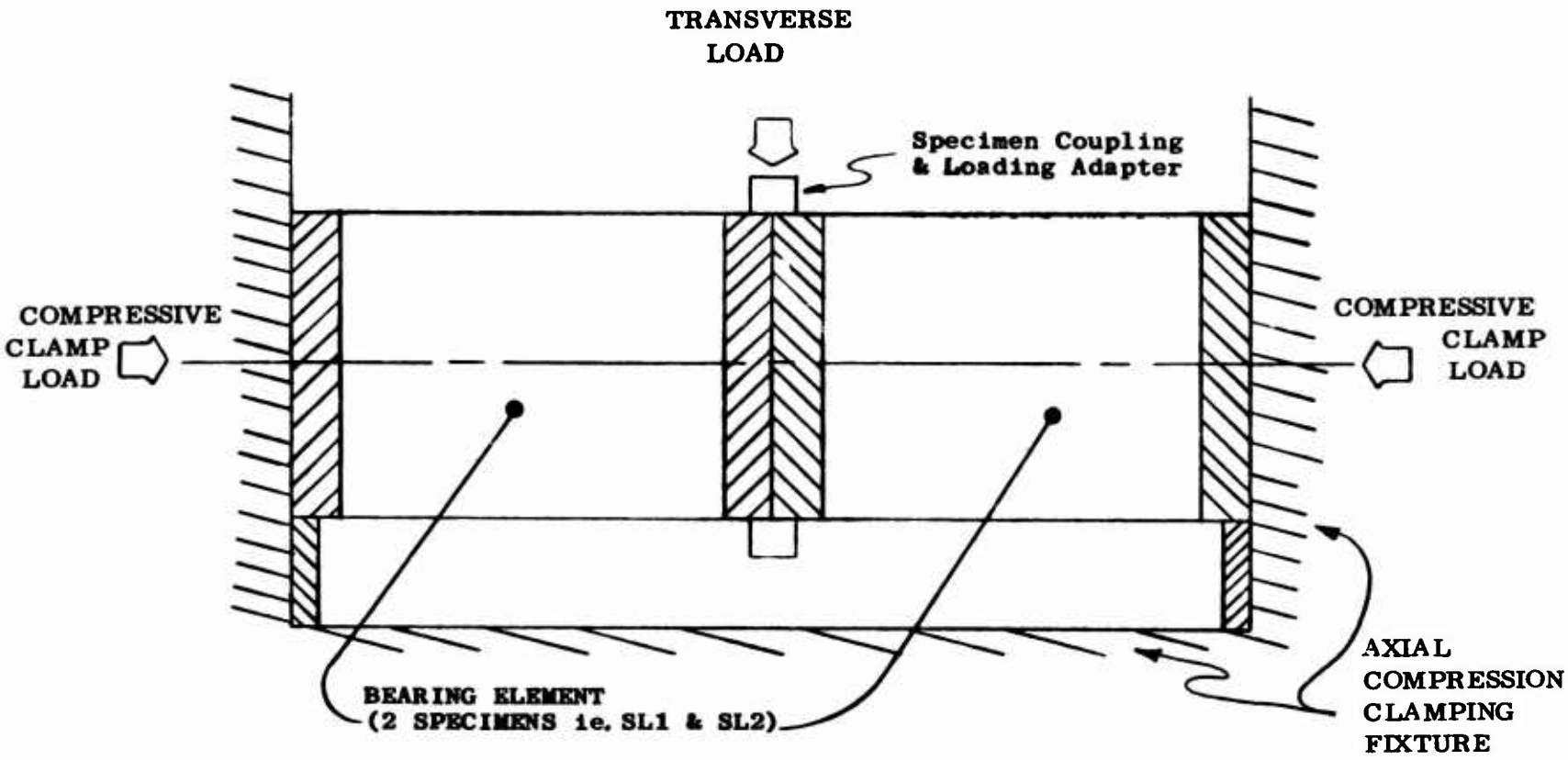

Figure 2. Transverse Shear Test Fixturing Concept

per minute from zero strain to 15% strain and back to zero strain, completing one cycle. Each specimen pair shall be subjected to two (2) cycles of loading with a load deflection plot being continuously recorded for each cycle. The results obtained for a specimen pair shall also be valid for each specimen of the pair. Strain limit values for each specimen pair are presented in Table IV. Upon reaching the maximum strain limit value during the last cycle for each specimen pair, still photographs shall be taken as specified in section 7.2 .

4.2 Inspection

Prior to the stability test each specimen shall be physically inspected to determine specimen height (h_c) and end to end plate parallelism with both being recorded. Each specimen shall be marked prior to test to relate orientation of inspection and position in the test machine.

5.0 TEST REQUIREMENTS

5.1 Test Fixture

For the stability tests a wedge plate shall be placed between the moveable head of the test machine and the upper end plate of each test specimen. Each specimen shall be tested with each of two wedge plate configurations

TABLE IV

STRAIN LIMIT VALUES FOR THE
TRANSVERSE SPRING RATE TEST

Specimen Designation	Axial Deflection (in)				Transverse Deflection (in)
	0%	5%	10%	15%	15% Strain
SL1 & SL2		.138	.275	.413	0.648
SL3 & SL4		.083	.165	.248	0.483
SL5 & SL6		.050	.099	.149	0.384
SL7 & SL8		.100	.200	.300	0.480
SL9 & SL10		.060	.120	.180	0.360
SL11 & SL12		.036	.072	.108	0.288
SL13 & SL14		.075	.150	.225	0.366
SL15 & SL16		.045	.090	.135	0.276
SL17 & SL18		.027	.054	.081	0.222

as shown in Figure 3. The wedge plates shall be of sufficient area to cover the entire surface of the specimen end plates to induce an initial specimen tilt. Wedge plate "A" shall have a tilt angle of 1^{o} (tan = 0.0175) with wedge plate "B" having a tilt angle of 2.5^{o} (tan = 0.0437).

5.2 Lateral Deflection Measurement

For each test the lateral deflection of each specimen shall be measured by a dial indicator. The indicator shall be initially located at the mid-point of each specimen in the plane of tilt (ref Figure 3), which is the anticipated plane of lateral deformation. If the deformation wave begins to form in another area, the load on the specimen shall be released as soon as possible and the dial indicator moved to the area where maximum lateral deformation occurs.

5.3 Stability Test

5.3.1 1 Degree Tilt

Each specimen shall be installed in the test machine using wedge plate "A" (1^{o} tilt). With the specimen and wedge plate in place, sufficient axial loading shall be applied to seat the wedge plate and locate the dial indicator as specified in Section 5.2. After locating

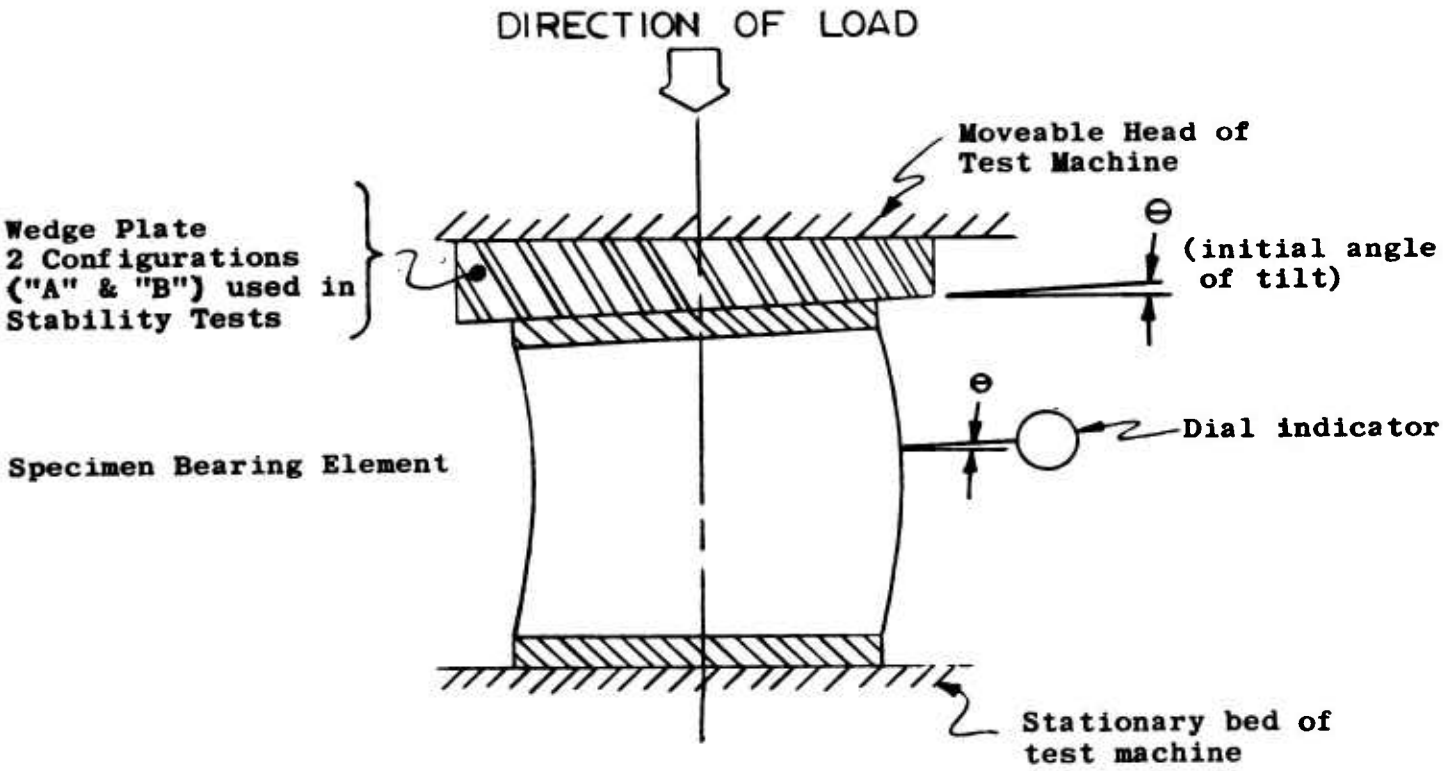

Wedge Plate "A" = 1^{o} (tan = 0.0175)
Wedge Plate "B" = 2.5^{o} (tan = 0.0437)

Figure 3. Installation of Axial Compression and Stability Test Specimens in Test Machine

the dial indicator and recording the load level, axial loading shall be continued at a rate of 0.02 inches per minute with axial loading continuously recorded and lateral deflection recorded in 5,000 pound increments of axial loading. The compressive axial loading shall continue until an approximate 10% drop off in the stiffness characteristics of the specimen occurs as evidenced by a reversal in stiffness trend (ref Figure 4), at which time the test will be terminated. It is suggested that a template depicting the 10% change in stiffness be prepared for the chosen load-deflection scale to facilitate the determination of test termination. Prior to unloading each specimen, still photographs shall be taken as specified in Section 7.3.1 and the orientation of the lateral wave recorded. After load release each specimen shall be inspected for specimen height (h_c) and end plate parallelism.

5.3.2 2.5 Degree Tilt

Each specimen shall also be tested according to Section 5.3.1 using wedge plate "B" (2.5^{o} tilt).

5.3.3 Fatigue Test

After the tests of sections 5.3.1 and 5.3.2 have been conducted, each specimen shall be tested to complete

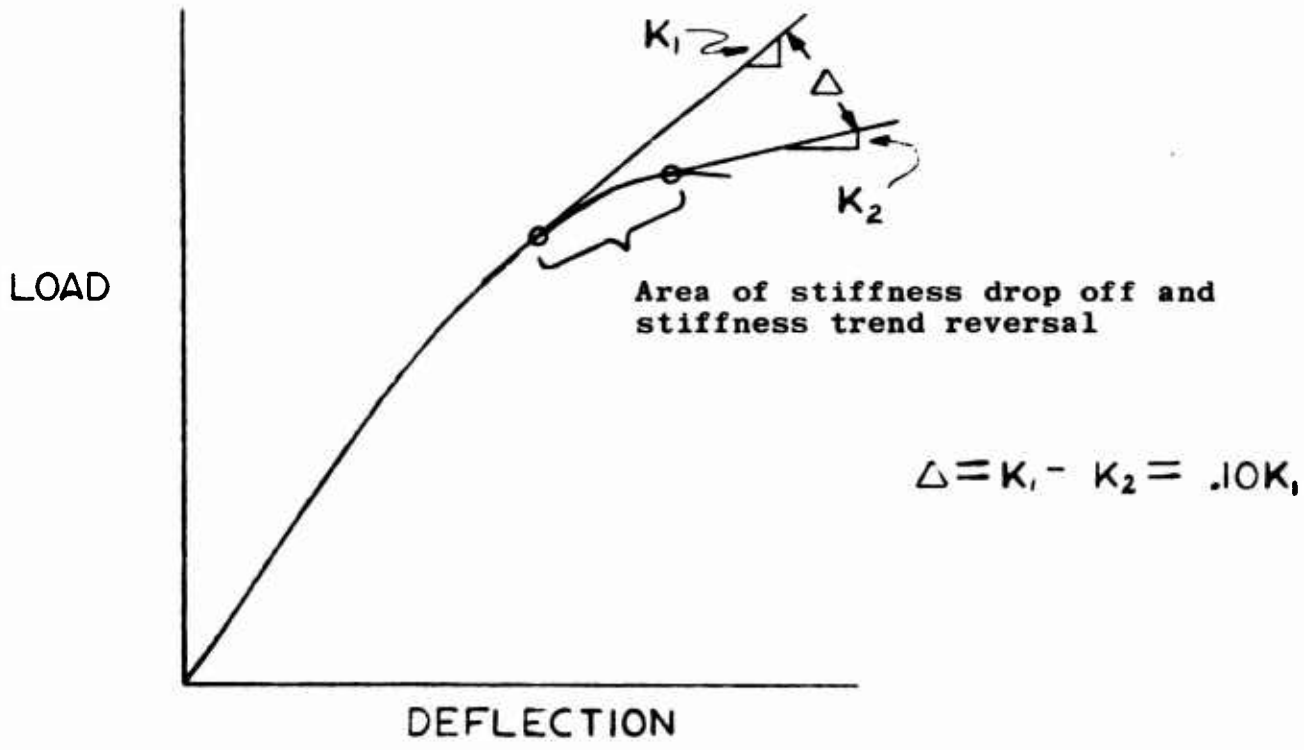

$$\Delta = .10K_1 = K_1 - K_2$$

$$K = \frac{\Delta \text{ Load}}{\Delta \text{ Deflection}}$$

Figure 4. Sample of Load Deflection Curve

failure. This test shall be conducted with both end plates of the specimen parallel to each other and perpendicular to the specimen axis. Each specimen shall be positioned in the test fixture so that the wave area, as noted from the tests of section 5.3.1 and 5.3.2, is in line with the dial indicator. If the wave does not occur in the same area the procedures of section 5.2 shall be followed. After the dial indicator has been properly positioned and the load level recorded, each specimen shall be continuously loaded at 0.02 inches per minute until stiffness trend reversal occurs (ref Figure 4). At that point the lateral deflection shall be recorded at sufficient intervals of loading to define the changing specimen shape as a function of changing load. Loading shall then continue until failure, as defined by a 30% drop in loading or specimen collapse. Photographic coverage for this test is defined in section 7.3.2.

6.0 INSTRUMENTATION

6.1 Static Test Instrumentation

For the static tests a plotter shall be used in conjunction with the test machines to present a continuous record of load and deflection relationships.

6.2 Stability And Fatigue Test Instrumentation

For the stability and fatigue tests a plotter shall be used in conjunction with the test machine to present a continuous record of load and deflection relationships. A dial indicator shall also be used to measure the amount of lateral deformation of each specimen during stability testing.

7.0 PHOTOGRAPHY

7.1 Photographic Coverage of the CSR Test

Upon reaching the maximum strain limit value during the last cycle of the CSR Test (ref Section 4.1.2) for each specimen, still photographs shall be taken to depict the following:

a) The entire specimen

b) A close up of a single rubber lamination bounded by the steel shims at the location of maximum rubber bulge.

7.2 Photographic Coverage of the TSR Test

Upon reaching the maximum strain limit value during the last cycle of the TSR Test (ref Section 4.1.3) for each specimen, still photographs shall be taken to depict the following:

a) Each specimen of the pair at each axial compressive load.

b) The upper tensile surface of each specimen of the pair showing any deformation in the edge of the rubber laminate at each axial compressive load.

c) The lower compressive surface of each specimen of the pair showing any deformation in the rubber laminate at each axial compressive load.

7.3 Photographic Coverage of the Stability Test

7.3.1 1 and 2.5 Degree Tilt

Prior to unloading each specimen in the stability tests of section 5.3.1 and 5.3.2, still photographs shall be taken of the entire specimen showing the lateral wave.

7.3.2 Photographic Coverage of the Fatigue Test

During the interval between stiffness trend reversal and specimen fatigue in the stability test of section 5.3.3,several still photographs shall be taken of the developing specimen shape as a function of changing load.

8.0 REPORTS

Test reports, provided by the Development Lab, for the

stability test of Type I specimens, shall consist of the following:

1. Test logs which present the history of the test.
2. A short summary report containing actual test procedures, results and data, still photographs, test anomalies and a history of part life.

AMENDMENT 1

TEST PLAN FOR CYCLIC FATIGUE TESTING OF TYPE I SPECIMENS

Project Nos.
CR101-02-01
CR102-01-01
CR103-01-01

17 January 1974

NOW:

Specimen Designation	Axial Compression (in) (50% Strain)	Torsion (deg) (100% Strain)
A1	0.075	7
A2	0.100	9
A3	0.125	11
A4	0.150	13
R2	0.100	9
R4	0.150	13
C1	0.075	7
C2	0.100	9
SA1A	0.150	13
SA4A	0.300	26
SA1B	0.150	13
SA4L	0.300	26

Amendment 1

TWR-7468, "Test Plan for Cyclic Fatigue Testing of Type I Specimens", dated 17 September 1973 is amended as follows:

TABLE II, PAGE 7

WAS:

Specimen Designation	Axial Compression (in) (50% Strain)	Torsion (deg) (100% Strain)
A1	0.008	1.93
A2	0.010	2.57
A3	0.013	3.21
A4	0.015	3.86
R2	0.010	2.57
R4	0.015	3.86
C1	0.008	1.93
C2	0.010	2.57
SA1A	0.015	3.86
SA4A	0.030	7.72
SA1B	0.015	3.86
SA4B	0.030	7.72

TEST PLAN FOR CYCLIC FATIGUE TESTING OF TYPE I SPECIMENS

Project Nos. CR101-02-01
CR102-01-01
CR103-01-01

17 September 1973

1.0 INTRODUCTION

This test plan defines the torsional cyclic fatigue test requirements to be performed on a natural rubber compound utilizing flat laminate, annular shaped, Type I elastomeric bearing specimens designed and built by Thiokol Chemical Corporation. The tests will be conducted at the Thiokol Chemical Corporation Engineering and Development Laboratories.

2.0 TEST OBJECTIVES

The primary objective is to generate fatigue life data for Type I Specimens having a natural rubber elastomer with the strain level and geometry of the elastomer treated as variables.

3.0 TEST ITEM DESCRIPTION

3.1 For the cyclic fatigue test, each specimen will be a composition of two (2) annular laminates of elastomer bounded by steel rings as shown in Figure 1. A total of five (5) basic elastomeric configurations (ref. Figure 1 Detail A and Table I) will be evaluated.

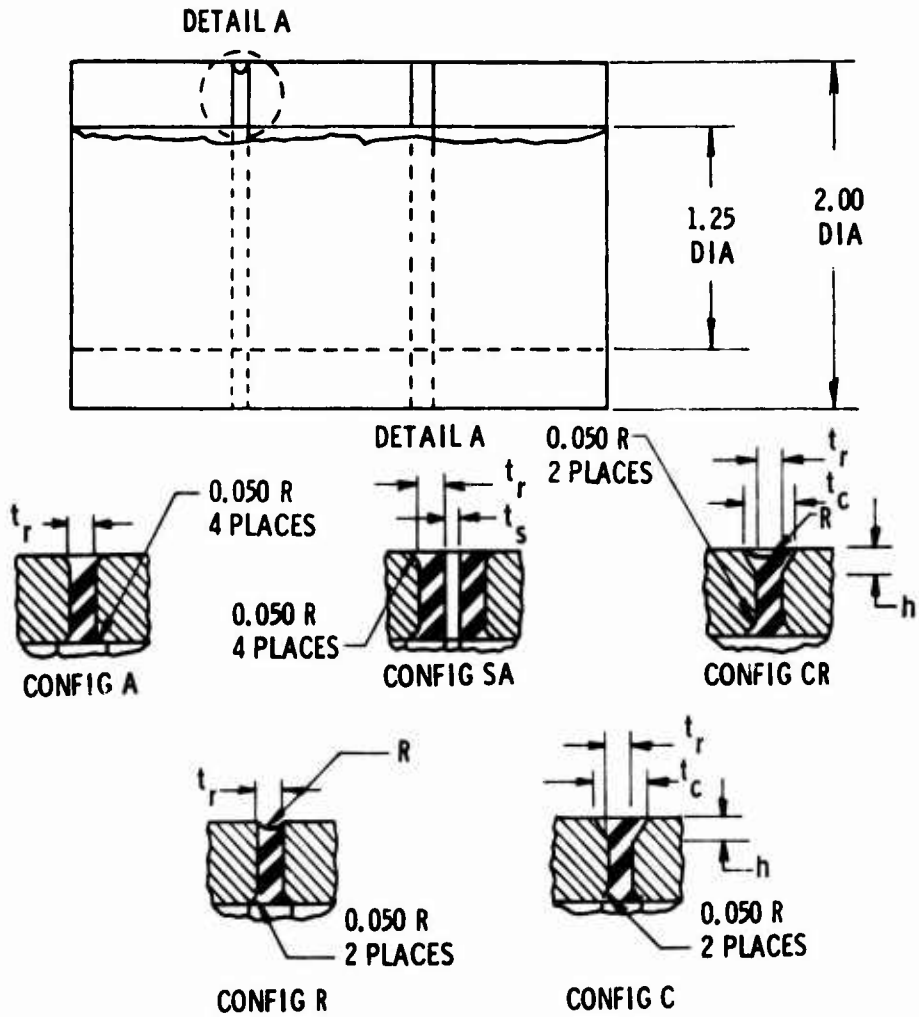

Figure 1. Type I Specimen Configurations

TABLE I

TYPE I SPECIMEN CONFIGURATION DIMENSIONS

Specimen Designation	t_r	t_s	R	t_c	h
A1	0.075				
A2	0.100				
A3	0.125				
A4	0.150				
R2	0.100		0.050		
R4	0.150		0.075		
C1	0.075			0.125	0.150
C2	0.100			0.150	0.150
CR2	0.100		0.075	0.150	0.150
SA1A	0.075	0.037			
SA4A	0.150	0.037			
SA1B	0.075	0.063			
SA4B	0.150	0.063			

3.2 Up to ten (10) specimens may be installed on the Cyclic Fatigue Testing Machine at one time. The machine will induce a cyclic torsional mode of motion about the specimen axis of symmetry while an axial compression load is held as a steady state mode. (See Figure 2)

4.0 PRETEST REQUIREMENTS

4.1 Static Test

Prior to each cyclic fatigue test, each specimen will undergo a static test at room temperature. The static test will consist of a compression load-deflection test, to determine the compressive spring rate (k_C) and the torsional spring rate (k_T). These tests will produce the data points for monitoring the change in bearing stiffness as a result of the decay of the mechanical integrity of the elastomeric material.

4.2 Compressive Test

Each specimen shall be subjected to a static axial compressive load test up to an axial strain level of 50 percent at a load rate of 0.02 inches per minute.

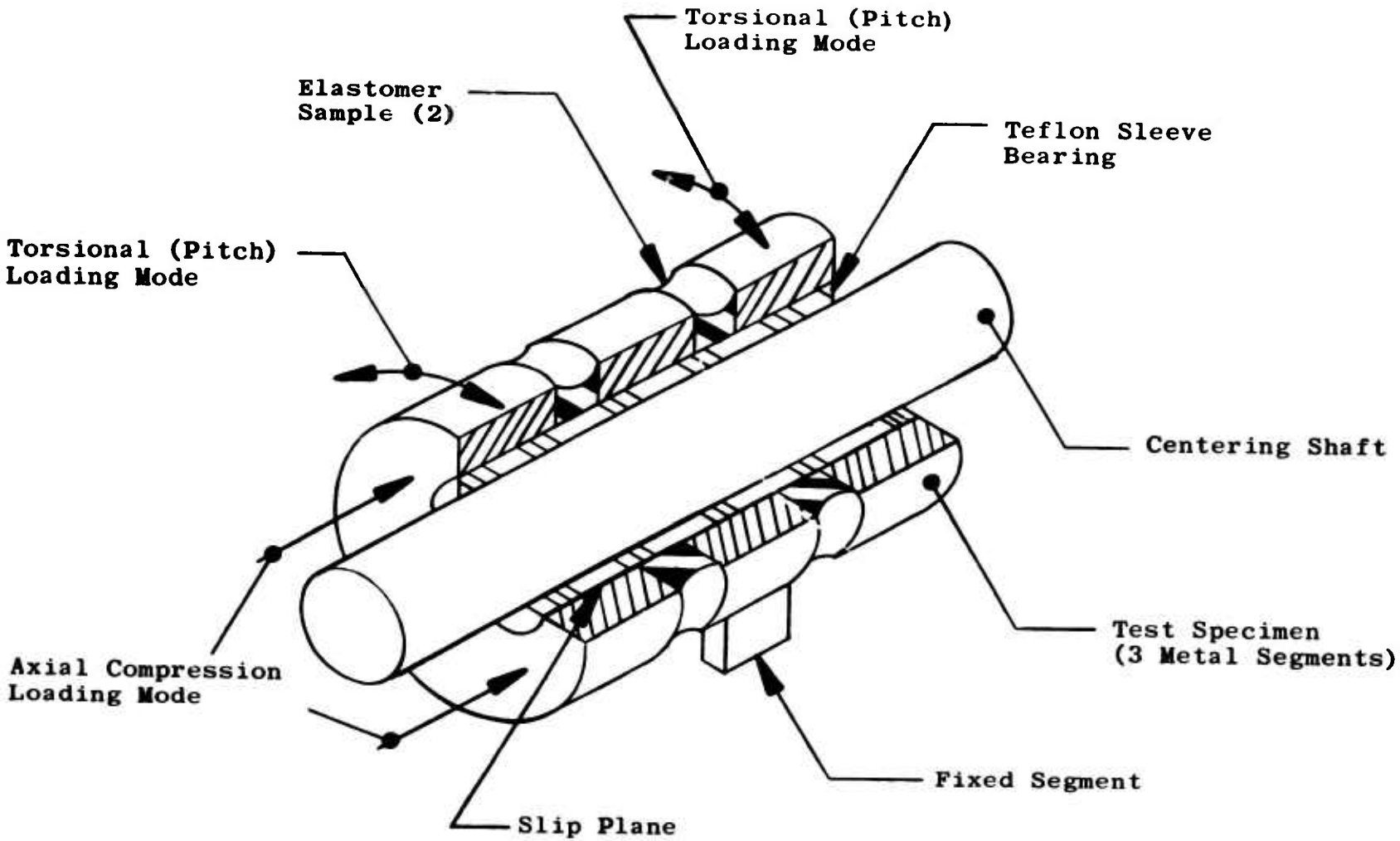

Figure 2. Type I Cyclic Fatigue Specimen

A total of five (5) loading cycles will be run from 0 to 50 percent strain and back down to 0 again. The first four (4) cycles will be run to "stress soften" the specimen with no recording of data. During the fifth cycle the load and deflection measurements will be continually recorded.

4.2.1 Compressive Strain (ϵ_c)

Percent ϵ_c is defined by the following equation:

$$\% \epsilon_c = \frac{\text{axial deflection}}{\text{total rubber thickness}} \times 100$$

The total axial deflection to be induced into each of the respective specimen types to achieve a 50% compressive strain level is presented in Table II.

4.2.2 Compressive Spring Rate (k_c)

The k_c for each specimen is determined from the slope of a line drawn tangent to the load vs axial deflection curve generated during the loading phase through a point at 25% ϵ_c (See Figure 3A). The k_c is given by the following equation:

$$k_c = \frac{\Delta \text{ load}}{\Delta \text{ deflection}} = \text{lb/in}$$

TABLE II

STRAIN LIMIT VALUES FOR AXIAL

COMPRESSION AND TORSIONAL STATIC TESTING

Specimen Designation	Axial Compression (in) (50% Strain)	Torsion (deg) (100% Strain)
A1	0.008	1.93
A2	0.010	2.57
A3	0.013	3.21
A4	0.015	3.86
R2	0.010	2.57
R4	0.015	3.86
C1	0.008	1.93
C2	0.010	2.57
SA1A	0.015	3.86
SA4A	0.030	7.72
SA1B	0.015	3.86
SA4B	0.030	7.72

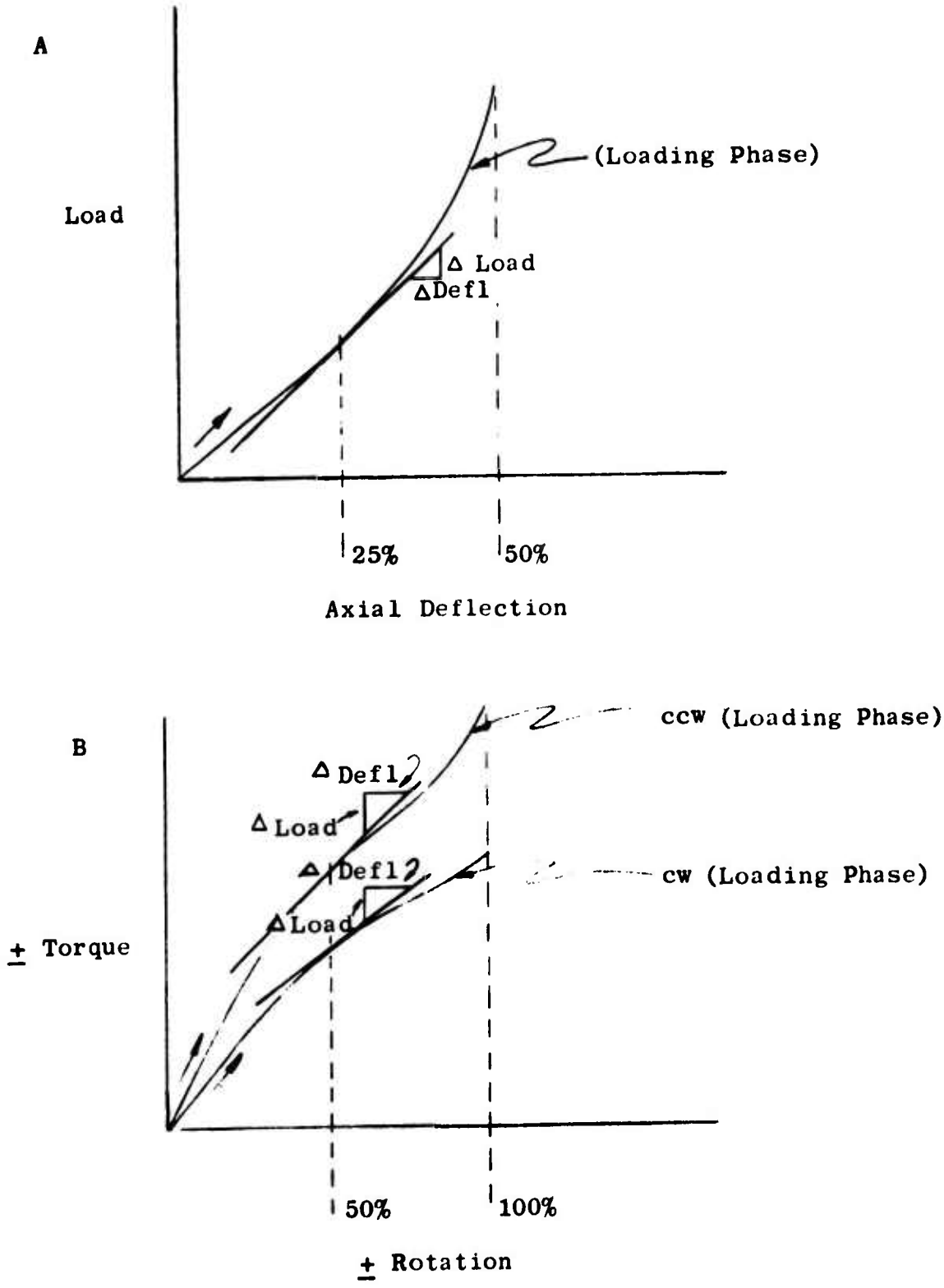

Figure 3. Samples of Load-Deflection Curves

4.3 Torsion Test

Each specimen shall also be subjected to a static torsional load-deflection test up to 100 percent strain in both the clockwise (cw) and counter clockwise (ccw) directions. It will be necessary to mark each specimen cw and ccw to establish a constant orientation for subsequent testing. A total of five (5) cycles will be run, taking the specimen from 0 to 100 percent strain and back down to 0 again. The first four (4) of these cycles will be run to "stress soften" the specimen with no recording of data. During the fifth cycle the load and deflection measurements will be continuously recorded.

4.3.1 Torsional Strain (γ)

Percent γ is given by the equation:

$$\% \gamma = \arctan \frac{0.0175\Theta}{t_\gamma} \times 100$$

Where:

Θ = rotation in degrees

t_γ = total rubber thickness in inches

The total torsional deflection to be induced into each of the respective specimen types to achieve a 100% torsional strain level in one direction is presented in Table II.

4.3.2 Torsional Spring Rate (k_T)

The k_T for each specimen is determined from the slope of a line drawn tangent to the torque vs rotation curve (loading phase) through a point at 50% strain (See Figure 3B).

It is possible that two (2) curves will be generated for each specimen, one for cw rotation and one for ccw rotation. In this case k_T for the specimen shall be an arithmetic average of the two individual values generated from each curve.

The k_T is given by the equation:

$$k_T = \frac{\Delta \text{ torque}}{\Delta \text{ angular rotation}} = \text{in-lbs/degree}$$

5.0 TEST REQUIREMENTS

5.1 Material Screening

For the initial material screening tests, the test specimen configurations and test variables are defined in Table III. Two different materials, material X and material Y, will be tested using the R2 configuration. Prior to the cyclic fatigue test, the specimens will be subjected to the static compression and torsional requirements of Section 4.0.

TABLE III
MATERIAL SCREENING TEST PARAMETERS

Torsional Rotation
L1-L5 = ± 1.8°
R1-R5 = ± 1.8°

Frequency = 250 cpm

Test Position	Specimen* Type	Rubber** Type	Axial Compressive Strain (%)	Torsional Strain (±%)	Specimen S/N
L1	XR2-001	X	15	± 30	XR2-001
L2	XR2-002	X	15	± 30	XR2-002
L3	XR2-003	X	15	± 30	XR2-003
L4	XR2-004	X	15	± 30	XR2-004
L5	XR2-005	X	15	± 30	XR2-005
R1	YR2-001	Y	15	± 30	YR2-001
R2	YR2-002	Y	15	± 30	YR2-002
R3	YR2-003	Y	15	± 30	YR2-003
R4	YR2-004	Y	15	± 30	YR2-004
R5	YR2-005	Y	15	± 30	YR2-005

*Geometry of XR2 and YR2 is same as R2
**Arbitrary descriptions for two candidate formulations

5.1.1 Cyclic Fatigue

For the cyclic fatigue test, a steady state axial compression will be applied prior to and maintained during the test. Torsional strain will be applied as a sinusoidal function with the strain amplitude treated as a variable. Loading will be continuous having a tolerance of $\pm$ 5% with interruptions only for spring rate checks as specified. The test will be run for 105 $\pm$ 15 hours or until the specimen fails at a frequency of 250 cycles per minute. Specimen failure is defined as complete rupture of the elastomer or when an approximate 90% loss in stiffness is detected. If the specimen should not fail during the 105 hour fatigue test, a compressive and torsional static test shall be made per Sections 4.2 and 4.3, deleting the four (4) "stress softening" cycles defined in Sections 4.2 and 4.3. After the static test the specimen will be re-installed in the Cyclic Fatigue Testing Machine and run under the conditions listed above until failure occurs. During all cyclic fatigue tests, a counter will be attached to the machine to record the cumulative number of torsional cycles subjected on the specimen.

5.2 Material Characterization

For the material characterization test one of the two materials tested in the material screening test will be selected and used. A total of three (3) different groups of specimens, as defined in Tables IV, V and VI, will be tested. Prior to the cyclic fatigue tests, the specimens will be subjected to the static compressive and torsional load deflection requirements of sections 4.2 and 4.3.

5.2.1 Cyclic Fatigue

For the cyclic fatigue test a steady state axial compression will be applied prior to and maintained during the test. Torsional strain will be a sinusoidal function with the strain amplitude treated as a variable. Loading will be continuous having a tolerance of $\pm$ 5% with interruptions for spring rate checks as specified. The duration of this test (predicted fatigue life) will be determined by the average fatigue life of the chosen material as demonstrated in the material screening test (Section 5.1). The predicted fatigue life is given by the following equation:

$$\text{Predicted Fatigue Life (PFL)} = \frac{\text{Total No. of Cycles}}{\text{No. of Specimens}}$$

After the PFL has been determined, it will be divided into four (4) equal increments as pictorially defined in Figure 4. The specimens will then undergo cyclic

TABLE IV

MATERIAL CHARACTERIZATION TEST REQUIREMENTS TEST 1

Torsional Rotation

L1-L5 = ± 1.35°
R1-R5 = ± 1.8°

. Frequency = 250 cpm

Test Position	Specimen Type	Axial Compressive Strain (%)	Torsional Strain (±%)	Specimen S/N
L1	A1	15	± 30	A1-001
L2	C1	15	± 30	C1-001
L3	CR2	15	± 22	CR2-001
L4	A2	15	± 22	A2-001
L5	A4	15	± 15	A4-001
R1	R2	0	± 30	R2-001
R2	R2	15	± 30	R2-002
R3	R2	20	± 30	R2-003
R4	R2	25	± 30	R2-004
R5	R2	30	± 30	R2-005

TABLE V

MATERIAL CHARACTERIZATION TEST REQUIREMENTS TEST 2

. Torsional Rotation

L1-L5 = $\pm$ 1.8°
R1-R5 = $\pm$ 2.25°

. Frequency = 250 cpm

Test Position	Specimen Type	Axial Compressive Strain (%)	Torsional Strain ($\pm$%)	Specimen S/N
L1	A2	15	$\pm$ 30	A2-002
L2	C2	15	$\pm$ 30	C2-001
L3	CR2	15	$\pm$ 30	CR2-002
L4	R4	15	$\pm$ 20	R4-001
L5	A1	15	$\pm$ 40	A1-002
R1	A3	15	$\pm$ 30	A3-001
R2	CR2	15	$\pm$ 38	CR2-003
R3	C1	15	$\pm$ 50	C1-002
R4	A2	15	$\pm$ 38	A2-003
R5	A1	15	$\pm$ 50	A1-003

TABLE VI

MATERIAL CHARACTERIZATION TEST REQUIREMENTS TEST 3

Torsional Rotation'

L1-L5 = ± 2.7°
R1-R5 = ± 2.7°

. Frequency = 250 cpm

Test Position	Specimen Type	Axial Compressive Strain (%)	Torsional Strain (±%)	Specimen S/N
L1	R4	15	± 30	R4-002
L2	SA1A	15	± 30	SA1A-001
L3	SA1B	15	± 30	SA1B-001
L4	A4	15	± 30	A4-002
L5	R2	15	± 45	R2-006
R1	SA4A	15	± 30	SA4A-001
R2	SA4B	15	± 30	SA4B-001
R3	R4	15	± 60	R4-003
R4	SA1A	15	± 60	SA1A-002
R4	SA1B	15	± 60	SA1B-002

TABLE VI

MATERIAL CHARACTERIZATION TEST REQUIREMENTS TEST 3

Torsional Rotation'

L1-L5 = ± 2.7°
R1-R5 = ± 2.7°

. Frequency = 250 cpm

Test Position	Specimen Type	Axial Compressive Strain (%)	Torsional Strain (±%)	Specimen S/N
L1	R4	15	± 30	R4-002
L2	SA1A	15	± 30	SA1A-001
L3	SA1B	15	± 30	SA1B-001
L4	A4	15	± 30	A4-002
L5	R2	15	± 45	R2-006
R1	SA4A	15	± 30	SA4A-001
R2	SA4B	15	± 30	SA4B-001
R3	R4	15	± 60	R4-003
R4	SA1A	15	± 60	SA1A-002
R4	SA1B	15	± 60	SA1B-002

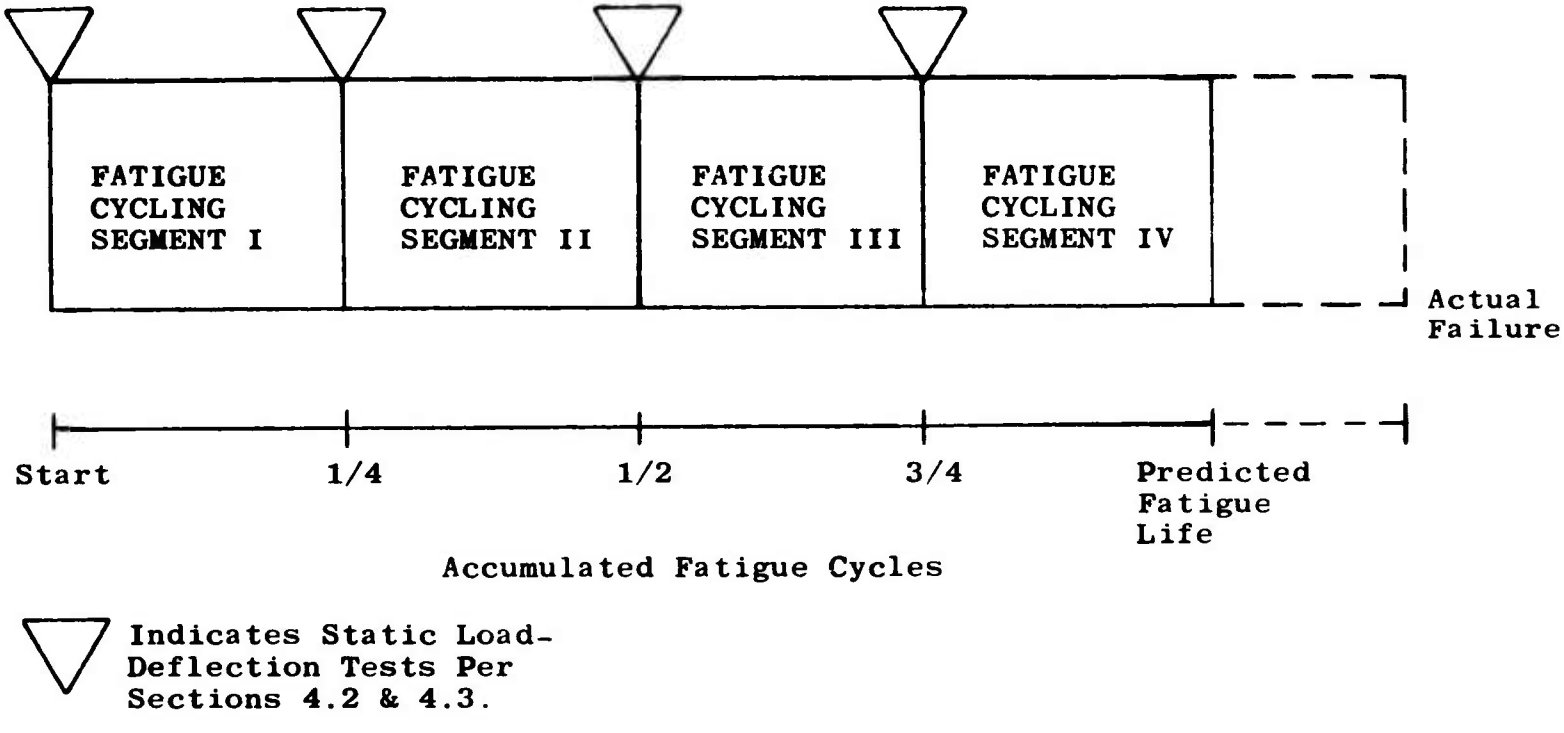

Figure 4. Type I Fatigue Specimen Material Characterization Testing Environment

fatigue testing for the first quarter increment; at the end of which static tests per sections 4.2 and 4.3 will be conducted, deleting the four (4) "stress softening" cycles. This procedure will then be followed for the remaining three (3) segments except that the fourth segment of fatigue testing will be continued until all specimens have failed.

6.0 INSTRUMENTATION

6.1 Static Test Instrumentation

The plotter on the universal test machines shall be used to give a continuous record of load and deflection relationship.

6.2 Fatigue Test Instrumentation

Visual counters shall be used to indicate the cumulative number of cycles.

7.0 PHOTOGRAPHY

Still photographs of each specimen shall be taken before testing, at each stop interval of cyclic testing, and after failure.

8.0 REPORTS

Test Reports, provided by the Development Lab for the cyclic fatigue test of Type I Specimens, will consist of the following:

1. Test logs which present the history of the tests.
2. A short summary report containing actual test procedures, results and data, still photographs, test anomalies, history of part life and definition of change in spring rate.

APPENDIX B

CONSULTATION WITH DR. A. N. GENT

The following is a summary of notes taken during the visit of Dr. A. N. Gent. Dr. Gent is considered by industry to be one of the leading experts in the United States in the area of fracture mechanics work relative to elastomers used in mechanical systems. The service life study effort which is a major part of the Elastomeric Bearing Design Criteria Program (CR-1) will fall into this area of endeavor, where parameters affecting both the initiation and propagation of fracture as a function of fatigue cycles will be studied. A few of the pertinent points brought out during the course of discussion are highlighted below.

GENERAL DISSERTATION

1. Natural rubber is a strain crystalline material which forms a crystalline structure at the apex of a crack. The crystal acts as a reinforcement and retards crack growth.
2. Natural rubber has the broadest temperature range for strain crystalline materials.
3. Triaxial tension exceeding 75% (elastic modulus) will initiate immediate rupture due to cavitation.
4. Heat generation and dissipation must be considered when designing relative to fatigue environments.
5. Free edge shape of the elastomer is critical.
6. Both antioxidants and antiozonants are a must for any natural rubber formation used for mechanical components. The two gases react with the rubber in independent ways.

CRITIQUE OF PROGRAM

1. The TR-3005 material used in the C3 bearing is not a good formulation choice for fatigue applications.
2. In stress-relaxation tests, a nonsoluble oil should be used in place of N_2 for external pressurization.
3. A beam bending specimen will give the truest elastic modulus values for small strains.
4. The Type II radial bearing with integral shims and outer housing will have significant thermal shrinkage stresses which will cause premature failure.
5. The nonlinear finite element is not practical when correlating predicted stress with fatigue test data.

SERVICE LIFE ANALYSIS

1. Bondline termination geometry has two effects:
   a. May change service life considerably.
   b. If proper geometry is selected, analyses (stress and service life) are simplified.
2. A criterion for service life based upon a reduction in bearing stiffness was suggested.
3. Service life should be determined from laboratory specimens having the same termination and thickness to width ratio as the bearing being analyzed.
4. Service life data from laboratory specimens should be plotted against applied stress, shear stress at failure initiation, or energy release rate at the failure initiation point.
5. Miner's law appears to apply to service life predictions for rubbers.

6. Specimens having typical edge shape conditions and stress field mode from a clear elastomer (SOLITHANE®) to facilitate visible witness of crack initiation and propagation would be advantageous.

STABILITY

1. The S-shaped buckling curves can be eliminated by using angled wedges at top and bottom of compressive stability specimens.
2. The critical buckling load is calculated using an iterative procedure that accounts for the pad thickness reduction due to axial loading.

APPENDIX C

ADHESIVE FRACTURE - THEORY AND APPLICATIONS

by

Garron P. Anderson

THIOKOL/WASATCH DIVISION
A Division of Thiokol Corporation
Brigham City, Utah

ABSTRACT

Stresses as determined from linear elastic analyses become unbounded at various locations for particular geometries and material property combinations. Typical stress behavior in the vicinity of these locations is discussed. In many adhesive systems, stress oscillations near the point of debonding have been shown to occur, both analytically and numerically. The effect of these oscillations upon the calculation of the stresses and strain energy is discussed with the conclusion that finite element codes can be used with sufficient precision for fracture analysis.

Several different adhesive fracture test specimens were tested and analyzed. In each specimen, the bulk behavior of the adherends and adhesives was linearly elastic. The specimens tested failed in various combinations of the three loading modes. It is shown that debond does not always originate at the expected mathematical singular points but may originate at inherent flaws within the bondline. Bondline normal stress is shown to be an acceptable failure criterion for this condition.

SINGULAR POINTS

Sharp corners in homogeneous materials have been recognized for many years as points from which fracture propagates. As demonstrated for two individual examples by Sneddon[1] in 1946 and later generalized by Williams,[2] linear elastic analyses of plane problems yielded series solutions for the stresses near a sharp notch in the form

$$\sigma_{ij} = \frac{K}{r^{1/2}} f(\theta) + O(r^{1/2}) + \ldots \quad (1)$$

where r, θ are polar coordinates with origin at the crack tip. For a general enclosed material angle of β, equation (1) may be written

$$\sigma_{ij} = \frac{K}{r^{\lambda}} f(\theta) + \ldots \quad (2)$$

where λ is a function of β as plotted in Figure 1a. For material angles less than π no singular term is present ($\lambda = 0$) while for 2π the square root of r singularity of equation (1) is retained.

In many recent applications such as rocket motor grain retention systems and elastomeric bearings, multimaterial bondlines must be considered. In these cases the stresses near the bondline terminus may be written

$$\sigma_{ij} = \frac{K}{r^{\lambda}} f \left[\theta, \begin{pmatrix} \sin \\ \cos \end{pmatrix} (b \ln r) \right] + \ldots \tag{3}$$

For plane problems in which one material is bonded at an angle β to a semi-infinite sheet of a second more rigid material[3] ($E_1 = 0.001 \; E_2$, $\nu_1 = \nu_2 = 0.2$), values of λ and b are plotted as in Figure 1b. The function b in (3) obviously depends upon material properties since for a homogeneous material b is zero for all material angles. For the nonhomogeneous case, no singularity exists ($\lambda = 0$) until a material angle of over 60 degrees is obtained. Thus fillet angles less than 60 degrees are advisable for such systems. For material angles greater than 210 degrees a nonzero value of b is obtained. In addition to the mathematically infinite stresses at debond terminus which are characteristic of cohesive fractures, the analytical solutions now have an oscillatory character as the debond terminus is approached. The bounding singularity is still of the form $r^{-\lambda}$, however. the signs of the stresses alternate between plus and minus for very small values of r.

As noted by several authors, the oscillations in the analytically determined stresses are not physically realistic. In fact, the analytically determined displacements on the two adjacent faces of the crack oscillate in a manner that would require the material on one side of the crack to intersect the material on the adjacent face in the crack tip vicinity. Thus one must conclude that the analytical solutions are not valid in this area. This phenomenon has not destroyed the usefulness of the analytical solution for predicting strength of the singularity near the crack tip or the stress intensity factor.

The largest value of r for which the sign change is noted ($r = r_o$) depends upon material properties. For example the two semi-infinite sheet geometry shown in Figure 2 has bondline stresses of the form[4]

$$\tau_{xy} = \frac{2(1-\nu)\, Q e^{-\pi b}}{\pi (2ar)^{1/2}} \sin \left(b \ln \frac{r}{2a} \right) + \ldots \tag{4}$$

$$\sigma_y = \frac{2(1-\nu)\, Q e^{-\pi b}}{\pi (2ar)^{1/2}} \cos \left(b \ln \frac{r}{2a} \right) + \ldots \tag{5}$$

Thus as the point r = o is approached the first sign change takes place when

$$b \ln \frac{r_o}{2a} = -\pi/2 \tag{6}$$

The constant b for plane strain conditions simplifies to

$$b = \frac{1}{2\pi} \ln (3 - 4\nu_1) \tag{7}$$

when the modulus of material 2 is much larger than that of material 1 and equation 6 reduces to

$$r_o/a = 2\, e^{-\pi^2/\ln (3 - 4\nu_1)} \tag{8}$$

The character of the variation is given in the following table where, in particular, it may be noted that for an incompressible material $r_o = 0$; i.e., the stresses do not oscillate.

POISSON'S RATIO VERSUS DISTANCE FROM CRACK TIP

ν	r_o/a
0	2.5×10^{-4}
0.10	6.5×10^{-5}
0.20	7.3×10^{-6}
0.30	1.0×10^{-7}
0.40	3.6×10^{-13}
0.48	4.0×10^{-56}
0.499	$4.3 \times 10^{-1,040}$
0.50	0

In addition, two other points are evident: first, the stress oscillation is of a very localized nature for all values of Poisson's ratio; and second, the interval of oscillation decreases monotonically with increasing values of Poisson's ratio.

As stated by England[5] "the probable cause of the oscillatory result is the use of both an idealized physical model and the classical linear theory of elasticity." It would be interesting, if only from an academic viewpoint, to numerically analyze some problem of this type on a computer of sufficient size that the grid mesh in the crack tip vicinity was small enough to reproduce some of the analytically

determined oscillations. If the analytical solutions are due only to the idealized physical model, one may be then able to show the true singularity behavior in this manner.

A second geometry pertinent to bond terminations is shown in Figure 3. The plot of λ in Figure 3 indicates that singular values are expected for all non-homogeneous bond systems with the two quarter plane geometry. However, the order of the singularity is smaller than found in sharp notches. Thus most non-filleted bondlines in practice, have singularity points and the applicability of a strain or stress failure criterion may be questioned when linear elastic analyses are used.

NUMERICAL ASPECTS

Normally one relies on an energy balance approach for geometries which contain singular points. Since for complex geometries, finite element computer programs are used to obtain stresses and energy release rates, one questions the accuracy of these values for systems where analytical oscillations are observed.

Oscillations have also been noted in the stresses in the vicinity of a boundary condition discontinuity as calculated by the standard finite element computer programs (reformulated) which use linear displacement or constant strain elements.[6] This oscillation is much more pronounced under the following conditions: (a) in areas of high stress gradient such as at the terminus of a fixed free boundary ($E_1/E_2 \ll 1$), (b) for nearly incompressible materials, (c) for highly constrained systems (higher amplitude of oscillation for plane strain than for plane stress problems), and (d) compatible elements (relaxing the compatibility requirements normally reduces the magnitude of the oscillations).

An example of the stress oscillation is given in Figure 4. The analysis for these data was performed for a finite dimension sheet approximating the two-material infinite sheet geometry analyzed by Erdogan[4] as shown in Figure 2. The modulus of the second material (E_2) was assumed infinite.

The computer program used a constant strain element with a grid consisting of 880 nodes. The width of the smallest element was 0.002 inch as compared to a total bond length of 2 inches. The height of the first row of elements above the crack tip is 0.001 inch. In the particular program used in this study, each quadrilateral element is divided into four triangular elements by the computer. The stresses at the centroid of each element are then calculated, and the four triangular stresses are averaged to give a single value for the quadrilateral element stress. Thus some degree of smoothing of the stress oscillations is automatically accomplished. The width of the smallest element is many orders of magnitude larger than the largest radius from the crack tip at which the analytically determined stresses oscillate ($r_o \backsim 10^{-1,000}$ since $\nu = 0.499$ was used). Therefore, all the "natural" oscillations occur within a very small portion of the first element. Since the numerical oscillations become more pronounced

with high values of Poisson's ratio (the inverse being true of the "natural" oscillation), and since the "natural" oscillations all occur in a very small portion of the two elements adjacent to the crack tip, it seems unlikely that the two phenomena are related.

Comparisons of numerical and analytical results as presented in reference 7 have demonstrated that even though rather severe oscillations are seen in the stresses at bi-material interfaces for the usual finite element formulations, stress values sufficient for most engineering applications can be obtained by suitable smoothing of the numerical values. In addition, energy release rate obtained from these codes has compared favorably in all cases for which analytical and numerical results were compared.

APPLICATIONS

As shown above, infinite stresses are predicted at the tip of V notches and at the ends of bi-material interfaces for linear elastic analysis. Infinite stresses are not seen in real materials since the linearity assumption is violated as stresses become large. In practice, the stresses do become relatively large near singular points. These points are certainly potential fracture initiation points. For example, in applying a tensile load to two cylinders bonded with a butt joint as shown in Figure 5, points 1, 3, 7 and 9 are singular points and therefore strong candidates for failure initiation. However, experience with poker chip test specimens demonstrates that point 5 must also be considered as a potential failure initiation point. Systems of this type were tested[8] using PMMA adherends bonded with Solithane 113. Debonds were found to initiate in the high stress regions away from end discontinuities (points 2 and 8 of Figure 5).

The butt joint is a special case of a conical test specimen (Figure 6) developed at the University of Utah for studying loading mode effects on fracture.[8] For conical specimens with cone angles from 5 through 90 deg (butt joint), the bondline stress distributions demonstrated identical patterns. As an example, the bondline normal and shear stress for a 5 deg cone are plotted in Figure 7. A 0.06 in. initial debond was built into these specimens. However, debond initiated in the high stress region away from the theoretical singular points (A and B of Figure 7). One could therefore assume that the higher (singular) stresses extend over such a small (plastic) region; they do not affect fracture. However it is conceivable that in an ideally elastic system, the energy release rate from a naturally existing flaw in a high stress region is greater than that from an initial debond in a low stress region. Thus even for ideal linear elastic materials, debonds could propagate from inherent flaws away from end induced singular points.

When the cone angle is reduced to zero (cylinder test), the stress pattern changes to that shown in Figure 8. The large normal stress at the bondline center is missing and debond propagated from the 0.06 in. initial debond region (point A). Note from Figure 1b that the order of the stress singularity is greater at point A than at point B.

A more complete discussion of cone test results is presented in references 8 and 9. However the above brief discussion points out some of the difficulties in analysis of complex bondline systems such as found in elastomeric bearings or rocket motor grain retention systems. The weakest point in the system is not always obvious.

In cone test specimens where debond initiated away from bond termination singular points, the bondline normal stress was shown[9] to be a reasonably reliable failure criterion. Solithane-PMMA cone test specimens of 5, 45, and 90 degrees all failed at a normal stress within 5 percent of 493 psi.

In test specimens where failures occurred at bond termination points an energy balance was used for failure criterion As shown in reference 10 the effective value of adhesive fracture energy (γ_a) changes with direction of load application (loading mode). The magnitudes of these changes are very significant, at least for a PMMA-Solithane bond system, as shown in the following table:

Loading Mode	γ_a (in. lb/sq in.)
I	0.17
II	0.40
III	0.58

As shown in reference 11, γ_a values are also rate and temperature dependent. Thus with the present state of the art, one must select laboratory tests for which temperature, loading rate, and loading mode duplicate as nearly as possible those in the bondline being analyzed. If there is difficulty in obtaining the desired load rate and/or temperature in the laboratory it is possible to test specimens at a number of different load rates and temperatures. Then by applying a time-temperature shift of the resulting γ_a data in a manner similar to that used in obtaining relaxation modulus for viscoelastic materials, one can obtain a master γ_a versus log of reduced time, log (time/temperature shift factor), curve which may cover many decades of time. A thorough explanation of this procedure is given in reference 11.

Although the γ_a data show large changes due to loading mode, the engineering implications are not as severe as one might suspect since the critical loads are generally related to the square root of γ_a. Thus, if the actual γ_a value is somewhere between the Mode I and Mode II values such as 40 percent higher than the Mode I value, a critical load predicted using the Mode I value would be conservative by less than 20 percent.

REFERENCES

1. Sneddon, I. N., "The Distribution of Stress in the Neighborhood of a Crack in an Elastic Solid," Proceeding, Royal Soc. London, Vol. A-187 (1946).

2. Williams, M. L., "On the Stress Distribution at the Base of a Stationary Crack," Transactions, Am. Soc. Mechanical Engineers, J. of Applied Mechanics (1957).

3. Hein, V. L. and Erdogan, F., "Stress Singularities in a Two-Material Wedge," Int. Journ. of Fracture, 7 (1973) 317-330.

4. Erdogan, F., Journal of Applied Mechanics, 30 (1963) 232.

5. England, S. H., Journal of Applied Mechanics, 30 (1965) 400.

6. Anderson, J. M. and Christiansen, H. N., Bulletin Sixth Meeting of the ICPPG Mech. Behavior Working Group (1967).

7. Anderson, G. P., DeVries, K. L. and Williams, M. L., "Finite Element in Adhesion Analyses," Int. Journal of Fracture Mechanics (to be published).

8. Anderson, G. P., "Applied Adhesive Fracture Mechanics," Ph. D Dissertation, Mechanical Engineering Department, University of Utah, Salt Lake City, Utah, 1973.

9. Anderson, G. P., DeVries, K. L. and Williams, M. L., "Stress Field Effect in Adhesive Fracture," Int. Journal of Fracture Mechanics (to be published).

10. Anderson, G. P., DeVries, K. L. and Williams, M. L., "The Influence of Loading Direction Upon the Character of Adhesive Debonding," Journal of Colloid and Interface Sciences (to be published).

11. Bennett, S. J., Ph. D Dissertation, Mechanical Engineering Department, University of Utah, Salt Lake City, Utah, 1973.

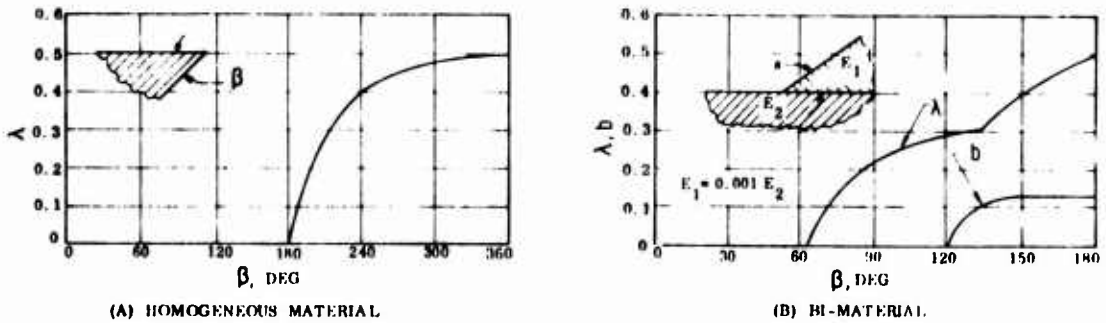

Figure 1. Singular Eigenvalues-Half Plane to Wedge

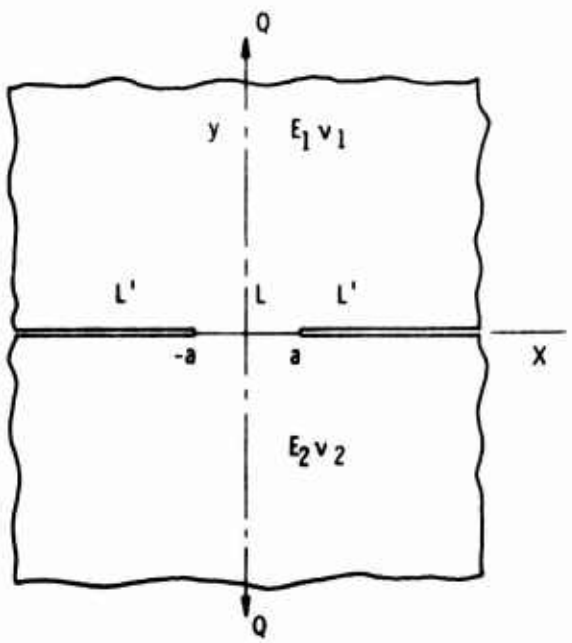

Figure 2. Two Semi-Infinite Crack Geometry and Load Analyzed

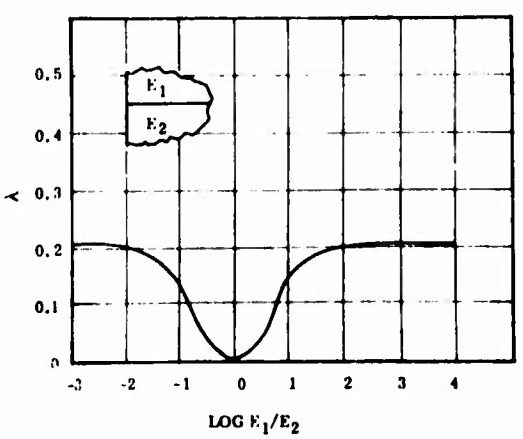

Figure 3. Singular Eigenvalues-Two Quarter Planes

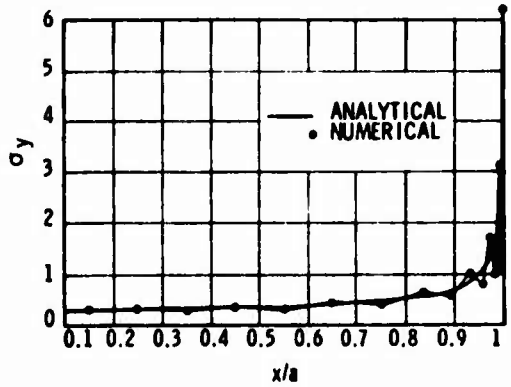

Figure 4. Bondline Stresses Calculated Numerically and Analytically for $\mu_2 = \infty$

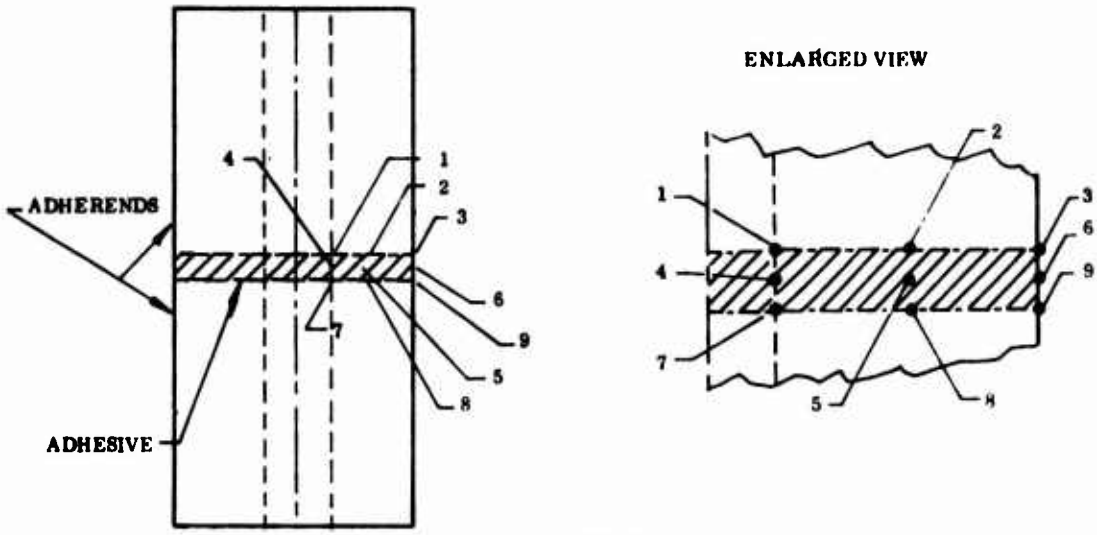

Figure 5. Potential Failure Initiation Points in a Butt Joint

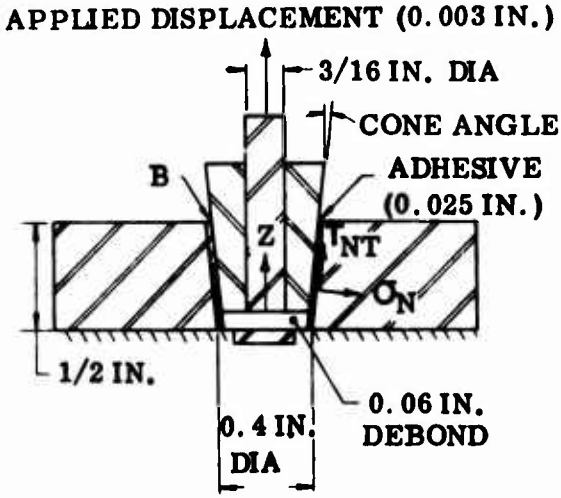

Figure 6. Cone Configuration Analyzed

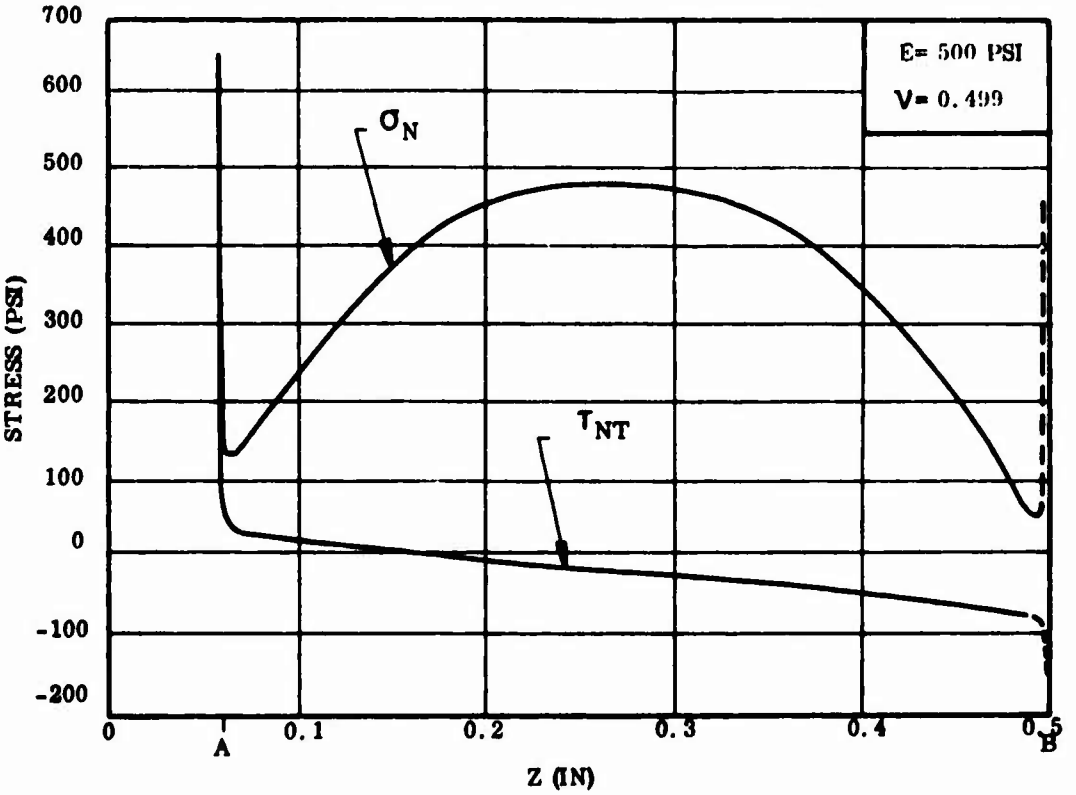

Figure 7. Normal and Shear Stress Components for 5 Degree Cone

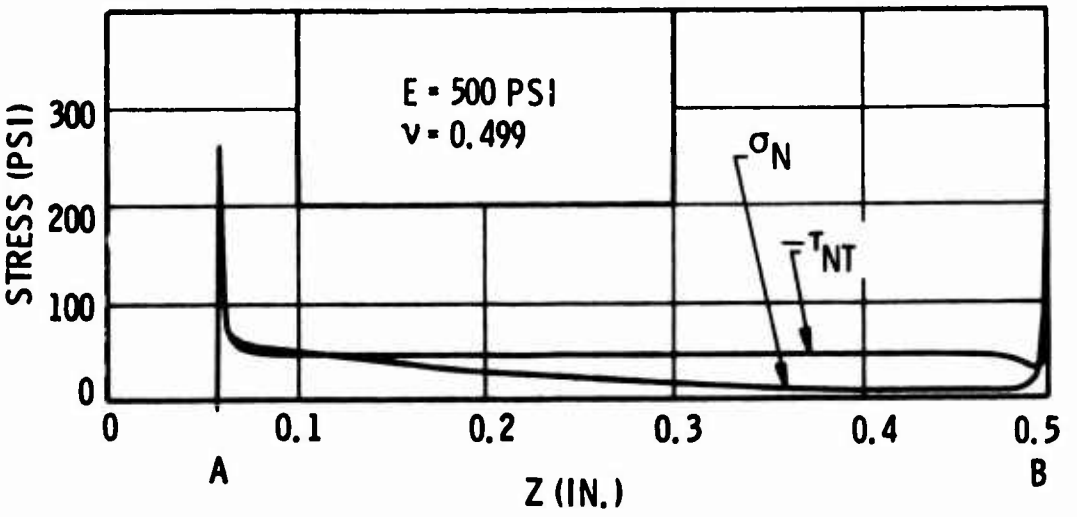

Figure 8. Normal and Shear Stress Components for 0 Degree Cone

LIST OF SYMBOLS

COORDINATE SYSTEM

Rectangular (Cartesian)

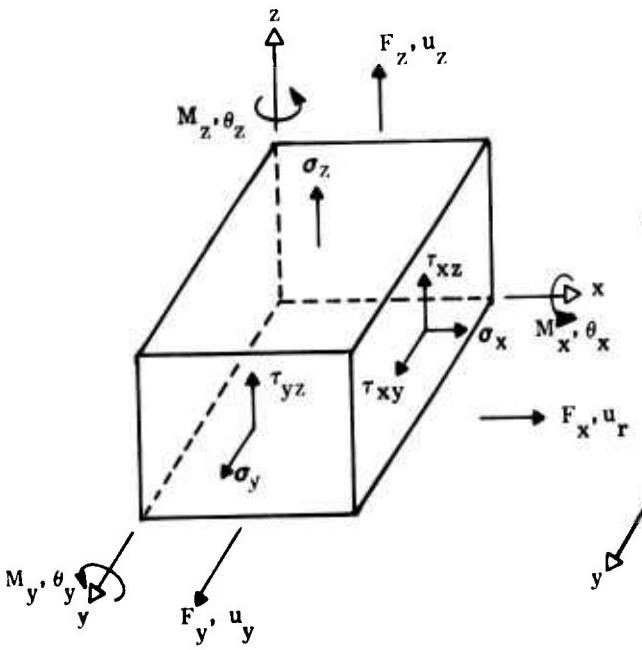

Cylindrical (Polar)

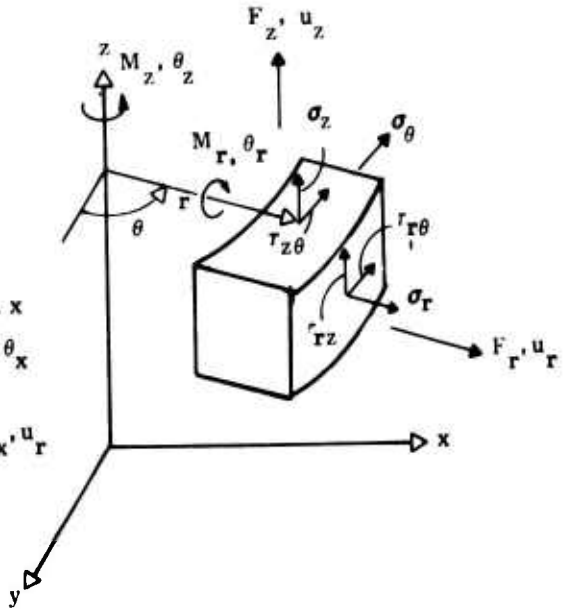

Spherical

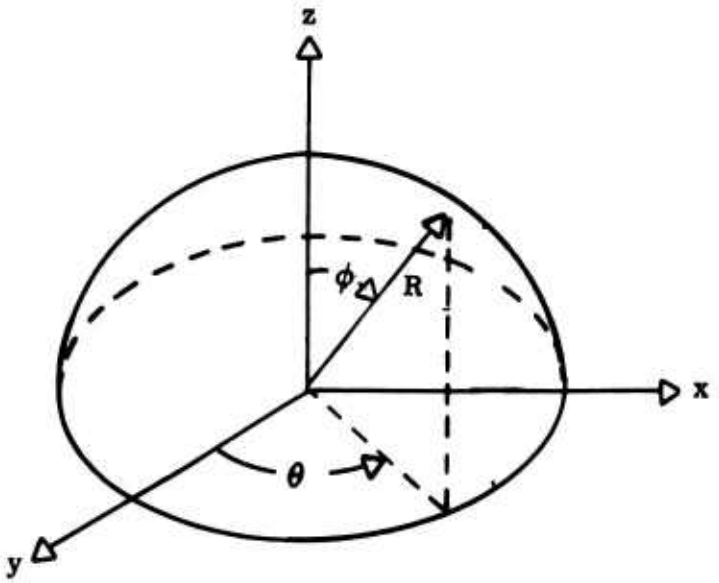

LIST OF SYMBOLS (Cont)

Loads and Displacements

Symbol	Identity	Unit of Measure
F	Force, Load	lb
M	Moment	in.-lb
u	Displacement	in.
θ	Rotation	rad
σ	Normal Stress	lb/sq in.
$\bar{\sigma}$	Hydrostatic Stress	lb/sq in.
τ	Shear Stress	lb/sq in.
ϵ	Normal Strain	in/in.
γ	Shear Strain	in/in.
F^c	Critical Load	lb

Stiffnesses

K_z	Axial	$\left(= \frac{F_z}{u_z}\right)$	lb/in.
K_r	Radial	$\left(= \frac{F_r}{u_r}\right)$	lb/in.
K_{θ_x}	Flap	$\left(= \frac{M_x}{\theta_x}\right)$	in.-lb/rad
K_{θ_y}	Lead-Lag	$\left(= \frac{M_y}{\theta_y}\right)$	in.-lb/rad
K_{θ_z}	Torsion	$\left(= \frac{M_z}{\theta_z}\right)$	in.-lb/rad
K_{θ_r}	Vector	$\left(= \frac{M_r}{\theta_r}\right)$	in.-lb/rad

Note: Minimum, Maximum, Average or Allowable values are denoted by superscripts.

LIST OF SYMBOLS (Cont)

Geometric Properties

Symbol	Identity	Unit of Measure
h	Elastomer Pad Thickness	in.
t	Shim Thickness	in.
h^T	Total Elastomer Thickness	in.
t^T	Total Shim Thickness	in.
n	Number of Elastomer Pads	
r_i	Minimum Inner Pad Radius	in.
r_o	Minimum Outer Pad Radius	in.
R	Mean Spherical Radius of Pad	in.
A	Cross-Sectional Area	in.
S	Shape Factor	—
V	Volume	$in.^3$
V_o	Initial Volume	$in.^3$
J	Polar Moment of Inertia	$in.^4$
I	Moment of Inertia	$in.^4$
η	Buckling End Fixity Coefficient	
L	Bearing Length	in.

Material Properties

E	Young's Modulus	lb/sq in.
E_A	Apparent Compression Modulus	lb/sq in.
G	Shear Modulus	lb/sq in.
G_{rel}	Shear Relaxation Modulus	lb/sq in.
G^*	Complex Shear Modulus	lb/sq in.
G', G''	Real and Imaginary Parts of Complex Shear Modulus	lb/sq in.
k	Bulk Modulus	lb/sq in.
k_1, k_2	Nonlinear Material Properties	
ν	Poisson's Ratio	

LIST OF SYMBOLS (Cont)

Material Properties (Cont)

Symbol	Identity	Unit of Measure
Tan δ	Loss Tangent	
α	Coefficient of Linear Thermal Expansion	in./in./° F
	Miscellaneous	
U	Strain Energy Density	in.-lb/in.^{3}
U^T	Total Strain Energy	in.-lb
c	Crack or Debond Length	in.
T	Temperature	°F
ΔT	Change in Temperature ($=T_{final} - T_{initial}$)	°F
P	Pressure	psi
N	Cycles to Failure	
$\frac{dc}{dN}$	Crack Growth Rate	in/cycle
γ_t	Tearing Energy	in.-lb/sq in.
γ_c	Cohesive Fracture Energy	in.-lb/sq in.
γ_a	Adhesive Fracture Energy	in.-lb/sq in.
A_f	Fracture Surface Area	sq in.
f	Frequency	Hz